Study of Excited State Intra- and Inter-molecular Proton Transfer in Few Azole Derivatives

A dissertation
as partial fulfilment for the degree of
Doctor of Philosophy in Chemistry

by

Ila
146122035

Department of Chemistry
Indian Institute of Technology Guwahati
Guwahati 781039
Assam, India

TH-2834_146122035

TH-2834_146122035

Statement

The work contained in this thesis titled "Study of Excited State Intra- and Inter- molecular Proton Transfer in Few Azole Derivatives" is the outcome of the research work carried out by me under the supervision of Prof. G. Krishnamoorthy, Department of Chemistry, Indian Institute of Technology Guwahati, India.

In the present thesis, the general practices of the scientific observations are reported. Whenever needed, the findings of other investigators are described and duly acknowledged. This thesis is not submitted anywhere else for the award of any degree.

Ila

April 16, 2021
Guwahati

Ila
Department of Chemistry,
IIT Guwahati
Guwahati, Assam, India-781039

TH-2834_146122035

TH-2834_146122035

INDIAN INSTITUTE OF TECHNOLOGY GUWAHATI
Guwahati 781 039, Assam, India

Dr. G. Krishnamoorthy
Dean of Industrial Interactions and
Special Initiatives & Professor of Chemistry

Tel: +91–361–258 2315 (W), 258 4315 (H) Fax: +91–361–2582349
E-mail: gkrishna@iitg.ac.in, gkrishna_2000@yahoo.com

Certificate

It is certified that the work contained in thesis titled "Study of Excited State Intra- and Inter- Molecular Proton Transfer in Few Azole Derivatives" by Ila is an authentic record of the results obtained from the research work carried out under my supervision in the Department of Chemistry, Indian Institute of Technology Guwahati, India.

April 16, 2021
Guwahati

G. Krishnamoorthy

TH-2834_146122035

TH-2834_146122035

Dedicated to my grandparents

TH-2834_146122035

TH-2834_146122035

~Acknowledgement~

First of all, I express my sincere gratitude to my supervisor Dr. G. Krishnamoorthy for his guidance and support. I thank him for being patient when I was feeling demotivated. I acknowledge my doctoral committee members, Prof. Anumita Paul (chairperson), Prof. S. Ravi and Dr. Kingsuk Mahata, for their valuable suggestions during annual evaluation, which helped improve my thesis.

I thank IIT Guwahati for the fellowship. I am thankful to IIT Guwahati, Department of Chemistry (& staff) and Central Instruments Facilities (& staff), to provide research and instrumental facilities. I acknowledge HPC, IIT Guwahati, for theoretical calculations. My special regards to Dr. Babulal Das and Mr. Aniruddha Gogoi for their support.

I would like to thank my teachers at Miranda House, IIT Roorkee and IIT Guwahati for teaching me excellent Chemistry. I am thankful to Dr. Naseem Ahmed's lab (IITR) for my first research experience during my M.Sc. dissertation. I also want to thank all my teachers from school. My special regards to Late Mr. Satyadeo Ojha for igniting my interest in Chemistry. Thanks Aaron and Alexandra for your fight towards making science accessible.

I would like to thank Dr. Suranjan Dey for teaching me column chromatography. I thank my former and present labmates Dr. Francis (for helping me with DFT), Dr. Santosh (for conceptualizing the work done in chapter 7), Dr. Saugata (For teaching me instrumentation), Dr. Ashim, Himadree, Minati, Aditya, Arup and Mongoli for their help and support. Thank you, Minati, Tapasi, Trusna, Sarita and Suresh and my other batchmates, for making my Ph.D. bearable. I thank Arup, Mongoli, Reshmi, Pravesh, and Sanjeev for help with some of the work. I thank everyone who did their bachelor's and master's dissertations in my lab during my Ph.D (Thanks Bhushan for helping me with TOC). Thank you Sumit Bhai, Dikshant, Anmol, Arshad, Paulomi and AOL family, for your valuable friendship during my Ph.D. I am thankful to my friends from school and college (especially Richa, Swasti, Rashmi, Sanju, Suchi, Shruti, Anu, Ashwin, Madhu, Aakanksha, Preeti, Varsha, Abu, Animesh). I am grateful to Anindita for her constant support during the last three years. I thank Ms. Namrata Naomi Rynjah for her guidance. I want to thank the Disha family, especially Dr. Srinivasan Krishnaswami (EEE) and Dr. Sriparna Bhattacharya (Mathematics). A small note of thanks to Dr. S. S. for the last-minute encouragement.

I thank my grandparents (Mankeshwar Prasad and Ramgyani Devi, Vinayak Chandra Dutt and Savita Dutt) for their blessings. How do I thank my mother for giving me a life she always wanted for herself? It is impossible to thank my parents (Tanuja Dutt and Suresh Kumar Verma) and younger sister, Isha and our pet Bravo for their love. I am grateful to my extended family, especially my aunts (Mukta, Anita and Late Mrs. Meera), uncles (Prabhat and Pranav) and cousins (Awanish (& family), Manish (& family), Ravi, Rahul, Surabhi (& Vaibhav jiju), Ishaan and Shivaansh for their support. I am thankful to my cousin Vinish (& family) and his friends (Krishna, Shrawan, Amresh & others) for always treating me like their little sister. Lastly, I would like to thank everyone who is/was part of my journey and have helped me to grow.

Sincerely,
Ila

TH-2834_146122035

TH-2834_146122035

-Synopsis-

Proton transfer (PT) is a fundamental process in biology and chemistry. Excited state intramolecular proton transfer (ESIPT) takes place upon light excitation when acidic (e.g., OH, $–NH_2$ etc.) and basic groups (e. g. =O, =N etc.) are close enough to form an intramolecular hydrogen bond. Usually, ESIPT shows dual emission, one from the normal excited state (N*) and the second one from a lower energy excited state tautomer (T*) (**Scheme 1**). It is very sensitive to the medium and surrounding environment.

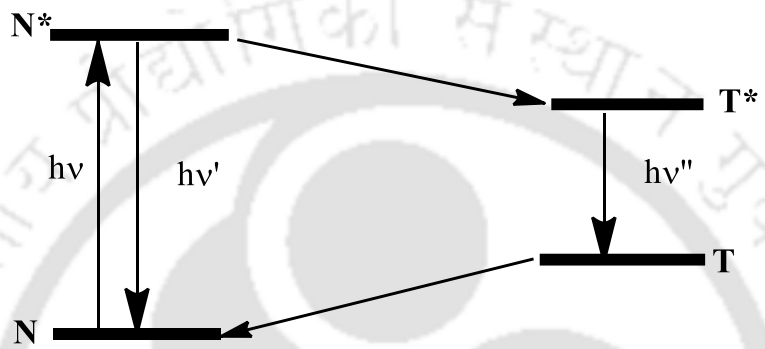

Scheme I. A simple schematic diagram of proton transfer.

Proton transfer between donor and acceptor groups of two different molecules is called intermolecular proton transfer. In such cases, proton transfer may occur between two molecules via dimer formation or through solvent assistance. In biological systems, the proton is transported by a chain of water molecules by accepting and donating protons. In chemical systems, it is observed with alcohol or water chain in a similar fashion. These kinds of proton transfers (known as relay proton transfer) have attracted a lot of interest from experimental as well as theoretical chemists.

Excited state proton transfer in hydroxyarenes have been studied for several decades. However, new prospects are still opening for this fundamental proton transfer process. Steady state and time resolved photoluminescence, transient electronic spectroscopy, femtosecond fluorescence up-conversion measurements and quantum mechanical calculations are employed to elucidate the mechanism of ESIPT. As a result of new substrates, new instrumentation for ultrafast processes, and new calculation tools, a fairly reliable picture of proton transfer has emerged.

The effect of different environment on the PT process of a few azole derivatives are studied. The thesis is divided into eight chapters and a summary of all the chapters are given in brief ahead.

TH-2834_146122035

Chapter 1: Introduction

Chapter 1 gives a brief description of PT, different types of PT and effect of various factors on PT, along with relevant studies from the literature. A brief introduction about charge transfer and aggregation induced enhanced emission (AIEE) are also given, along with suitable examples from literature. The motivation to carry out this research work is given at the end of the chapter.

Chapter 2: Materials, Method and Instrumentation

Chapter 2 lists all the chemicals and instruments used in the thesis work. The synthetic procedures of all the synthesized compounds are reported here. This chapter also contains details about the preparation of solutions. Computational and other methods used in this work are also presented in brief.

Chapter 3: The origin of longer wavelength emission in 2-(4-Fluorophenylamino)-5-(2,4-dihydroxybenzeno)-1,3,4-thiadiazole and its analogue 2-Phenylamino-5-(2-hydroxybenzono)-1,3,4-thiadiazole

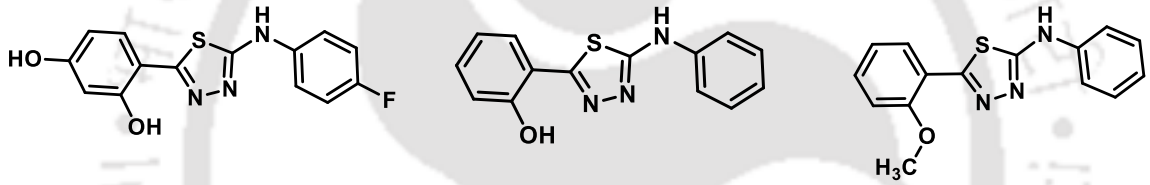

FABT **PHBT** **PMBT**

Chart I. Structures of FABT, PHBT and PMBT.

2-(4-fluorophenylamino)-5-(2,4-dihydroxybenzeno)-1,3,4-thiadiazole (FABT, **Chart I**) has been studied for its pharmacological properties, especially the anticancer activity by many research groups. In an aqueous solution, FABT emits dual emission and the longer wavelength emission in FABT was assigned to the combination of aggregation and change in conformation in the literature. However, FABT has proton donor and acceptor groups in close proximity and therefore, the longer wavelength emission may originate from excited state tautomer.

In this work, an analogue of FABT, 2-phenylamino-5-(2-hydroxybenzono)-1,3,4-thiadiazole (PHBT, **Chart I**), was synthesized to determine the origin of the longer wavelength emission. The luminescence of PHBT and its methoxy derivatives 2-phenylamino-5-(2-methoxybenzono)-1,3,4-thiadiazole (PMBT, **Chart I**) were studied and compared with that of FABT. The longer wavelength emission band was assigned to the excited state tautomer (**Figure I**).

TH-2834_146122035

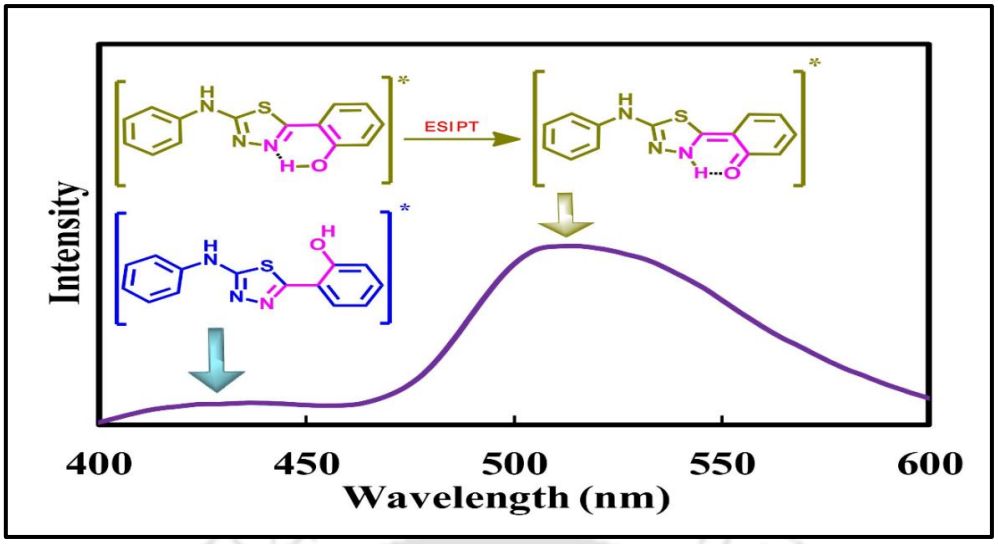

Figure I. ESIPT in PHBT.

Chapter 4: Effect of pH and host-guest complexation on PTTPT of 3,5-bis(2-hydroxyphenyl)-1H-1,2,4-triazole

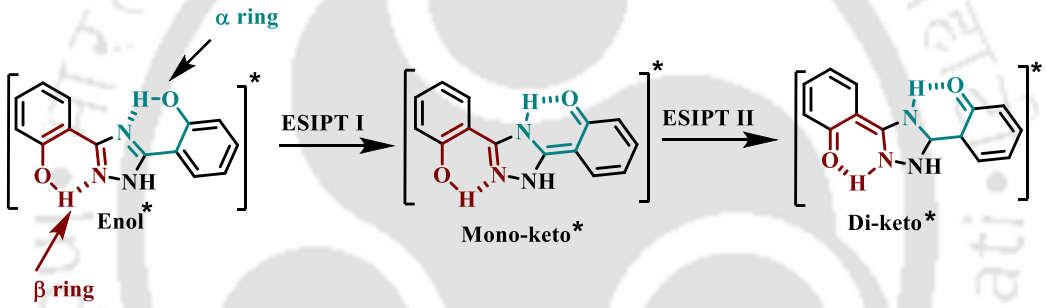

Scheme II. PTTPT pathway in bis-HPTA.

A special kind of PT called Proton transfer triggered proton transfer (PTTPT) in 3,5-bis(2-hydroxyphenyl)-1H-1,2,4-triazole (bis-HPTA) was reported recently (**Scheme II**). This fluorophore has two proton donor-acceptor pairs. But the first proton transfer (ESIPT-I) is feasible only in one pair.

The other pair did not show proton transfer (ESIPT-II) initially due to annular tautomerism. ESIPT-II is only feasible after ESIPT-I because of the decrease in annular tautomerism. In other words, ESIPT-I triggers ESIPT-II. Therefore, this PT was named PTTPT.

Water is an important solvent for fluorescence study for understanding biological systems and application point of view. ESIPT properties of molecules are dictated by a change in pH. Therefore, PTTPT of bis-HPTA was studied in aqueous media. Cyclodextrins (CDs) have been used to study excited state processes such as proton transfer and charge transfer. *β*-CD is considered the best system for studying inclusion complexes. Its interior is hydrophobic and the external wall is hydrophilic. The hydrophobic nature of the cavity increases the

TH-2834_146122035

solubility and hence the fluorescence of organic guests. Therefore, PTTPT properties of bis-HPTA in water and *β*-CD were explored.

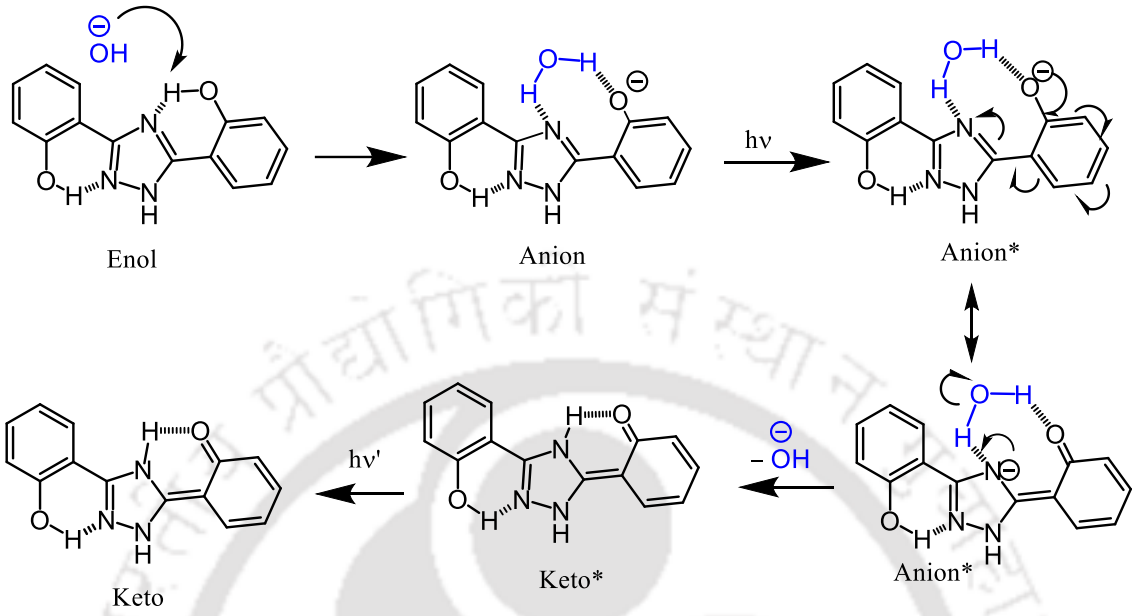

Scheme III. Tautomer formation via intermolecular proton transfer in the bis-HPTA anion.

PTTPT of bis-HPTA was more favoured in water compared to organic solvents. However, it was reduced inside *β*-CD. Photoexcitation induced intermolecular proton transfer in the anion of bis-HPTA in water. In the excited state, the anion rearranged to form the keto tautomer (**Scheme III**). Bis-HPTA was encapsulated inside *β*-CD in such a way that the triazole ring and most parts of the α-ring are entirely inside. The encapsulation prevents the intermolecular proton transfer in the anion. Hence, no tautomer emission was observed from bis-HPTA anion inside *β*-CD.

Chapter 5: Effect of micelles and reverse micelles on PTTPT of 3,5-bis(2-hydroxyphenyl)-1H-1,2,4-triazole

Micelles and reverse micelles are interesting micro-heterogeneous systems. As ESIPT is susceptible to surroundings, the confined environments such as micelles and reverse micelles significantly alter this photophysical process. Therefore, the effects of micelles and reverse micelles on the proton transfer of bis-HPTA were studied.

The keto band intensity increases upon increasing the micelle concentration. This increase indicates the encapsulation of the molecule inside the micellar interior. The less polar and restricted environment of the micellar interior decreases the nonradiative decay. Tautomer formation from anion via intermolecular proton transfer is not observed in micelles. In Aerosol-

TH-2834_146122035

OT (AOT)/*n*-heptane/water reverse micelles, on increasing the water amount, the tautomer emission decreases along with the increase in normal emission.

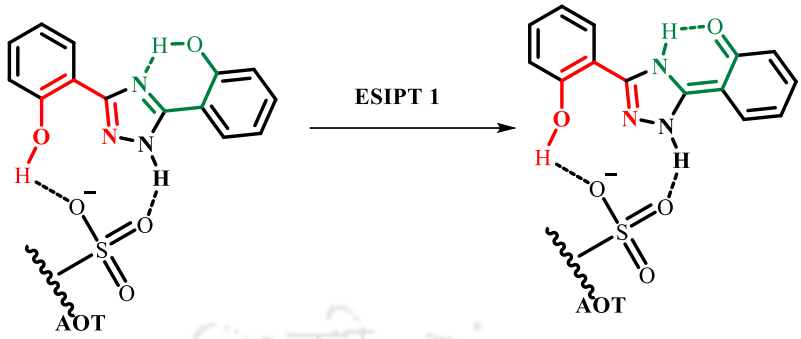

Scheme IV. ESIPT I in the bis-HPTA-AOT hydrogen-bonded complex.

The β-ring of bis-HPTA is opened to form an intermolecular hydrogen bond with the sulpho- group of AOT. The molecule then undergoes ESIPT I in the α-ring to form only monoketo (**Scheme IV**). Water breaks the α-ring to give solvated enol. The solvated enol emits only normal emission. On increasing the water quantity, the tautomer emission decreases and a little enhancement was found in the normal emission.

Chapter 6: The suppression of Intramolecular Charge Transfer by tautomerism in 2-(4′-amino-2′-hydroxyphenyl)-1H-imidazo[4,5-c]pyridine: Intramolecular Proton Transfer Versus Intermolecular Proton Transfer

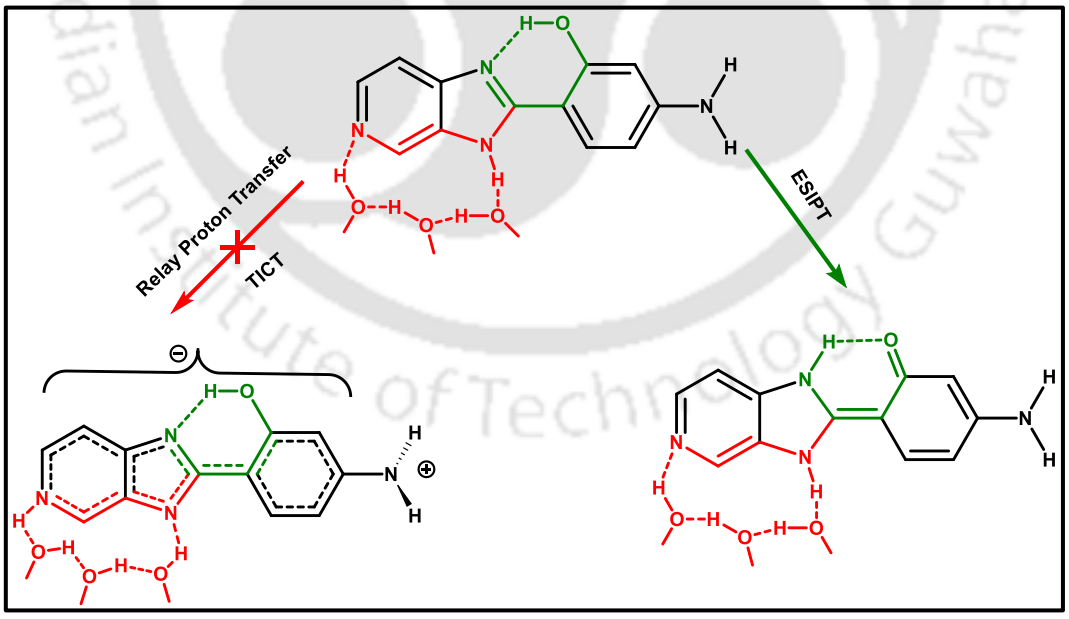

Scheme V. Suppression of twisted intramolecular charge transfer (TICT) by ESIPT in AHPIP-c.

TH-2834_146122035

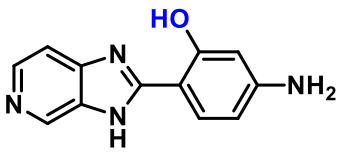

AHPIP-c

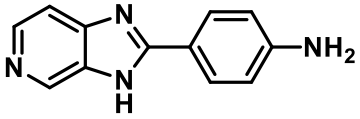

APIP-c

Chart II. Structures of AHPIP-c and APIP-c.

2-(4′-Aminophenyl)-1H-imidazo-[4,5-c]pyridine (APIP-c, **Chart II**) undergoes relay proton transfer in methanol that induced TICT emission (**Scheme V**). But its hydroxy derivative, 2-(4′-amino-2′-hydroxyphenyl)-1H-imidazo[4,5-c]pyridine (AHPIP-c, **Chart II**) emits only tautomer emission along with normal emission in methanol. The cause for the absence of TICT emission of AHPIP-c in methanol was unknown. Therefore, theoretical calculations were performed using a polar continuum model with methanol molecules to understand the mechanism.

The barrier heights for proton transfer of both the processes in ground states are more compared to excited states (**Figure II**). Due to lesser barrier height in excited states, these proton transfers would be favoured in excited states than in the ground states.

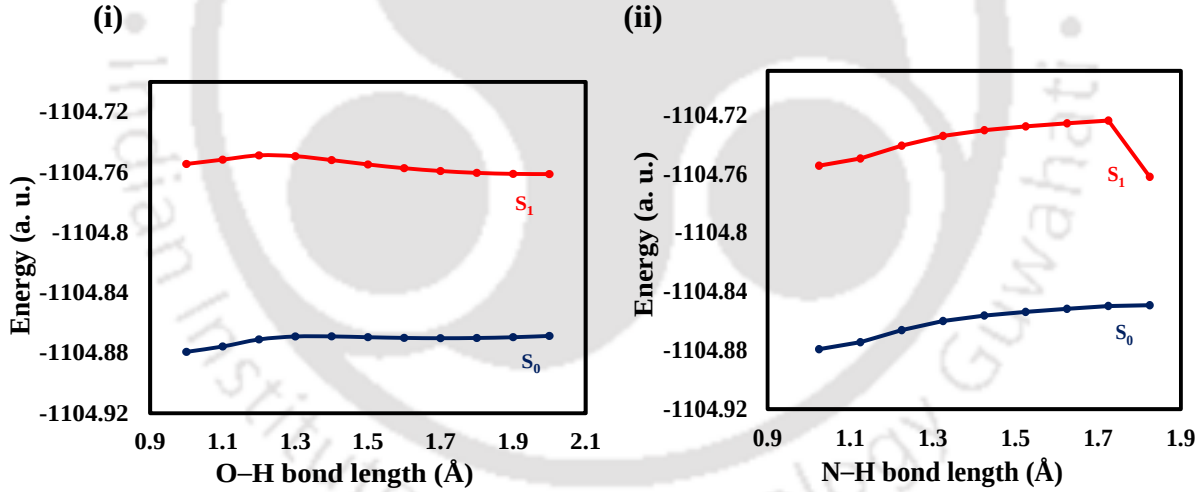

Figure II. The potential energy curve for the intramolecular (i) and intermolecular (ii) proton transfer.

The lesser barrier height for ESIPT shows that the ESIPT is favoured over solvent assisted proton transfer in the excited state (**Figure II**).

Chapter 7: Turning on intramolecular charge transfer emission in 2-(4′-amino-2′-hydroxyphenyl)-1H-imidazo-[4,5-c]pyridine by intermolecular proton transfer

AHPIP-c, (**Chart III**) emits only ESIPT emission. Its methoxy counterpart, 2-(4′-amino-2′-methoxyphenyl)-1*H*-imidazo[4,5-c]pyridine (AMPIP-c) (**Chart III**) cannot undergo ESIPT due to the absence of proton donor '-OH' group but gives ICT emission in methanol. In

TH-2834_146122035

AHPIP-c, the binding of proton to the pyridyl nitrogen might increase the charge flow from donor to acceptor moiety and hence, may induce the ICT emission.

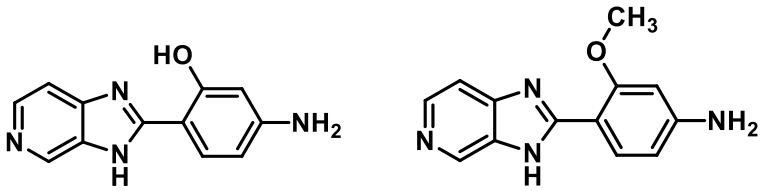

AHPIP-c **AMPIP-c**

Chart III. Structures of AHPIP-c and AMPIP-c.

AHPIP-c forms two kinds of monoanions. Both are formed by the deprotonation of charge donor groups. One of them emits the TICT emission. Both AHPIP-c and AMPIP-c forms three monocations namely MC1, MC2 and MC3 and dications, DC1, DC2 and DC3. MC3 and DC3 of both the molecules emit TICT fluorescence. MC3 of AHPIP-c also undergoes ESIPT in acetonitrile to emit tautomer emission.

Chapter 8: Summary and scope for future work

The last chapter of the thesis gives a summary of the present work and scope for future work.

TH-2834_146122035

TH-2834_146122035

Contents

		Page
Acknowledgement		ix
Synopsis		xi
List of Abbreviation		xxiii
List of Charts		xxv
List of Figures		xxvii
List of Schemes		xxxi
List of Tables		xxxii
References		xxxiii
Chapter 1: Introduction		
1.1.	Fluorescence	3
1.2.	Dual fluorescence	3
1.3.	Proton transfer	3
1.3.1.	Excited state intermolecular proton transfer	4
1.3.2.	Excited state intramolecular double proton transfer	6
1.3.2.1	Effect of molecular geometry on ESIPT	9
1.3.2.2.	Effect of substituents on ESIPT	10
1.3.2.3.	Effect of solvent on ESIPT	11
1.3.2.4.	Effect of pH on ESIPT	12
1.4.	Effect of heterogeneous media on PT	13
1.4.1	Effect of micelles on PT	14
1.4.2.	Effect of reverse micelles on PT	15
1.4.3.	Effect of supramolecular hosts on PT	16
1.5.	Intramolecular charge transfer	17
1.5.1	The role of hydrogen bonding in intramolecular charge transfer	19
1.6.	Coupled proton and charge transfer systems	19
1.7.	Aggregation induced enhanced emission	21
1.8.	Motivation for the present work	22
Chapter 2: Materials, Methods and Instrumentations		
2.0.	Introduction	27
2.1.	Materials	27
2.1.1.	Solvent	27
2.1.1.1.	For spectroscopic measurements	27
2.1.1.2.	For synthesis and purification	27
2.1.2.	Starting materials and reagents	28
2.1.3.	Other chemicals	28
2.2.	Synthetic procedures	28
2.2.1.	Synthesis of 2-(phenylamino)-5-(2-hydroxybenzono)-1,3,4-thiadiazole (PHBT) and 2-(phenylamino)-5-(2-methoxybenzono)-1,3,4-thiadiazole (PMBT)	28
2.2.2.	Synthesis of 3,5-bis(2'-hydroxyphenyl)-1H-1,2,4-triazole (bis-HPTA)	29
2.2.3.	Synthesis of 2-(4′-amino-2′-hydroxyphenyl)-1H-imidazo-[4,5-c]pyridine (AHPIP-c)	30
2.3.	Sample preparation	31
2.3.1.	Preparation of stock solutions	31
2.3.2.	Solvatochromic studies	31

TH-2834_146122035

2.3.3.	Prototropic studies	31
2.3.4.	Micellar and β-CD solutions	31
2.3.5.	Reverse micellar solutions	31
2.4.	Methods	32
2.4.1.	Quantum Yield and relative fluorescence quantum yield	32
2.4.2.	Quantum mechanical calculations	32
2.5.	Instruments	32
2.5.1.	pH meter	32
2.5.2.	UV-visible spectrophotometer	33
2.5.3.	Steady state fluorimeter	33
2.5.3.1.	Basic parts of a fluorimeter	33
2.5.4.	Time resolved fluorimeter	35
2.5.5.	Other instruments	37
Chapter 3: The Origin of Longer Wavelength Emission in 2-(4-Fluorophenylamino)-5-(2,4-dihydroxybenzeno)-1,3,4-thiadiazole and its Analogue 2-Phenylamino-5-(2-hydroxybenzono)-1,3,4-thiadiazole		
3.0.	Introduction	41
3.1.	Spectral characteristics of PHBT and PMBT	42
3.1.1.	The excited state proton transfer	42
3.2.	Ground state equilibrium	47
3.3.	Aggregation assisted ESIPT	51
3.4.	Conclusion	53
Chapter 4: Effect of pH and Host-Guest Complexation on PTTPT of 3,5-Bis(2-hydroxyphenyl)-1H-1,2,4-triazole		
4.0.	Introduction	57
4.1.	Electronic spectra of bis-HPTA in aqueous solution	58
4.1.1	Neutral bis-HPTA	58
4.1.2	Anionic bis-HPTA	60
4.2	Effect of pH on electronic spectra of bis-HPTA in the presence of β-CD	67
4.3	Effect of β-CD on electronic spectra of bis-HPTA	62
4.4	Conclusion	68
Chapter 5: Effect of Micelles and Reverse Micelles on PTTPT of 3,5-Bis(2-hydroxyphenyl)-1H-1,2,4-triazole		
5.0.	Introduction	71
5.1.	Effect of micelle on neutral bis-HPTA	72
5.2.	Effect of micelle on the anion of bis-HPTA	74
5.3.	Effect on electronic spectra of bis-HPTA in the presence of AOT/*n*-heptane/water	76
5.4.	Conclusion	79
Chapter 6: The Suppression of Intramolecular Charge Transfer by Tautomerism in 2-(4′-Amino-2′-hydroxyphenyl)-1H-imidazo[4,5-c]pyridine: Intramolecular Proton Transfer versus Intermolecular Proton Transfer		
6.0	Introduction	83
6.1	Absorption maximum	84
6.2	Structure of the enol complex	84
6.3	Structure of Tautomer complexes	88
6.4	Potential energy curves of the proton transfers	90
6.5	Electronic transitions	92
6.6	Isosurface of hole and electron distribution and heat map	95

TH-2834_146122035

6.7	Conclusion	97
Chapter 7: Turning on Intramolecular Charge Transfer Emission in 2-(4′-Amino-2′-hydroxyphenyl)-1H-imidazo-[4,5-c]pyridine by Intermolecular Proton Transfer		
7.0	Introduction	101
7.1	Neutral-monoanion equilibria	102
7.2	Neutral-monocation equilibria	105
7.3	Monocation-dication equilibria	112
7.4	Trication of AHPIP-c and AMPIP-c	115
7.5	Conclusion	116
Chapter 8: Summary and Scope for Future Work		
8.1.	Summary of the present work	119
8.2.	Scope for the future work	121

TH-2834_146122035

TH-2834_146122035

List of Abbreviations

ADC	Analogue to digital converter
AHPIP-c	2-(4′-amino-2′-hydroxyphenyl)-1H-imidazo[4,5-c]pyridine
AIE	Aggregation induced emission
AOT	Aerosol OT
AIEE	Aggregation induced enhanced emission
AMPIP-c	2-(4′-amino-2′-methoxyphenyl)-1H-imidazo[4,5-c]pyridine
APIP-c	2-(4′-aminophenyl) imidazo[4,5-c]pyridine
Bis-HPTA	3,5-bis(2-hydroxyphenyl)-1H-1,2,4-triazole
BODIPY	Boradiazaindacene
CB	Cucurbit
CD	Cyclodextrin
CT	Charge transfer
CTAB	Cetyltrimethylammonium bromide
DFT	Density functional theory
DK	Diketo
DNA	Deoxyribonucleic acid
DMABN	4-Dimethylaminobenzonitrile
DMAPIP-b	2-(4′-N,N-dimethylaminophenyl) imidazo[4,5-b]pyridine
DMAPIP-c	2-(4′-N,N-dimethylaminophenyl) imidazo[4,5-c]pyridine
DMF	*N*,*N*-Dimethyl formamide
DMSO	*N*,*N*-Dimethyl sulfoxide
ESIPT	Excited state intramolecular proton transfer
ESDPT	Excited state double proton transfer
ESIDPT	Excited state intramolecular double proton transfer
ESPT	Excited state proton transfer
eV	electron volt
FABT	2-(4-Fluorophenylamino)-5-(2,4-dihydroxybenzeno)-1,3,4-thiadiazole
FC	Franck-Condon
GSPT	Ground state proton transfer
HPBI	2-(2′-Hydroxyphenyl) benzimdazole
HPBO	2-(2′-Hydroxyphenyl) benzoxazole
HPIP-b	2-(2′-Hydroxyphenyl)-3H-imidazo-[4, 5-b] pyridine
HPIP-c	2-(2'-Hydroxyphenyl)-3H-imidazo-[4,5-c] pyridine
HPLC	High-performance liquid chromatography
HRMS	High resolution mass spectrometry
ICT	Intramolecular Charge Transfer
IEFPCM	Integral equations formalism- polarizable continuum model
IRF	Instrument response function
K1	Monoketo
K2	Diketo
LASER	Light Amplification by Stimulated Emission of Radiation
LE	Locally Excited
LED	Light emitting diode
NMR	Nuclear Magnetic Resonance
PHBT	2-Phenylamino-5-(2-hydroxybenzono)-1,3,4-thiadiazole
PMBT	2-Phenylamino-5-(2-methoxybenzono)-1,3,4-thiadiazole
PMT	Photomultiplier tube
PT	Proton Transfer
PTTPT	Proton Transfer Triggered Proton Transfer
SDS	Sodium Dodecyl sulfate
TAC	Time to amplitude converter
TCSPC	Time-correlated Single Photon Counting

TH-2834_146122035

TDDFT	Time-dependent density functional theory
THF	Tetrahydrofuran
TICT	Twisted Intramolecular Charge Transfer
TX-100	Triton-X 100
UV	Ultra violet
˚C	˚Centigrade
$\in$	Extinction coefficient
λ_{max}^{ab}	Absorption maximum
λ_{max}^{ex}	Excitation maximum
λ_{max}^{em}	Emission maximum
λ_{ex}	Excitation wavelength
λ_{em}	Emission wavelength
Φ_f	Quantum yield of fluorescence
τ	Fluorescence lifetime
$\tilde{\nu}_{ss}$	Stokes' shift

TH-2834_146122035

List of Charts

Chapter 1	
Chart 1.1	I) Phenol-quinoline and (II) intramolecular H-bond in a conjugated ring, where d_{DA} is the proton donor-acceptor distance and θ is the dihedral angle.
Chart 1.2	Chemical structure of 2-(2′-aminophenyl)benzothiazole (APBT) and effect on proton transfer upon various substitutions.
Chart 1.3	Substituted HPBI derivatives studied by Douhal et. al.
Chart 1.4	Three enol conformers and keto tautomer of HPBI.
Chart 1.5	4,5-dimethyl-2-(2'-hydroxyphenyl)imidazole (I) and 2-(2'-hydroxyphenyl)-5-phenyloxazole (II).
Chart 1.6	Structure of 3-Hydroxyflavone.
Chart 1.7	Structure of sodium bis(2-ethylhexyl) sulfosuccinate or Aerosol-OT (AOT).
Chart 1.8	Structure of 1,7-bis(4-hydroxy-3-methoxyphenyl)-1,6-hepatadiene-3,5-dione or Curcumin.
Chart 1.9	Structure of *β*-cyclodextrin.
Chart 1.10	Structure of 1-hydroxy-2-napthaldehyde.
Chart 1.11	Structure of 4-dimethylaminobenzonitrile (DMABN).
Chart 1.12	The chemical structure of 7-aminocoumarin.
Chart 1.13	6-Dodecanoyl-2-dimethylaminonaphtalene (laurdan).
Chart 1.14	Structures of aminosalicylates.
Chart 1.15	HPBO derivatives studied by Park et al.
Chart 1.16	HPBT derivative.
Chart 1.17	Structures of N,N′-di[3-hydroxy-4-(2′-benzothiazole)phenyl]isophthalic amide (I) and N,N′-di[3-Hydroxy-4-(2′-benzothiazole)phenyl]5-tert-butyl-isophthalic amide (II).
Chart 1.18	Boradiazaindacene (BODIPY) derivative.
Chapter 3	
Chart 3.1	Structures of FABT, PHBT and PMBT.
Chart 3.2	Different conformers and tautomers of PHBT and FABT.
Chart 3.3	*cis*-enol and solvated enol conformers of PHBT.
Chapter 4	
Chapter 5	
Chapter 6	
Chart 6.1	Structures of 2-(4′-amino-2′-phenyl)-1H-imidazo[4,5-c]pyridine (APIP-c), 2-(2′-hydroxyphenyl)-1H-imidazo[4,5-c]pyridine (HPIP-c), 2-(4′-amino-2′-hydroxyphenyl)-1H-imidazo[4,5-c]pyridine (AHPIP-c) and 2-(4′-dimethylamino-2′-phenyl)-1H-imidazo[4,5-c]pyridine (DMAPIP-c).
Chart 6.2	Structures of (a) enol and (b) keto forms of AHPIP-c.
Chapter 7	
Chart 7.1	Structures of AHPIP-c (I) and AMPIP-c (II).
Chart 7.2	Different possible monoanions of AHPIP-c.
Chart 7.3	Different possible monocations of AHPIP-c.
Chart 7.4	Different possible dications of AHPIP-c.
Chart 7.5	Conformers of MC3.
Chart 7.6	Trication of AHPIP-c.

TH-2834_146122035

List of Figures

Chapter 2	
Figure 2.1	Block diagram of a double beam- UV-visible spectrophotometer.
Figure 2.2	Block diagram of steady state fluorescence spectrophotometer.
Figure 2.3	Block diagram of a TCSPC instrument.
Chapter 3	
Figure 3.1	Normalized absorption spectra of (a) PHBT and (b) PMBT in toluene (1), ethyl acetate (2), acetonitrile (3) and methanol (4).
Figure 3.2	Normalized emission spectra of PHBT in toluene (1), dioxane (2), ethyl acetate (3), acetonitrile (4) and methanol (5), λ_{ex} = 340 nm.
Figure 3.3	Normalized emission spectra of PMBT in toluene (1), dioxane (2), ethyl acetate (3), acetonitrile (5) and methanol (5), λ_{ex} = 330 nm.
Figure 3.4	Fluorescence decay of PHBT monitored at (b) λ_{em} = 395 nm and (c) λ_{em} = 520 nm in 1,4-dioxane, λ_{ex} = 336 nm, (a) Instrument response function.
Figure 3.5	The excitation spectra of PHBT in dioxane at λ_{em} = 400 nm (1) and 520 nm (2) along with its absorption spectrum (dashed line).
Figure 3.6	Ground state optimized geometry of PHBT *cis*-enol (a) and trans-enol (b).
Figure 3.7	Ground state optimized geometry of FABT *cis*-enol (a) and trans-enol (b).
Figure 3.8	Normalized absorption spectra of PHBT in the water of pH value 7.2 (dashed line) and 13.0 (solid line).
Figure 3.9	Normalized emission spectra of PHBT at pH values 7.2 (dashed line) and 13.0 (solid line) in water (λ_{ex} = 340 nm), * water Raman.
Chapter 4	
Figure 4.1	Normalized absorption spectra of bis-HPTA in the water of pH 4.0 to 12.0.
Figure 4.2	(a) Normalized emission spectra of bis-HPTA in water of pH 4.0 to 12.0, λ_{ex} = 300 nm. (b) Normalized excitation spectra of bis-HPTA in water of pH 4.0 to 12.0, λ_{em} = 420 nm.
Figure 4.3	(a) Normalized emission spectra of neutral bis-HPTA in water, λ_{ex} = 270 nm (1), 280 nm (2), 290 nm (3), 300 nm (4), 310 nm (5), 320 nm (6), 330 nm (7). (b) Normalized excitation spectra of neutral AHPIP-c in water, λ_{em} = 360 nm (1), 380 nm (2), 400 nm (3), 420 nm (4), 440 nm (5), 460 nm (6).
Figure 4.4	(b) Fluorescence decay of bis-HPTA in water (pH 4.0), λ_{ex} = 308 nm and (a) instrument response function.
Figure 4.5	(a). Normalized emission spectra of anionic bis-HPTA in water, λ_{ex} = 270 nm (1), 280 nm (2), 290 nm (3), 300 nm (4), 310 nm (5), 320 nm (6), 330 nm (7). (b). Normalized excitation spectra of anionic bis-HPTA in water, λ_{em} = 380 nm (1), 400 nm (2), 420 nm (3), 440 nm (4), 460 nm (5), 480 nm (6), 500 nm (7).
Figure 4.6.	(b) Fluorescence decay of bis-HPTA in water (pH 12.0), λ_{ex} = 336 nm and (a) instrument response function.
Figure 4.7	Normalized absorption spectra of bis-HPTA in β-CD (12.0 mM) of pH 1.0 to 12.0.
Figure 4.8	Emission spectra of bis-HPTA in β-CD (12.0 mM) of pH 1.0 to 12.0.
Figure 4.9	(b) fluorescence decay of bis-HPTA in β-CD (12.0 mM) at pH 4.0. (a) Instrument response function
Figure 4.10	Absorption spectra of bis-HPTA in different concentrations of β-CD in aqueous solution (at pH 4.0).
Figure 4.11	Emission spectra of bis-HPTA in different concentrations of β-CD in aqueous solution (at pH 4.0), λ_{ex} = 290 nm.
Figure 4.12	Benesi-Hildebrand plot showing 1:1 binding of bis-HPTA and β-CD.
Figure 4.13	Optimized geometries of bis-HPTA and β-CD complexes.

TH-2834_146122035

Chapter 5	
Figure 5.1	Emission spectra of neutral bis-HPTA in different concentrations of CTAB in water, λ_{ex} = 300 nm.
Figure 5.2	Emission spectra of neutral bis-HPTA in water (1), CTAB (2), SDS (3) and TX-100 (4), λ_{ex} = 300 nm, *water Raman.
Figure 5.3	Fluorescence decay of neutral bis-HPTA in (b) water and (c) CTAB. (a) IRF.
Figure 5.4	Absorption spectra of bis-HPTA in SDS at different pH.
Figure 5.5	(a) Absorption and (b) emission spectra of anionic bis-HPTA in water (1), CTAB (2), SDS (3) and TX-100 (4), λ_{ex} = 300 nm.
Figure 5.6	Absorption spectra of bis-HPTA in AOT/n-heptane/water with changing w_o values.
Figure 5.7	Emission spectra of bis-HPTA in AOT/*n*-heptane/ water with changing w_o values, λ_{ex} = 300 nm.
Chapter 6	
Figure 6.1	The optimized structures of AHPIP-c.$(CH_3OH)_3$ complex in the ground and first excited states.
Figure 6.2	Simulated infrared spectra of AHPIP-c.$(CH_3OH)_3$ complex in the ground (solid line) and excited states (dashed line). Inset represents the normalized spectra depicting O17-H28 (1, 1'), O19-H18 (2, 2'), N7-H27 (3, 3'), O22-H21 (4, 4') and O25-H24 (5, 5') stretching frequencies.
Figure 6.3	The excited state optimized structure of the tautomers, (I) keto, pyridinyl (IIA) normal tautomer and (IIB) amino twisted tautomer.
Figure 6.4	. Simulated infrared spectra of keto (solid line) and pyridinyl tautomer (dotted) AHPIP-c.$(CH_3OH)_3$ complex in the excited states.
Figure 6.5	The potential energy curve for the intramolecular proton transfer in methanol.
Figure 6.6	The potential energy curve for the intermolecular proton transfer from imidazole N7─H27 to the methanol molecule.
Figure 6.7	Natural transition orbitals (NTOs) generated for the first excited states of enol, keto (I), pyridinyl tautomer (IIA) and amino twisted pyridinyl tautomer (IIB).
Figure 6.8	TDDFT simulated emission spectra of enol (1) and keto (2) tautomers of AHPIP-c in methanol (dashed line is the experimental spectrum).
Figure 6.9	Heat map and isosurface of hole, electron and overlap distribution of first excited state of different forms of AHPIP-c.$(CH_3OH)_3$.
Chapter 7	
Figure 7.1	(a). Absorption spectra of neutral-monoanionic equilibria of AHPIP-c in water. (b). Emission spectra of neutral-monoanionic equilibria of AHPIP-c in water, λ_{ex} = 300 nm.
Figure 7.2	(a). Normalized emission spectra of MAs of AHPIP-c in water, λ_{ex} = 320 nm (1), 335 nm (2), 350 nm (3), *water Raman. (b). Normalized excitation spectra of MAs of AHPIP-c in water, λ_{em} = 430 nm (1) and 510 nm (2).
Figure 7.3	(a). Absorption spectra of neutral-monoanionic equilibria of AMPIP-c in water. (b). Emission spectra of neutral-monoanionic equilibria of AMPIP-c in water, λ_{ex} = 300 nm, *water Raman.
Figure 7.4	Absorption spectra of neutral-monocation equilibrium of (a) AHPIP-c and (b) AMPIP-c in water.
Figure 7.5	Emission spectra of neutral-monocation equilibria of AHPIP-c in water, λ_{ex} = 335 nm.
Figure 7.6	(a). Normalized emission spectra of MCs of AHPIP-c in water, λ_{ex} = 320 nm (1), 335 nm (2), 350 nm (3), 370 nm (4). (b). Normalized excitation spectra of MCs of AHPIP-c in water, λ_{em} = 395 nm (1), 410 nm (2), 430 nm (3), 450 nm (4), 490 nm (5), 510 nm (6).

TH-2834_146122035

Figure 7.7	(a). Normalized emission spectra of MCs of AMPIP-c in water, λ_{ex} = 290 nm (1), 325 nm (2), 350 nm (3), 370 nm (4). (b). Normalized excitation spectra of MCs of AHPIP-c in acetonitrile, λ_{em} = 390 nm (1), 430 nm (2), 460 nm (3), 480 nm (4), 510 nm (5).
Figure 7.8	Absorption spectra of neutral-monocation equilibrium in (a) methanol and (b) acetonitrile.
Figure 7.9	Fluorescence spectra of neutral-monocation equilibrium in (a) methanol and (b) acetonitrile, λ_{ex} = 340 nm. *water Raman.
Figure 7.10	(a). Normalized emission spectra of MCs of AHPIP-c in methanol, λ_{ex} = 320 nm (1), 340 nm (2), 360 nm (3), 390 nm (4). (b). Normalized excitation spectra of MCs of AHPIP-c in methanol, λ_{em} = 360 nm (1), 410 nm (2), 440 nm (3), 470 nm (4), 500 nm (5).
Figure 7.11	(a). Normalized emission spectra of MCs of AHPIP-c in acetonitrile, λ_{ex} = 320 nm (1), 340 nm (2), 360 nm (3), 390 nm (4). (b). Normalized excitation spectra of MCs of AHPIP-c in acetonitrile, λ_{em} = 360 nm (1), 380 nm (2) 410 nm (3), 440 nm (4), 470 nm (5), 500 nm (6).
Figure 7.12	(a). Normalized emission spectra of MCs of AMPIP-c in acetonitrile, λ_{ex} = 290 nm (1), 320 nm (2), 330 nm (3), 340 nm (4), 350 nm (5), 370 nm (6). (b). Normalized excitation spectra of MCs of AMPIP-c in acetonitrile, λ_{em} = 400 nm (1), 420 nm (2) 440 nm (3), 460 nm (4), 480 nm (5), 500 nm (6).
Figure 7.13	Absorption spectra of monocation-dication equilibria of AHPIP-c (a) and AMPIP-c (b) in water.
Figure 7.14	Emission spectra of monocation-dication equilibria of AHPIP-c in water, λ_{ex} = 320 nm (a) and λ_{ex} = 350 nm (b), *water Raman.
Figure 7.15	Normalized emission spectra of DCs of AHPIP-c in water, λ_{ex} = 300 nm (1), 320 nm (2), 335 nm (3), 350 nm (4), 370 nm (5). (b) Normalized excitation spectra of DCs of AHPIP-c in water, λ_{em} = 395 nm (1), 410 nm (2), 430 nm (3), 450 nm (4), 490 nm (5), 510 nm (6).
Figure 7.16	(a). Normalized emission spectra of DCs of AMPIP-c in water, λ_{ex} = 292 nm (1), 325 nm (2), 350 nm (3), 420 nm (4). (b). Normalized excitation spectra of DCs of AMPIP-c in water, λ_{em} = 390 nm (1), 430 nm (2), 460 nm (3), 480 nm (4), 510 nm (5).
Figure 7.17	Absorption spectra of monocation-dication equilibria of AHPIP-c in (a) methanol and (b) acetonitrile.
Figure 7.18	Normalized (1) excitation (λ_{em} = 430 nm) and (2) emission (λ_{ex} = 350 nm) spectra TC of (a) AHPIP-c and (b) AMPIP-c in water.

TH-2834_146122035

List of Schemes

Chapter 1	
Scheme 1.1	Perrin-Jablonski diagram.
Scheme 1.2	A simple schematic diagram of (I) Intramolecular and (II) Intermolecular proton transfer.
Scheme 1.3	Excited state intermolecular proton transfer of 7-azaindole dimer in 3-methylpentane.
Scheme 1.4	ESDPT mechanism of 7-azaindole cyclically H-bonded to an alcohol molecule.
Scheme 1.5	A schematic diagram of ESIPT.
Scheme 1.6	Intrinsic proton relay in 7-hydroxyquinoline-8-carboxylic acid.
Scheme 1.7	ESIDPT in 2,2′-bipyridyl-3,3′-diol via the sequential and concerted mechanism.
Scheme 1.8	Effect of pH on benzothiazole based Schiff's base.
Scheme 1.9	Spirobenzopyran based ratiometric pH responsive probe.
Scheme 1.10	Dual emission from a TICT fluorophore.
Scheme 1.11	Excited state coupled intramolecular proton and charge Transfer of 2-(4′-*N*,*N*-diethylamino-2′-hydroxyphenyl)benzimidazole derivatives (X = NH and NMe).
Scheme 1.12	Excited state intramolecular proton and charge transfer of 2-phenyl-1H-imidazo-[4,5-c]pyridine derivatives.
Chapter 2	
Scheme 2.1	Synthesis of PHBT (R=H) and PMBT (R=CH_3).
Scheme 2.2	Synthesis of the precursor of bis-HPTA.
Scheme 2.3	Synthesis of bis-HPTA.
Scheme 2.4	Synthesis of AHPIP-c.
Chapter 3	
Chapter 4	
Scheme 4.1	ESIPT pathway in bis-HPTA.
Scheme 4.2	Annular tautomerism in bis-HPTA.
Scheme 4.3	Tautomer formation via intermolecular proton transfer in bis-HPTA anion.
Chapter 5	
Scheme 5.1	ESIPT I in the bis-HPTA-AOT hydrogen-bonded complex.
Scheme 5.2	Formation of solvated open enol from *cis*-enol.
Chapter 7	
Scheme 7.1	Electronic spectral shifts upon binding of H^+ with donor (D) and acceptor (A) groups.
Scheme 7.2.	ESIPT and TICT in MC3 of AHPIP-c.
Scheme 7.3	Formation of different dications from monocations.
Chapter 8	
Scheme 8.1	Organization of the thesis

TH-2834_146122035

List of Tables

Chapter 3	
Table 3.1	Experimental absorption band maxima (λ_{abs}, nm), log εmax, fluorescence emission band maxima (λ_{em}, nm) and relative fluorescence yield (F) of PHBT in different solvents.
Table 3.2	Experimental absorption band maxima (λ_{abs}, nm)), log ε_{max}, fluorescence emission band maxima (λ_{em},nm)), quantum yield (Φ), Stokes' shift ($\tilde{\nu}_{ss}$, cm^{-1}) of PMBT in different solvents.
Table 3.3	Theoretically calculated emission wavelength maximum for enol and keto species of PHBT in few selected solvents.
Table 3.4	Fluorescence lifetime (τ, ns) of PHBT and PMBT, λ_{ex} = 336 nm.
Table 3.5	Ground state optimized energies of FABT and PHBT and excitation spectral maximum (λ_{ex}, nm).
Table 3.6	The O-H bond and the N···H hydrogen bond distance of the *cis*-enol in the ground and the excited states.
Table 3.7	The fluorescence maximum (λ_f^{max}, nm) and Stokes' shift ($\bar{\nu}_{SS}$, cm^{-1}) of the emissions.
Chapter 4	
Table 4.1	Absorption maximum (λ_{ab}^{max}, nm), excitation maximum (λ_{em}^{max}, nm), emission maximum (λ_{em}^{max}, nm) and fluorescence lifetime (τ, ns) of bis-HPTA in water.
Table 4.2	Absorption maximum (λ_{ab}^{max} (nm)), emission maximum (λ_{em}^{max} (nm)) and fluorescence lifetime (τ, ns) of bis-HPTA in 12.0 mM *β*-CD.
Table 4.3	Relative energy (kJ/mol), stabilization energy (kJ/mol) and relative population (%) of *β*-CD and bis-HPTA complexes.
Chapter 5	
Table 5.1	Absorption maximum (λ_{ab}^{max}, nm), emission maximum (λ_{em}^{max}, nm), fluorescence lifetime (τ, ns) of bis-HPTA in Water, CTAB, SDS and TX-100.
Table 5.2	Absorption maximum (λ_{ab}^{max}, nm), emission maximum (λ_{em}^{max}, nm), excitation maximum (λ_{ex}^{max}, nm) of anion of bis-HPTA in micelles.
Table 5.3	Absorption maximum (λ_{ab}^{max}, nm), emission maximum (λ_{em}^{max}, nm) and fluorescence lifetime (τ, ns) of bis-HPTA in AOT/*n*-heptane/water at different w_0 values.
Chapter 6	
Table 6.1	Calculated and experimental absorption spectral maximum (λ_{max}, nm).
Table 6.2	Calculated bond lengths (Å) and vibrational frequencies ($\bar{\upsilon}$, cm^{-1}) of O–H and N–H bonds of AHPIP-c.$(CH_3OH)_3$ complex in the ground and the excited states.
Table 6.3	O17–H28, N9–H28, N7—H27, O25—H27, N7—H18, O19—H18 bond lengths N7—H27—O25 and N7—H18—O19 bond angles for enol, keto, pyridinyl tautomer (normal and amino twisted) in the excited state (Refer figure 6.3 for structures).
Table 6.4	Major absorption transitions, wavelength maximum (λ_{max}, nm), oscillator strength (*f*) and corresponding contributing molecular orbitals of Enol form of AHPIP-c.$(CH_3OH)_3$.
Table 6.5	Theoretical (λ_{max}^{theo}, nm) and experimental emission maximum (λ_{max}^{exp}, nm) of enol and keto forms of AHPIP-c.
Table 6.6	The emission transition of different forms, emission maximum (λ_{max}), Oscillator strength (*f*) and corresponding contributing molecular orbitals of Different forms of AHPIP-c.$(CH_3OH)_3$.
Table 6.7.	Δr and t indices of first excited state of different forms of AHPIP-c.$(CH_3OH)_3$.
Chapter 7	

TH-2834_146122035

Table 7.1	Absorption wavelength maximum (λ_{ab}^{max}, nm), excitation wavelength (λ_{ex}^{max}, nm) and emission wavelength (λ_{em}^{max}, nm) of different species of AHPIP-c and AMPIP-c in water.
Table 7.2	Absorption maximum (λ_{ab}^{max}, nm), emission maximum (λ_{em}^{max}, nm) and excitation maximum (λ_{ex}^{max}, nm)of different species of AHPIP-c in methanol and acetonitrile.

TH-2834_146122035

TH-2834_146122035

Chapter 1

Introduction

TH-2834_146122035

TH-2834_146122035

1.1 Fluorescence

A fluorophore is a molecule that absorbs the energy of a particular wavelength and emits energy at a different but specific wavelength.[1] The intensity and wavelength of the emission energy depend on the molecular structure of the fluorophore and the surrounding chemical environment.[2]

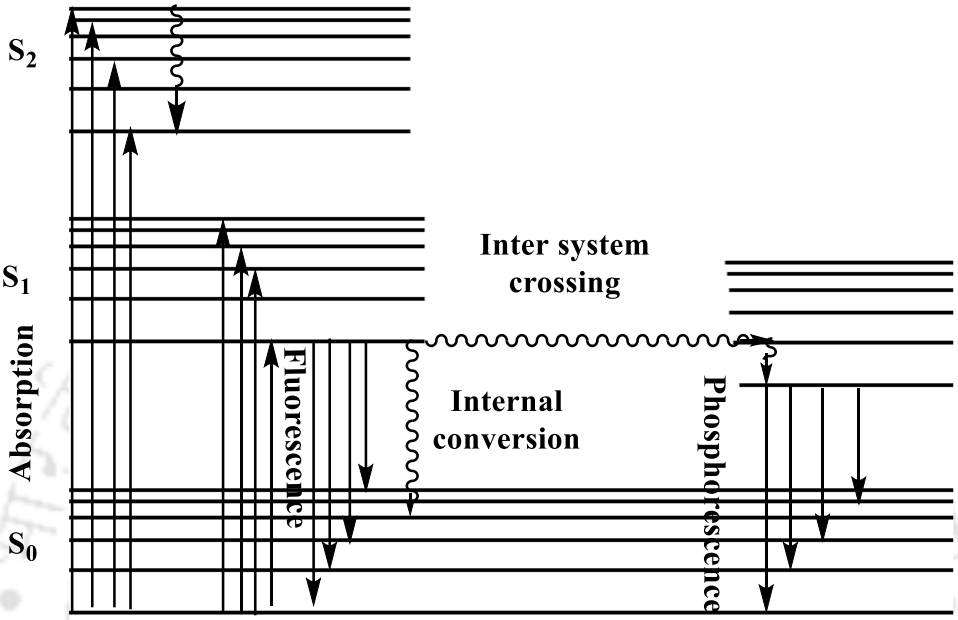

Scheme 1.1. Perrin-Jablonski diagram.

Luminescence is the common term used for radiative decays.[2] Fluorescence is the term given to radiative decays occurring from the singlet state after photo-excitation (**Scheme 1.1**). The lifetime of fluorescence is ~10^{-9} to 10^{-7} s. The fluorescence efficiency is measured in terms of fluorescence quantum yield. It is defined as the ratio of emitted photons to absorbed photons. The emitted photons are of lesser energy than the absorbed photons. This difference in wavelength is known as Stokes' shift. Fluorescence is a widely used technique in chemical and life sciences.[2,3]

1.2. Dual fluorescence

Many processes such as proton transfer,[4,5] charge transfer,[6,7] energy transfer[8,9] etc. are characterized by dual emission,[10] when another radiative species from a molecule is formed in its excited state.

1.3. Proton transfer

Proton transfer (PT) is a fundamental process in biology and chemistry.[4,5,11,12] Photo-induced proton transfer has been reported in respiration,[13] photosynthesis,[14] DNA base-

TH-2834_146122035

pairs,[15,16] ATP synthesis,[17] proton channels,[13] proton pumps,[18,19] and photoreceptors[20]. In addition, PT molecules find application in LASER dyes,[21–23] LEDs,[24–26] Solar cells,[27,26] sensors[28–31] etc. Therefore, the interest in proton transfer systems is not purely basic research. It also opens channels for the development of novel materials for numerous applications.

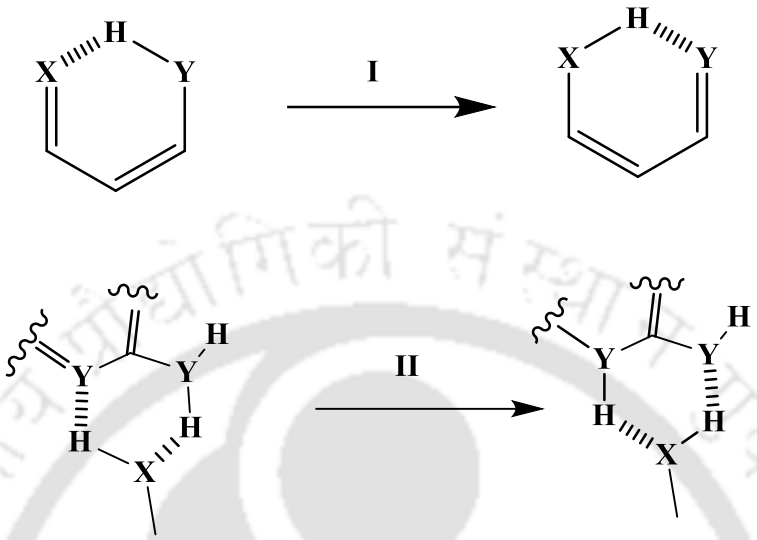

Scheme 1.2. A simple schematic diagram of (I) Intramolecular and (II) Intermolecular proton transfer.

As the name suggests, PT is the transfer of a proton from an acidic to a basic centre.[4] Hydrogen bond formation between a proton donor and acceptor is essential for proton transfer (**Scheme 1.2**).[32.33] If proton transfer occurs between two different molecules, it said to be intermolecular proton transfer.[33–37] If the acidic and basic moieties of the same molecule are involved, then called intramolecular proton transfer.[38–40] If PT occurs in the ground state, it is called the ground state proton transfer (GSPT).[41–43] If PT takes place upon light excitation, then it is known as the excited state proton transfer (ESPT).[35,44,45] There are different sub-types and mechanisms reported for proton transfers.[36,46,47] Some of these types of PT and effects of the various factors on them will be discussed in subsequent sections.

1.3.1. Excited state intermolecular proton transfer

Proton transfer occurring between donor and acceptor groups of two different molecules is called intermolecular proton transfer.[33,35–37] In such cases, proton transfer may occur between two molecules via dimer formation or through solvent assistance.[48–53]

1.3.1.1. Excited state intermolecular proton transfer without solvent assistance

Excited state intermolecular proton transfer between a hydrogen bonded donor-acceptor pair are useful for understanding the mutagenesis in DNA.[16,54–56] Proton transfer in

TH-2834_146122035

hydrogen bonded DNA base pairs and model systems have been studied extensively.[16,49,57–60] Many researchers have shed light on the mechanism of excited state double proton transfer (ESDPT) of 7-azaindole as a model system[57,61–65] It undergoes intermolecular proton transfer after dimer formation. The dimers of 7-azaindole and similar molecules are prototypical to the hydrogen bonded adenine–thymine base pair with two hydrogen bonds. It gives a violet emission in ether.[61] However, in 3-methyl pentane, it shows green emission.[61]

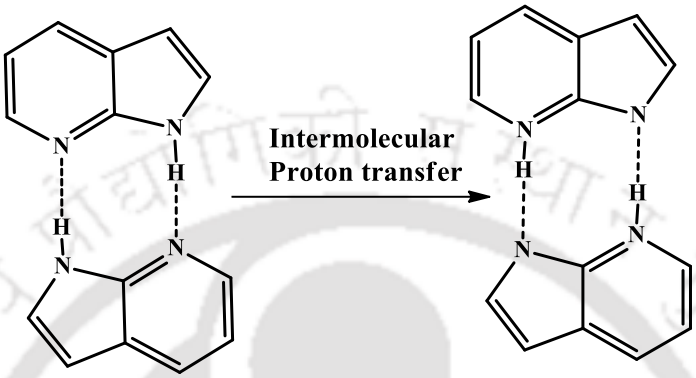

Scheme 1.3. Excited state intermolecular proton transfer of 7-azaindole dimer in 3-methylpentane.

The violet emission comes from the normal form. The green appears from the tautomer. In 3-methylpentane solution, the molecule exists in dimer form, whereas it exists in monomer form in ether. A low-lying tautomer is formed from the dimer via concerted double proton transfer in the excited state (**Scheme 1.3**). The mechanism of PT in 7-azaindole has been fiercely debated in the scientific community. Douhal et al. proposed that ESDPT of 7-azaindole follows the stepwise mechanism.[62] Folmer et al. confirmed this proposition by arresting the reaction intermediate.[66] Catalán et al. proposed the concerted mechanism.[16] Sekiya and Sakota concluded that the reaction occurs in a concerted manner in gas phase.[67] Crespo-Otero et al. established that stepwise mechanism is kinetically and thermodynamically unfavorable in 7-azaindole.[65] Similar PT is also observed in salicylic acid dimer.[5]

1.3.1.2. Excited state intermolecular proton transfer with solvent assistance

Biological systems often show solvent-mediated long-ranged proton relay transfer.[52,53,68] Proton is transported by a chain of water molecules by accepting and donating protons. It is also observed in many chemical systems with alcohol, water, formic acid, acetic acid or ammonia chain.[69–74] These kinds of proton transfers have attracted a lot of interest from theoretical chemists as well. They have used different parameters such as bond lengths and

TH-2834_146122035

angles, vibrational analysis, hydrogen bond strengths and potential energy surface diagrams in the ground and excited states to study relay proton transfer.[75–78]

Recently, imidazopyridines have been studied for solvent mediated proton transfer in methanol by many research groups[75,76,79,80] Relay proton transfer in quinolone–pyrazole has been reported in methanol solvent.[81] Similar solvent mediated proton transfer was also reported in 2-(1H-pyrazol-5-yl)pyridine in 1-propanol.[82]

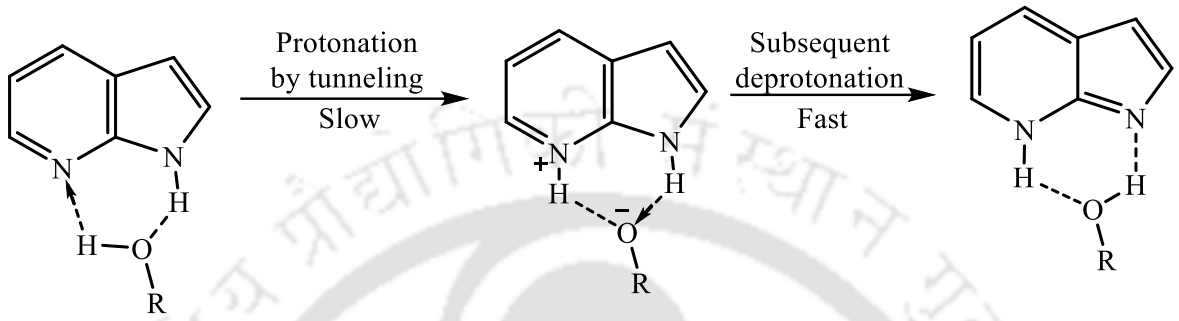

Scheme 1.4. ESDPT mechanism of 7-azaindole cyclically H-bonded to an alcohol molecule.[83]

The involvement of polar protic solvents such as alcohol and water in ESDPT of 7-azaindole is also well reported (**Scheme 1.4**).[69,83–87] Chou et al. reported that 7-azaindole undergo water catalyzed ESPT in neutral water.[83] Stairs et al. suggested that excited state proton transfer in the gas phase hydrated 7-azaindole monomer may be possible via a water proton bridge.[84] Full tautomerization may not be feasible, but the transfer of a proton from the 7-azaindole monomer to the solvating water is possible. They also studied the rate of proton transfer in 7-azaindole complexed with two, three and four water molecules. The rate increased in 7-azaindole monomer with four water molecules compared to two and three waters. 7-azaindole and water complexes formed in aprotic solvents are also reported to undergo ESDPT.[88]

1.3.2. Excited state intramolecular proton transfer

Excited state intramolecular proton transfer (ESIPT) takes place when an acidic (e.g. –OH, $–NH_2$ etc.) and basic groups (e.g. =O, =N etc.) are close enough to form an intramolecular hydrogen bond.[5,39,44,56,89–93] The basicity of the proton acceptor and the acidity of the proton donor groups of an aromatic molecule increases upon light excitation and this induces proton transfer. ESIPT is a superfast[36,94] light induced proton transfer facilitated by intramolecular hydrogen bonding. It is characterized by dual fluorescence, normal emission and a large Stokes' shifted emission (~6000-12000 cm^{-1}) (**Scheme 1.5**). ESIPT is attractive both for

TH-2834_146122035

mechanistic studies and practical applications. Steady state and time-resolved photoluminescence, transient electronic spectroscopy, femtosecond fluorescence up-conversion measurements and quantum-mechanical calculations are employed to elucidate the mechanism of ESIPT.[47,95,96,] It is very sensitive to medium and surroundings environment.[45,97–99]

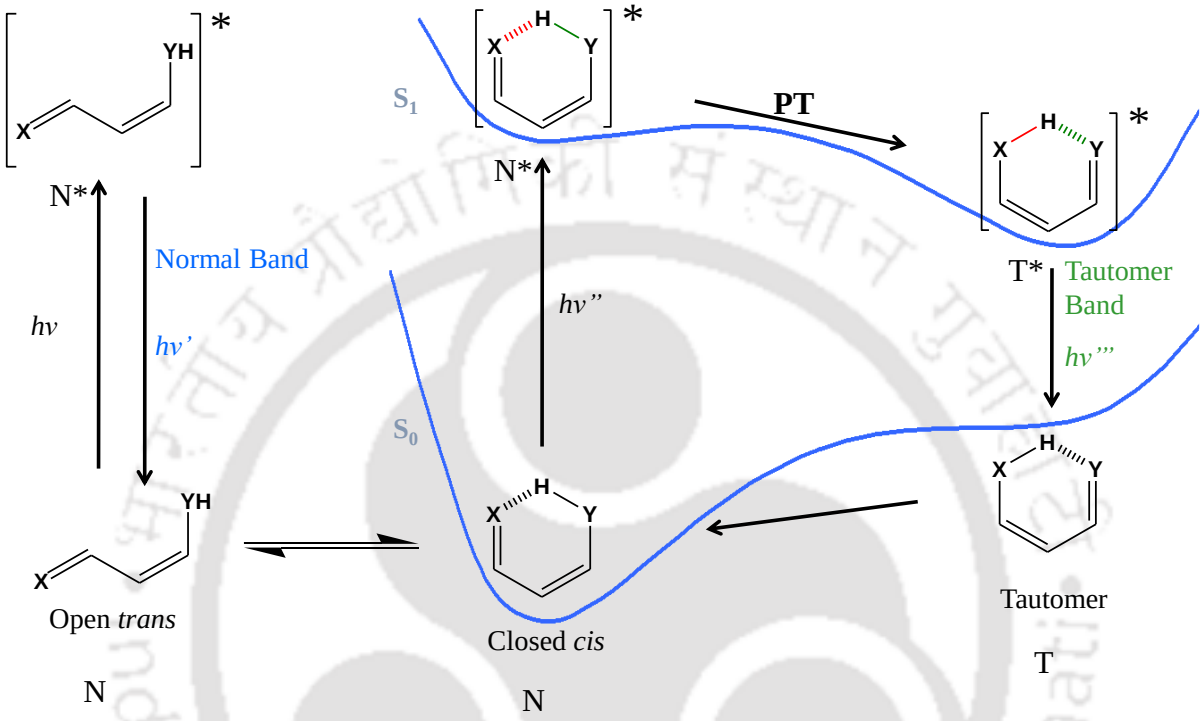

Scheme 1.5. A schematic diagram of ESIPT.

ESIPT exhibits four level cyclic photo-physical scheme (**Scheme 1.5**).[90] First step is light absorption by the normal form of the molecule for N→N* excitation. Then, proton transfer occurs in the excited state resulting in excited tautomer formation (N*→T*) followed by emission from the excited tautomer (T*→T). Finally, the back transfer of the proton takes the molecule back to its normal form (T→N). If the intramolecular hydrogen bond breaks, the molecule emits normal emission. As both the normal and tautomer forms emit light, ESIPT usually results in dual fluorescence. Various effects on ESIPT are generally analyzed by observing normal to tautomer intensity ratio. It depends on factors such as substituent, solvent polarity, pH, temperature, etc. Therefore, it finds many applications as fluorescent probes and luminescent materials.[39,42,77,100–102] Normal to tautomer intensity ratio can be anywhere between 0 to 1 depending upon molecular structures and surrounding environment. The effects of different factors on ESIPT are discussed later.

TH-2834_146122035

1.3.2.1 Excited state intramolecular double proton transfer

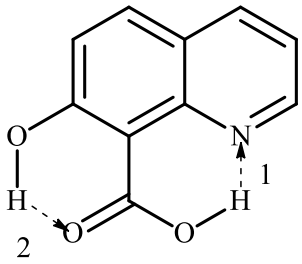

Scheme 1.6. Intrinsic proton relay in 7-hydroxyquinoline-8-carboxylic acid.

7-Hydroxyquinoline-8-carboxylic acid was shown to undergo excited-state intramolecular double proton transfer (ESIDPT) (**Scheme 1.6**).[48] The cooperative effect of ESIDPT in the molecule was shown by chemically blocking each proton donating site one by one. Theoretical results favored a concerted mechanism with a small barrier. This study indicates that 7-hydroxyquinoline-8-carboxylic acid is an intrinsic proton relay system. A similar relay type intramolecular double proton transfer has been also reported in 1,8-dihydroxy-2-naphthaldehyde.[103] ESIDPT of 2,2′-bipyridyl-3,3′-diol[104–107] and 2,2′-bipyridyl-3,3′-diamine[107,108] are reported using different techniques and in various media. One of the fundamental issues addressed in all the above examples is whether the proton transfer process of the two hydrogens proceeds in a concerted manner with a single transition state or through a stepwise pathway by forming an intermediate species (**Scheme 1.7**).

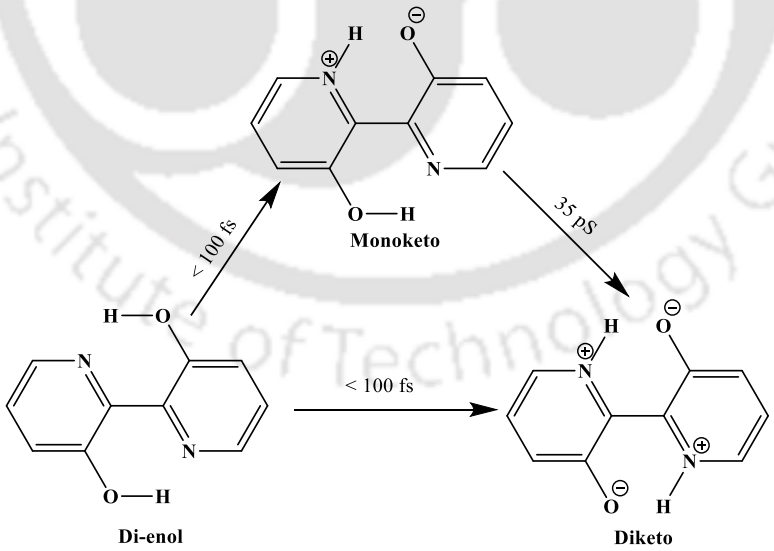

Scheme 1.7. ESIDPT in 2,2′-bipyridyl-3,3′-diol via the sequential and concerted mechanism.

Lischka et al. reported that the mechanism is sequential in 2,2′-bipyridyl-3,3′-diol.[104]A femtosecond fluorescence up-conversion study of 2,2′-bipyridyl-3,3′-diamine concluded that it

TH-2834_146122035

undergoes ESIDPT consisting of two trajectories: (a) ultrafast double proton transfer (<100 fs) followed by twisting (~250 fs); (b) combined double proton transfer and twisting (~250 fs).[91]

1.3.2.2. Effect of molecular geometry on ESIPT

Molecular planarity plays a crucial role in intramolecular proton transfer as the planar structure is ideal for forming intramolecular hydrogen bonds. The influence of hydrogen bond geometry on the dynamics of ESIPT and photoinduced tautomerization in a series of phenol-quinoline compounds was studied by Zietz et al. (**Chart 1.1)**.[109]

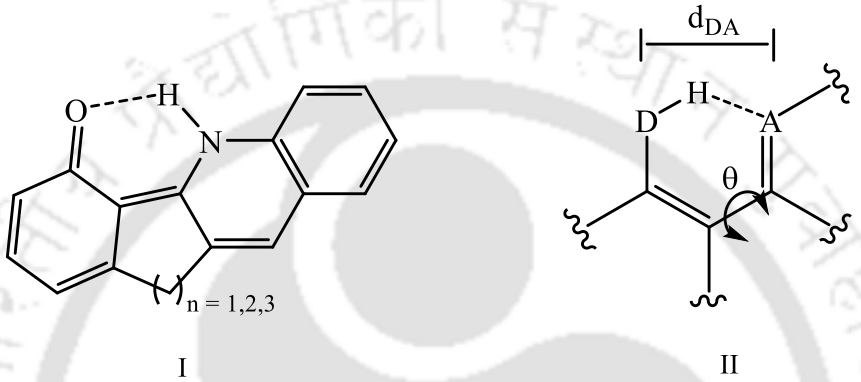

Chart 1.1. (I) Phenol-quinoline and (II) intramolecular H-bond in a conjugated ring, where d_{DA} is the proton donor-acceptor distance and θ is the dihedral angle.[76]

Different donor-acceptor distance (d_{DA}) and dihedral angle between the proton donor-acceptor subunits was achieved by adding methylene straps of increasing lengths to link the phenol and quinoline. They showed that a longer d_{DA} resulted in a higher barrier for ESIPT. At the same time, a large dihedral angle opened very efficient deactivation paths after ESIPT, thereby preventing the formation of the fully relaxed tautomer.

With increasing dihedral angle between the donor and acceptor groups, the ease of the proton transfer is reduced. The non-planarity of the cyclic hydrogen bond ring structure in the ground state can also lead to a higher non-radiative decay rate of an ESIPT species. This increase in non-radioactive decay decreases the fluorescence lifetime of the ESIPT state. 1-methyl-2-(2'-hydroxyphenyl)benzimidazole has a non-planar *cis*-enol structure in the ground state.[110] The excited state lifetime of its keto tautomer is very low (one-tenth) in comparison to the keto tautomer of a similar 2-(2'-hydroxyphenyl)benzimidazole (HPBI) molecule. It was reported that the excited keto tautomer of HPBI and related molecules undergo a non-radiative decay induced by torsional rotation.[111] In 1-methyl-2-(2'-hydroxyphenyl)benzimidazole, this non-radiative path is much faster because the molecule is non-planar.

TH-2834_146122035

1.3.2.3. Effect of substituents on ESIPT

In aromatic molecules, the electron donating substituents on the donor moiety and electron withdrawing groups on the acceptor site promote ESIPT.[112] In simple words, ESIPT is enhanced when both/either of the acid and base groups become stronger acids or bases in the excited state. As we know that there are two sides of ESIPT molecules, i.e., proton donor (acidic) and proton acceptor (basic). Substituents that increase acidity of the donor or increase the basicity of the acceptor favor ESIPT.

Chou et al. have studied the substituent effect on 2-(2′-aminophenyl)benzothiazole (APBT) by synthesizing a series of compounds with electron withdrawing (EWG) (-$COCH_3$, -tosyl) and donating substituents (EDG) (-CH_3) on the donor group (**Chart 1.2**).[93] APBT does not undergo ESIPT. When the –NH_2 group has methyl substitution, ESIPT is still not feasible. But slow proton transfer takes place upon acyl substitution on –NH_2. However, ultrafast proton transfer is observed upon tosyl substitution. Carbon para to the amino group was also substituted with donating (-NH_2) and withdrawing groups (–CN). The electron withdrawing cyano- group increases the rate of ESIPT.

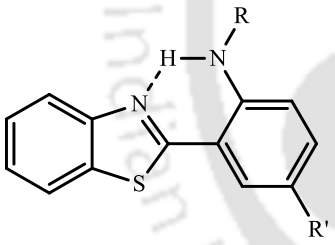

R	R’	Proton transfer
CH_3	H	No
H	H	No
CH_3	CN	Slow
H	CN	Slow
$COCH_3$	H	Slow
Tosyl	NH_2	Ultrafast
Tosyl	H	Ultrafast
Tosyl	CN	Ultrafast

Chart 1.2. Chemical structure of 2-(2′-aminophenyl)benzothiazole (APBT) and effect on proton transfer upon various substitutions.[93]

Douhal et al. showed that substitution of electron donating groups at 5-position (para to -OH) produces a red shift in the absorption and the fluorescence spectra by inducing resonance effect in HPBI (**Chart 1.3**).[113]

TH-2834_146122035

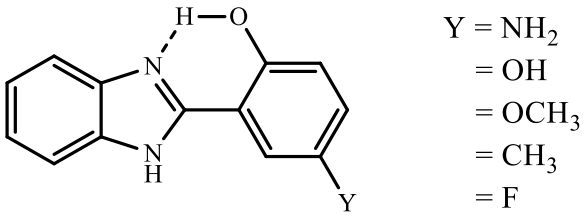

Chart 1.3. Substituted HPBI derivatives studied by Douhal et. al.[113]

They have also reported the photophysics of two 2-(2'-hydroxyphenyl)benzoxazole (HPBO) derivatives, where the benzene ring of benzoxazole was substituted by $–NH_2$ group at different positions in the acceptor ring.[114] In this study, they showed that the presence and position of the amino group in substituted HPBO can change both the ground and excited state behaviors of the intramolecular proton transfer. Contrary to HPBO, these amino derivatives do not show any proton transfer process. Only the emissions of the open enol (**Scheme 1.5**) were observed just like the methylated derivatives of the studied molecules. Hence, amino being EDG at the acceptor side hampers ESIPT in these substituted HPBO derivatives.

1.3.2.4. Effect of solvent on ESIPT

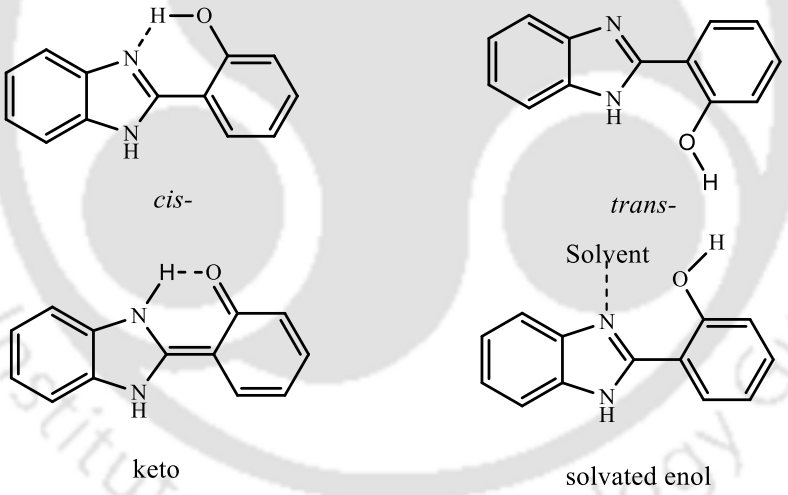

Chart 1.4. Three enol conformers and keto tautomer of HPBI.[115]

The dielectric environment around the molecule produces a substantial impact on the proton transfer process. ESIPT is affected by solute-solvent interactions. Therefore, solvent dependent intensity variations are key characteristics of ESIPT dyes. The effects of solvent on ESIPT have been studied in a variety of solvents both experimentally and theoretically[77,89,116–120] Usually, the solvent effect is governed by two factors, i.e. polarity and hydrogen bonding ability.[121] The normal to tautomer ratio is highly dependent on solvent polarity in ESIPT molecules.[77,83] The effect of solvent on the relative intensities of normal and tautomer emission

TH-2834_146122035

of ESIPT molecule depends on *cis*-*trans* equilibrium.[111,115] The *cis*-conformer of a molecule possesses intramolecular hydrogen bond between the donor and the acceptor (**Chart 1.4**).[122] The cyclic intramolecular hydrogen bonded ring is the precondition for ESIPT. Another conformer called *trans*-conformer also exists where donor and acceptor groups are trans with respect to each other. It is the *cis*-conformer which gives phototautomer upon light excitation. Non-polar solvents aid in ESIPT process and tautomer formation. This is due to two reasons. First, they do not hamper intra-molecular hydrogen bonding (hence, *cis*- conformer predominates) and second, tautomer being less polar than the normal form is more stable in non-polar solvents.

Intermolecular hydrogen bonding with polar protic solvents such as alcohols break the intra-molecular hydrogen bond and hence, inhibit ESIPT. It favours the normal emission.[77,99] Polar solvents cause a bathochromic shift in the normal band and hypsochromic shift in the tautomer band. Tautomer to normal band ratio is inversely proportional to the solvent polarity.

4,5-dimethyl-2-(2'-hydroxyphenyl)imidazole (**I, Chart 1.5**) exhibits only blue-green tautomer emission in dried non-polar solvents.[123] However, the intensity of the normal emission is enhanced in polar protic solvents.

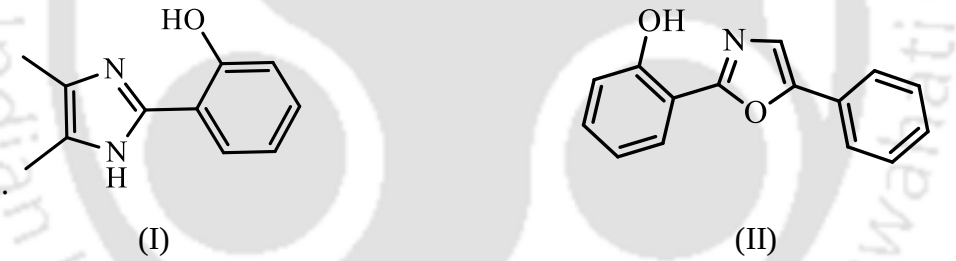

(I) (II)

Chart 1.5. 4,5-Dimethyl-2-(2'-hydroxyphenyl)imidazole (I) and 2-(2'-hydroxyphenyl)-5-phenyloxazole (II).

This is due to shifting of equilibrium from *cis*- to *trans*- conformer of the molecule upon increasing the polarity and hydrogen bonding capacity of solvents. In 2-(2'-hydroxyphenyl)-5-phenyloxazole (**II, Chart 1.5**), the tautomer emission is 210 times higher than that of the normal emission in octane.[124] Solvent polarity also dictates the wavelength shift of these two bands, polarity causing red shift in the normal band and blue shift in the tautomer band.[100,115,125]

1.3.2.5. Effect of pH on ESIPT

Molecule is more sensitive towards the pH in the excited state than ground state.[2] The pKa of the molecule in the excited state is different than ground state pKa. Therefore, excited state processes like ESIPT are pH dependent. The donor and acceptor sites of ESIPT molecules

TH-2834_146122035

can get altered by changing pH. Lower pH can lead to protonation of the basic site while higher pH can lead to deprotonation of the acidic site. If protonation happens at the photo-basic site or deprotonation at the photo-acidic site then, ESIPT is hampered. Therefore, these molecules have been utilized as pH responsive probes. [126,127]

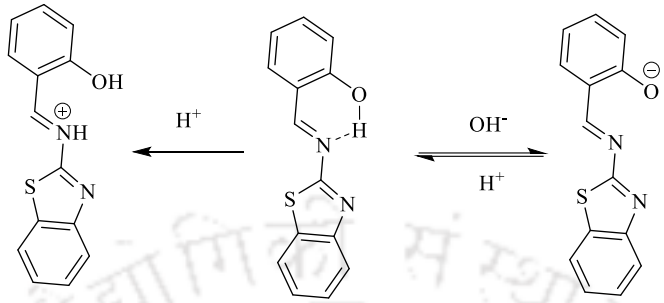

Scheme 1.8. Effect of pH on benzothiazole based Schiff's base.

A benzothiazole-based Schiff-base (**Scheme 1.8**) was used for pH sensing and tested for intracellular imaging.[126] The molecule shows violet fluorescence in pH range 1.0-5.0, yellow in 6.0-8.0 and green in 9.0-14.0. The yellow fluorescence in the pH range 6.0-8.0 is due to the tautomer emission.

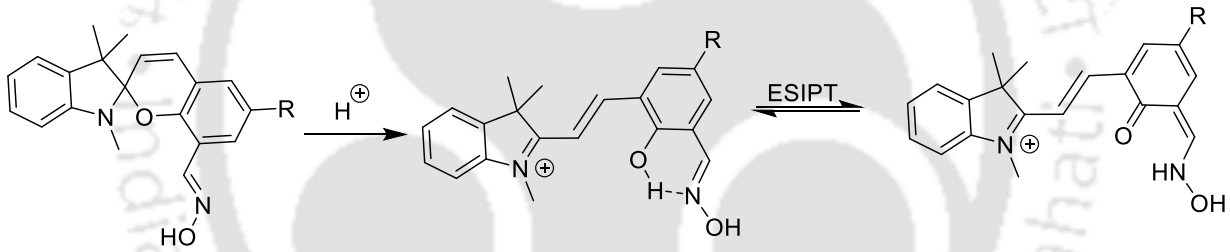

Scheme 1.9. Spirobenzopyran based ratiometric pH responsive probe.

Spirobenzopyran based ratiometric pH responsive probes were synthesized by Shuang et al.[127] ESIPT gets turned on in the probe on adding H^+. The longer to shorter wavelength intensity increased 68 times on changing the pH from 8.0 to 4.0 (**Scheme 1.9**).

1.4. Effect of heterogeneous media on PT

Proton transfer is sensitive to the local environment such as polarity and viscosity.[77,117,128,129] These properties make them useful fluorescent probes of heterogeneous environments, e.g. micelles and reverse micelles, supramolecular cavities, etc.[96,130–132] Many photophysical processes have been studied in these systems using steady state and time resolved emission spectroscopy.[133] These supramolecular entities are not just passive hosts. Hydrophobic and electrostatic interactions in these clusters profoundly influence the guest's chemical properties, leading to novel and often interesting host-guest chemistry.[134] Water

TH-2834_146122035

molecule are confined within these supramolecular hosts.[135,136] This confined water is different from bulk water. As proton transfer is highly affected by the surrounding micro-environment, the ESIPT properties of a molecule vary greatly in these systems compared to aqueous solutions. Therefore, many ESIPT molecules have been studied in these organized media.[137–140]

1.4.1. Effect of micelles on PT

Micelles form a part of micro-heterogeneous systems uniformly distributed in aqueous solution.[136,141–143] Surfactants, detergents or amphiphiles are molecules with distinct hydrophobic and hydrophilic regions within the same molecule that can form micelles. The polarity decreases as we go from the interfacial region to the micellar core. In an aqueous medium, surfactant molecules dynamically and spontaneously associate to form aggregates known as micelles above a characteristic concentration, critical micelle concentration (CMC). Association between the hydrophobic chains and repulsion between the surfactants' polar head groups is responsible for micelle formation. As a general rule of thumb, the longer the hydrocarbon chain, the lower the CMC. They can be cationic [e.g., hexadecyltrimethylammonium bromide (CTAB)], anionic [e.g., sodium dodecyl sulfate (SDS)], neutral [e.g., polyoxyethylene(9.5)octylphenol (TritonX-100)], and zwitterionic [e.g., 3-(dimethyldodecylammonio)propane-l-sulfonate].

ESIPT of HPBI was studied in micelles.[144] Above the CMC, the intensity of the normal emission band, decreased and a large enhancement tautomer emission along with a 20 nm red shift of the emission maxima was observed. The fluorescence decay of the normal emission was unaffected. However, the lifetime of tautomer emission of HPBI increased sharply above the CMC. The enhanced tautomer emission is due to the penetration of HPBI molecules residing in the micelles' non-polar and aprotic interior.

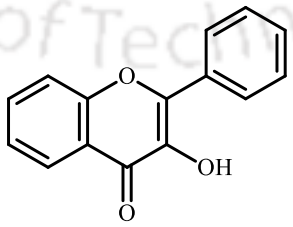

Chart 1.6. Structure of 3-hydroxyflavone.

ESIPT on 3-hydroxyflavone (**Chart 1.6**) was studied in aqueous micelles.[145] The ESIPT dynamics of 3-hydroxyflavone in aqueous micelles is similar to that in polar, protic solvents like methanol and water, where dual emission is also observed. In both micelles and

TH-2834_146122035

polar protic solvents, ground state intermolecular proton transfer occurs, producing the anion which emits independently.

Hazra et al. have studied ESIDPT of 2,2′-bipyridyl-3,3′-diol in micelles and bile salts aggregates.[96] ESIDPT follows sequential pathways in all these supramolecular assemblies (**Scheme 1.7**). However, the time-range for the proton transfer was different in different systems. The first proton transfer was faster in these systems, while the second was much slower than water. The different proton transfer dynamics in these supramolecular aggregates were attributed to the variation of water molecules in the probe's vicinity.

1.4.2. Effect of reverse micelles on PT

Surfactants having suitable lipophilic hydrophobic balance [e.g. sodium bis(2-ethylhexyl)sulfosuccinate (Aerosol-OT or AOT)] (**Chart 1.7**) undergo self-association in non-polar solvents.[146,147]

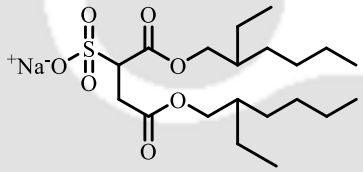

Chart 1.7. Structure of sodium bis(2-ethylhexyl) sulfosuccinate or Aerosol-OT (AOT).

These surfactants can solubilize a large number of water molecules. These surfactant/non-polar solvent/water systems form reverse micelles. The molar ratio (w_0) of added water or polar solvent to the surfactant is given by (w_0 = [Polar solvent]/[surfactant]). A water-in-oil microemulsion is produced with nanometer sized water droplets, called water pool, surrounded by a layer of surfactant molecules dispersed in the non-polar organic solvent. The water molecules in the water pool are highly structured, less mobile and have a polarity less than that of ordinary bulk water. On adding water to reverse micelles in micro-quantities, a substantial amount of water can be solubilized inside a non-polar solvent like *n*-heptane. In *n*-heptane, the radius of the water pool is roughly $2w_0$ (Å). For small water pools (w_0 up to 10), the water molecules are held very tightly by the polar head groups of the surfactant, while for large pools (w_0 = 10 to 30), the water molecules (mainly at the center) are relatively free.

Dual emission of HPBI was studied in the reverse micelle.[131] The increase in the tautomer emission in reverse micelles, compared with *n*-heptane, was attributed to decreased non-radiative rates. It was also inferred that the polarity of the water pool is less than that of ordinary bulk water.

TH-2834_146122035

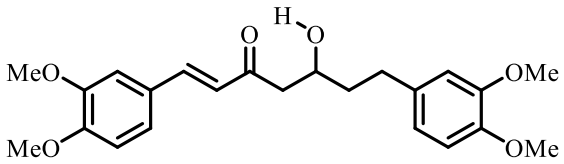

Chart 1.8. Structure of 1,7-bis(4-hydroxy-3-methoxyphenyl)-1,6-hepatadiene-3,5-dione or Curcumin.

Curcumin (**Chart 1.8**), an ESIPT active natural yellow pigment, was studied in AOT reverse micelle. The AOT micellar interface was modulated by using different hydrogen-bond-donor and non-hydrogen-bond-donor core solvents such as water, amides, glycols and glycerol and *n*-heptane as bulk solvent.[148] On increasing the amount of core solvents, the emission intensity and lifetime of curcumin increased with substantial red shift inside the reverse micelle. The confined probe's lifetime values in the micellar environment were significantly longer than those observed in pure homogeneous solvents.

ESDPT in 7-Azaindole in AOT reverse micelle has been reported.[149,150] The emission changed from dual to single on increasing w_0.[149] The fluorophore molecules were found to reside at the bound-water regions of AOT reverse micelle.[150] The decrease of proton transfer in the bound-water regions was due to the increased free energy of solvation to form a prerequisite cyclic 1:1 7-azaindole:water complex.

1.4.3. Effect of supramolecular hosts on PT

Host-guest inclusion complexes are formed when a small guest molecule becomes encapsulated in a sizeable cage-like host cavity.[151–154] These complexes represent a simple supramolecular system as they are bound only by non-covalent interactions. There is a dynamic equilibrium between free host, guest and the complex because of the lack of host-guest covalent bond.

Organic hosts such as cyclodextrins (CDs) and cucurbit[n]urils (CB-n) or (CB[n]) are very popular supramolecular hosts. Their bindings have been studied with many fluorescent guests.[132,133,155–159] Cyclodextrins (CDs) consist of glucose subunits cyclic ring, joined by α-1,4 glycosidic bonds.[160] CDs have a nanosized cavity of different sizes and shapes labelled as *α, β, γ*. Their methylated variants are also used as a host. *β*-CD is considered the best system for studying inclusion complexes (**Chart 1.9**). Its interior is hydrophobic and the external wall is hydrophilic. The hydrophobic nature of the cavity increases the solubility and hence fluorescence of organic guests. CDs have been used to study the effect of encapsulation on the excited state processes such as proton transfer and charge transfer etc. [130,132,155,158,161–165]

TH-2834_146122035

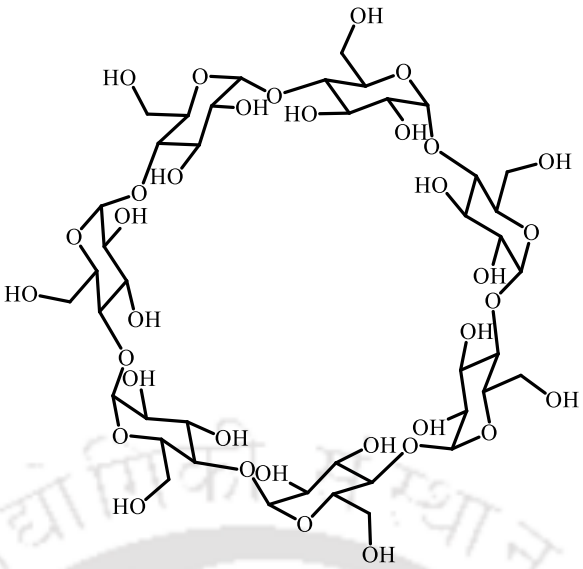

Chart 1.9. Structure of *β*-cyclodextrin.

The effects of CDs on HPBI, HPBO and 2-(2′-hydroxyphenyl)benzothiazole (HPBT) were studied in the ground and excited states in water by Warner et al.[163] Their results suggested HPBO exists as a planar conformer and HPBT and HPBI both exist as twisted. The molecules were stable inside CD cavities which were suggested by an increase in absorbance and bathochromic shift in absorption spectra as compared to water. They showed weak intramolecular hydrogen bonding in HPBI and the formation of strong intermolecular hydrogen bonds with the hydroxyl groups of the CD. Also, they reported that phototautomers of all these azoles exist as zwitterions inside *β*-CDs and *γ*-CD.

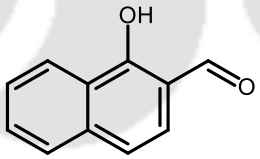

Chart 1.10. Structure of 1-hydroxy-2-napthaldehyde.

Guchhait et al. studied the ESIPT of 1-hydroxy-2-napthaldehyde (**Chart 1.10**) in the presence of CDs.[156] Enhanced tautomer emission in the encapsulated state predicted favourable ESIPT reaction in CDs. Benesi−Hildebrand plots indicated 1:2, 1:1, and 1:1 complexation for *α*-, *β*-, and *γ*-CD, respectively. Hazra et al. studied 2,2′-bipyridyl-3,3′-diol in CB [7] and *β* -CD. The ESIDPT in water and *β*-CD takes place via a two-step sequential mechanism, but it changes to concerted inside CB [7] (**Scheme 1.7**).

1.5. Intramolecular charge transfer

Intramolecular charge transfer (ICT) is another process in fluorophores that can result in dual emission.[166–168] ICT occurs when a spacer or single bond connects a charge donor and

TH-2834_146122035

a charge acceptor. This photoinduced phenomenon results in a highly polar ICT state. Molecule emits from both locally excited and charge transfer state hence resulting in dual emission. ICT also plays an important role in biological systems and has many practical applications.[114,167,169–173] When the donor group gets twisted to prevent back transfer of the charge, the process is called twisted intramolecular charge transfer (TICT) (**Scheme 1.10**).[168,169,174] Due to this charge separation, the fluorescence of a TICT molecule is strongly dependent on the polarity.

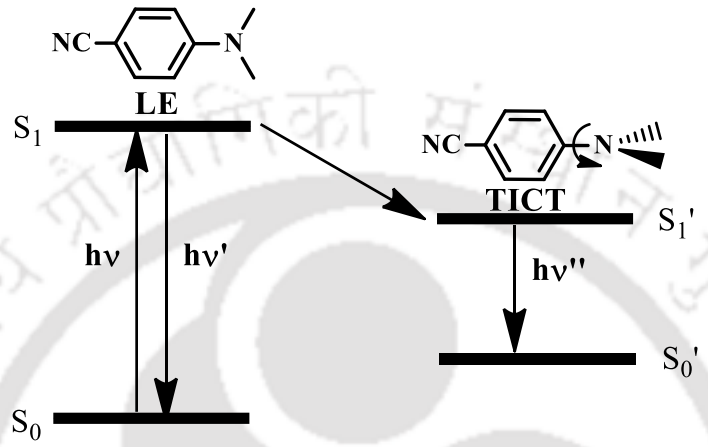

Scheme 1.10. Dual emission from a TICT fluorophore.

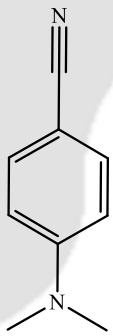

Chart 1.11. Structure of 4-dimethylaminobenzonitrile (DMABN).

4-Dimethylaminobenzonitrile (DMABN, **Chart 1.11**) is a popular donor-acceptor system emitting dual fluorescence in polar solvents because of TICT.[7,175] The hydrogen bonding ability of solvent, pH and micro-viscosity or rotational hindrance posed by the local environment also affect TICT. The dipole moments of these dyes are greater in the excited state compared to their ground state. Therefore, one of the significant characteristics of ICT emission is the bathochromic shift in emission spectra with an increase in solvent polarity. This positive solvatochromism is exactly the opposite of ESIPT. Due to the polar nature of the TICT state, the rate of formation and stabilization of the ICT state increases on increasing the polarity of the environment.

TH-2834_146122035

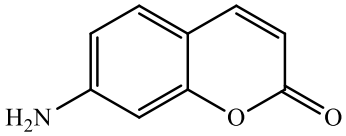

Chart 1.12. The chemical structure of 7-aminocoumarin.

7-aminocoumarin (**Chart 1.12**) and its substituted derivatives were widely studied as TICT probes.[42,176–178] Due to ICT in the excited state, 7-aminocoumarins show a highly polar excited state. Sometimes the ICT is followed by twisting of the amino group in the excited state to give TICT emission in these molecules.

1.5.1. The role of hydrogen bonding in intramolecular charge transfer

The fluorescence of 6-dodecanoyl-2-dimethylaminonaphtalene (laurdan) (**Chart 1.13**) was studied in pure and mixed solvents.[179] It shows a large solvent shift as a function of the solvent polarity. This shift was attributed to the ICT emission.

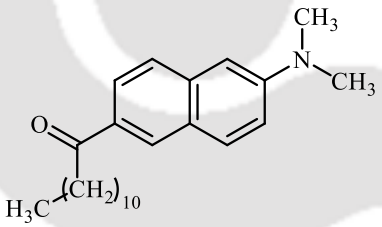

Chart 1.13. 6-Dodecanoyl-2-dimethylaminonaphtalene (laurdan).

The difference of ICT emission of laurdan in methylcyclohexane–tetrahydrofuran and methylcyclohexane–ethanol was explained by the absence and presence of hydrogen bond. The presence of isosbestic point in absorption spectra of laurdan in methylcyclohexane–ethanol confirmed the formation of 1:1 complex between laurdan and ethanol. In aminophenylpyridoimidazoles, hydrogen bonding with protic solvents is essential to obtain TICT emission. Fasani et al. showed that 2-(4'-aminophenyl)pyridoimidazoles (APIPs) emit single emission in non-polar and polar aprotic solvents, but dual emission from both locally excited state and ICT state in alcoholic solvents.[180] TICT emission is also reported from dimethylamino derivatives of APIPs.[181,182]

1.6. Coupled proton and charge transfer systems

When both ESIPT and ICT groups are combined in the same fluorophore, their photophysical properties become very interesting. Coupled proton and charge transfer reactions play an important role in chemical and biological processes.[183–187] ICT can occur either before or after PT and often these two processes compete with each other.

TH-2834_146122035

Kasha et al. demonstrated that all the three states of p-dimethylaminosalicylate, i.e. the locally excited state, the ICT and tautomer can emit and therefore, compete with each other (**Chart 1.14**).[188–190]

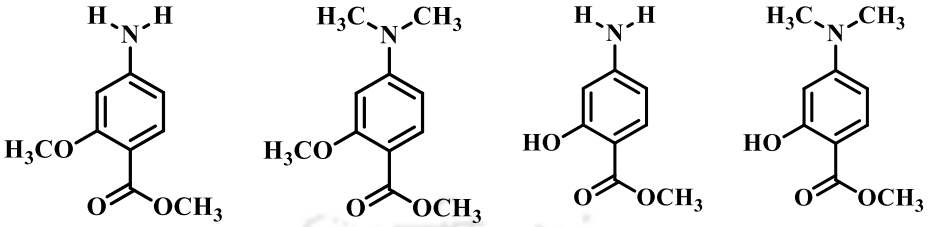

Chart 1.14. Structures of aminosalicylates.

Park et al. studied two HPBO derivatives substituted with electron acceptor substituents (**Chart 1.15**).[191] These substituents can rearrange themselves as dipolar push-pull systems after ESIPT. The keto emission of these two dyes showed a large red shift with an increase in solvent polarity and a negligible shift in enol emission. However, HPBO shows a slight blue shift on increasing the solvent polarity. This opposite behaviour in these two HPBO derivatives was attributed to the ICT process followed by ESIPT.

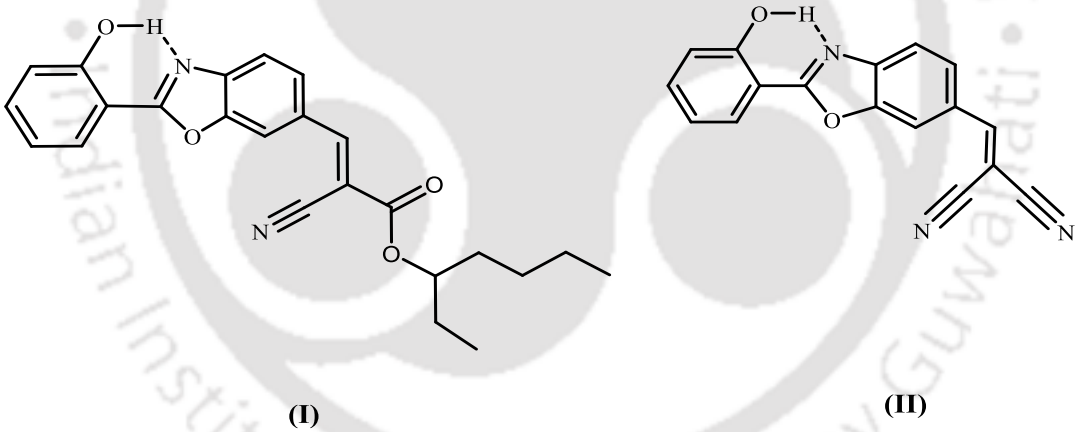

(I) **(II)**

Chart 1.15. HPBO derivatives studied by Park et al.

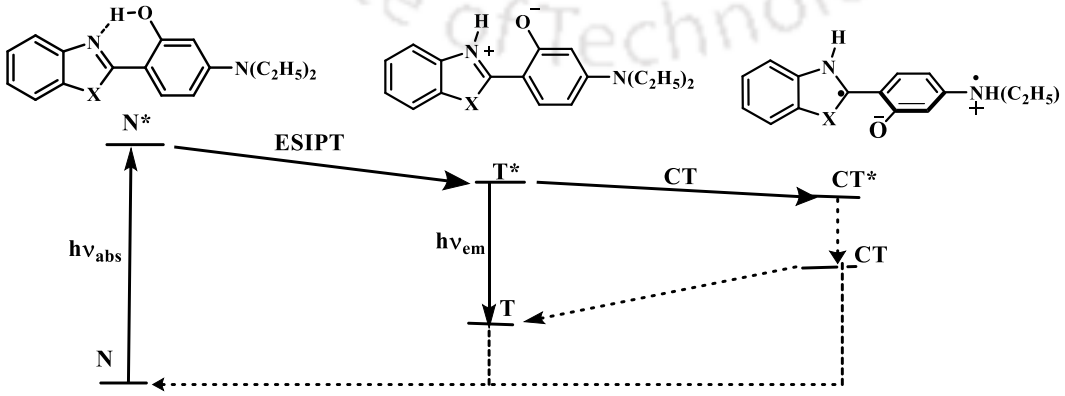

Scheme 1.11. Excited state coupled intramolecular proton and charge Transfer of 2-(4′-*N*,*N*-diethylamino-2′-hydroxyphenyl)benzimidazole derivatives (X = NH and NMe).

TH-2834_146122035

Rodríguez et al. reported that 2-(4′-*N*,*N*-diethylamino-2′-hydroxyphenyl)benzimidazole and its methylated derivative emit normal and tautomer emissions and no ICT emission (**Scheme 1.11**).[192] However, they proposed ICT from the zwitterionic molecule, which resulted in a non-fluorescent tautomer. The same mechanism was also reported in 1-methyl-2-(2‘-hydroxyphenyl)benzimidazole.[192]

1.7. Aggregation induced enhanced emission

Aggregation-caused quenching is responsible for fluorescence quenching in concentrated solutions and solids. The π–π stacking interaction between the fluorophore molecules is responsible for this quenching. This notorious phenomenon poses a hindrance to the practical application of fluorophores. An entirely opposite phenomenon called aggregation-induced emission (AIE) or aggregation-induced enhanced emission (AIEE) causes fluorescence enhancement in aggregates.[193–195] The mechanism of AIE is proposed to be the restriction of intramolecular rotation (RIR) and intramolecular vibrations. AIE-active ESIPT and TICT fluorophores are well reported.[196–201]

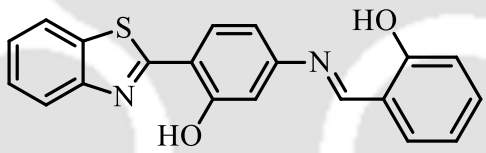

Chart 1.16. HPBT derivative.

Substituted HPBT derivative given in **Chart 1.16** gives dual emission in methyltetrahydrofuran, methylcyclohexane and methanol.[202] The ratio of normal to tautomer band intensity is dependent on solvent polarity. The molecule’s solubility is significantly less in methyltetrahydrofuran and methylcyclohexane, which results in poor emission intensity of the molecule in these two solvents. When the temperature is decreased, the emissions of the molecule increases in all three solvents. A ~28 fold increase in emission was observed in methylcyclohexane when the temperature was reduced from 298 to 140 K; This enhancement was attributed to AIEE due to RIR upon bringing the temperature to freezing point of the solvent. This molecule also shows AIEE in water methanol mixtures. In 90% water, 20 times emission enhancement of the keto band was observed compared to pure methanol.[126]

HPBT based ESIPT molecules, *N*,*N*′-di[3-Hydroxy-4-(2′-benzothiazole)phenyl]isophthalic amide and *N*,*N*′-di[3-Hydroxy-4-(2′-

TH-2834_146122035

benzothiazole)phenyl]5-*tert*-butyl-isophthalic amide were synthesized by Yang et al. (**Chart 1.17).**.[199]

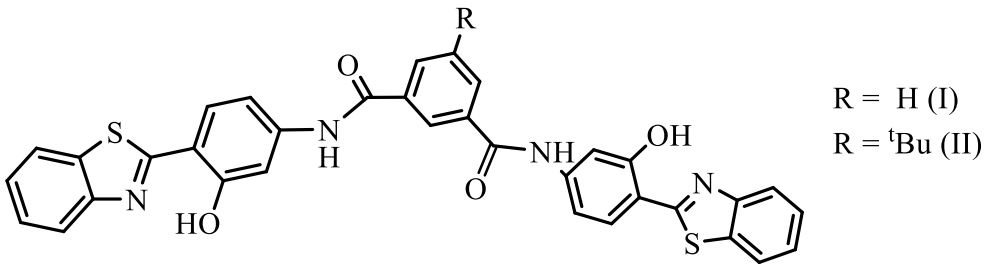

Chart 1.17. Structures of *N,N′*-di[3-hydroxy-4-(2′-benzothiazole)phenyl]isophthalic amide (I) and *N,N′*-di[3-Hydroxy-4-(2′-benzothiazole)phenyl]5-tert-butyl-isophthalic amide (II).

They were weakly emissive in THF. These two molecules in THF/H_2O mixture exhibited AIEE due to RIR. In solid state, II showed more enhancement than I due to the steric hindrance by the tert-butyl group.

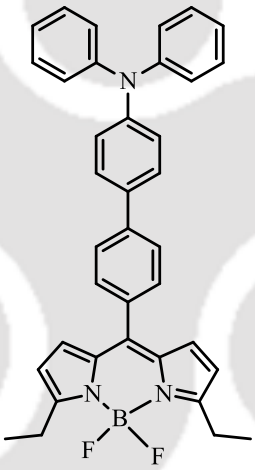

Chart 1.18. Boradiazaindacene (BODIPY) derivative.

Combined AIE-TICT effect has been studied in boradiazaindacene (BODIPY) derivative (**Chart 1.18**).[198] The studied BODIPY derivative emits at 685 nm in pure THF. The spectrum undergoes a 15 nm red shift in THF–water (90:10) mixture due to an increase in solvent polarity. The emission remains weak up to 65% water content, and after that, it starts to increase. In 99% water, fluorescence intensity increases to 70 times as compared to 50% water with blue-shifted emission at 658 nm.

1.8. Motivation for the present work

Excited state proton transfer from hydroxyarenes has been studied for decades. However, new horizons are still opening for this fundamental proton transfer process. As a result of new substrates, new instrumentations and new calculation tools, a fairly consistent

TH-2834_146122035

proton transfer picture has emerged. The present thesis is focused on the proton transfer in three model systems, (i) 2-phenylamino-5-(2-hydroxybenzono)-1,3,4-thiadiazole (PHBT), (ii) 3,5-bis(2-hydroxyphenyl)-1H-1,2,4-triazole (bis-HPTA) and (iii) 2-(4′-amino-2′-hydroxyphenyl)-1*H*-imidazo-[4,5-c]pyridine (AHPIP-c). PT mechanism was studied in these systems using UV-visible spectroscopy, steady state and time resolved photoluminescence and theoretical calculations.

2-(4-fluorophenylamino)-5-(2,4-dihydroxybenzeno)-1,3,4-thiadiazole (FABT) has been studied for its pharmacological properties, especially the anticancer activity.[203] In aqueous solution, FABT emits dual emission and the longer wavelength emission in FABT was assigned to the combination of aggregation and change in conformation.[204] FABT has proton donor and acceptor groups in close proximity and therefore, the longer wavelength emission may originate from excited state tautomer. An analogue of FABT, PHBT was synthesized to determine the origin of the longer wavelength emission. The luminescence of PHBT and its methoxy derivatives 2-phenylamino-5-(2-methoxybenzono)-1,3,4-thiadiazole (PMBT) were studied and compared with that of FABT. Based on the experimental and theoretical studies, the origin of the longer wavelength emission was revealed.

A special kind of ESIDPT called Proton transfer triggered proton transfer (PTTPT) in a triazole derivative, bis-HPTA, was reported recently.[205] The fluorophore has two proton donor-acceptor pair. But the first proton transfer (ESIPT-I) is feasible only in one pair. The other pair did not show proton transfer (ESIPT-II) initially due to annular tautomerism. ESIPT-II is only feasible after ESIPT-I because of a decrease in annular tautomerism. In other words, ESIPT-I triggers ESIPT-II. Therefore, this ESIDPT was named PTTPT. As we know, pH plays an important role for dictating the ESIPT properties of molecules. Water is an important solvent for fluorescence study for understanding biological systems and application point of view. As discussed in this chapter, the ESIPT processes is highly sensitive to the environment and micelles, reverse micelle and CD provide a heterogeneous environment. Therefore, the proton transfer process of bis-HPTA was investigated in micelle and β-CD to find the effect of these micro heterogeneous system on PTTPT of bis-HPTA in aqueous media.

2-(4′-Aminophenyl)-1H-imidazo-[4,5-c]pyridine (APIP-c) emits TICT emission in methanol (**Scheme 1.12**).[180] But its hydroxy derivative, AHPIP-c, emits only tautomer emission along with normal emission in methanol.[206] No TICT emission is observed in AHPIP-c in methanol. DFT calculations were performed using the polar continuum model with methanol molecules to understand the PT mechanism in AHPIP-c. TDDFT calculations were used for vibrational frequency analysis in the excited state.

TH-2834_146122035

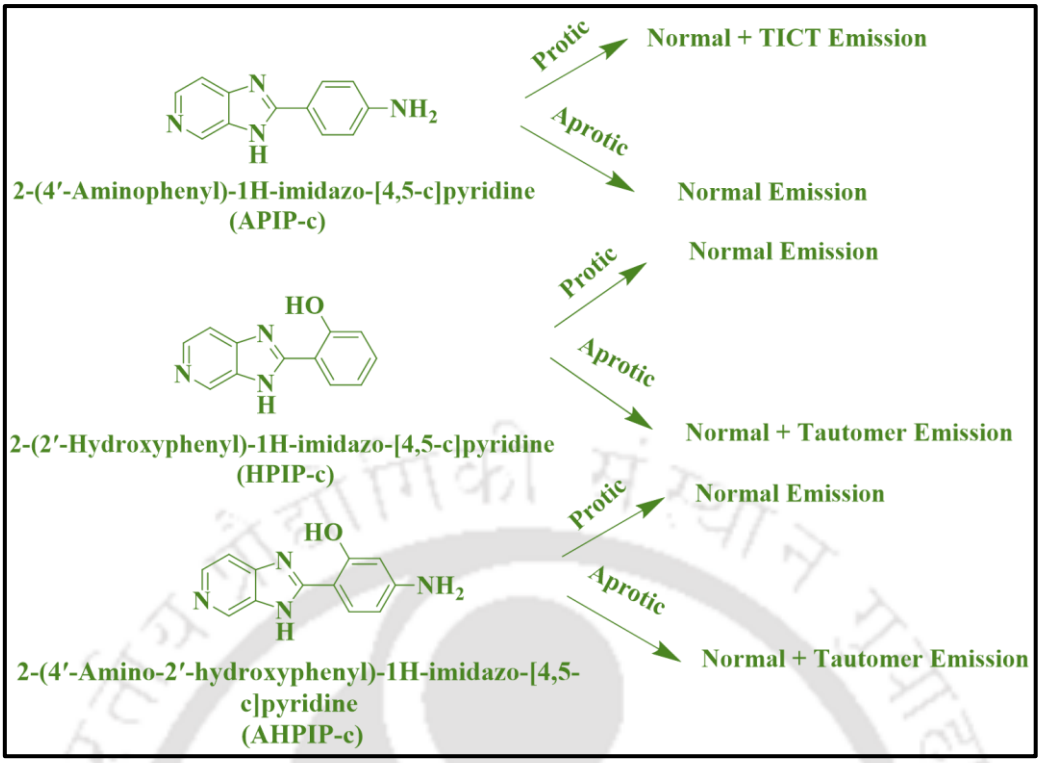

Scheme 1.12. Excited state intramolecular proton and charge transfer of 2-phenyl-1H-imidazo-[4,5-c]pyridine derivatives.

The fluorescence properties of molecules may vary drastically on changing the pH. In AHPIP-c, the binding of proton to pyridyl/imidazole nitrogen should increase the charge flow from donor to acceptor moiety and increase the ICT emission. Spectral characteristics of AHPIP-c and its methoxy derivative were studied at different pH in water. The study was further extended to acetonitrile and methanol to determine the polarity dependence on emission. The study aimed to find whether ICT emission is possible in the prototropic species in AHPIP-c.

TH-2834_146122035

Chapter 2

Materials, Methods and Instrumentations

TH-2834_146122035

TH-2834_146122035

2.0. Introduction

This chapter gives the details of the chemicals, solvents, instruments, synthetic procedures and various methods used in this thesis work.

2.1. Materials

2.1.1. Solvents

2.1.1.1. For spectroscopic measurements

- *n*-Heptane ($CH_3(CH_2)_5CH_3$), (HPLC grade, Merck)
- Toluene ($C_6H_5CH_3$), (HPLC grade, Rankem India)
- Ethyl acetate ($CH_3COOCH_2CH_3$), (HPLC grade, Spectrochem India)
- 1,4-Dioxane ($C_4H_4O_2$), (HPLC grade, Spectrochem India)
- Tetrahydrofuran, THF (C_4H_8O), (HPLC grade, Spectrochem India)
- Acetonitrile (CH_3CN), (HPLC grade, Spectrochem India)
- N,N-Dimethylformamide (C_3H_7NO), (HPLC grade, Spectrochem India)
- Dimethyl sulphoxide (C_2H_6OS), (HPLC grade, Spectrochem India)
- 1-Propanol ($CH_3(CH_2)_2OH$), (HPLC grade, Spectrochem India)
- 1-Butanol ($CH_3(CH_2)_2OH$), (HPLC grade, Spectrochem India)
- 2-Butanol ($(CH_3)_2CHCH_2OH$), (HPLC grade, Spectrochem India)
- 2-Propanol ($(CH_3)_2CHOH$), (HPLC grade, Spectrochem India)
- Methanol (CH_3OH), (HPLC grade, Spectrochem India)
- Water (H_2O), (Elix, Merck Millipore)
- Chloroform-d ($CDCl_3$), (Sigma Aldrich)
- Dimethylsulfoxide-d6 (C_2D_6OS), (Sigma Aldrich)

2.1.1.2. For synthesis and purification

- Acetonitrile (CH_3CN), (AR grade, Spectrochem India)
- Ethanol (CH_3CH_2OH)
- Xylenes ($C_6H_4(CH_3)_2$), (AR grade, Merck)
- Pyridine (C_6H_5N), (AR grade, Merck)
- Methyl tetrahydrofuran ($C_4H_7OCH_3$), (AR grade, Merck)
- Diethyl ether (CH_3OCH_3), (AR grade, Merck)
- Hexanes (C_6H_{12}), (AR grade, Merck)
- Ethyl acetate ($CH_3COOCH_2CH_3$), (AR grade, Spectrochem India)
- Dichloromethane (CH_2Cl_2), (AR grade, Merck)

TH-2834_146122035

- Methanol (CH_3OH), (AR grade, Merck)

2.1.2. Starting materials and reagents

- Dichloro dicyano benzoquinone (DDQ) (Sigma Aldrich)
- 3,4-Diaminopyridine (Sigma Aldrich)
- 4-Amino-2-hydroxybenzoic acid (Sigma Aldrich)
- Phosphorus oxychloride ($POCl_3$)
- Sulphonyl chloride ($SOCl_2$)
- Salicylic acid (98%, Merck)
- Salicylamide (99%, Sigma Aldrich)
- Hydrazine monohydrate (80% solution in water) (Merck)

2.1.3. Other chemicals

- Silica gel (SiO_2) (60-120 mesh) (Merck India)
- Silica gel for TLC (SiO_2), (Merck India)
- Silica gel GF254 (SiO_2), (Merck India)
- Cetyl trimethylammonium bromide or hexadecyltrimethylammonium bromide (CTAB) (Sigma Aldrich)
- Sodium dodecyl sulfate (SDS) (Sigma Aldrich)
- Polyethylene glycol tert-octyl phenyl ether (Triton-X 100) (Sigma Aldrich)
- Sodium bis(2-ethylhexyl) sulfosuccinate (AOT) (Sigma Aldrich)
- *β*-Cyclodextrin hydrate (Sigma Aldrich)
- Sodium bicarbonate (Merck)
- Sodium hydroxide (Merck)
- Sodium sulphate anhydrous (Merck India)
- Sulfuric acid (AR grade, Merck)
- Buffers (pH 4.0, 7.0 and 9.2) (Merck)

2.2. Synthetic procedures

2.2.1. Synthesis of 2-(Phenylamino)-5-(2-hydroxybenzeno)-1,3,4-thiadiazole (PHBT) and 2-(phenylamino)-5-(2-methoxybenzeno)-1,3,4-thiadiazole (PMBT)

PHBT and its methoxy derivative, PMBT, were synthesised using the procedure reported for the synthesis of similar molecules.[207] A mixture of appropriate thiosemicarbazone (0.25 mmol) (hydroxyl for PHBT and methoxy for PMBT) and DDQ (0.25 mmol) was stirred in acetonitrile (2.0 ml) at room temperature for an hour.

TH-2834_146122035

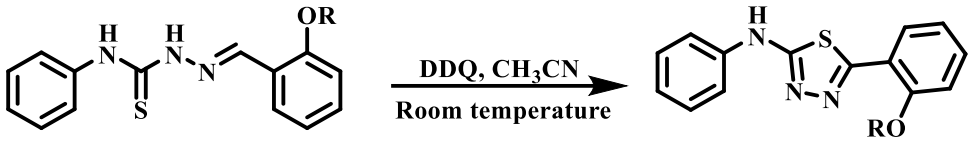

Scheme 2.1. Synthesis of PHBT (R=H) and PMBT (R=CH_3).

After the completion of the reaction, acetonitrile was removed under reduced pressure. Water was added to the reaction mixture and the compound was extracted by ethyl acetate. The organic layer was separated, dried using anhydrous sodium sulfate, filtered. Ethyl acetate was removed under reduced pressure.

The crude PHBT was purified using column chromatography using a 70:30 hexane-ethyl acetate mixture. The final product was a white powder. The product was confirmed using ^{1}H and ^{13}C spectra (**Annexure A**) and mass data.

PHBT (^{1}H NMR, 600 MHz, Chloroform-d): δ 6.93 (t, 1H), 7.10 (d, 1H), 7.19 (m, 1H), 7.36 (m, 2H), 7.44 (m, 4H), 9.57 (s, 1H), 11.19 (s, 1H). Mass $[M+H]^+$ 270.0733.

The crude PMBT was obtained as red and white solid. It was washed with methanol to remove red impurity and recrystallised with ethyl acetate. The final product was a white crystalline solid. The product was confirmed by ^{1}H and ^{13}C NMR, single crystal X-ray diffraction (SCXRD) analysis (**Annexure A**) and mass data.

PMBT (^{1}H NMR, 600 MHz, Chloroform-d): δ 3.99 (s, 3H),7.02 (d, 1H), 7.11 (t, 2H), 7.48-7.40 (m, 5H), 8.40 (dd, 1H). Mass $[M+H]^+$ 284.0897.

2.2.2. Synthesis of 3,5-bis(2'-hydroxyphenyl)-1H-1,2,4-triazole (bis-HPTA)

Bis-HPTA was synthesised in two steps by using the procedure reported in the literature.[208] First, 2-(2'-hydroxyphenyl)-4H-1,3-benzoxazin-4-one i.e. the precursor for Bis-HPTA, was synthesised. 0.01 M of salicylic acid, 0.01 M salicylamide and a catalytic amount of pyridine were stirred in a 25 ml round bottomed flask with 15 ml xylene maintaining a temperature of 65˚C. An equivalent amount of thionyl chloride was added in batches over 4 hours time period. The reaction was carried at 65˚ C for another 30-40 minutes after the complete addition of $SOCl_2$. The reflux condenser was then removed and the reaction mixture was heated for another 30 minutes to remove excess $SOCl_2$. Xylene was evaporated at low pressure using ethanol as a co-solvent. For completely drying, methyl THF was added to the round-bottomed flask and left overnight in ice. The precipitate was washed with ethyl acetate, dried and weighed. No purification was needed after this step.

TH-2834_146122035

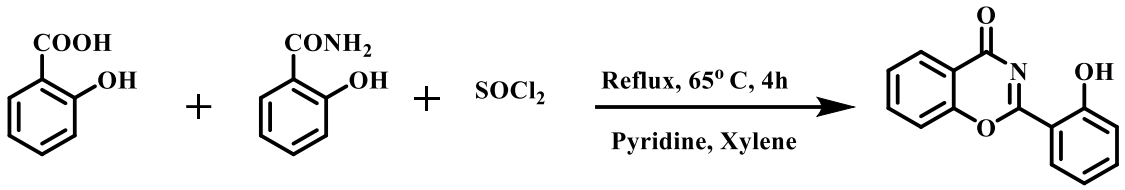

2-(2'-hydroxyphenyl)-4*H*-benzoxazin-4-one

Scheme 2.2. Synthesis of the precursor of bis-HPTA.

In the final step, the equimolar amounts of 2-(2'-hydroxyphenyl)-4H-benzoxazin-4-one and hydrazine monohydrate were taken into diethyl ether and left for reaction overnight at room temperature to obtain bis-HPTA. The compound was purified by column chromatography using the ethyl acetate and hexane mixture. The molecule was characterised by proton and ^{13}C NMR (**Annexure B**) and ESI-mass spectrometry.

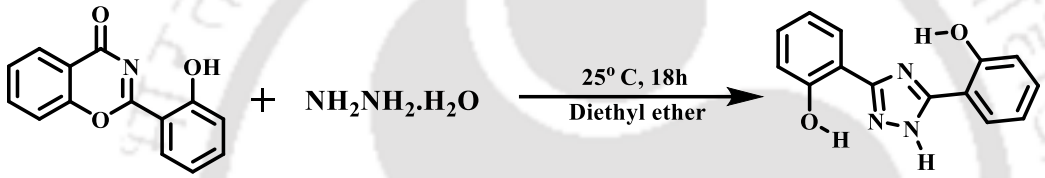

3,5-bis(2-hydroxyphenyl)-1H-1,2,4-triazole (bis-HPTA)

Scheme 2.3. Synthesis of bis-HPTA.

Bis-HPTA (^{1}H NMR, 600 MHz, DMSO-d6): δ 11.46 (s, 2H), 8.02 (dd, *J* = 7.8, 1.6 Hz, 2H), 7.35 (t, *J* = 7.7 Hz, 2H), 7.03 (d, *J* = 8.1 Hz, 2H), 7.00 (t, *J* = 7.5 Hz, 2H).

2.2.3. Synthesis of 2-(4′-amino-2′-hydroxyphenyl)-1*H*-imidazo-[4,5-c]pyridine (AHPIP-c)

AHPIP-c were synthesised by refluxing 3,4-diaminopyridine and 4-amino-2-hydroxybenzoic acid in $POCl_3$ at 110 °C.[209] After 8 hours, the reaction mixture was cooled to room temperature and poured into ice-cold water. The hydrochloric acid formed as a byproduct was neutralised by a concentrated sodium hydroxide solution. The precipitates were filtered and dried. The compound was purified by column chromatography using the dichloromethane-methanol mixture. The final compound was brown in colour. The identity of the compounds was confirmed by ^{1}H NMR spectroscopy.

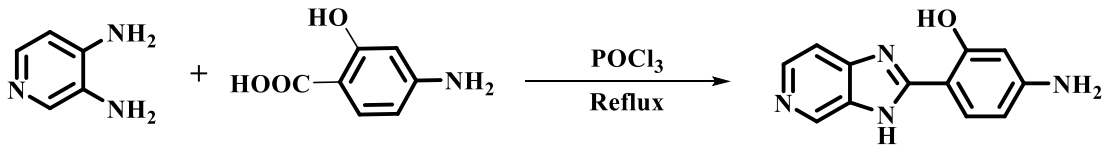

AHPIP-c

TH-2834_146122035

Scheme 2.4. Synthesis of AHPIP-c.

AHPIP-c (^{1}H NMR, 600 MHz, DMSO-d6): δ 8.10 (s, 1H), 7.57 (d, 1H), 7.06 (d, 1H), 7.01 (d, 1H), 5.56 (d, 1H), 5.48 (s, 1H).

2.3. Sample preparation

2.3.1. Preparation of stock solutions

The stock solutions (1 mM) of PHBT, PMBT and AHPIP-c were prepared in acetonitrile. 1 mM stock solution of bis-HPTA was prepared in methanol.

2.3.2. Solvatochromic studies

50 μL (for 5 μM) or 100 μL (for 10 μM) of the stock solutions were pipetted out to a 10 ml volumetric flask. The solution was dried under nitrogen. 10 ml of required solvents were added to each volumetric flask containing the dried compound.

2.3.3. Prototropic studies

The aqueous solutions of different pH were prepared by adding an appropriate amount of acid (sulfuric acid) and base (sodium hydroxide) to distilled water. The solution of pH 3.0 to 11.0 were prepared by adding the appropriate amount of dil. acid and base. The solutions of pH 11.0-13.0 were obtained by using conc. sodium hydroxide. The solutions of pH 1.0-3.0 were prepared by adding conc. sulfuric acid to distilled water. These solutions were then added to the volumetric flask containing 10 μM of the dried compound.

2.3.4. Micellar and *β*-CD solutions

The stock solutions of surfactants and *β*-CD were prepared in a 100 ml volumetric flask by adding an appropriate quantity of CTAB/SDS/Triton-X 100/*β*-CD in distilled water. The stock solutions were then added to the volumetric flasks. The pH of the solutions was adjusted by adding little dilute sulfuric acid or sodium hydroxide solution. These solutions were then added to the volumetric flask containing the dried compound.

2.3.5. Reverse micellar solutions

AOT/*n*-heptane/water reverse micelle solutions were prepared by mixing the required amount of water to *n*-heptane-AOT solution. The water quantity in the reverse micellar system is expressed in terms of the molar ratio (w_0) of water to the surfactant. The AOT concentration (0.1 M) was kept fixed and the amount of water was varied to obtain solutions of different w_0 values. These solutions of different w_0 values were then added to the volumetric flask containing the dried compound.

TH-2834_146122035

2.4. Methods

2.4.1. Quantum Yield and relative fluorescence quantum yield

Quantum yield (Φ_f) is the ratio of the number of photons emitted to the number of photons absorbed.[99]

$$\Phi_f = \frac{\text{Number of photons emitted}}{\text{Number of photons absorbed}} \quad (2.1)$$

The relative fluorescence quantum yields are determined with respect to a known standard by using the below equation,

$$\Phi_S = \Phi_{RX} \frac{{n_S}^2}{{n_R}^2} \times \frac{A_R}{A_S} \times \frac{I_S}{I_R} \quad (2.2)$$

I_S and I_R are the area under curve for the emission spectra of the sample and reference, respectively. A_S and A_R are the absorbance for the sample and reference, respectively. n_S and n_R are the refractive indices for the solvent used for the sample and the reference solutions, respectively. Quinine sulphate in 1N sulphuric acid (Φ_f = 0.55) is used as the reference in the work done in this thesis.

2.4.2. Quantum mechanical calculations

Theoretical calculations were performed by density functional theory (DFT)[210] and time-dependent density functional theory (TDDFT)[211] methods using Gaussian09 and Gaussian16.[212] Becke's three-parameter hybrid exchange function with the Lee-Yang-Parr gradient-corrected correlation functional B3LYP, CAM-B3LYP and B3LYP-D3 were employed as functions[213–216] Solvent effect was included using integral equation formalism-polarisable continuum model (IEF-PCM).[217] 6-31G ++ (d, p), DGTZVP, aug-CC-PVTZ were used as basis sets. LanL2DZ was used as basis set to optimize *β*-cyclodextrin in chapter 4. IR vibrational frequencies were also calculated to rule out imaginary frequencies. UV-visible and emission spectra were calculated using the same theoretical parameters. Potential energy curves in S_0 and S_1 states were obtained to determine the barrier height by using modified redundant coordinates and scan features in Gaussian09. In chapter 6, the isosurfaces of hole, electron and hole electron overlap were done by using Multiwfn[218] wavefunction analyzer.

2.5. Instruments

2.5.1. pH meter

A pH meter consists of a glass electrode to measure the H^+ concentration. The electrode is connected to a small electronic device to display the results. The pH of different solutions

TH-2834_146122035

were measured using Jenway 3510 and Eutech instruments (pH 700) pH meters. Calibration was done before every experiment using three standard buffer solutions (pH 4.0, pH 7.0 and pH 9.2) within a range of ± 0.01-0.02 units.

2.5.2. UV-visible spectrophotometer

UV-visible or absorption spectrophotometer is an instrument that measures the absorption wavelength and molar extinction coefficient of the chromophore. It consists of two light sources (for UV and visible range), a monochromator (for wavelength segregation), a detector (to detect the incoming light), an amplifier (to amplify signals) and a recorder (**Figure 2.1**).

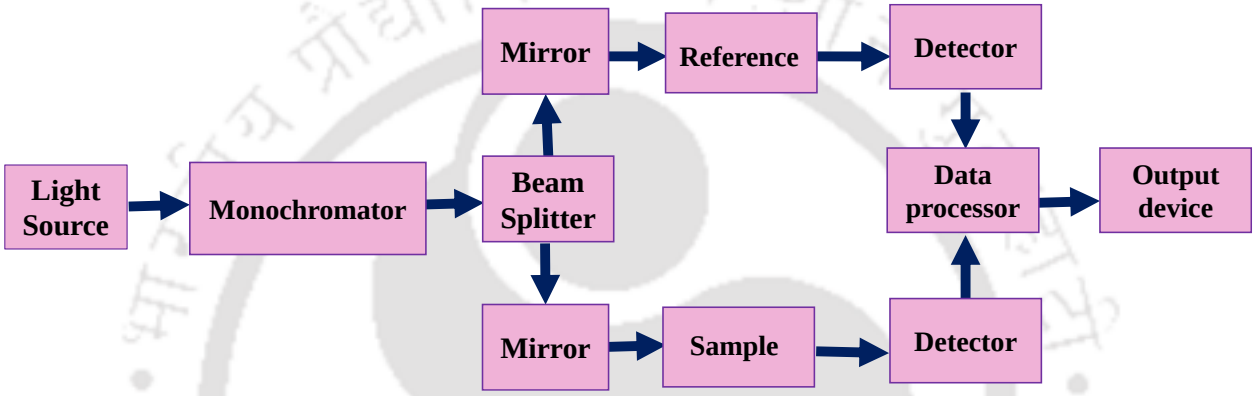

Figure 2.1. Block diagram of a double beam UV-visible spectrophotometer.

In the present work, the absorption spectra were recorded on a Perkin Elmer Lambda 35 double beam UV-visible spectrometer. It uses deuterium (for UV) and tungsten (for visible) lamps as light sources. It has two photo-diode detectors each for reference and sample beams.

2.5.3 Steady state fluorimeter

Steady state measurements are carried out by constantly illuminating a sample with a continuous source of light.[1] The rate of excitation and emission are equal in this case. Hence, this state is called a steady state. The basic components of a steady state fluorimeter are a light source (Xenon arc lamp), excitation and emission monochromators (diffraction gratings), a detector and a recorder (computer).

2.5.3.1 Basic parts of a fluorimeter

The optics of a fluorimeter contains a light source, a sample holder, monochromators, shutters, polarisers if necessary, and a beam splitter consisting of a quartz plate reflecting a fraction of the exciting light towards a quantum counter or a photodiode (**Figure 2.2**). Fluorescence is collected at 90° with respect to the incident light, i.e. the placement of light source and detector are at the right angle to each other. Most of the fluorimeters use xenon

TH-2834_146122035

lamp as the light source. It provides a relatively uniform intensity from UV to near infra-red. Monochromators are used to select excitation and emission wavelengths. Diffraction gratings are usually utilised as monochromators. Motorised monochromators are used for the automatic scanning of wavelengths.

Emission Spectrum: It represents the emitted photons count over a chosen wavelength range by keeping the excitation wavelength fixed. Usually, emission spectra and quantum yields are independent of excitation wavelength.

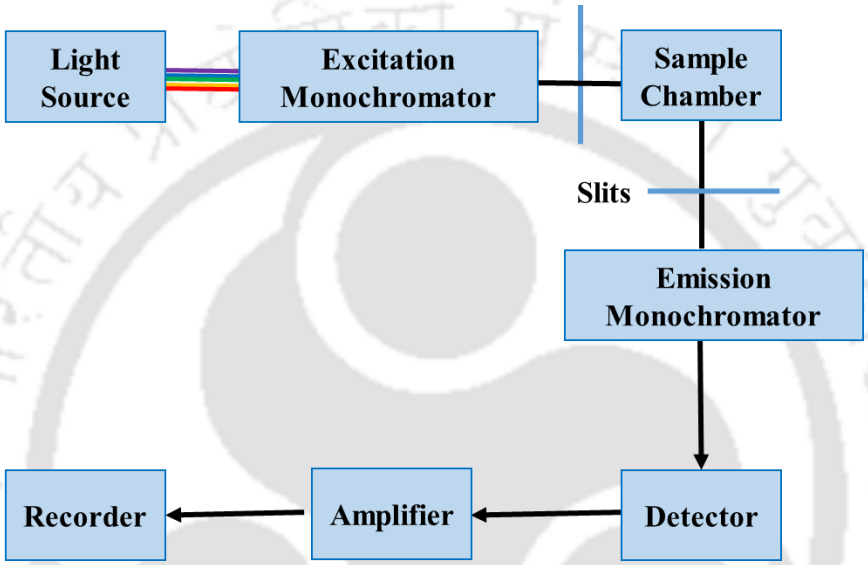

Figure 2.2. Block diagram of steady state fluorescence spectrophotometer.

Excitation Spectrum: It represents the relative emission at a particular emission wavelength of the fluorophore at each excitation wavelength. The excitation spectrum of a fluorophore can be usually superimposed on its absorption spectrum. However, exact matching absorption and excitation spectra are rarely observed because the excitation intensity is different at each wavelength.

The spectra are recorded as a function of wavelength and not wavenumber because the monochromators employ diffraction gratings. For a given input and output slit widths, the monochromators operate at a constant bandpass expressed in wavelength (nm).

The fluorescence spectra are corrected for the distortion caused by the wavelength dependence of several instrumental components.

Spectral correction for emission spectra

The distortion in the emission spectrum is due to the wavelength dependence of the emission monochromator efficiency and detector response. The correction factors are

TH-2834_146122035

measured by a calibrated tungsten lamp or a standard fluorescent dye whose corrected emission spectrum is available.

Spectral Correction for excitation spectra

The excitation spectrum is distorted due to the wavelength dependence of the lamp intensity and transmission efficiency of the excitation monochromator. The ratio of the fluorescence signal from the sample to that of the photodiode (as a function of λ_{ex}) provides the corrected excitation spectra. However, such correction procedures may not suffice for correct measurements (e.g. for comparing absorption and excitation spectra). The optical geometry of the reference channel is not identical to the main channel. The wavelength dependence of optical parts (e.g. focal length of lenses) may introduce some distortion too. It is then recommended to use correction factors obtained by using a fluorescent compound that absorbs in the same wavelength range as the sample and has identical absorption and excitation spectra. The ratio of the excitation spectrum to the absorption spectrum of this reference provides the correction factors that can be stored in the computer. Spectrofluorometers with photodiode need further correction because the wavelength response of the photodiode is not linear over the complete wavelength range. Most commercially available instruments come with a file containing the correction factors.

Jobin-Yvon Fluoromax 4 and Fluoromax+ spectrofluorometers were used for this work to record emission and excitation spectra. Both the Fluoromax models have single excitation monochromators. Fluoromax 4 has 150 W Xe arc lamps as the light source. They use Hamamatsu red-sensitive PMT detector. The corrected spectra were recorded using the instrumental correction factors provided by the manufacturer.

2.5.4. Time resolved fluorimeter

The fluorescence decay of an excited fluorophore can be expressed as:

$$I(t) = I_0 e^{-\frac{t}{\tau}} \qquad (2.3)$$

I_0 is the fluorescence intensity at time 0 after the photoexcitation and $I(t)$ is the emission intensity after the time t. τ is the excited state lifetime of the molecule. τ is the time needed to drop $I(t)$ by 1/e (~37%). The fluorescence lifetime can also be expressed as

$$\tau = \frac{1}{k_r + k_{nr}} \qquad (2.4)$$

k_r and k_{nr} are radiative and non-radiative rate constants, respectively. Fluorescence lifetime is an intrinsic property of a fluorophore and is independent of how it is measured. It is a state function independent of fluorophore concentration, excitation wavelength, one- or multi- photon excitation, duration of light exposure and fluorescence intensity. It is unaffected

TH-2834_146122035

by photobleaching. As fluorescence occurs from an energetically unstable state. Therefore, the fluorescence lifetime is sensitive to internal and external factors. The internal factor is fluorophore structure and the external factors are polarity, temperature, viscosity and fluorescence quenchers etc.

The fluorescence lifetime of fluorophores are measured in frequency-domain or time-domain.[13] They have different instrumentation setups and follow different data acquisition methods. However, both approaches are mathematically equivalent and their data can be interconverted by Fourier transformation. In the frequency domain, the incident light is sinusoidally modulated at high frequencies such that the emission occurs at the same frequency as the incident light. The difference between the incident and emitted light is that the emitted light experiences a phase delay, and the amplitude of the emitted light is changed relative to the excitation light (demodulation). Data are acquired with photomultipliers or charge-coupled devices (CCD) equipped with a gain modulator.

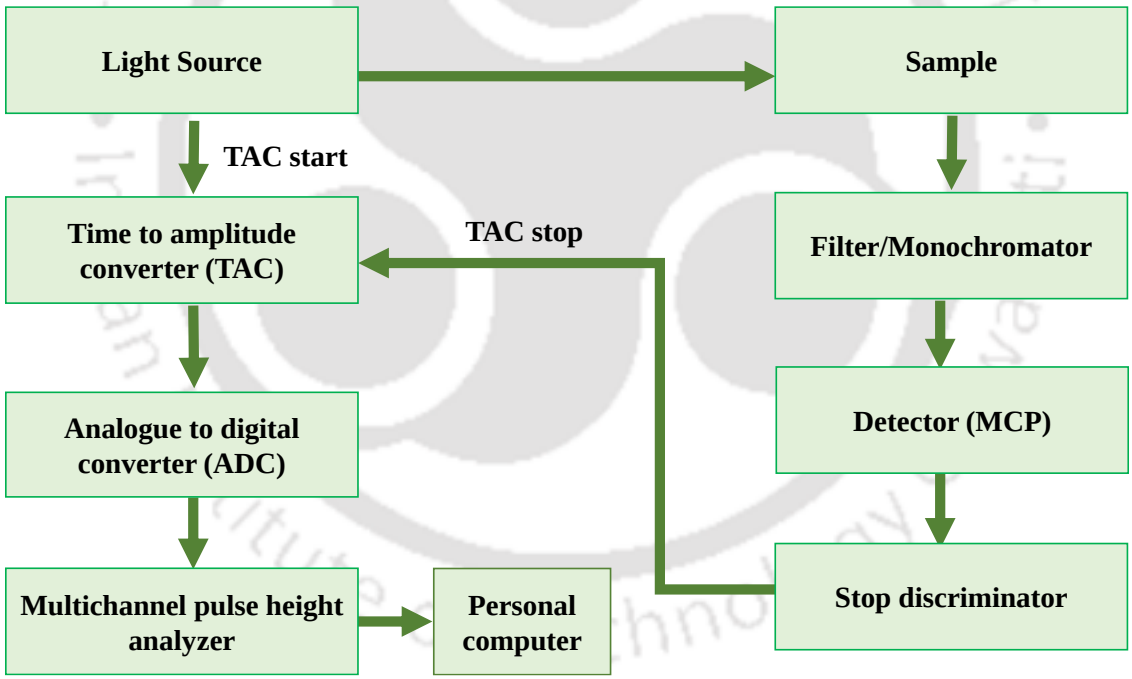

Figure 2.3. Block diagram of a TCSPC instrument.

In the time-domain, the sample is excited with a short light pulse from a flash lamp, pulsed laser, laser diode, or LED with sufficient delay between pulses. Various methods are available for data collection. Time-correlated single photon counting (TCSPC) which is used in this work.[13] **Figure 2.3** explains the working principle of a TCSPC instrument. The TCSPC method needs a highly repetitive light source to accumulate sufficient photons. The source light

TH-2834_146122035

beam is split into the start and stop signal pulses. The start pulse travels to a micro-channel plate (MCP) photomultiplier tube (PMT), which activates the time-to-amplitude converter (TAC). The stop pulse travels through the sample. The growth of the ramp signal in TAC is stopped by this pulse. The TAC output can be amplified by an amplifier, and this analogue pulse of height equal to a measured time of the signal goes through an analogue to digital converter (ADC).

The photons are not emitted all at once but with different relaxation times following their excitation. TCSPC detects and measures single photon arrival times to a reference signal from the light source. The time measurement of the start and stop sequence is represented by increasing the histogram memory value. Thus, this experiment should be repeated many times to collect sufficient photons in the full range of excitation and emission delays.

It is a statistical method and requires excellent statistical data precision. The resulting histogram of counts versus the time channels represents the fluorescence decay profile.

In this work, fluorescence lifetimes were measured with the LifeSpec II instrument from Edinburgh Instruments. It has a Hamamatsu MCP detector that has a 50 ps response time. The excitation light sources used were 290 nm, 308 nm and 336 nm LED from PicoQuant and 375 nm laser diode from Edinburgh. Data were analysed by Discrete Component Analysis using the FAST software provided by the manufacturer. χ^2 and residual plots determined the goodness of fit.

2.5.5. Other instruments

Fourier transformed nuclear magnetic resonance (FTNMR) spectra were recorded as the standard for ^{1}H nuclei on AVANCE III 600 MHz NMR spectrometer from Bruker. The high resolution mass spectrometry (HRMS) data was obtained on Agilent technologies' Waters Instruments (Q-Tof Premier). Single crystal X-ray diffraction was recorded on Bruker SMART APEX-II CCD diffractometer. Structural illustrations were drawn with MERCURY for Windows.

TH-2834_146122035

TH-2834_146122035

Chapter 3

The Origin of Longer Wavelength Emission in 2-(4-Fluorophenylamino)-5-(2,4-dihydroxybenzeno)-1,3,4-thiadiazole and its Analogue 2-Phenylamino-5-(2-hydroxybenzono)-1,3,4-thiadiazole

TH-2834_146122035

TH-2834_146122035

3.0. Introduction

2-Amino-1,3,4-thiadiazoles show a broad spectrum of medicinal properties[219] such as anticancer,[220] antimicrobial,[221,222] antiinflammatory,[223] antidepressant,[224] anticonvulsant,[225] antifungal,[226,227] etc. 2-(4-Fluorophenylamino)-5-(2,4-dihydroxybenzeno)-1,3,4-thiadiazole (FABT, **Chart 3.1**) is an important molecule of this class. Researchers have studied FABT for its pharmacological properties, in particular, the anticancer activity.[203,228,229]

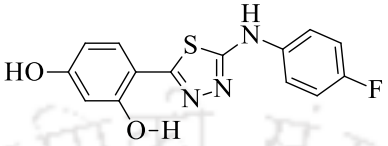

2-(4-Fluorophenylamino)-5-(2, 4-dihydroxybenzeno)-1,3,4-thiadiazole (FABT)

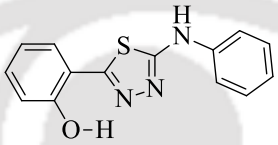

2-(Phenylamino)-5-(2-hydroxybenzono)-1,3,4-thiadiazole (PHBT)

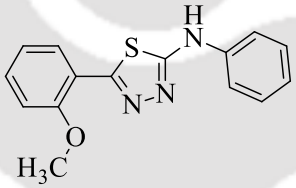

2-(Phenylamino)-5-(2-methoxybenzono)-1,3,4-thiadiazole (PMBT)

Chart 3.1. Structures of FABT, PHBT and PMBT.

Photophysical properties of FABT and a few other 1,3,4-thiadiazoles are reported.[204,230–232] Gagoś et al. studied the polymorphism, solvatochromism and prototropism of FABT.[204,232,] They observed dual emission of FABT in water.[204] They attributed this dual emission to two factors, the specific conformational change and aggregation. They assigned the longer wavelength absorption and emission bands to the enol conformer. However, the keto tautomer usually absorbs and emits at a longer wavelength than the normal/enol form. In suitable conformers of FABT and similar molecules, excited state intramolecular proton transfer (ESIPT) is feasible. Therefore, the viability of ESIPT in a structurally similar 2-amino-1,3,4-thiadiazoles was studied. To understand the ground state and the dual fluorescence of 2-amino-1,3,4 thiadiazole molecules with 'phenolic' substitution, 2-(phenylamino)-5-(2-hydroxybenzono)-1,3,4-thiadiazole (PHBT) and its methoxy derivative (PMBT) (**Chart 3.1**) were synthesized. PHBT is a structurally similar but simpler molecule than FABT. It has phenol in place of the resorcyl ring and does not have fluorine substitution. PMBT has a

TH-2834_146122035

methoxy group in place of hydroxyl. In PMBT, the acidic 'OH' proton is replaced by a methyl group. Therefore, it cannot undergo ESIPT to form a keto tautomer.

3.1. Spectral characteristics of PHBT and PMBT

3.1.1. The excited state proton transfer

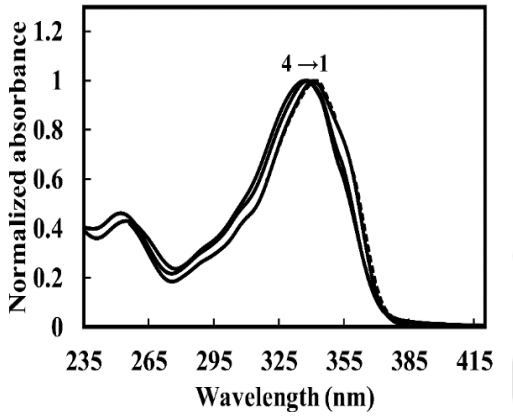

Figure 3.1. (a). Normalized absorption spectra of PHBT in toluene (1), ethyl acetate (2), acetonitrile (3) and methanol (4).

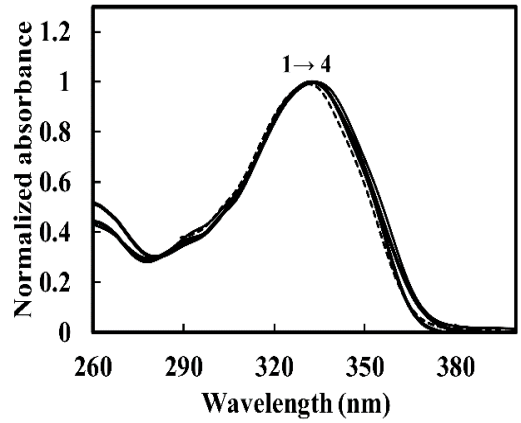

Figure 3.1. (b). Normalized absorption spectra of PMBT in toluene (1), ethyl acetate (2), acetonitrile (3) and methanol (4).

Figure 3.1. (a) shows the absorption spectra of PHBT in selected solvents. The complete data in all studied solvents are in **Table 3.1**. Like FABT[204], PHBT has maximum absorbance around 340 nm. This longer wavelength absorption maximum is blue shifted in PMBT in most of the solvents (**Figure 3.1. (b) and Table 3.2**). This blue shift is also observed upon methoxy substitution in other ESIPT molecules.[183,205,206] It is because the 'OH' proton of the hydroxyl derivative forms an intramolecular hydrogen bond, and the methoxy derivative cannot. In hydrogen bond accepting polar solvents like DMF and DMSO, the difference in the spectral maxima is small. The absorption spectra of PMBT are little red shifted compared to

TH-2834_146122035

TH-2834_146122035

Table 3.1. Experimental absorption band maxima (λ_{abs}, nm), log ε_{max}, fluorescence emission band maxima (λ_{em}, nm) and relative fluorescence yield (F) of PHBT in different solvents.

Solvent	λ_{abs} (log ε_{max})	λ_{em} (F)[a]	$\tilde{\nu}_{ss}$ (cm^{-1})[b]	$\tilde{\nu}_{ss}'$ (cm^{-1})[b]	I_T/I_N[c]
Toluene	343 (4.30)	395 (0.0008), 531 (0.0031)	3838	10322	1.9
1,4-Dioxane	341 (4.26)	395 (0.02), 520 (0.0003)	4009	10095	0.12
Tetrahydrofuran	341 (4.26)	400 (0.02), 526 (0.0002)	4326	10168	0.17
Ethyl acetate	341 (4.48)	397 (0.03), 530 (0.0002)	4137	10458	0.13
Acetonitrile	337 (4.25)	412 (0.01)	5402		
N,N-Dimethyformamide	340 (4.39)	409 (0.25)	5081		
Dimethyl sulphoxide	338 (4.25)	416 (0.42)	5547		
1-Propanol	341 (4.58)	408 (0.11)	4816		
1-Butanol	342 (4.58)	410 (0.12)	4850		
2-Butanol	342 (4.48)	411 (0.12)	4909		
2-Propanol	340 (4.26)	408 (0.14)	4902		
Methanol	335 (4.38)	425 (0.04)	6321		

[a]*Values in parenthesis are relative fluorescence yields.*[26]

[b]$\tilde{\nu}_{ss}$ and $\tilde{\nu}_{ss}'$ are Stokes' shifts for shorter and longer wavelength emission respectively.

[c]I_T/I_N *represents the longer wavelength band's relative intensity with respect to the shorter wavelength band.*

the hydroxyl derivative. It may be due to the formation of a *trans*-enol conformer, which does not have the intramolecular hydrogen bond (see later).

Table 3.2. Experimental absorption band maxima (λ_{abs}, nm, log ε_{max}), fluorescence emission band maxima (λ_{em},nm), quantum yield (Φ), Stokes' shift ($\tilde{\nu}_{ss}$, cm^{-1}) of PMBT in different solvents.

Solvent	λ_{abs} (log ε_{max})	λ_{em} (Φ)	$\tilde{\nu}_{ss}$
Toluene	335 (4.48)	390 (0.31)	4210
Ethyl acetate	331 (4.48)	396 (0.27)	5086
1,4-Dioxane	334 (4.26)	403 (0.33)	4877
Tetrahydrofuran	336 (4.30)	406 (0.47)	5607
Acetonitrile	332 (4.16)	415 (0.01)	6197
N,N-Dimethyformamide	339 (4.26)	418 (0.44)	5969
Dimethyl sulphoxide	340 (4.26)	416 (0.35)	5545
1-Propanol	336 (4.50)	417 (0.24)	5781
1-Butanol	336 (4.00)	418 (0.36)	5838
2-Butanol	336 (4.48)	418 (0.30)	5838
2-Propanol	335 (5.20)	418 (0.21)	5927
Methanol	331 (5.15)	426 (0.01)	6737

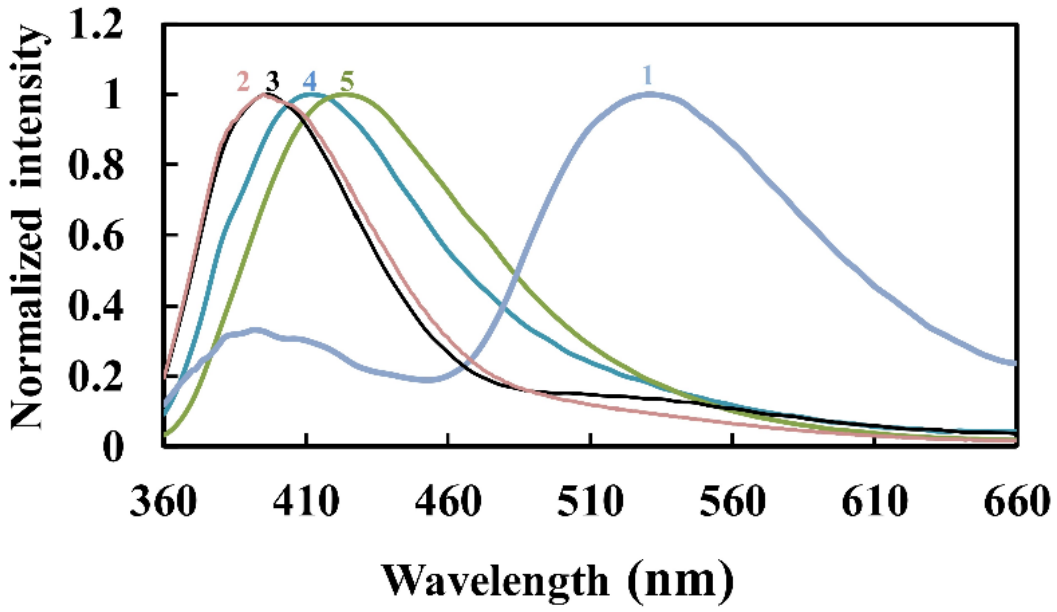

Figure 3.2. Normalized emission spectra of PHBT in toluene (1), dioxane (2), ethyl acetate (3), acetonitrile (4) and methanol (5), λ_{ex} = 340 nm.

PHBT gives dual emission in nonpolar solvents (**Figure 3.2, Table 3.2**). The significant Stokes' shift observed for the longer wavelength emission suggests a substantial change in this emitting state's molecular structure. The intensity of the longer wavelength emission is greater than, the shorter wavelength emission in toluene. The relative intensity for shorter is to longer wavelength band decreases with the increase in polarity. Even in a solvent such as dioxane, the shorter wavelength emission is predominant over the longer wavelength emission. The shorter wavelength emission undergoes a bathochromic shift with an increase in solvent polarity and hydrogen bonding capacity (**Table 3.1**). It is because polar solvents stabilize the excited state

TH-2834_146122035

more than the ground state. This relative stabilization decreases the energy gap between the two states that results in a bathochromic shift.

On the other hand, the increase in solvent polarity produces a hypsochromic shift in the longer wavelength emission. This shows that the excited state is less polar compared to the corresponding ground state. Such a nature is a characteristic feature of the keto emission in the ESIPT molecules.[97,115,120,233] The calculated dipole moment of the keto tautomer (8.5 D in the ground state and 3.3 D in the excited state) confirms this. Therefore, the longer wavelength emission can be assigned to the keto tautomer emission. The shorter wavelength fluorescence corresponds to the normal emission from the excited enol. The calculated ground state dipole moment and the excited state dipole moment of the *trans*-enol are 4.7 D and 13.9 D, respectively. This is consistent with the red shift of the normal emission with an increase in polarity.

Table 3.3. Theoretically calculated emission wavelength maximum for enol and keto species of PHBT in few selected solvents.

Solvent	λ_{em}^{enol} (nm)	λ_{em}^{keto} (nm)
Cyclohexane	350	486
Toluene	350	471
THF	422	441
Methanol	416	–

The DFT calculations also predicted that the emission maximum of the normal emission is red shifted and that of the keto tautomer emission is blue shifted (**Table 3.3**).

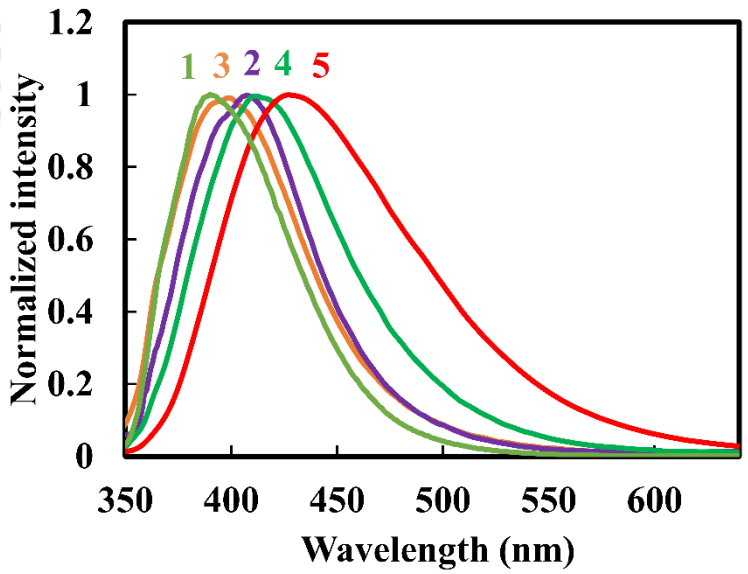

Figure 3.3. Normalized emission spectra of PMBT in toluene (1), dioxane (2), ethyl acetate (3), acetonitrile (5) and methanol (5), λ_{ex} = 330 nm.

TH-2834_146122035

To confirm the longer wavelength emission assignment to the keto tautomer formed by ESIPT, the emission characteristics of the methoxy derivative, PMBT, were studied. PMBT emits only one emission. Similar to the normal emission of the PHBT, a bathochromic shift is observed in the fluorescence spectrum of PMBT with an increase in polarity and hydrogen bonding capability of the solvent. In PMBT, the acidic 'OH' proton is replaced by the methyl group and therefore, it cannot undergo ESIPT to form the keto tautomer. The absence of the longer wavelength emission from the excited methoxy derivative confirms that the longer wavelength in the hydroxyl derivative (PHBT) is due to keto fluorescence (**Figure 3.3**).

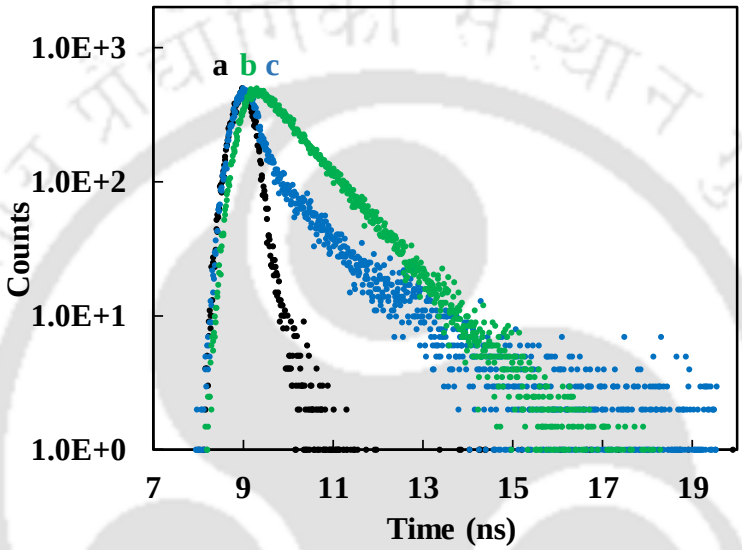

Figure 3.4. Fluorescence decay of PHBT monitored at (b) λ_{em} = 395 nm and (c) λ_{em} = 520 nm in 1,4-dioxane, λ_{ex} = 336 nm, (a) Instrument response function.

Table 3.4. Fluorescence lifetime (τ, ns) of PHBT and PMBT, λ_{ex} = 336 nm.

	PHBT		PMBT	
Solvent	**λ_{em}^{mon} (nm)**	**τ (ns)**	**λ_{em}^{mon} (nm)**	**τ (ns)**
Toluene	532	0.15 (63.1 %) 2.65 (36.9 %)	390	0.84 (100 %)
1,4-Dioxane	399 523	1.38 (100 %) 0.06 (56.7 %) 1.29 (43.3 %)	386	1.08 (100 %)
Tetrahydrofuran	400	1.08 (100 %)	397	1.51 (100 %)
Ethyl acetate	398	0.88 (100 %)	397	1.32 (100 %)
Dimethyl sulphoxide	425	1.88 (100 %)	420	1.77 (100 %)
N,N-Dimethyformamide	409	1.75 (100 %)	418	1.76 (100 %)
1-Propanol	408	1.49 (100 %)	420	1.38 (100 %)
2-Butanol	408	1.62 (100 %)	416	1.53 (100 %)
1-Butanol	415	1.54 (100 %)	420	1.45 (100 %)
2-Propanol	430	1.49 (100 %)	413	1.40 (100 %)
Methanol	425	1.01 (100 %)	428	0.90 (100 %)

TH-2834_146122035

The fluorescence decay of the normal emission of PHBT is single exponential and is about 1–2 ns (**Figure 3.4(b) and Table 3.4**). These lifetimes match with the fluorescence lifetime of the methoxy derivative. The fluorescence decays of PHBT monitored at the longer wavelength are biexponential decay (**Figure 3.4(c) and Table 3.4**). The relative amplitude of the shorter lifetime is greater than that of the longer lifetime species (**Table 3.4**). Therefore, the shorter lifetime can be assigned to the keto tautomer. The other lifetimes correspond to the normal emission. The lifetime data thus substantiate the assignment of shorter wavelength and longer wavelength emissions to the normal emission and tautomer emission, respectively.

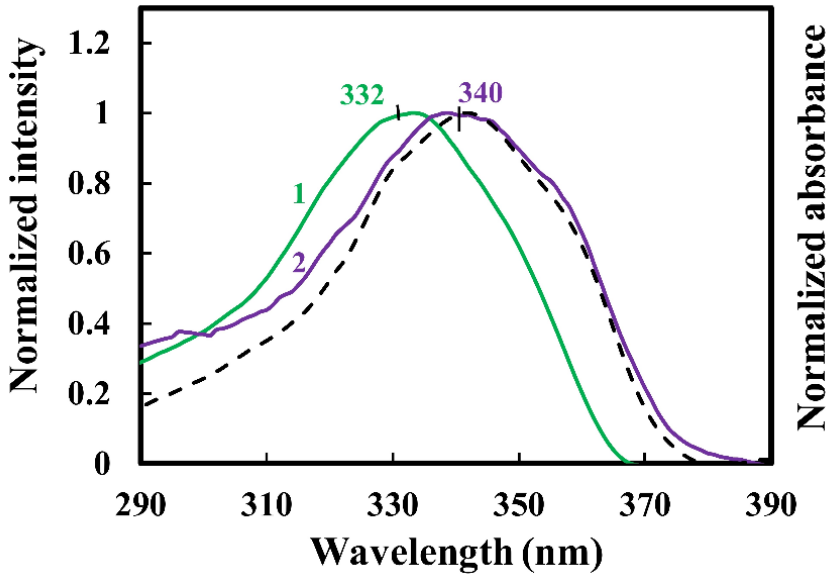

Figure 3.5. The excitation spectra of PHBT in dioxane at λem = 400 nm (1) and 520 nm (2) along with its absorption spectrum (dashed line).

Since the excitation spectrum provides the information about the ground state species which is excited, the excitation spectra were recorded at emission wavelengths. The excitation spectra of both emissions are different (**Figure 3.5**). This shows that both emissions originate from different ground states.

3.2. Ground state equilibrium

Based on the "OH" group orientation, FABT and PHBT can exist in two conformers (**Chart 3.2**). Gagoś et al. label the two conformers as "S" and "N" conformers.[204] In the "N" conformer, the "OH" group is oriented towards the thiadiazole nitrogen and an intramolecular hydrogen bond exists between the "OH" group and the thiadiazole nitrogen. In the "S"

TH-2834_146122035

conformer, the "OH" group is oriented towards the thiadiazole sulphur and therefore, intramolecular hydrogen is not feasible.

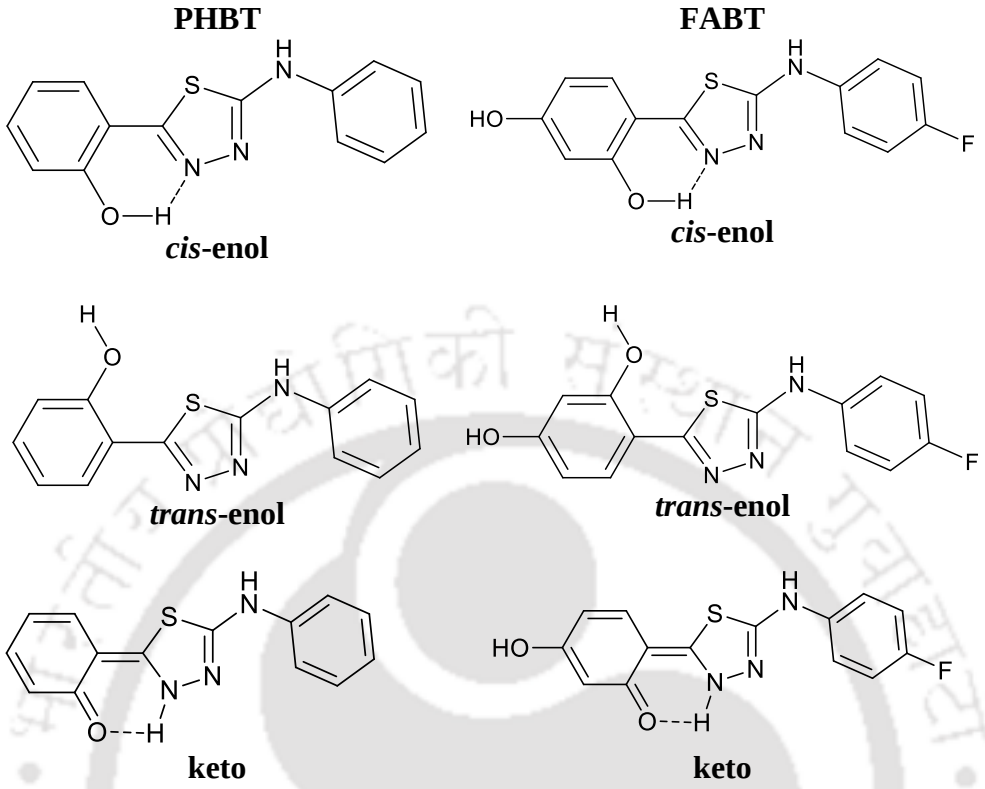

Chart 3.2. Different conformers and tautomers of PHBT and FABT.

Conventionally, the conformer that possesses the intramolecular hydrogen bond in ESIPT molecules is labelled as *cis*-enol and the other conformer is called as *trans*-enol.[115] By the convention, the "N" and or "S" conformers (labeled by Gagoś et al.) are referred to as *cis* and *trans* conformers (**Chart 3.2**) in this work.

The ground state geometries of both the conformers of PHBT were optimized by the DFT method (**Figure 3.6**). The *cis*-enol is more stable than the *trans*- enol (**Table 3.5**).

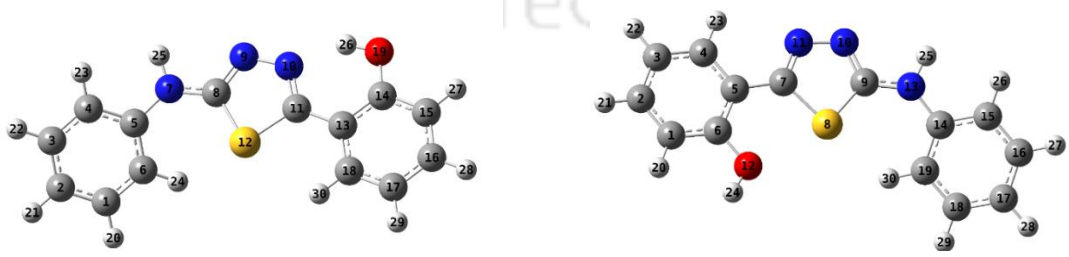

(a) **(b)**

Figure 3.6. Ground state optimized geometry of PHBT *cis*-enol (a) and *trans*-enol (b).

TH-2834_146122035

Table 3.5. Ground state optimized energies of FABT and PHBT and excitation spectral maximum (λ_{ex}, nm).

	FABT		PHBT	
	***cis*-enol**	***trans*-enol**	***cis*-enol**	***trans*-enol**
Relative energy (eV)	0.00	0.34	0.00	0.41
λ_{ex} (nm)	352	347	355 (340)	352 (332)

Values in parenthesis represent experimental data.

The stabilization of *cis*-enol over the *trans*-enol is due to the intramolecular hydrogen bond between the acidic and basic centers. Upon photoexcitation, ultrafast proton transfer occurs through this bond due to the increase in the acidity and the basicity of the acidic and basic groups, respectively.[234]

The increase in the molecular acidity and basicity is evident from the increase in the O–H bond distance and the decrease in the N- - -H hydrogen bond distance (**Table 3.6**).

Table 3.6. The O-H bond and the N···H hydrogen bond distance of the *cis*-enol in the ground and the excited states.

	FABT		PHBT	
	S_0	**S_1**	**S_0**	**S_1**
O-H (Å)	0.993	0.996	0.991	0.993
N···H (Å)	1.745	1.732	1.756	1.746

Since the *trans*-enol lacks the intramolecular hydrogen bond, it emits normal emission. In protic solvent, the intermolecular hydrogen bond interferes with the intramolecular hydrogen bond and the breaking of the intramolecular hydrogen bond decreases the relative population of *cis*-enol, leading to the formation of solvated enol (**Chart 3.3**). Since the solvated enol does not possess the intramolecular hydrogen bond, only the normal emission is observed in protic solvents. Due to the same in other ESIPT active molecules also, it was found that the relative intensity of the normal emission increased in protic solvents compared to in aprotic solvents.[36,115,235]

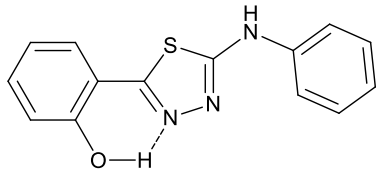

(I)

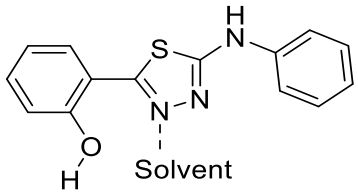

(II)

Chart 3.3. *cis*-enol and solvated enol conformers of PHBT.

TH-2834_146122035

The excitation spectrum of the longer wavelength emission is red shifted compared to the excitation spectrum of the shorter wavelength emission (**Figure 3.5**). Therefore, the 340 nm and 332 nm excitation spectra can be assigned to *cis*-enol and *trans*-enol, respectively. The bathochromic shift in the excitation spectrum of *cis*-enol compared to *trans*-enol is due to the intramolecular hydrogen bond. The theoretically predicted excitation maxima are also in good agreement with the experimental excitation spectral maxima (**Table 3.4**).

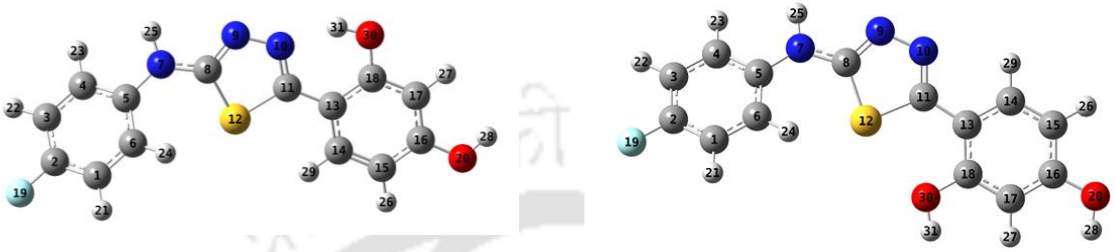

(a) **(b)**

Figure 3.7. Ground state optimized geometry of FABT *cis*-enol (a) and *trans*-enol (b).

The geometries of both the conformers of FABT were also optimized (**Figure 3.7**). Similar to the *cis*-enol of PHBT, the *cis*-enol of FABT is more stable than its *trans*-enol (**Table 3.5**). Gagoś et al. also reported that the *cis*-enol is more stable than *trans*-enol.[204] The longer wavelength absorption maximum of FABT is close to the theoretically predicted absorption maxima of *cis*-enol of FABT. The observation of the keto emission being longer than the enol emission specifies that the energy gap between the first excited state and the ground state is lesser in the keto than the enol form. Therefore, like the emission spectrum, the absorption spectrum of the keto tautomer should also be red shifted compared to the absorption spectrum of the enol.[236] As established earlier, the 340 nm band corresponds to the enol form. Gagoś et al. also assigned the 340 nm band to the enol form. However, similar to its analogue PHBT, no absorption band is observed for FABT at longer wavelength than the 340 nm absorption band of enol.[204] This suggests that FABT exists as enol and not as the keto tautomer in the ground state. To substantiate further, the keto geometry of FABT was put for optimization in the ground state to calculate its absorption theoretically. But attempts to optimize the keto geometry in the ground state resulted in the *cis*-enol. This states that the keto form is not stable in the ground state. This confirms that FABT exits as an enol, not in the keto form in the ground state. The relative fluorescence intensity of the tautomer emission (with the respective normal emission) is less in PHBT (**Table 3.1**) than in similar oxadiazole and triazole derivatives.[52,63] This may be the effect of the thiadiazole ring of PHBT. Similar behaviour was observed in

TH-2834_146122035

hydroxyphenylbenzthiazole than in the corresponding benzoxazole and benzimidazole derivatives.[115,174]

3.3. Aggregation assisted ESIPT

Table 3.7. The fluorescence maximum (λ_f^{max}, nm) and Stokes' shift ($\bar{\nu}_{ss}$, cm^{-1}) of the emissions.

	Shorter Wavelength		Longer Wavelength	
	λ_f^{max}	$\bar{\nu}_{ss}$	λ_f^{max}	$\bar{\nu}_{ss}$
FABT (in water, at pH = 7)[a]	410	5776	500	9425
PHBT (in water, at pH = 7)	425	6592	515	10703
PHBT (in cyclohexane)	410	4240	536	10721
PHBT (in toluene)	395	3838	531	10322

[a]*From reference* [204].

The absorption maximum in water at basic pH (13.0) is red shifted compared to that in neutral pH (7.2) (**Figure 3.8**). This is typical of phenolic compounds on deprotonation.[115] The spectral red shift occurs due to increased conjugation in the phenoxide ion compared to phenol.

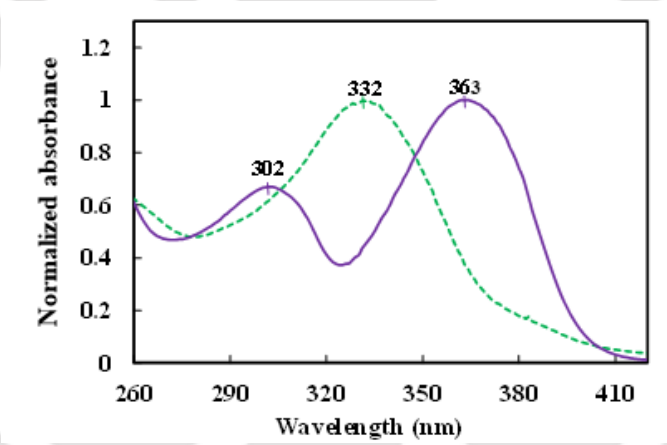

Figure 3.8. Normalized absorption spectra of PHBT in the water of pH value 7.2 (dashed line) and 13.0 (solid line).

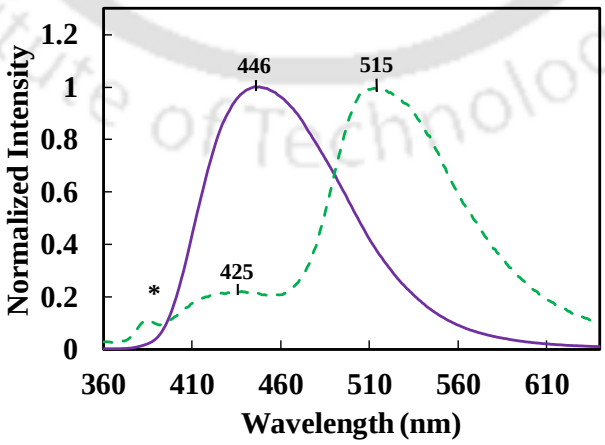

Figure 3.9. Normalized emission spectra of PHBT at pH values 7.2 (dashed line) and 13.0 (solid line) in water (λ_{ex} = 340 nm), *water Raman.

TH-2834_146122035

In an aqueous solution at neutral pH, like its analogue FABT, PHBT also emits dual emission (a strong emission at 515 nm along with a weak emission at 425 nm, **Figure 3.9, Table 3.7**). Gagoś et al. showed that at pH 7, FABT emits dual emission (**Table 3.7**).[204] They assigned the 410 nm band to the emission from the 'S' conformer. They associated the longer wavelength emission in an aqueous medium at pH 7 with the combination of aggregation and conformational change.[204] However, this proposition alone fails to explain the large difference in the emission maximum between the shorter wavelength and the longer wavelength fluorescence band and the large Stokes shift associated with the longer wavelength emission. The difference in the excitation maxima of *cis*- and *trans*- enols is only 5 nm (**Table 3.5 and Figure 3.8**). The difference in both the emission band maxima is huge (90 nm). Furthermore, since the difference in the excitation spectral maximum of both the conformers is very small, the difference in the Stokes shift of the emission spectra of both the conformers is also expected to be similar. The difference in the Stokes shift between the two emissions for both the molecules in water is large (**Table 3.7**). However, the Stokes shift of the shorter wavelength and the longer wavelength emission in water are comparable to that of the normal emission and tautomer emission. This shows that the longer wavelength emission cannot be assigned to the enol emission and clearly indicates that the longer wavelength emission is the tautomer emission from the keto tautomer. To confirm the assignment further, the emission maximum of the keto form of FABT were theoretically calculated using water as the solvent. Thus, the calculated emission maximum of 494 nm is in agreement with the experimental value (500 nm). The assignment of the longer wavelength emission to the tautomer emission can be easily confirmed in an aqueous solution. If the 'OH' proton (that is transferred during ESIPT) is removed by deprotonation, the ESIPT is not feasible. Then, the molecule can emit only the normal emission but not the tautomer emission (only a single emission will be observed). Upon deprotonation in the basic solution, no dual emission is observed from PHBT, and it emits only a single emission at 446 nm (**Figure 3.9**). Gagoś et al. also reported that in an alkaline solution at pH 12.0, FABT emits a single emission (431 nm).[204] Observation of the single emission upon deprotonation confirmed the dual emission attribution to ESIPT and the longer wavelength emission to the tautomer emission. The anionic fluorescence in PHBT and FABT are red shifted compared to the enol emission (normal fluorescence), but blue shifted relative to keto fluorescence (tautomer emission). It is typical behaviour of the anionic fluorescence in ESIPT molecules.[237,238] This is because the anion is formed from the enol form by the deprotonation of the 'OH' proton which increases the conjugation. The polarity and protic nature of the solvent favour the *trans*-enol. Water is the most polar and protic solvent. Nonetheless, not only

TH-2834_146122035

the relative intensity of the tautomer is higher than that of other solvents such as ethyl acetate, but the intensity of the tautomer emission is also higher than that of the normal emission (the intensity ratio of the tautomer emission to the normal emission is more than 1.0 i.e. 1.4). Gagoś et al. have shown the FABT aggregates in water.[204] Organic molecules aggregate in water due to hydrophobic interactions. In solution, the individual solute molecules are present in the solvent cage surrounded by solvent molecules in all directions. In the aggregated state, the individual organic molecules are not surrounded by solvent molecules and have limited solvent molecules exposure. This will reduce the solvent-solute interaction in aggregates. As a result, hydrophobicity of the environment increases. The hydrophobicity of the environment favours *cis*-enol. Thus, the *trans*-enol equilibrium towards the *cis*-enol in the aggregates is comparable to that in solution. This causes an enhancement in the tautomer emission. Such an aggregation induced enhancement in the tautomer emission was reported in several ESIPT exhibiting molecules. The tautomer emission of HPBI was reported to be enhanced due to the shift in the equilibrium.[115] A bis-hydroxyphenylbenzothiazole derivative emits an exclusive tautomer emission upon aggregation.[200] Another chloro substituted hydroxyphenylbenzothiazole derivative was shown to exhibit an enhanced keto emission in water due to aggregation.[201] More recently, a tetraphenylethylene based dye was reported to undergo aggregation assisted ESIPT in 99 : 1 water : tetrahydrofuran mixture.[196] The *cis*-enol possesses the intramolecular hydrogen bond, which is the prerequisite for ESIPT. As the *trans*-enol lacks the intramolecular hydrogen bond between the proton donor and the proton acceptor, it is incapable of undergoing ESIPT. Hence, the aggregation induced conformational change aided the ESIPT and it is the cause of dual emission. Thus, emitted tautomer fluorescence is enhanced due to aggregation induced emission enhancement (AIEE).[193,194]

3.4. Conclusion

Based on the study, it can be concluded that PHBT and FABT exist as enol in the ground state. Both these molecules do not exist in the keto form in the ground state. However, keto species is formed in the excited state from the *cis*-enol by ESIPT. The single emission from the methoxy derivative supports this conclusion. The *trans*-enol upon excitation emits normal emission. The longer wavelength emissions of FABT and PHBT in aqueous solutions are due to ESIPT. In water, the aggregation of the molecules reduces the solvent-solute interaction. This shifts the equilibrium from *trans*-enol to *cis*-enol that undergoes ESIPT to form a keto tautomer. Gagoś et al. also found that in an aqueous solution, FABT undergoes aggregation and conformational change. Upon deprotonation of the 'OH' proton (involved in the proton

TH-2834_146122035

transfer), only single emission is observed from the anion. This work is published in *Photochem. Photobiol. Sci*., 2020, **19**, 844–853.

TH-2834_146122035

Chapter 4

Effect of pH and Host-Guest Complexation on PTTPT of 3,5-Bis(2-hydroxyphenyl)-1H-1,2,4-triazole

TH-2834_146122035

TH-2834_146122035

4.0. Introduction

Host-guest systems are used to tune the photophysical properties of fluorescent dyes.[133,138,151,157] Organic hosts such as CDs are popular supramolecular hosts.[153] They have been used to study the excited state processes like proton and charge transfer.[239,186] Reduction of non-radiative decay was reported as the cause of enhancement of tautomer emission in 3,5,6-trichlorosalicylic acid in CD.[155] ESIPT of 1-hydroxy-2-naphthaldehyde was studied in supramolecular assemblies of CDs and micelles.[130] Enhanced tautomer emission in the encapsulated complexes predicted favourable ESIPT reaction in these assemblies. Heptakis(2,6-di-O-methyl)-*β*-cyclodextrin was used to study salicylic acid-loaded Pluronic F127 micelles as drug nanocarriers for controlled release.[240] ESIPT of 3-hydroxyflavone was more favourable in the CD hydrophobic cavity than in an aqueous solution.[164] Abu-Zaid studied excited state intramolecular double proton transfer (ESIDPT) of 2,2′-bipyridine-3,3′-diol in CDs. The molecule remains in the di-enol conformer inside the host cavities.[241] Hazra et al. also studied this molecule in CB[7] and *β*-CD.[242] While the double proton transfer in water and *β*-CD occurs via a two-step sequential process, the mechanism changes to concerted inside CB[7].

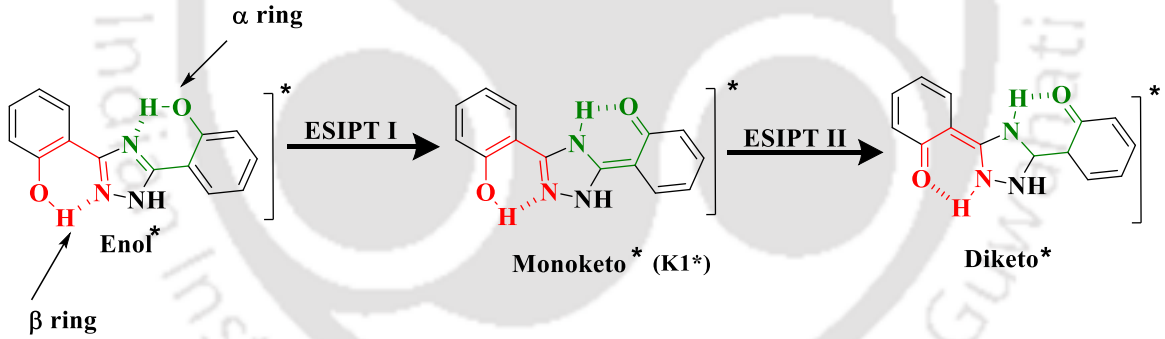

Scheme 4.1. ESIPT pathway in bis-HPTA.

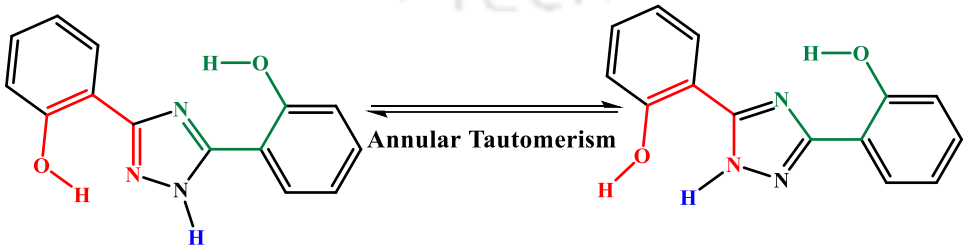

Scheme 4.2. Annular tautomerism in bis-HPTA.

TH-2834_146122035

Bis-HPTA undergoes a new type of proton transfer, PTTPT, where the first proton transfer triggers the inactive second proton transfer (**Scheme 4.1**).[205] It possesses two intramolecular cyclic rings, labelled as α and β. In β-ring, the annular tautomerism (**Scheme 4.2**) prevents the ESIPT-II. After the first proton transfer (ESIPT-I), the electronic distribution change obstructs the annular tautomerism promoting ESIPT-II. However, solvents like DMF strongly perturb PTTPT by forming intermolecular hydrogen bond complexes with the molecule and completely alter the ground state conformer equilibrium.[243] It not only prevents the PTTPT but also opens a new intermolecular proton transfer path. CDs have been used to study ESIPT and ESIDPT. [155,156,244] Hence, the effect of *β*-CD on the PTTPT of bis-HPTA are investigated. As water is used as a solvent to study the host-guest system. Therefore, the spectral properties of the molecule were first studied in an aqueous solution.

4.1. Electronic spectra of bis-HPTA in aqueous solution

4.1.1. Neutral bis-HPTA

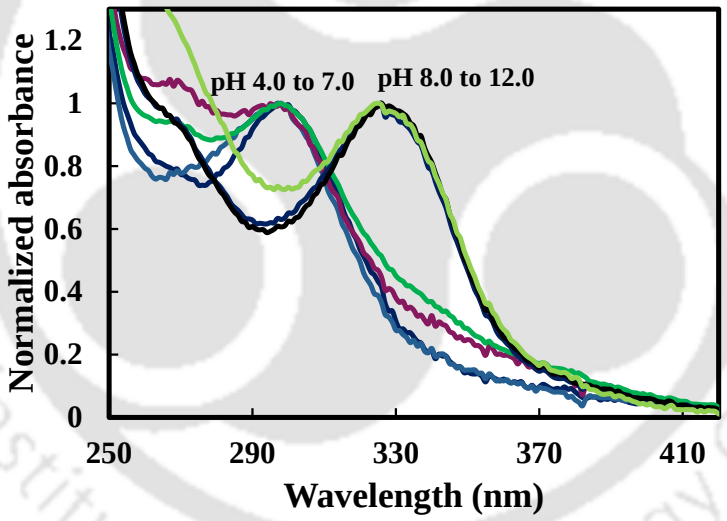

Figure 4.1. Normalized absorption spectra of bis-HPTA in the water of pH 4.0 to 12.0.

Unlike in organic solvents, the determination of pH is crucial for any study in aqueous solution. As discussed earlier, the presence of acidic and basic sites and hydrogen bonding in an ESIPT molecule are susceptible to pH change. Depending on the pH, the molecule may be in cationic, anionic or neutral form. If protonation or deprotonation does not happen at the phototautomerization site, then the molecule can still undergo ESIPT.[237,245] The absorption spectra of aqueous bis-HPTA in the pH range of 4.0 to 12.0 is given in **Figure 4.1**. The absorption maximum (λ_{ab}^{max}) of bis-HPTA in the water of pH 4.0 to 7.0 is 298 nm. This band

TH-2834_146122035

maximum is similar to the absorption maxima in organic solvents.[205]At higher pH, the λ_{ab}^{max} shifts towards red, indicating the deprotonation of the molecule.

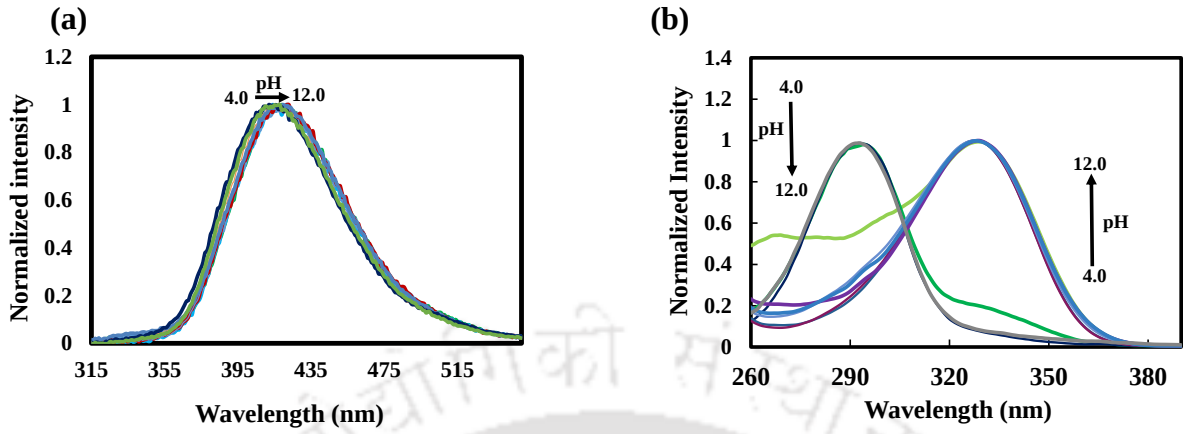

Figure 4.2. (a). Normalized emission spectra of bis-HPTA in water from pH 4.0 to 12.0, λ_{ex} = 300 nm. (b). Normalized excitation spectra of bis-HPTA in water from pH 4.0 to 12.0, λ_{em} = 420 nm.

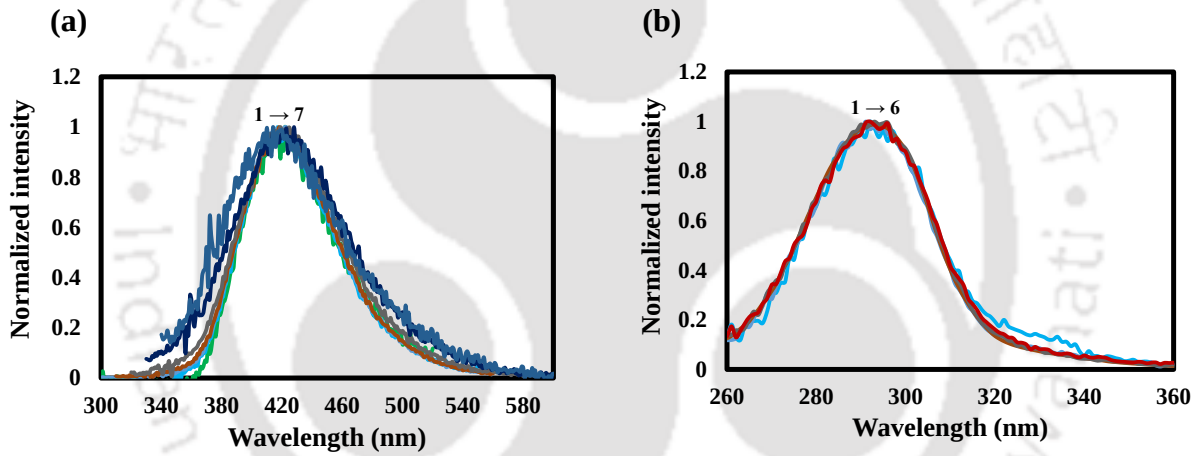

Figure 4.3. (a). Normalized emission spectra of neutral bis-HPTA in water at difference excitation wavelengths, λ_{ex} = 270 nm (1), 280 nm (2), 290 nm (3), 300 nm (4), 310 nm (5), 320 nm (6), 330 nm (7). (b). Normalized excitation spectra of neutral AHPIP-c in water at different emissions, λ_{em} = 360 nm (1), 380 nm (2), 400 nm (3), 420 nm (4), 440 nm (5), 460 nm (6).

In water (pH 4.0), the emission is observed at 420 nm and is highly Stokes' shifted (9748 cm^{-1}) than its absorption spectrum (**Figure 4.2 (a)**). Bis-HPTA emits high Stokes' shifted (10728 cm^{-1}) keto emission at ~460 nm in organic solvents.[205] The tautomer emission undergoes negative solvatochromism with an increase in polarity. The 420 nm band in water is 18 nm blue-shifted compared to the longer wavelength emission in methanol. The longer wavelength emission in other solvents (except in DMF) is due to the tautomer emission.[205,243] Therefore, the 420 nm emission band can be assigned to the tautomer formed by ESIPT. As discussed in the last chapter, the tautomer is less polar in the excited state than the ground state. The blue shift of the emission in water compared to the longer wavelength emission in organic

TH-2834_146122035

solvents supports the proposition that the tautomer emission undergoes negative solvatochromism.

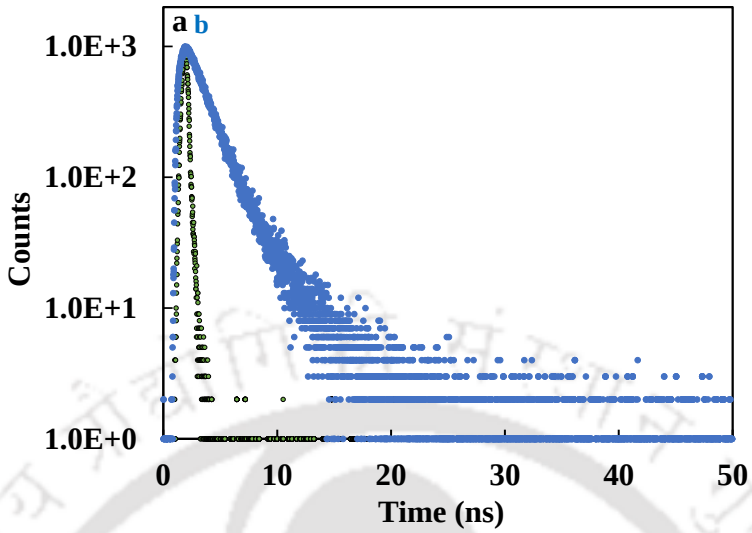

Figure 4.4. (b). Fluorescence decay of bis-HPTA in water (pH 4.0) at λ_{ex} = 308 nm and (a) IRF.

The fluorescence decay monitored at 420 nm emission of bis-HPTA in water is biexponential with lifetimes at 1.5 ns (73.3%) and 3.9 ns (26.7%) (**Figure 4.4 (b)**). The biexponential decay of the tautomer emission was also reported in other solvents.[205] As stated earlier, bis-HPTA emits two tautomer emissions; one is from the monoketo, K1 due to ESIPT-I from α-ring, and the second is from the diketo emission due to PTTPT (**Scheme 4.1**). The fluorescence lifetime of the diketo is shorter than the monoketo.[205] In methanol, the mono keto emission (52.0%) dominates over the diketo emission (48.0%). But in water, the shorter lifetime component's relative amplitude is more than the longer lifetime component. That means the diketo emission is relatively increased in water than the monoketo emission. This relative enhancement in the percentage of diketo shows that PTTPT is more favoured in water.

4.1.2. Anionic bis-HPTA

Anion absorption for this molecule in polar protic solvents and alkaline methanol was reported at ~340 nm.[205] The absorption spectra get red shifted on increasing pH. At pH 9.0, a new band appears at 328 nm (**Figure 4.1**). Bis-HPTA has three acidic centers. The acidic centers are two phenolic 'OH' and one 'NH' of the triazole ring. Deprotonation can occur at one of the acidic centers on increasing the pH. The 'OH' protons are more acidic than the 'NH' proton due to the greater electronegativity of oxygen than nitrogen. The deprotonation of 'OH' results in an increase in electron delocalization in phenolic molecules. This delocalization reduces the energy gap between the ground and excited electronic energy states, which results in a red shift in the absorption spectra. The unusual surprise is that on increasing the pH, the

TH-2834_146122035

absorption spectra (**Figure 4.1**) show anion formation, but the emission spectral maximum (**Figure 4.2 (a)**) is affected very little. However, the excitation spectrum is similar to the absorption spectrum of the anion (**Figure 4.2 (b)**). This confirms that the ground state precursor for the emission at higher pH (> 9.0) is the anion. In ESIPT molecules, the anion's emission spectrum is red-shifted with respect to normal emission and blue-shifted than the tautomer emission.[237,238]

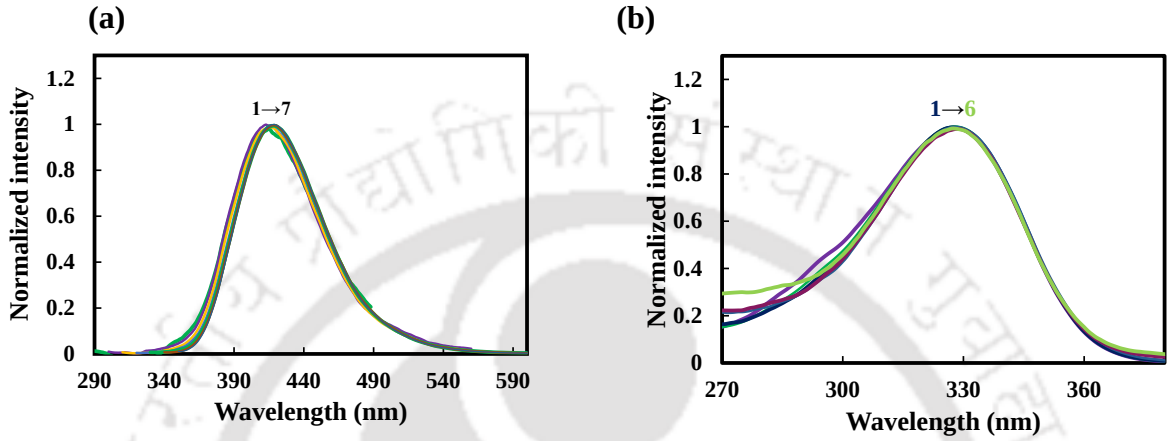

Figure 4.5. (a). Normalized emission spectra of anionic bis-HPTA in water, λ_{ex} = 270 nm (1), 280 nm (2), 290 nm (3), 300 nm (4), 310 nm (5), 320 nm (6), 330 nm (7). (b). Normalized excitation spectra of anionic bis-HPTA in water, λ_{em} = 400 nm (1), 420 nm (2), 440 nm (3), 460 nm (4), 480 nm (5), 500 nm (6).

The anion is formed from the enol form by the deprotonation of the 'OH' proton, which increases the conjugation. If the 'OH' proton (that participates in ESIPT) is deprotonated, the ESIPT is not feasible. Then, the molecule can emit the normal emission but not the tautomer emission. Only a single emission will be observed. The absence of the shift in the emission spectrum indicates the formation of tautomer from the anion.

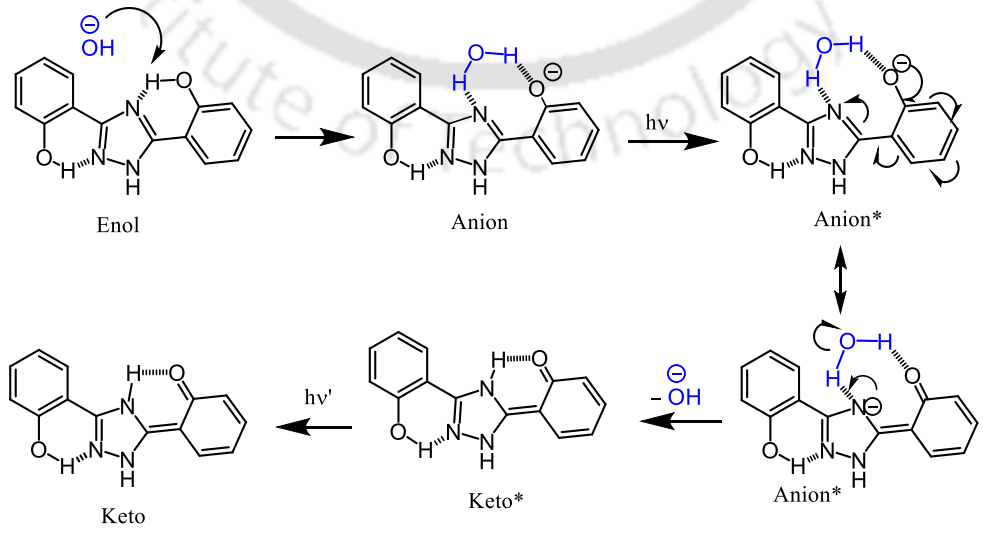

Scheme 4.3. Tautomer formation via intermolecular proton transfer in bis-HPTA anion.

TH-2834_146122035

The transformation of anion to tautomer occurs by intermolecular proton transfer in the excited state (**Scheme 4.3**). At higher pH due to an increase in the basicity, the 'OH' group deprotonates to form an anion. Upon excitation, the negative charge is shifted to azole nitrogen by resonance. The nitrogen whose basicity increased with negative charge abstract the proton from water to form keto tautomer. Thus, the formed excited state keto tautomer (keto*) emits tautomer emission. Depending upon the solution's pH, the excitation spectra recorded at 420 nm match the absorption spectra of the neutral or that of the anion (**Figure 4.2(b)**). Thus, keto tautomer is formed from both neutral and anionic species.

At pH 12.0, a single exponential emission decay is observed with a lifetime value of 1.7 ns. (**Figure 4.6**). This indicates the presence of single species. The environment significantly alters the PTTPT of bis-HPTA. Besides, photoexcitation also induced intermolecular proton transfer in the anionic form of bis-HPTA.

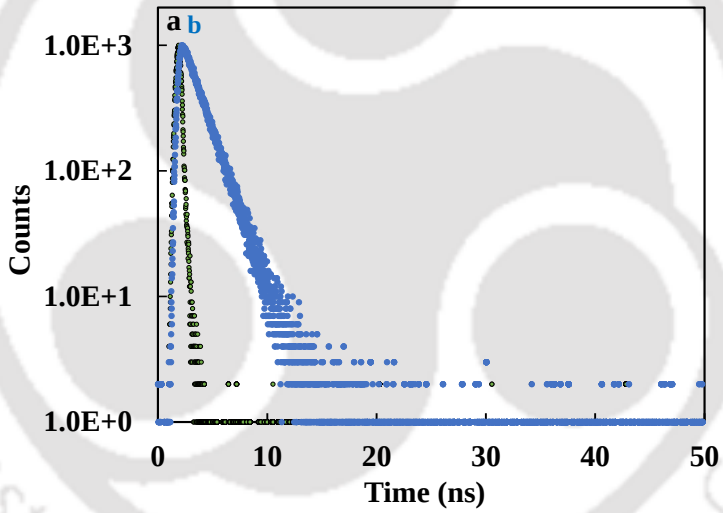

Figure 4.6 (b). Fluorescence decay of bis-HPTA in water (pH 12.0) at λ_{ex} = 336 nm and (a) IRF.

4.2. Effect of pH on electronic spectra of bis-HPTA in the presence of *β*-CD

The inclusion of a non-polar guest into a host molecule is favoured due to the release of the water molecules. It results in an increase in entropy.[151,160] It is also enthalpically favourable, as the released water molecules can then form hydrogen bonds with other water molecules in bulk. As the hydrophobicity of the cavity is different. It is interesting to find the effect of encapsulation by *β*-CD on the unique kind of proton transfer of bis-HPTA. In an aqueous *β*-CD solution, due to water presence, pH plays an important role. The molecule can be in different ionic forms depending upon the pH.[237,240,246] Therefore, the pH effect on the molecule was investigated first by absorption and emission spectroscopic techniques. **Figure**

TH-2834_146122035

4.7 shows the normalized absorption spectra of bis-HPTA at different pH in the presence of *β*-CD. The absorption maximum of bis-HPTA in the pH 1.0 to 6.0 range is 300 nm and 328 nm in pH 7.0 to 12.0.

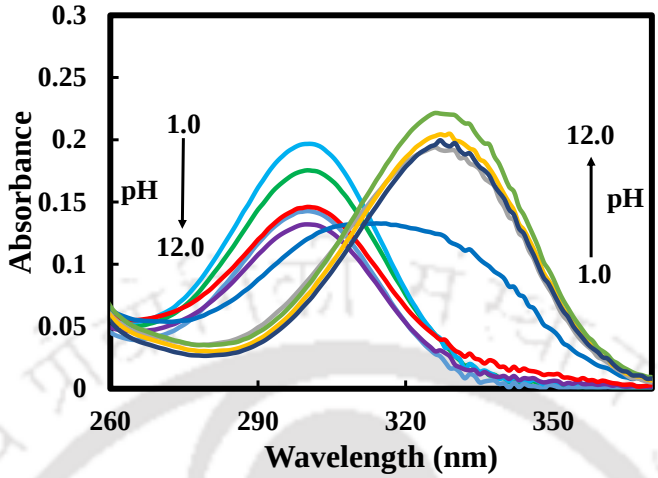

Figure 4.7. Normalized absorption spectra of bis-HPTA in *β*-CD (12.0 mM) of pH 1.0 to 12.0.

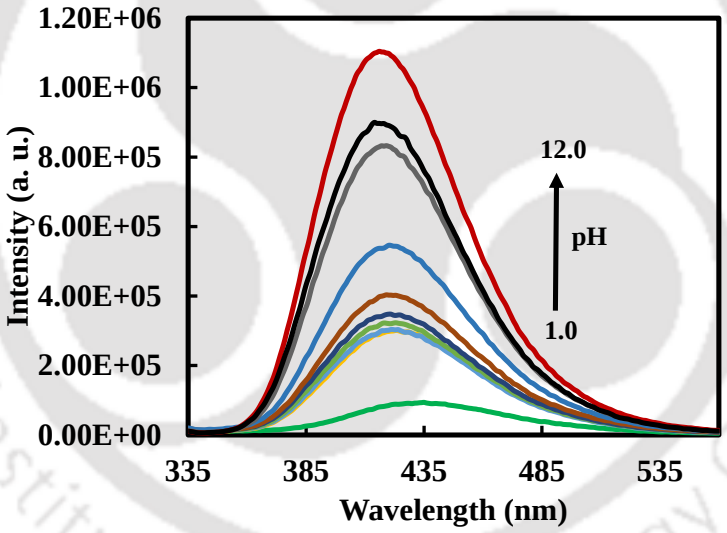

Figure 4.8. Emission spectra of bis-HPTA in *β*-CD (12.0 mM) of pH 1.0 to 12.0.

The red shift in the absorption spectra indicates the 'OH' group deprotonates to form an anion. The emission spectra of bis-HPTA in *β*-CD (12.0 mM) in pH range 1.0 to 12.0 is presented in **Figure 4.8**. Unlike in water, in CD, the emission spectrum was blue shifted, from 421 nm to 417 nm with increase in pH. The fluorescence lifetimes of the anion are also distinctly different from the fluorescence lifetimes of the tautomers (see later). The blue shift in the emission spectrum upon increasing the pH shows that the molecule is emitting in the anionic form, not as keto tautomer like water. As stated earlier, the blue shift in the emission spectrum compared to that of tautomer is a characteristic feature of the anion.[237] The anion

TH-2834_146122035

emission of ESIPT molecules are blue-shifted with respect to tautomer emission. The anionic emission of bis-HPTA is also blue-shifted compared to tautomer emission in alcohols.[205]

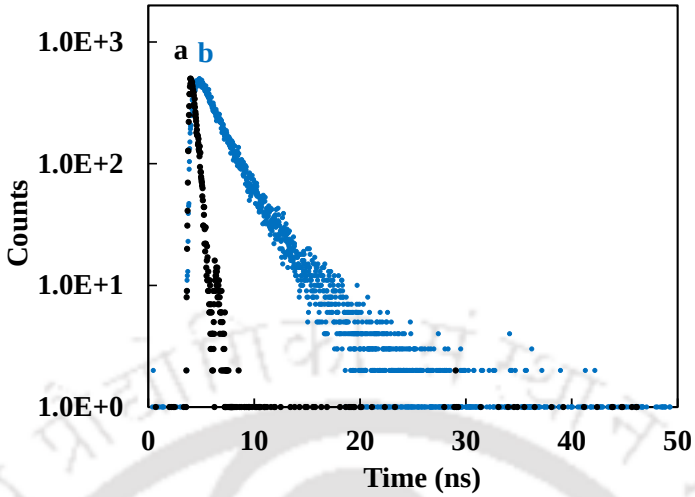

Figure 4.9 (a). Instrument response function and (b) fluorescence decay of bis-HPTA in *β*-CD (12.0 mM) at pH 4.0.

The fluorescence decay was monitored at 420 nm emission of bis-HPTA in 12.0 mM *β*-CD (pH 4.0). The decay is biexponential with lifetimes at 0.8 ns (35.0%) and 4.5 ns (65.0%) (**Figure 4.9**). As stated earlier, the fluorescence lifetime of the diketo is shorter than the monoketo. In water, the relative amplitude of diketo (73.3%) was higher than that of monoketo (26.7%). However, the relative amplitude of monoketo increases than diketo in *β*-CD. This increase shows that the PTTPT is more favoured in water than in *β*-CD. The excited state lifetime of anionic bis-HPTA (at pH 12.0) in *β*-CD is monoexponential (2.0 ns) and distinctly different from the tautomers.

4.3. Effect of *β*-CD on electronic spectra of bis-HPTA

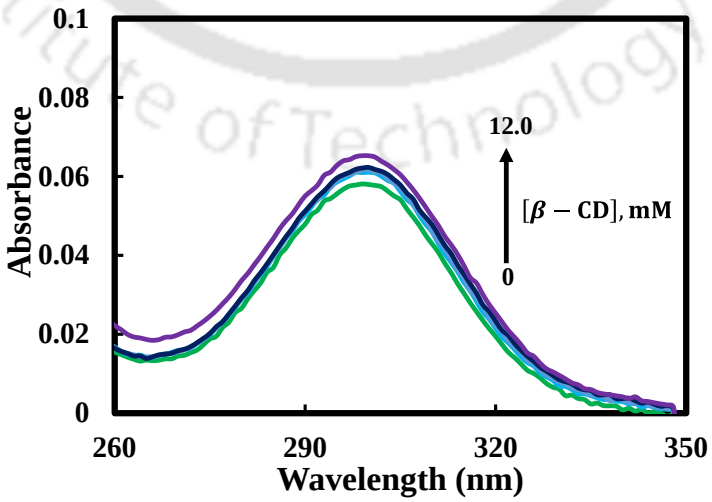

Figure 4.10. Absorption spectra of bis-HPTA in different concentrations of *β*-CD in aqueous solution (at pH 4.0).

TH-2834_146122035

Absorption spectra of bis-HPTA in the presence of *β*-CD is given in **Figure 4.10**. The addition of *β*-CD to bis-HPTA causes a slight increase in absorbance with a small red shift of 2 nm in absorption maximum. Such an increase in absorbance was reported when other non-polar guests were encapsulated in CD.[159]

The fluorescence spectra of bis-HPTA at different *β*-CD concentration are given in **Figure 4.11.** The fluorescence intensity of the molecule increases with a red shift gradually with the addition of *β*-CD. The emission intensity of bis-HPTA in 12.0 mM *β*-CD (**Figure 4.11**) is doubled compared to that in water. The CD cavity is relatively less polar than the bulk aqueous phase. The inclusion of guest molecules by CDs in an aqueous solution, results in a substantial rearrangement and removal of the water molecules originally solvated to CD. Due the restricted motion also, the local viscosity/rigidity are very different from the bulk liquid medium. This is reflected by the enhancement in fluorescence upon the addition of *β*-CD. The enhancement in fluorescence and the red shift indicates the encapsulation of the molecule inside the cyclodextrin. In CD, guest molecules are in a more confined and restrictive environment compared to that in solution.[154] Therefore, intramolecular rotations and other molecular motions of the guest molecule are significantly hindered upon inclusion compared to the free molecule in the bulk phase.

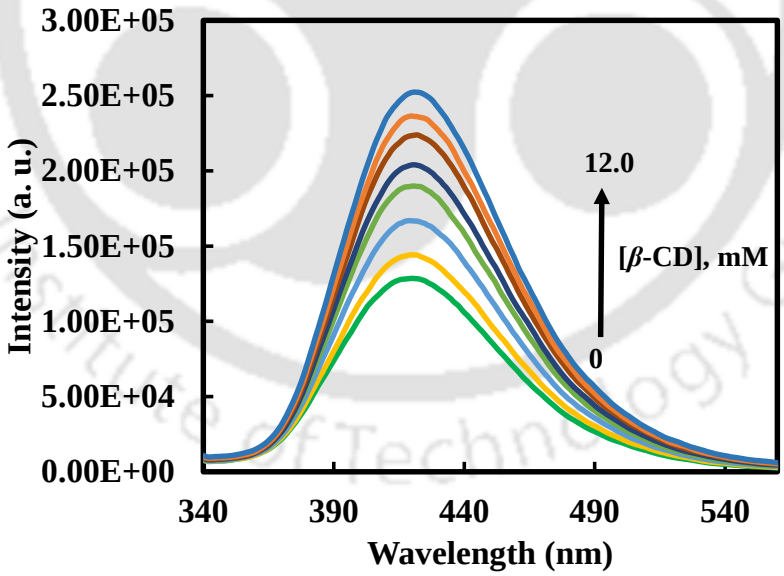

Figure 4.11. Emission spectra of bis-HPTA in different concentrations of *β*-CD in aqueous solution (at pH 4.0), λ_{ex} = 290 nm.

Due to these restrictions, the non-radiative decays of the guest were decreased in *β*-CD. This led to enhancement in the fluorescence lifetime of both the keto species. Like in water, the fluorescence decay of bis-HPTA in *β*-CD was also biexponential (**Figure 4.6**). But the

TH-2834_146122035

lifetimes of both species are different compared to water (**Figure 4.6**). The relative amplitude of the longer lifetime component to that of the shorter lifetime component in *β*-CD is more than water. This may be due to the reduced polarity of the environment. The other difference between the molecule in water and CD was the absence of intermolecular proton transfer in the anionic form to form tautomer in the excited state. In aqueous solution, the water molecule is near the triazole ring nitrogen. Therefore, it can form an intermolecular hydrogen bond, as shown in **Scheme 4.3**. However, in CD, since the triazole ring is present inside the cavity (**Figure 4.13**) (discussed later), it may not be able to form the hydrogen bond. Therefore, intermolecular proton transfer was prevented. Hence, the anion emits radiative emission instead of undergoing proton transfer to form tautomer.

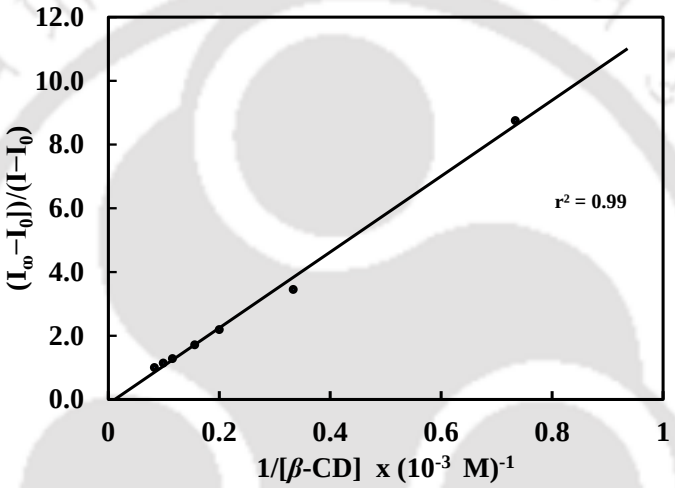

Figure 4.12. Benesi-Hildebrand plot showing 1:1 binding of bis-HPTA and *β*-CD.

Benesi-Hildebrand equation was used to find the stoichiometry of the binding (**Figure 4.12**).

The general form of the equation is

$$\frac{[I_\infty - I_0]}{[I - I_0]} = 1 + \frac{1}{K[\beta\text{-CD}]^n} \qquad (4.1)$$

for 1 : n ratio of host : guest. Here, I and I_0 are the emission intensity in the absence and the presence of CD. K is the binding constant. I_∞ is the limiting intensity. A good correlation coefficient (r^2 = 0.99) was obtained for n = 1 and K was calculated to be 8.4 x 10^1 M^{-1}. *β*-CD has portal and interior diameters of 6.0 and 6.5 Å and a height of 7.9 Å. The molecular dimensions of bis-HPTA are 12.3 Å X 4.6 Å. Therefore, bis-HPTA can be encapsulated inside *β*-CD. But, since the length is longer and the molecule formed 1:1 complex, it was only encapsulated partially. Accordingly, three different orientations of bis-HPTA inside the CD

TH-2834_146122035

were considered (I) the α-ring was inside the cavity, (II) the β-ring was inside the cavity, and (III) the triazole ring was completely inside and α-ring and β-ring were partially encapsulated

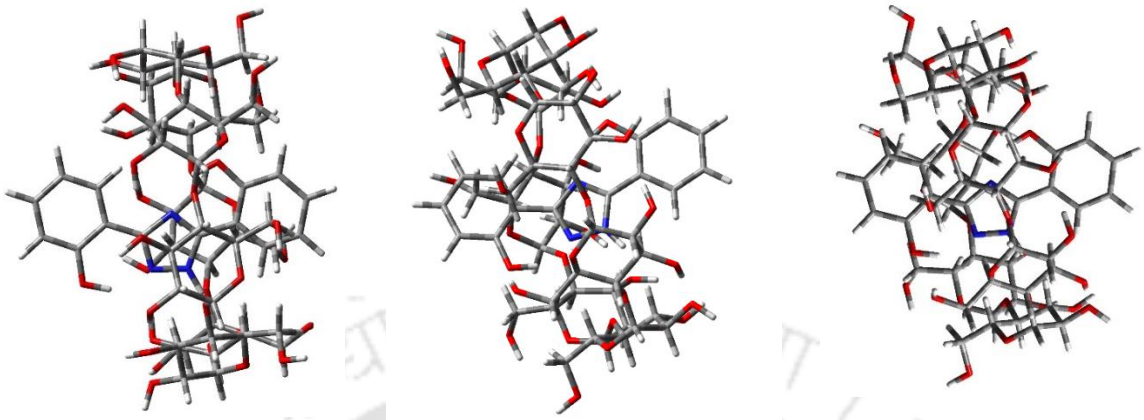

I **II** **III**

Figure 4.13. Optimized geometries of bis-HPTA and *β*-CD complexes.

Table 4.1. Relative energy (kJ/mol), stabilization energy (kJ/mol) and relative population (%) of *β*-CD and bis-HPTA complexes.

			Orientation		
	***β*-CD**	**Bis-HPTA**	**I**	**II**	**III**
Relative energy	82560.55	412536.44	0	0.47	0.41
Stabilization Energy			-2037.91	-2025.05	-2026.62
Relative population			98.43	0.55	1.02

The molecular geometries of all three inclusion complexes were fully optimized by DFT and the optimized geometries of all three complexes were shown in **Figure 4.13**. The stabilization energy (Es) of the host-guest complex was calculated by using the following equation.

$$E_s = E_{complex} - [E_{host} + E_{guest}] \quad (4.2)$$

Where E_{host}, E_{guest} and $E_{complex}$ are the energy of host, guest and complex obtained from DFT optimization. The optimized energies of the complexes along with the stabilization energies of all three different orientations, were compiled in **Table 4.1**. The calculations suggested that the orientation I (in which most parts of the α-ring along with triazole ring present inside the cavity) was the most stable and the relative population of the molecule in other orientations are negligible. In the inclusion complex, since triazole nitrogen is present inside the cavity, water is not accessible to triazole nitrogen. Therefore, it was not able to abstract the proton as in water and the molecule emits only anion emission, not the tautomer emission like water.

TH-2834_146122035

4.4. Conclusion

The PTTPT of bis-HPTA is significantly altered by the environment. Bis-HPTA is neutral at pH 4.0. PTTPT was more favoured in water than in organic solvents. However, it was reduced upon encapsulation by β-CD. Photoexcitation also induced intermolecular proton transfer in the anionic form of bis-HPTA in water. The anion rearranged to form the keto tautomer in the excited state. The orientation of host bis-HPTA inside β-CD is such that the triazole ring and most part of the α-ring are completely inside. The spectral changes in the presence of β-CD suggest that the relative position and orientation of the guest relative to the host impact the photophysics of the guest. The encapsulation prevents the intermolecular proton transfer in the anion and therefore, no tautomer emission was observed from the anion.

TH-2834_146122035

Chapter 5

Effect of Micelles and Reverse Micelles on PTTPT of 3,5-Bis(2-hydroxyphenyl)-1H-1,2,4-triazole

TH-2834_146122035

TH-2834_146122035

5.0. Introduction

Micelles and reverse micelles are interesting micro-heterogeneous systems.[142,143,147,247] The rigid environment around the molecule inside micelles decreases the nonradiative rate and consequently increases the fluorescence intensity of the encapsulated fluorophores.[136,248–253] As ESIPT is susceptible to surroundings, the confined environments such as micelles and reverse micelles significantly alter this photophysical process.[131,156,254,255]

Warner et al. studied the ESIPT of 10-hydroxybenzoquinoline and found that the tautomer emission increases in the presence of micelles.[132] Molecules residing inside a micellar interior experience a nonpolar, aprotic microenvironment. Therefore, they exhibit enhanced tautomer emission and lifetime. The mechanism of interaction of curcumin with soluplus micelle was studied.[140] Absorption and emission enhancement of curcumin was reported. The fluorescence anisotropy studies showed the presence of a rigid environment around curcumin upon encapsulation. The tautomer emission of salicylic acid was enhanced on increasing the F127 concentration.[256] Disruption of the intermolecular hydrogen bond in the ESIPT dye, 3-hydroxyflavone and the water molecules was reported inside cationic micelles.[257] The ESIPT of 4'-N,N'-dimethylamino-3-hydroxyflavone was studied in AOT/*n*-heptane/water.[258] ESIPT was hindered at w_o = 0, as the molecules were attached to the ionic AOT headgroups via intermolecular hydrogen bonding. The addition of water freed the molecules as water can form stronger hydrogen bonds with AOT headgroups. Hence, on increasing the w_o, ESIPT became faster.

In the last chapter, it was shown that the encapsulation affects the PTTPT of the neutral and intermolecular proton transfer of the anionic forms of bis-HPTA. Micelles are supramolecular molecular assemblies. Unlike CD, they are formed by the association. Water pool inside a reverse micelle behaves different than bulk water or the encapsulated water inside cyclodextrins. Therefore, the effect of micelles and reverse micelle may be different on bis-HPTA and the study would be interesting. Thus, in this work, the effects of cationic (CTAB) and anionic (SDS), non-ionic (Triton-X 100) and reverse (AOT/*n*-heptane/water) micelles on the proton transfer of bis-HPTA were studied using UV-visible, steady state and time resolved fluorescence spectroscopy.

TH-2834_146122035

5.1. Effect of micelle on neutral bis-HPTA

Neutral bis-HPTA emits keto emission at 420 nm (chapter 4). In all three micelles studied, the fluorescence spectrum of bis-HPTA is red shifted with an increase in surfactant concentration

(**Table 5.1**). The emission intensity also increases with the increase in surfactant concentration.

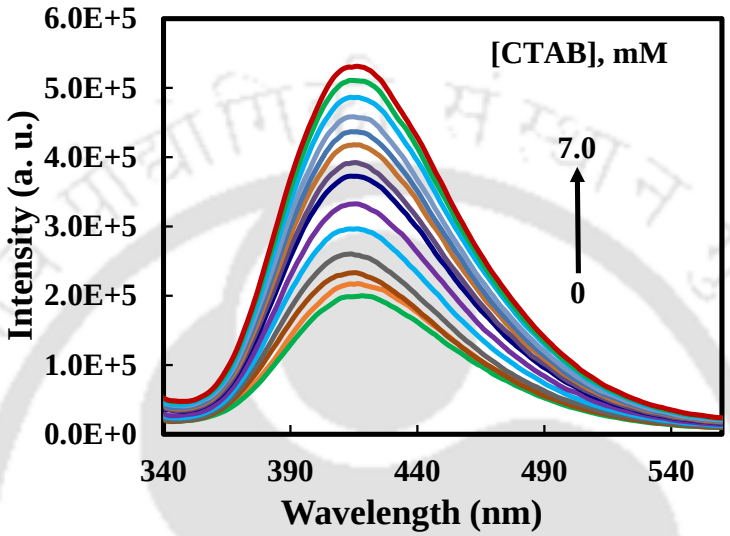

Figure 5.1. Emission spectra of neutral bis-HPTA in different concentrations of CTAB in water, λ_{ex} = 300 nm.

As a representative, the fluorescence spectra of bis-HPTA in different concentrations of CTAB are shown in **Figure 5.1**. Enhancement in fluorescence of bis-HPTA with surfactants concentration in micelles shows that the bis-HPTA enter inside the micelles. The fluorescence of fluorophore are enhanced in micelles due to a reduction in the nonradiative decay.[253] The confined environment hinders the rotation of the molecule. As a result, the nonradiative decay rate also decreases.

Table 5.1. Absorption maximum (λ_{ab}^{max}, nm), emission maximum (λ_{em}^{max}, nm), fluorescence lifetime (τ, ns) of bis-HPTA in Water, CTAB, SDS and TX-100.

	λ_{ab}^{max}	λ_{em}^{max}	τ
Water	297	420	1.5 (73.3%) 3.9 (26.7%)
CTAB	299	418	2.22 (58.2%) 5.44 (41.8%)
SDS	298	434	0.69 (66.9%) 1.95 (33.1%)
TX-100	303	433	1.97(39.1 %) 4.76(60.9 %)

TH-2834_146122035

As discussed earlier, the spectral shift provides information about the nature of the emission and the surrounding environment. The fluorescence spectrum of bis-HPTA in water and micelles are compared in **Figure 5.2**.

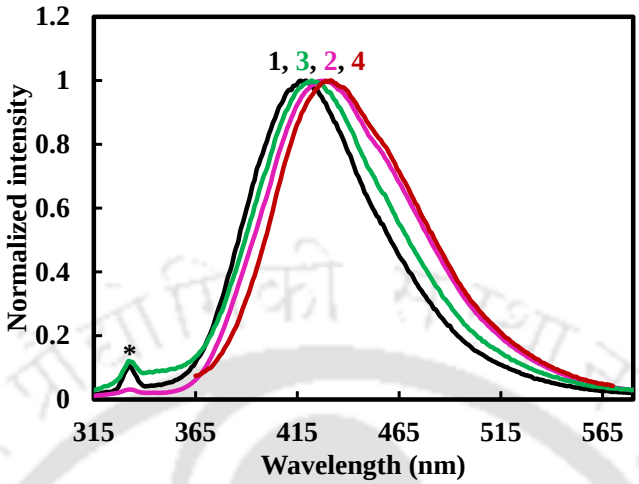

Figure 5.2. Emission spectra of neutral bis-HPTA in water (1), CTAB (2), SDS (3) and TX-100 (4), λ_{ex} = 300 nm, *water Raman.

The data are compiled in **Table 5.1**. The absorption spectra and the fluorescence spectra in micelles are red shifted compared to those in water (except fluorescence spectra in CTAB). The micelle environment weakens the intermolecular hydrogen bond and strengthens the intramolecular hydrogen bond. It results in a bathochromic shift in the absorption spectrum. The 420 nm emission in water corresponds to the tautomer emission (chapter 4). The fluorescence spectra of the bis-HPTA in SDS and TX-100 are bathochromically shifted than in water. As discussed earlier, the keto emission will be red shifted in a less polar environment. Since the polarity inside the micelle is less than water, the emission spectra in SDS and TX-100 are red shifted. But, in CTAB, despite the decreases in polarity, the fluorescence spectrum is little blue shifted than that in water. It may be due to the following reason. K1 tautomer emission spectrum is blue shifted than the diketo emission.[205] Enhancement in relative fluorescence of K1 than diketo may cause an apparent blue shift in the fluorescence spectrum. Though the relative fluorescence is enhanced in micelle, still it is less; therefore, the full time resolved area normalized spectra could not be obtained. However, the fluorescence lifetime was measured at fluorescence maxima (**Figure 5.3**). Same as in an aqueous medium, the fluorescence decay is bi-exponential. However, the relative amplitude of the longer lifetime component increased in CTAB (**Table 5.1**). This might be the cause of the small blue shift of the apparent fluorescence maximum. In TX-100 though the relative population of the K1 tautomer increases still a red shift was observed. In TX-100, it may be the shift in the

TH-2834_146122035

fluorescence spectra of the tautomer emission that dominates the relative increase in population. Both absorption and fluorescence spectra are also more shifted in TX-100 than other micelles. It indicates that the molecule is experiencing a lesser polar environment inside the TX-100 than SDS and CTAB. Comparative study of SDS, CTAB and TX-100 micelle showed that organic molecules experience less polar environment inside TX-100 than SDS and CTAB.[250]

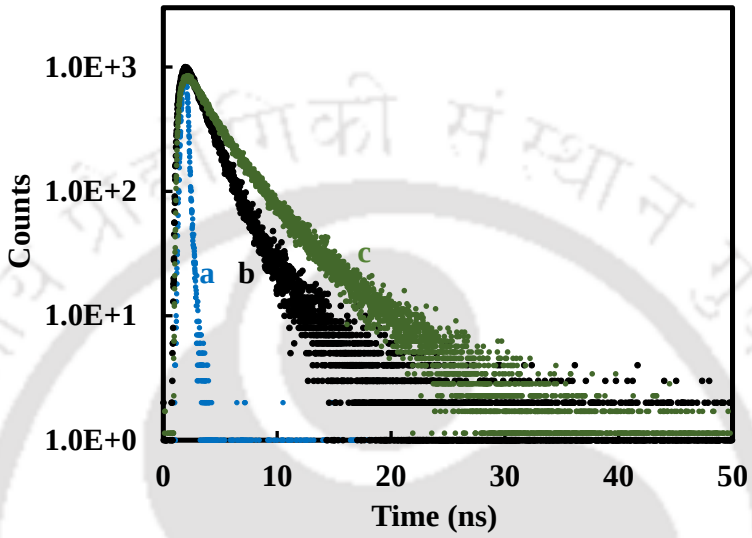

Figure 5.3. Fluorescence decay of neutral bis-HPTA in (b) water and (c) CTAB. (a) IRF.

5.2. Effect of micelle on the anion of bis-HPTA

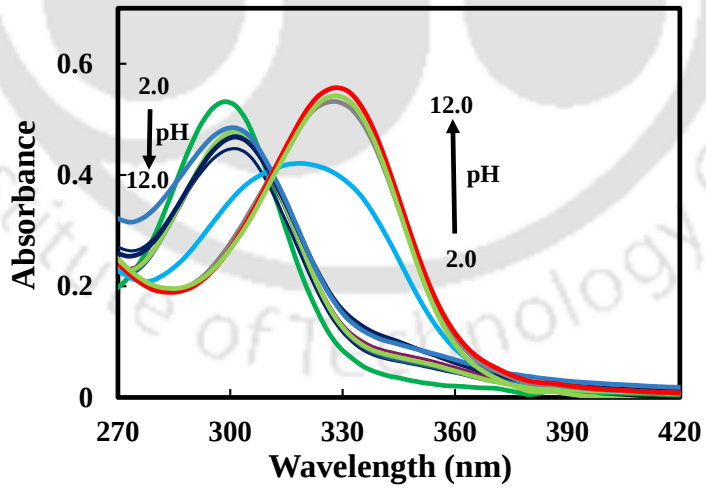

Figure 5.4. Absorption spectra of bis-HPTA in SDS at different pH.

The effect of pH on bis-HPTA in a micellar environment was investigated first. As a representative, the effect of pH on bis-HPTA in SDS is shown in **Figure 5.4**. In all the micelles, upon increasing the pH, the neutral molecule absorbance decreases and a new band appears at the longer wavelength. For example, in SDS, the neutral band's absorbance at 298 nm decreases

TH-2834_146122035

and a new band emerges at 328 nm. The increase in the absorbance of the longer wavelength absorbance band with increasing pH shows gradual deprotonation of the molecule upon increasing the base concentration. A quasi isosbestic point is observed at 316 nm. Similar changes are observed in CTAB and TX-100 also. These changes show that bis-HPTA is deprotonated to form an anion in the micelle.

Table 5.2 Absorption maximum (λ_{ab}^{max}, nm), emission maximum (λ_{em}^{max}, nm), excitation maximum (λ_{ex}^{max}, nm) of anion of bis-HPTA in micelles.

Medium	λ_{ab}^{max}	λ_{ex}^{max}	λ_{em}^{max}
Water	326	326	420
CTAB	333	333	408
SDS	328	328	416
TX-100	329	329	414

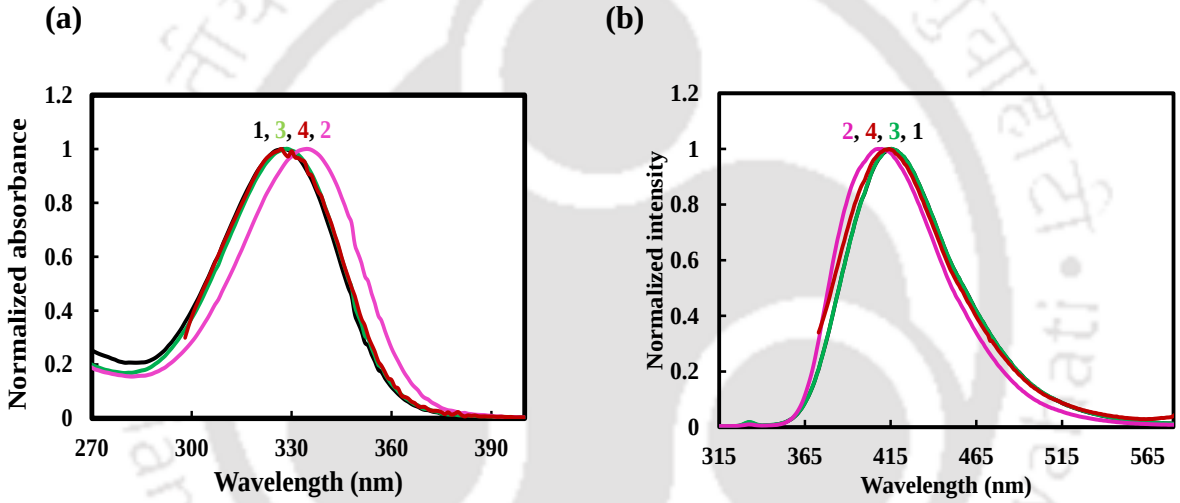

Figure 5.5 (a) Absorption and (b) emission spectra of anionic bis-HPTA in water (1), CTAB (2), SDS (3) and TX-100 (4), λ_{ex} = 300 nm.

The effect of different micelles on absorption spectrum and fluorescence spectrum of bis-HPTA anion are shown in **Figure 5.5** and the data are compiled in **Table 5.2**. The absorption spectra of the anion are red shifted and the fluorescence spectra are blue shifted in the micelles. As stated, the deprotonation increases the conjugation that produces a bathochromic shift. In water, the emission spectrum was unaffected when anion was excited. It was inferred that the tautomer was formed from the intermolecular proton transfer in the excited state. But in all three micelles, the anion's excitation resulted in the emission that is blue shifted than the tautomer emission. The blue shift in the emission is consistent with anionic emission in the ESIPT molecule.[259,] Unlike in water, the intermolecular proton transfer is prevented in micelles. Since the polarity and hydrogen bonding are reduced in the micelles, the intermolecular proton transfer is not feasible.

TH-2834_146122035

5.3. Effect on electronic spectra of bis-HPTA in the presence of AOT/*n*-heptane/water

Absorption spectra of the molecule were recorded in AOT/water/*n*-heptane at different w_0 values (**Figure 5.6**). Bis-HPTA at w_0 = 0, absorbs at 306 nm. On gradually increasing the w_0 value, we observe a decrease in absorbance at absorption maxima.

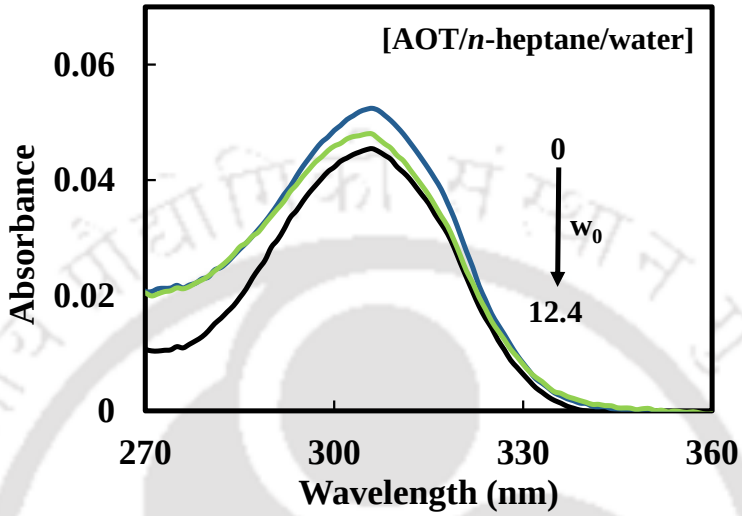

Figure 5.6. Absorption spectra of bis-HPTA in AOT/n-heptane/water with changing w_o values.

The emission spectra of bis-HPTA were recorded in AOT/water/*n*-heptane at different w_0 values (**Figure 5.7**). At w_0 = 0, only longer wavelength emission at 435 nm was observed. On increasing the w_0 value gradually, this band starts to decrease with a blue shift and a new band starts to appear at ~ 340 nm. The tautomer emission maximum is shifted to 430 nm in reverse micelle at w_0 = 18. But the intensity of the 340 nm band is very small even at w_0 = 12.4. Due to very weak intensity, the decay of the 340 nm band could not be measured, but that of the tautomer emission was measured.

Interestingly single exponential decay was observed for the longer wavelength emission in AOT/*n*-heptane/water reverse micelle (**Table 5.3**). Like the fluorescence intensity the fluorescence, lifetime of the longer wavelength emission decreases with increases in water quantity.

Table 5.3. Absorption maximum (λ_{ab}^{max}, nm), emission maximum (λ_{em}^{max}, nm) and fluorescence lifetime (τ, ns) of bis-HPTA in AOT/*n*-heptane/water at different w_0 values.

w_0	λ_{ab}^{max}	λ_{em}^{max}	τ
0	306	436	5.2 (100 %)
0.4	306	436	5.0 (100 %)
6.2	308	436	2.5 (100 %)
12.4	308	435	2.0 (100 %)

TH-2834_146122035

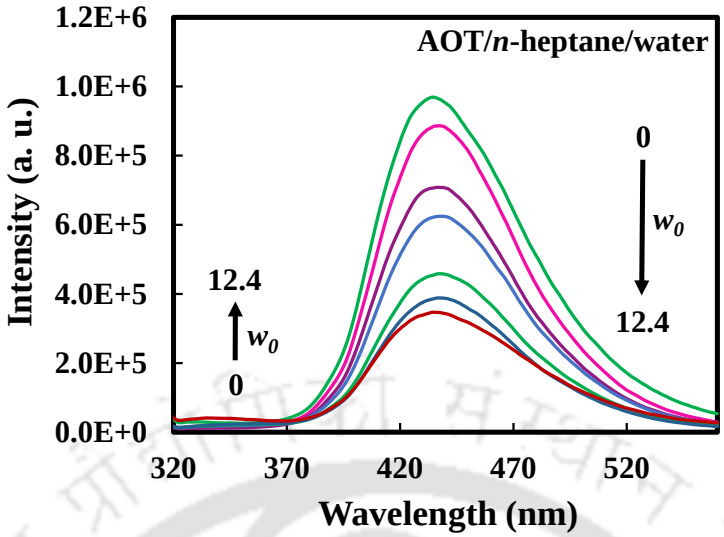

Figure 5.7. Emission spectra of bis-HPTA in AOT/*n*-heptane/ water with changing w_o values, λ_{ex} = 300 nm.

The 340 nm emission matches with the normal emission of bis-HPTA in methanol. Therefore, it can be assigned to the normal emission of bis-HPTA. The 436 nm band is close to the tautomer band in methanol.[205] In methanol, the decay is biexponential due to emission from K1 and diketo tautomers. But it is single exponential in AOT/*n*-heptane/water reverse micelle. In hydrogen accepting solvents like DMF also, bis-HPTA emits single tautomer emission.[205,243] The single tautomer emission of bis-HPTA suggests the presence of a single intramolecular hydrogen bond, like in DMF. But, in DMF, bis-HPTA emits the tautomer emission at 480 nm, where the tautomer is formed by ESIPT in β-ring. In AOT/*n*-heptane/water reverse micelles, bis-HPTA emits the tautomer emission at 435 nm, close to tautomer emission in methanol. The K1 tautomer emission is blue shifted compared to the diketo emission,[205] and the 435 nm emission is blue shifted compared to methanol, where mixed emission from K1 and diketo tautomers is observed. The tautomer fluorescence lifetime in AOT/*n*-heptane is close to that of K1 tautomer in other solvents, and diketo tautomer lifetime is shorter than this.[205] For example, in methanol, the fluorescence lifetimes of K1 and diketo are 0.7 ns and 3.0 ns, respectively.[205] This suggests the tautomer emission is most likely from K1 formed by ESIPT in the α-ring. It also indicates that the α-ring is intact. AOT is an anionic surfactant and it can act as a hydrogen bond acceptor. The proton of bis-HPTA can form an intermolecular hydrogen bond with a negatively charged sulpho group of AOT (**Figure 5.8**). It breaks the intramolecular hydrogen bond in the β-ring. Since, the complex has only one intramolecular

TH-2834_146122035

hydrogen bond. Therefore, excitation of this complex led to the formation of only K1 by ESIPT in α-ring.

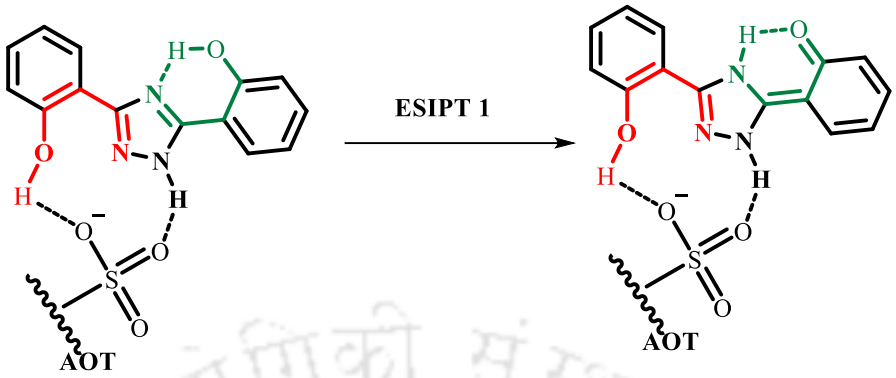

Figure 5.8. ESIPT I in the bis-HPTA-AOT hydrogen-bonded complex.

Reverse micelle has three different regions (i) oil phase, (ii) interfacial region with bound water and (iii) core water. The tautomer fluorescence maximum in AOT reverse micelle is blue shifted than nonpolar solvents and is red shifted than in methanol. Therefore, bis-HPTA is present not in the oil phase or core water but in the interfacial region with bound water. In this region, bis-HPTA can form an intermolecular hydrogen complex, as shown in **Figure 5.8**. The change in fluorescence intensity with water also suggests that the bis-HPTA is present in the region accessible to water. In ESIPT molecules, the keto ring's torsional rotation in the excited state via the ICT state is reported to be the major nonradiative decay.[192,111] In reverse micelles, the size of the water pool increases with the addition of water. The viscosity and polarity, therefore the nonradiative decays, increase with the size of the water pool.[131,148] The blue shift in the tautomer emission of bis-HPTA shows the rise in polarity and decrease in its lifetime, with water quantity support the increase in nonradiative decay with the addition of water.

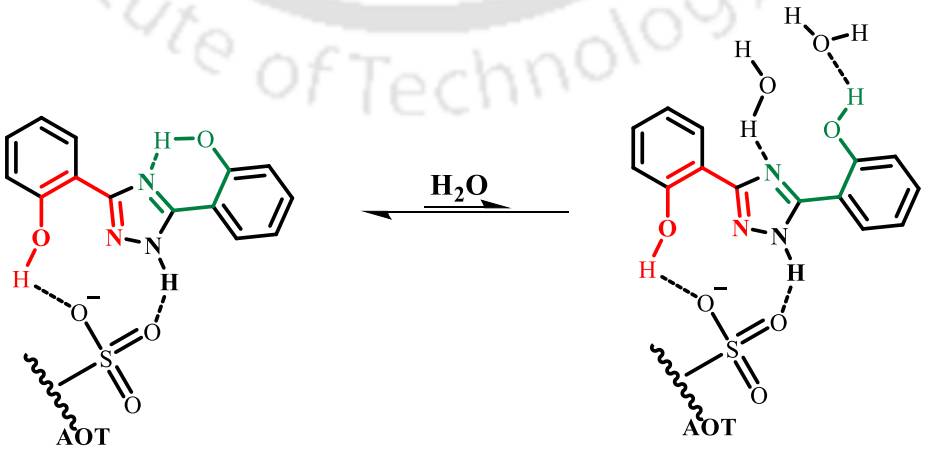

Figure 5.9. Formation of solvated open enol from *cis*-enol.

TH-2834_146122035

The increase in water amount enhances the nonradiative rate and breaks the intramolecular hydrogen bond in the α-ring (**Figure 5.9**). Thus, form the solvated enol. Due to the absence of an intramolecular hydrogen bond, the solvated enol emits only normal emission. Though in small amount bis-HPTA emits enol emission with the rise in the water pool size. The presence of isosemissive point confirms the conversion of *cis*-enol to open enol. This conversion to the solvated enol also contributes to the reduction in tautomer fluorescence.

5.4. Conclusion

The increase in the keto band emission intensity upon increasing the micelle concentration indicates the encapsulation of the molecule inside the micellar interior. The less polar and restricted environment of the micellar interior decreases the nonradiative decay. The molecule experiences a less polar environment in TX-100 as compared to CTAB and SDS. In CTAB, the relative population of the K1 tautomer increases. Tautomer formation from anion via intermolecular proton transfer is not observed in micelles. The normal emission of the molecule is absent in water and micelles. However, in AOT/*n*-heptane/water reverse micelles, on increasing the w_o, the tautomer emission decreases along with the normal emission increase. The β-ring of bis-HPTA can form an intermolecular hydrogen bond with hydrogen bond accepting polar head group of AOT. The molecule can then undergo ESIPT I in the α-ring to form only K1. On increasing the w_0, water can break this intermolecular hydrogen bond to give a solvated enol structure. The solvated enol structure emits only normal emission.

TH-2834_146122035

TH-2834_146122035

Chapter 6

The Suppression of Intramolecular Charge Transfer by Tautomerism in 2-(4′-Amino-2′-hydroxyphenyl)-1H-imidazo[4,5-c]pyridine: Intramolecular Proton Transfer versus Intermolecular Proton Transfer

TH-2834_146122035

TH-2834_146122035

6.0. Introduction

As mentioned earlier, intramolecular charge transfer followed by the torsional rotation of the donor results in TICT emission.[168,260,261] TICT requires a charge donor and acceptor connected by a spacer. Intramolecular hydrogen-bonded acid-base pair is a prerequisite for ESIPT. AHPIP-c (**Chart 6.1**) has both proton donor-acceptor and charge donor-acceptor pairs.

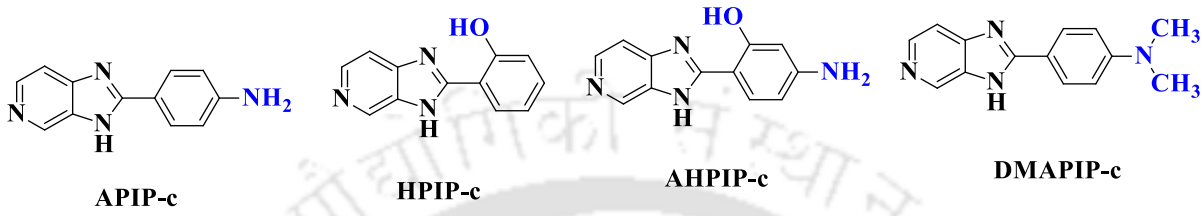

Chart 6.1. Structures of 2-(4′-amino-2′-phenyl)-1H-imidazo[4,5-c]pyridine (APIP-c), 2-(2′-hydroxyphenyl)-1H-imidazo[4,5-c]pyridine (HPIP-c), 2-(4′-amino-2′-hydroxyphenyl)-1H-imidazo[4,5-c]pyridine (AHPIP-c) and 2-(4′-dimethylamino-2′-phenyl)-1H-imidazo[4,5-c]pyridine (DMAPIP-c).

APIP-c **(Chart 6.1**) shows normal emission in aprotic solvents and normal plus TICT emission in alcohols.[180] (HPIP-c, **Chart 6.1**) emits only tautomer emission in a nonpolar solvent like cyclohexane.[262] But it emits both normal and tautomer emissions in polar and protic solvents. Torsional rotation of the keto tautomer after ESIPT is a main non-radiative deactivation path for HPIP-c and its analogues.[111] The photophysics of (AHPIP-c, **Chart 6.1**), which is a combination of APIP-c (**Chart 6.1**) and HPIP-c (**Chart 6.1**) and its methoxy derivative, AMPIP-c, was investigated.[206] APIP-c and AMPIP-c emit TICT emission in methanol.[180,206] AHPIP-c emits dual emission.[206] But the negative solvatochromism indicated that the longer wavelength in all organic solvents, including methanol, is due to keto emission (**Chart 6.2**). No TICT emission is observed. The experimental emission maxima match the theoretically calculated maxima.[206] Omidyan and Iravani studied the ESIPT and non-radiative deactivation path of AHPIP-c in the gas phase theoretically.[263] They found a conical intersection between the S_1/S_0 states along the torsional relaxation path of the keto. They proposed non-radiative deexcitation from the excited to the ground state via the conical intersection. It explains the low fluorescence quantum yield of AHPIP-c. Zhou et al. studied the solvent effect on the ESIPT of AHPIP-c by DFT.[77] They showed that the proton transfer barrier is inversely proportional to the solvent polarity.

In systems like AHPIP-c, it is essential to understand the cause of suppression of one process by the other. In general, the ESIPT process is hampered by alcohols and they induce

TH-2834_146122035

the TICT process in APIP-c. But the ESIPT process suppressed the TICT of AHPIP-c in alcohols. However, the cause of the suppression was not understood. But it is necessary to understand the competing ESIPT and TICT. It will also be useful for identifying and designing photoswitches with multiple reaction coordinates.[264–266]

(a) **(b)**

Chart 6.2. Structures of (a) enol and (b) keto forms of AHPIP-c.

The theoretical studies with explicit solvent molecules gained momentum and provided more detailed insight into the molecular interaction.[75,77,80,263,267] Therefore, The theoretical studies to determine the cause for the suppression of the TICT process by ESIPT in AHPIP-c are discussed in this chapter.

6.1. Absorption maximum

The absorption spectral maxima calculated using the 6-31G++(d, p) basis set are close to the experimental value than those calculated by other functionals (**Table 6.1**). Therefore, it was used for TDDFT optimizations and the potential energy curves.

Table 6.1. Calculated and experimental absorption spectral maximum (λ_{max}, nm).

	λ_{max}	
	$S_0 \rightarrow S_1$	$S_0 \rightarrow S_2$
B3LYP/6-31G ++ (d, p)	349	293
B3LYP/DGTVZP	331	291
B3LYP/aug-cc-PVTZ	326	297
Experimental[206]	342	303

6.2. Structure of the enol complex

Though hydrogen bonding may influence the TICT emission, it is predominantly the polarity that determines the TICT.[168] APIP and their dimethylamino derivatives are special kind of TICT emitting molecules.[180,182] Hydrogen bonding of the solvent plays an essential role in the TICT emission of the molecules.[180–182,268] Protic environment is necessary to obtain TICT emission in these molecules. For example, no TICT emission is observed from APIP-c in aprotic solvents, including polar acetonitrile.[180] On the other hand, it emits TICT emission in alcohols, such as ethanol, propanol and butanol, whose dielectric constants are lesser than acetonitrile. After numerous experimental and theoretical studies, the proton transfer induced

TH-2834_146122035

TICT emission mechanism of these molecules was revealed (**Scheme 6.1**).[181,182,269,270] The intermolecular proton transfer from the imidazole 'NH' to the pyridyl 'N' increases the acceptor's electron withdrawing ability. It induces the charge transfer from the donor amino/dimethylamino to the acceptor imidazopyridine ring. This intramolecular charge transfer accompanies the torsional rotation of the donor to form the TICT state. Calculated emission energies of the TICT state of these molecules matched well with the experimental longer wavelength emission.[206,80,182]

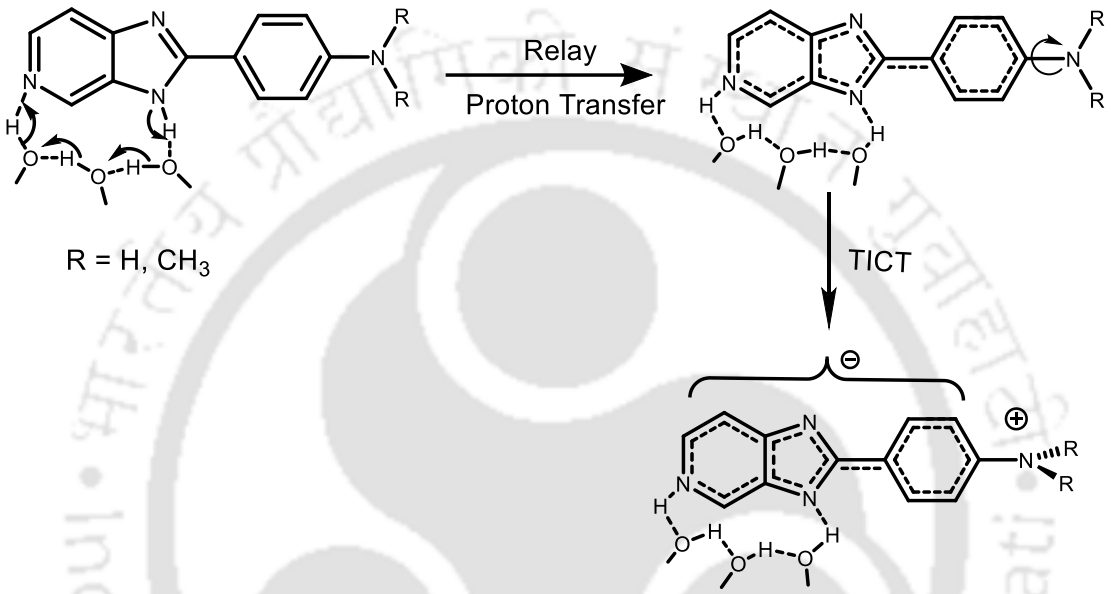

Scheme 6.1. The intermolecular proton transfer induced TICT in APIP-c (R=H) and DMAPIP-c (R=CH_3).

In imidazo[4,5-b]pyridine analogues, 2-(4′-amino-2′-phenyl)-1H-imidazo[4,5-b]pyridine (AHPIP-b) and its dimethylamino derivative, 2-(4′-dimethylamino-2′-phenyl)-1H-imidazo[4,5-b]pyridine (DMAPIP-b), single solvent molecule connects the intermolecular proton donor 'NH' and the proton acceptor pyridyl 'nitrogen'.[26] In imidazo[4,5-c]pyridine analogues, three solvent molecules are required to bridge the proton donor 'NH' group with the acceptor pyridyl 'N'.[182,267] In DMAPIP-c **(Chart 6.1**), the intermolecular relay proton transfer via a wire of three solvent molecules induced the TICT emission (**Scheme 6.1**).[182] Yang et al. performed detailed theoretical studies on DMAPIP-c.$(CH_3OH)_3$ and validated the mechanism.[80] They also suggested that more than three methanol molecules cannot hold the cyclic structure. They also considered 2-(2′-phenyl)-1H-imidazo[4,5-c]pyridine (PIP-c) with three methanol molecules to study the intermolecular proton transfer.[267] Therefore, a cyclic complex of AHIPIP-c with three methanol molecules [AHPIP-c.$(CH_3OH)_3$] was considered in the present work.

TH-2834_146122035

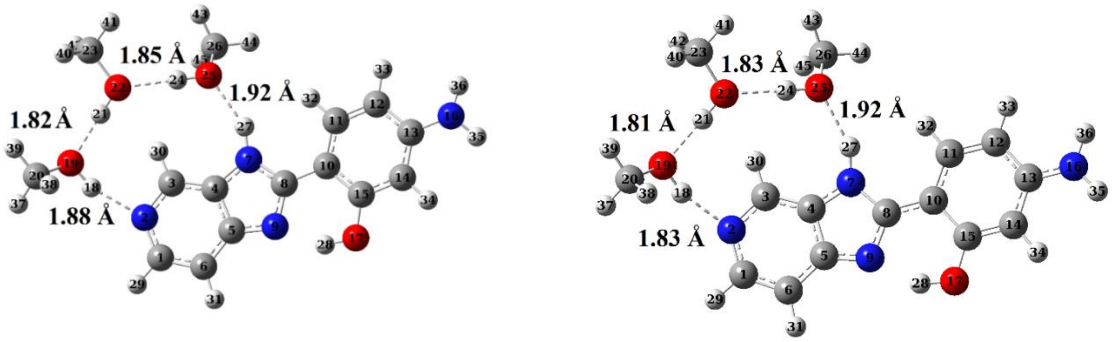

Ground State **Excited State**

Figure 6.1. The optimized structures of AHPIP-c.$(CH_3OH)_3$ complex in the ground and first excited states.

The ground state optimized geometry of AHPIP-c.$(CH_3OH)_3$ complex is shown in **Figure 6.1**. The bond angles involved in the hydrogen bonding, N7—H27—O25 and N2—H18—O19, are 152.4° and 159.6°, respectively. The hydrogen bond length between the hydrogen bond donor 'NH' group (N7—H27) and the methanol oxygen (the solvent accepting hydrogen bond) is 1.92 Å. The hydrogen bond length between the pyridyl nitrogen (N2) (hydrogen bond acceptor) and the methanol (the solvent donating hydrogen bond) is 1.88 Å. The hydrogen bond distance is smaller when methanol act as the donor than when it acts as the acceptor. Methanol being a protic solvent is a stronger hydrogen bond donor than an acceptor.

The electronic structure of the complex changes in the excited state. To understand the effect of change in the electronic state on the hydrogen bond strength, AHPIP-c.$(CH_3OH)_3$ complex was optimized in the first excited state (**Figure 6.1**). The N7—H27—O25 and N2—H18—O19 bond angles are 153.9° and 161.5°, respectively, in the excited state. In the excited state, the hydrogen bond's length with solvent as an acceptor is unaffected and the bond length remains 1.92 Å. But the solvent donating hydrogen bond length decreases to 1.83 Å, which shows the strengthening of this hydrogen bond. It is due to the increase in charge density on the pyridyl nitrogen, N2 in the excited state. The charge density on the pyridyl nitrogen in the ground and excited states are – 0.222 and – 0.244. However, the pyridyl nitrogen (N2) and the methanol hydrogen bond length of AHPIP-c.$(CH_3OH)_3$ cyclic complex is still longer than the same bond length in DMAPIP-c.$(CH_3OH)_3$ cyclic complex (1.77 Å).[80,182] The other interesting aspect is methanol-methanol hydrogen bond lengths. The hydrogen bond length between the two methanol molecules in the cyclic structure of AHPIP-c.$(CH_3OH)_3$ are 1.83 Å and 1.81 Å. On the other hand, in DMAPIP-c.$(CH_3OH)_3$, they were 1.80 Å and 1.77 Å.[80,182] All these

TH-2834_146122035

evidence suggest that the AHPIP-c.$(CH_3OH)_3$ cyclic structure is relatively weaker than DMAPIP-c.$(CH_3OH)_3$ cyclic complex.

Vibrational frequencies analysis also provides information about the strength of the bond. The theoretically calculated infrared spectrum of AHPIP-c.$(CH_3OH)_3$ complex in the ground and the excited states were shown in **Figure 6.2**. The OH and NH stretching frequencies of the complex are compared in **Table 6.2** to evaluate the strengthening or weakening of the bonds in the excited state. The frequencies of all the hydrogen bond donors reduced in the excited state, indicating a weakening of these bonds in the excited state. Compared to other 'O–H' or 'N–H' bonds, the frequency shift is more for the O17–H28 bond, which forms H-bond with imidazole nitrogen. This bond is clearly elongated in the excited state. This elongation shows the increase in the acidity of the O17–H28 group, which is an indication of its ease to undergo proton transfer. In other words, the intramolecular proton transfer is more favoured over the intermolecular proton transfer. Further, the distance between the 'OH' proton of AHPIP-c and imidazole nitrogen is reduced from 1.70 Å in the ground state to 1.67 Å in the excited state.

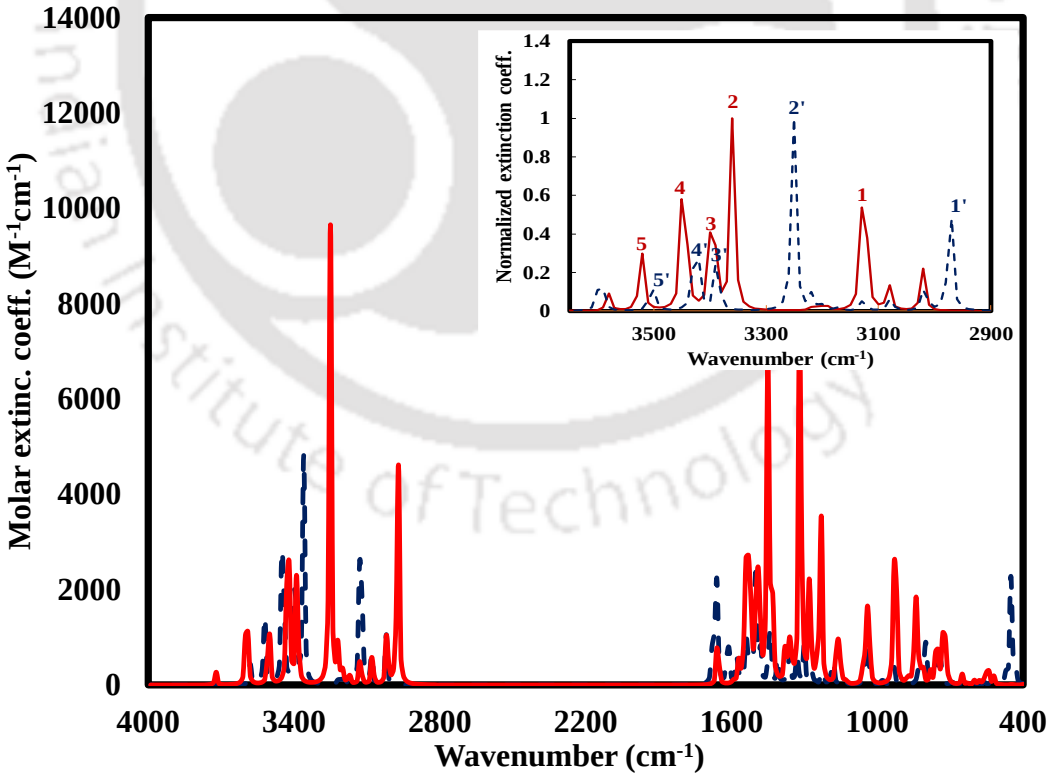

Figure 6.2. Simulated infrared spectra of AHPIP-c.$(CH_3OH)_3$ complex in the ground (solid line) and excited states (dashed line). Inset represents the normalized spectra depicting O17-H28 (1, 1'), O19-H18 (2, 2'), N7-H27 (3, 3'), O22-H21 (4, 4') and O25-H24 (5, 5') stretching frequencies.

TH-2834_146122035

Table 6.2. Calculated bond lengths (Å) and vibrational frequencies ($\bar{\upsilon}$, cm^{-1}) of O–H and N–H bonds of AHPIP-c.$(CH_3OH)_3$ complex in the ground and the excited states.

	Bond length		Vibrational frequency		Vibrational frequency
	S_0	S_1	S_0	S_1	S_0-S_1
O17–H28	1.00	1.01	3125	2972	153
O19–H18	0.99	0.99	3359	3251	108
N7–H27	1.02	1.02	3395	3387	8
O22–H21	0.99	0.99	3446	3425	21
O25–H24	0.98	0.98	3522	3504	18

The 'O–H' stretching frequency of the methanol molecule formed the hydrogen bond with pyridyl nitrogen (O19–H18) in AHPIP-c.$(CH_3OH)_3$ complex is 3359 cm^{-1}. But the 'O–H' stretching frequency of the methanol molecule that formed the hydrogen bond with pyridyl nitrogen (O19–H18) in DMAPIP-c.$(CH_3OH)_3$ complex was reported as 3318 cm^{-1}.[80] If the methanol 'O–H' bond forms a stronger hydrogen bond with pyridyl nitrogen, its strength reduces and its vibrational frequency decreases. It shows that the 'O–H' bond of methanol that formed a hydrogen bond with pyridyl nitrogen in AHPIP-c.$(CH_3OH)_3$ complex is stronger than the same in DMAPIP-c.$(CH_3OH)_3$ complex. It means that the intermolecular hydrogen bond formed with pyridyl nitrogen is weaker in AHPIP-c.$(CH_3OH)_3$ than DMAPIP-c.$(CH_3OH)_3$. Therefore, the intermolecular proton transfer is less favoured in AHPIP-c.$(CH_3OH)_3$ complex.

6.3. Structure of Tautomer complexes

Excited state optimized structures of the possible tautomers are given in **Figure 6.3,** along with selected geometrical parameters in **Table 6.2**. The intramolecular proton transfer from the 'OH' group to azole nitrogen results in keto tautomer **I**. In the keto tautomer, N9–H28 hydrogen bond shrunk to 1.02 Å as the covalent bond O17–H28 bond elongated as a hydrogen bond. The intermolecular relay proton transfer in the cyclic ring produces pyridinyl tautomer **IIA.** In this tautomer methanol complex, hydrogen bonds (H27---O25 and H18---N2) are shortened to form covalent bonds (1.00 Å and 1.02 Å). The bond length of H18–O19 and H25–N7 increases to 2.14 Å and 1.81 Å, respectively and convert to hydrogen bonds. The other molecules involved in the hydrogen-bonded ring also rearrange accordingly to change the covalent bonds to hydrogen bonds and vice-versa. The torsional rotation of the amino group of the tautomer leads to the TICT state formation. Thus, the structure of the amino twisted tautomer **IIB** was also fully optimized. When the amino group is twisted, the N9–H28 bond becomes a covalent bond and the O17–H28 bond becomes a hydrogen bond, indicating the conversion of enol to keto tautomer. The observed vibrational frequency 1466 cm^{-1} of the

TH-2834_146122035

amino twisted tautomer IIB is close to the vibrational frequency at 1474 cm^{-1} of the keto tautomer (**I**), which corresponds to the 'C=O' stretching frequency. It shows that intramolecular proton transfer is more favoured in the excited state.

Table 6.3. O17–H28, N9–H28, N7—H27, O25—H27, N7—H18, O19—H18 bond lengths N7—H27—O25 and N7—H18—O19 bond angles for enol, keto, pyridinyl tautomer (normal and amino twisted) in the excited state (Refer figure 6.3 for structures).

Bond length (Å)/ angle (°)	Enol	Keto tautomer	Pyridinyl tautomer	
			Normal	Amino twisted
O17–H28	1.01	1.98	1.03	1.97
N9–H28	1.67	1.02	1.59	1.01
N7–H27	1.03	1.03	1.81	1.85
O25–H27	1.92	1.88	1.00	0.99
N2–H18	1.83	1.84	1.02	1.02
O19–H18	0.99	0.99	2.14	2.12
N7–H27–O25	153.93	154.51	171.13	170.66
N2–H18–O19	161.55	161.12	138.26	139.02

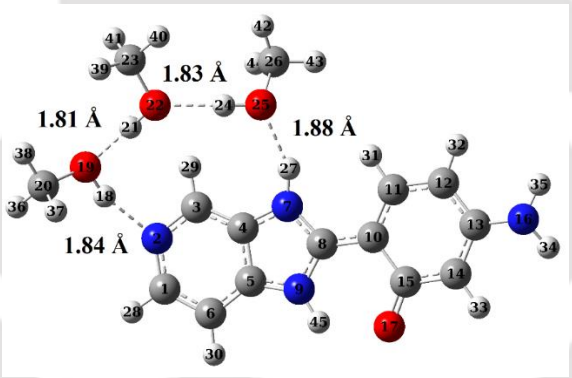

(I) Keto Tautomer

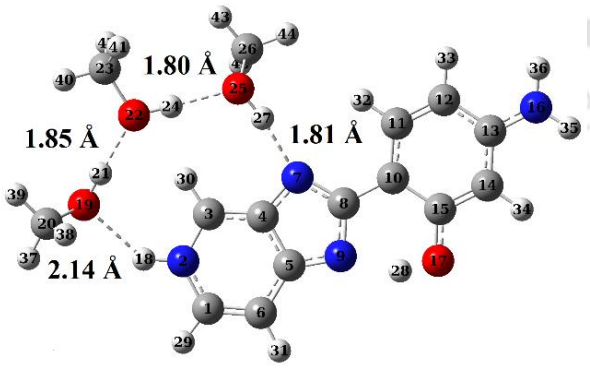

(IIA) Pyridinyl Normal

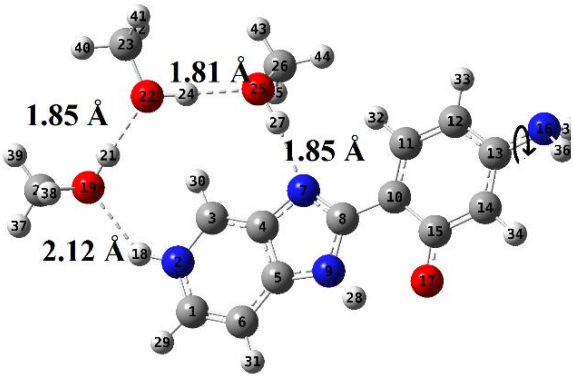

(IIB) Pyridinyl Amino Twisted

Figure 6.3. The excited state optimized structure of the tautomers, (I) keto, pyridinyl (IIA) normal tautomer and (IIB) amino twisted tautomer.

TH-2834_146122035

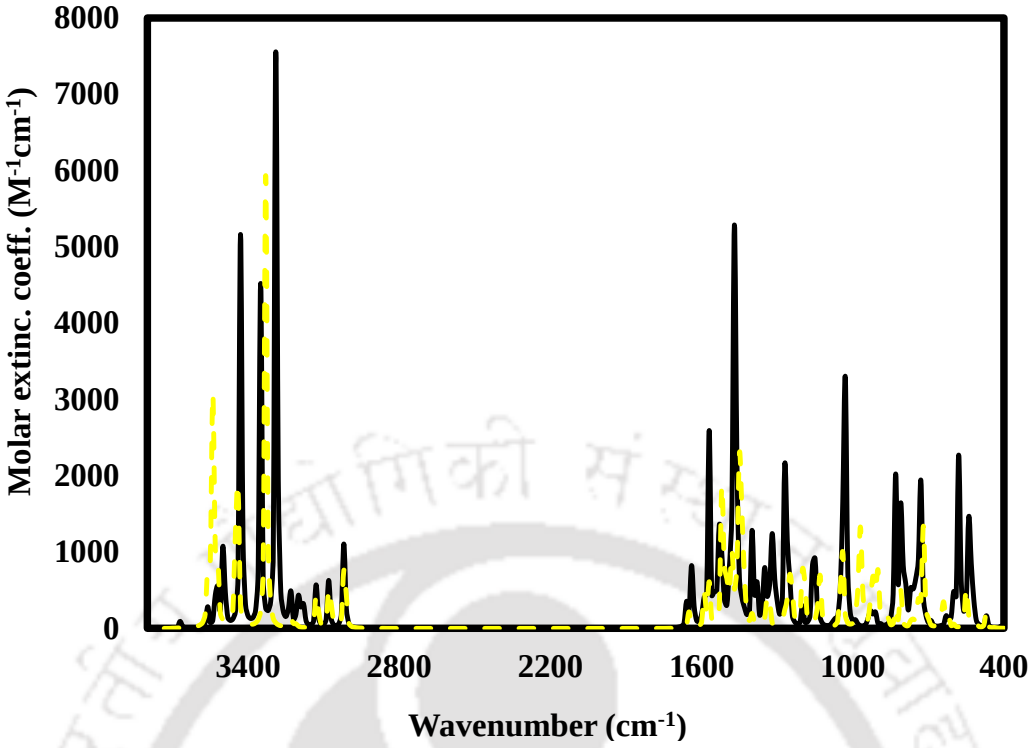

Figure 6.4. Simulated infrared spectra of keto (solid line) and pyridinyl tautomer (dotted) AHPIP-c.$(CH_3OH)_3$ complex in the excited states.

6.4. Potential energy curves of the proton transfers

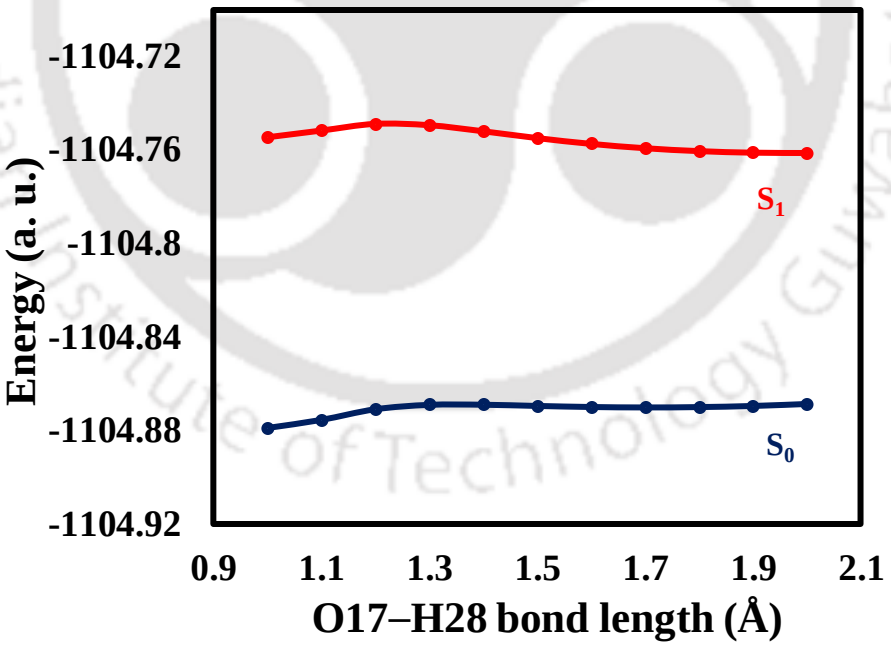

Figure 6.5. The potential energy curve for the intramolecular proton transfer in methanol.

TH-2834_146122035

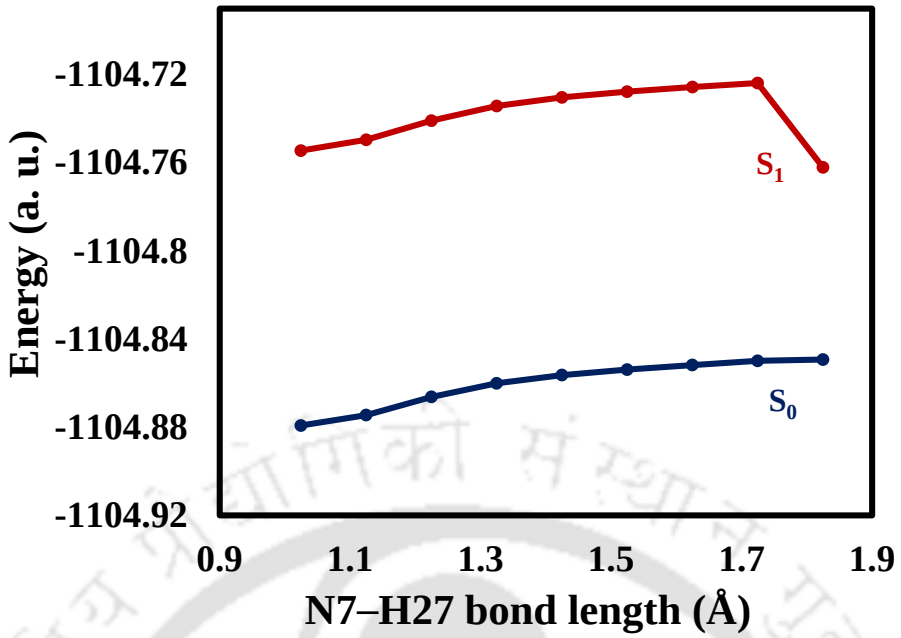

Figure 6.6. The potential energy curve for the intermolecular proton transfer from imidazole N7─H27 to the methanol molecule.

Potential energy curves were obtained for both the proton transfer processes in the ground and excited states (**Figures 6.5 and 6.6**). Enol 'O–H' (O17–H28) distance was increased stepwise (step size = 0.1 Å) in the ground and excited states and the energies were calculated at each point to construct the plot. The initial and final bond lengths were kept as obtained from the optimized geometries of the tautomers. Similarly, imidazole 'N–H' (N7–H27) distance was increased to obtain the plot for the intermolecular proton transfer from imidazole to methanol (**Figure 6.3**, **IIA**). This normal pyridinyl tautomer may create the TICT state by twisting the amino group (**Figure 6.3**, **IIB**). The barrier heights for both proton transfer processes in the excited states (13.6 and 80.5 kJ/mol) decreases compared to the ground states (27.0 and 81.1 kJ/mol). Due to reduced bareer height, these proton transfers would be favoured in excited states than in the ground states. The reduction in the barrier height of the ESIPT is significant, but that of intermolecular proton transfer is negligible. The barrier height for ESIPT is also significantly less than that of solvent assisted proton transfer from imidazole to pyridyl nitrogen. Omidyan et al. calculated the ESIPT barrier in AHPIP-c as 13.5 kJ/mol.[263] They concluded that the proton transfer dynamics of AHPIP-c should be similar to HPIP-c (**Chart 6.1**). Hence, ESIPT is much favoured over solvent assisted proton transfer from imidazole to pyridyl nitrogen.

The theoretical rate constant (k) for the ESIPT was calculated by using the Arrhenius equation,

TH-2834_146122035

$$k = A.\exp(-E_a/RT)$$

$$\text{where, } A = \frac{k_B T}{h}\exp(\Delta S/R)$$

A is pre-exponential factor. E_a is the activation energy calculated by subtracting the enthalpy of the reactant from the enthalpy of the transition state. R is the universal gas constant. T is the absolute temperature, i.e. taken as 298K (room temperature), k_B and h are the Boltzmann and Planck's constants, respectively. The change is entropy (ΔS) is calculated by subtracting the entropy of the reactant from the entropy of the transition state. The transition state was taken as the maximum of the PES diagram and optimized. The thermochemical data (enthalpy and energy) were obtained from frequency calculation results. The theoretical rate constant of ESIPT in AHPIP-c.$(MeOH)_3$ was calculated to be 6.2 x 10^{12} s^{-1}. This is in accordance with literature reports on the rate constant of ESIPT reactions.[271]

6.5. Electronic transitions

Table 6.4. Major absorption transitions, wavelength maximum (λ_{max}, nm), oscillator strength (*f*) and corresponding contributing molecular orbitals of Enol form of AHPIP-c.$(CH_3OH)_3$.

Transition	λ_{max}	*f*	Contributing Molecular Orbitals
$S_0 \rightarrow S_1$	349	1.2069	HOMO → LUMO (97%)
$S_0 \rightarrow S_2$	293	0.0489	HOMO – 1 → LUMO (81%) HOMO → LUMO + 1 (11%) HOMO → LUMO + 4 (4%)

Surface cubes for the frontier molecular orbitals (FMOs) were generated to understand the nature of the electronic transitions in various forms of AHPIP-c.$(CH_3OH)_3$ complex (**Annexure C**). The details of the absorption transitions are provided in **Table 6.4**. The longest wavelength absorption is predominantly a single excitation from the highest occupied molecular orbital (HOMO) to the lowest unoccupied molecular orbital (LUMO). It is a $\pi \rightarrow \pi^*$ transition. This transition is highly allowed (higher oscillator strength) than the other higher energy transitions. The higher energy transitions involve multiple excitations and have relatively lower oscillator strengths. The natural transition orbitals (NTOs)[272] generated for the first excited states of all the four forms (enol, keto and pyridinyl tautomers) of AHPIP-c.$(CH_3OH)_3$ are the same as their respective HOMO and LUMO (**Figure 6.7**). They show that the transitions are primarily HOMO-LUMO transition.

TH-2834_146122035

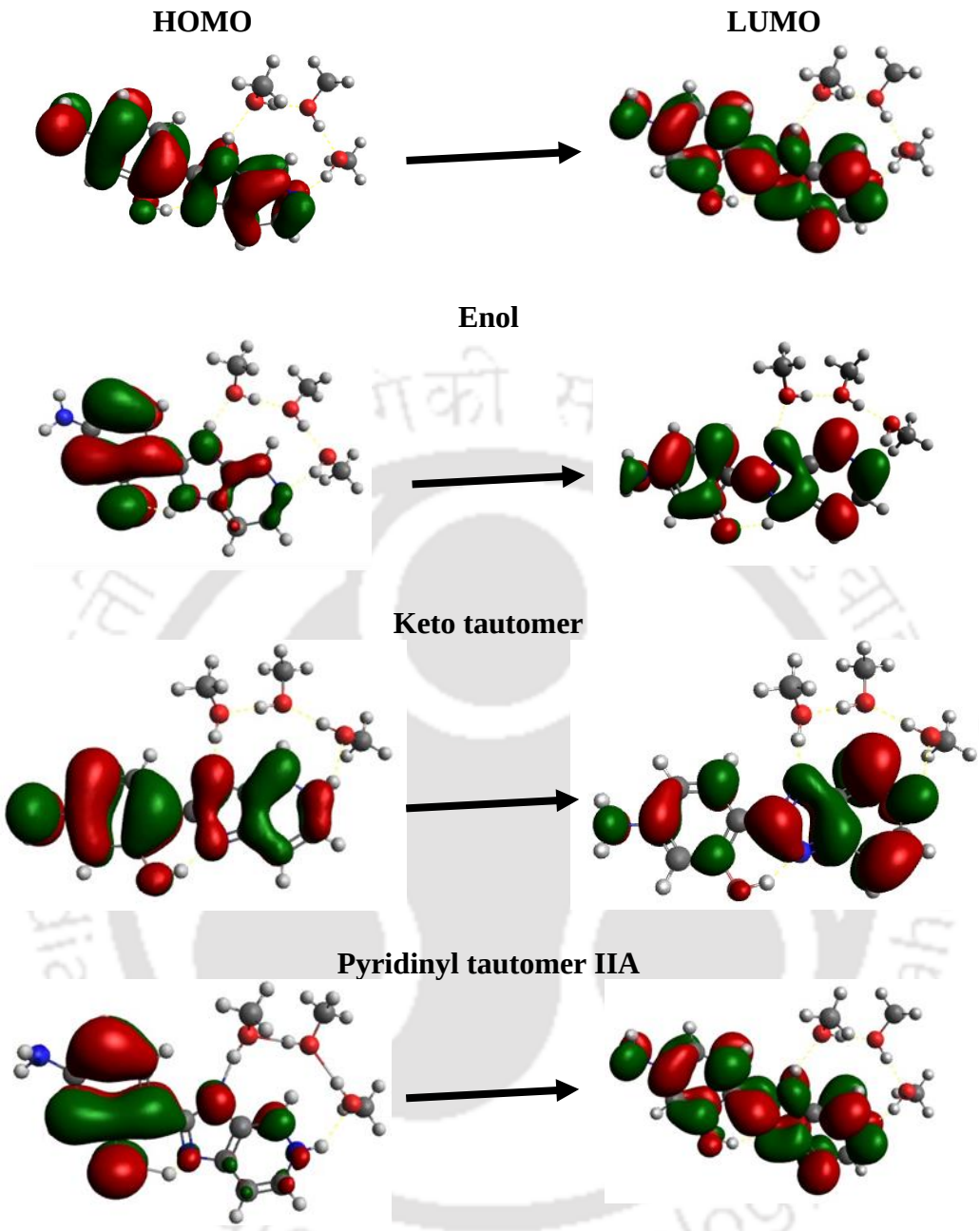

Figure 6.7. Natural transition orbitals (NTOs) generated for the first excited states of enol, keto (I), pyridinyl tautomer (IIA) and amino twisted pyridinyl tautomer (IIB).

TH-2834_146122035

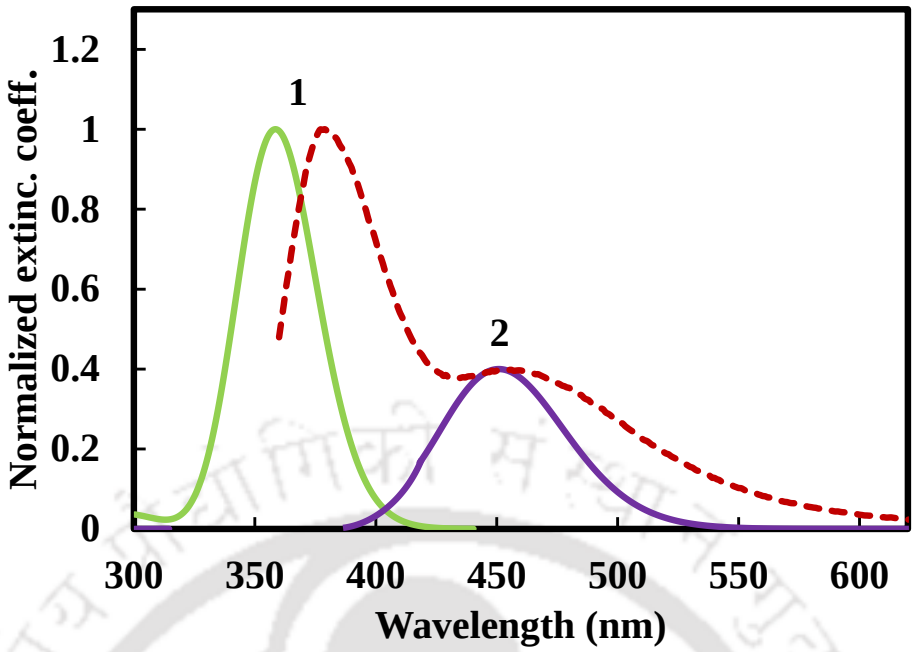

Figure 6.8. TDDFT simulated emission spectra of enol (1) and keto (2) tautomers of AHPIP-c in methanol (dashed line is the experimental spectrum).

Table 6.5. Theoretical (λ_{max}^{theo}, nm) and experimental emission maximum (λ_{max}^{exp}, nm)[206] of enol and keto forms of AHPIP-c.

Forms	λ_{max}^{theo}	λ_{max}^{exp}
Enol	358	379
Keto	441	451

Table 6.6. The emission transition of different forms, emission maximum (λ_{max}), Oscillator strength (*f*) and corresponding contributing molecular orbitals of Different forms of AHPIP-c.$(CH_3OH)_3$.

Forms	λ_{max} (nm)	*f*	Contributing Molecular Orbitals
Enol	358	1.0408	LUMO → HOMO (98%)
Keto (I)	441	0.5002	LUMO → HOMO (98%)
Pyridinyl Tautomer (II A)	400	0.5520	LUMO → HOMO (99%)
Amino Twisted Pyridinyl Tautomer (II B)	546	0.1308	LUMO → HOMO (100%)

The frontier molecular orbitals are shown in **Annexure C**.

The experimental absorption maxima for the enol form of AHPIP-c in methanol are 303 and 342 nm (**Table 6.1**).[206] The theoretically obtained absorption maxima (293 and 349 nm) match well with experimental maxima (**Table 6.4**). The shorter wavelength emission (corresponding to normal form) and longer wavelength emission maxima (corresponding to

TH-2834_146122035

keto form) are 379 and 451 nm, respectively.[206] The stimulated emission spectra of keto and enol forms are shown in **Figure 6.8**. The emission maxima (358 nm) of the normal form are quite close to the experimental value. The calculated keto emission (441 nm, **Table 6.5**) also matches well with the observed keto emission (451 nm). The theoretically calculated TICT emission maximum (amino Twisted Pyridinyl Tautomer, II B, **Table 6.6**) is the longest (546 nm) and is not observed experimentally.[206]

6.6. Isosurface of hole and electron distribution and heat map

The isosurfaces of hole, electron and hole electron overlap were done by the approach proposed by Chen et al.[273] using Multiwfn[218] wavefunction analyzer (**Figure 6.9**). The corresponding Δr and t indices were also obtained using the Multiwfn program (**Table 6.7**).[32,33] The contribution of all non-hydrogen atoms to hole and electron are also shown as the heat map in **Figure 6.9**. The x-axis on the heat map denotes the no. assigned to individual atoms in the Z-matrix of optimized output in Gaussian09. The colour scale on the right represents percentage contribution.

Table 6.7. Δr and t indices of first excited state of different forms of AHPIP-c.$(CH_3OH)_3$.

Forms	Δr index (Å)	t index (Å)
Enol	1.94	-0.78
Keto	2.68	0.49
Pyridinyl (II A)	3.93	1.49
Amino twisted pyridinyl (II B)	4.66	2.84

In a single-electron excitation process, hole and electron distributions respectively indicate the region where an electron leaves and goes to. The Δr index is a quantitative indicator of an electron excitation mode.[274] A smaller Δr index value indicates the likelihood of excitation to be a locally excited state. If the Δr index for a state is smaller than 2.0, then the state can be characterized as the locally excited state. However, in exceptional cases, it may be large. Other indices are proposed to assign locally excited, charge transfer or Rydberg character to an electronic state. For example, t index[275] also gives details about the separation of hole-electron. $t > 0$ means the separation is clear.

Figure 6.9 presents the isosurfaces of distribution of hole, electron and hole-electron overlap of the S_1 state of enol, keto, pyridinyl and pyridinyl twisted forms of AHPIP-c.$(CH_3OH)_3$. The corresponding Δr and t indices are also given in **Table 6.7**.

TH-2834_146122035

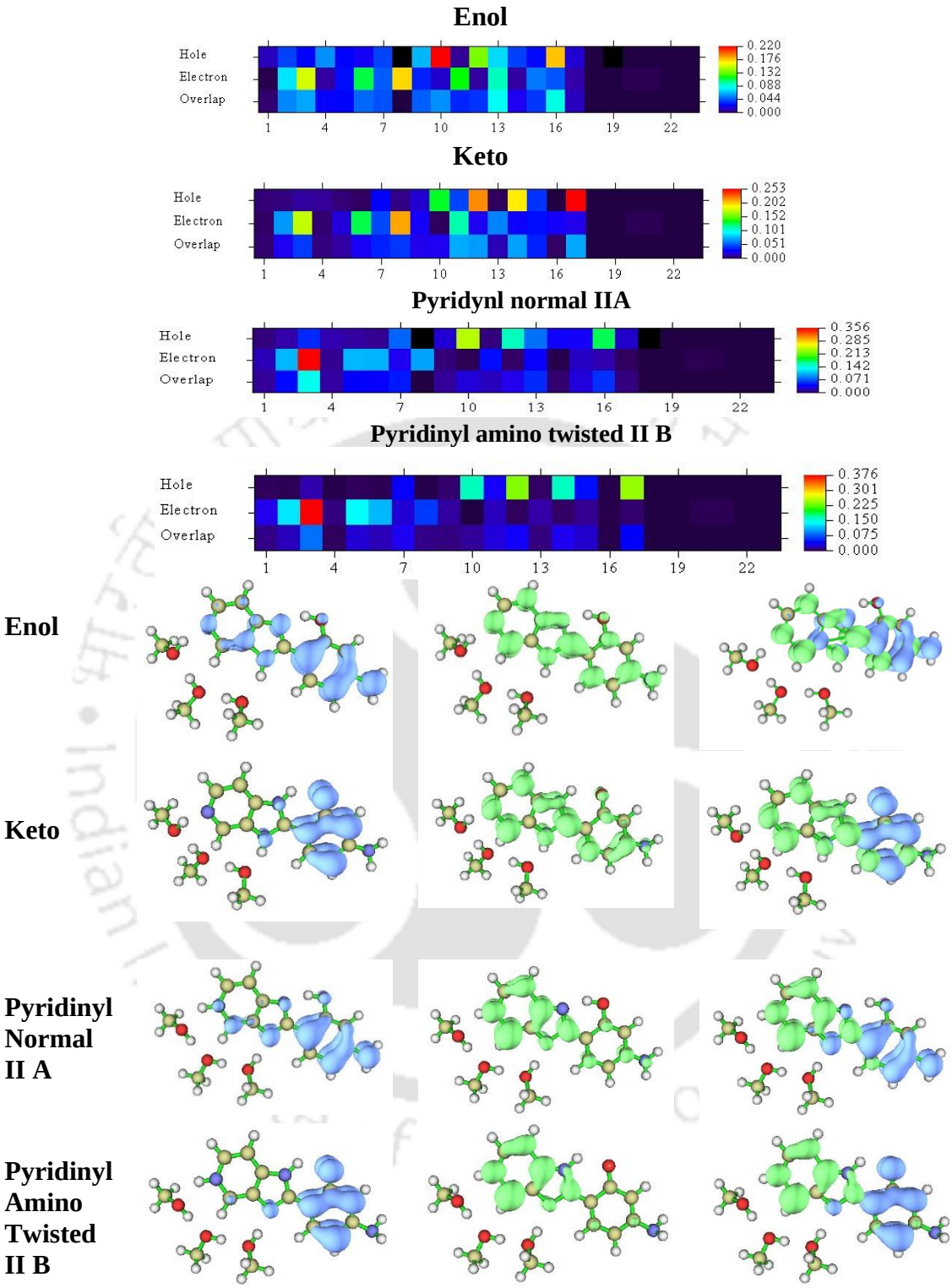

Figure 6.9. Heat map and isosurface of hole, electron and overlap distribution of first excited state of different forms of AHPIP-c.$(CH_3OH)_3$.

Figure 6.9 clearly shows that in the case of enol, hole and electron overlap over each other. $\Delta r < 2$, t (-0.775 Å) is negative also indicate that hole and electron overlap. In the case

TH-2834_146122035

of keto, the hole is concentrated on the aminophenol ring, but the electron is distributed over the whole molecule. The hole electron separation in the first excited state is more apparent in pyridinyl tautomers than keto (**Figure 6.9**). The charge transfer character increases in the order of keto < pyridinyl IIA < pyridinyl II B.

6.7. Conclusion

The proton transfer mechanism of AHPIP-c was investigated in methanol using TDDFT. The calculations suggest that AHPIP-c.$(CH_3OH)_3$ cyclic structure is weaker than DMAPIP-c.$(CH_3OH)_3$ cyclic structure. The decrease in vibrational frequency in the S_1 state in the enol O–H bond is more than the imidazole N–H bond. It shows that breaking of the enol O–H bond is more favourable than the N–H bond in the excited state. The barrier heights for proton transfer-processes is reduced in the excited state compared to the ground state in both proton transfer. Potential energy curves also suggested that the intramolecular proton transfer is favoured over the intermolecular proton transfer. Thus, ESIPT dominates over TICT in AHPIP-c and AHPIP-c emits only tautomer emission along with normal emission. This work is published in *J. Photochem. Photobiol. A Chem.*, 2021, 113199.

TH-2834_146122035

TH-2834_146122035

Chapter 7

Turning on Intramolecular Charge Transfer Emission in 2-(4′-Amino-2′-hydroxyphenyl)-1H-imidazo-[4,5-c]pyridine by Intermolecular Proton Transfer

TH-2834_146122035

TH-2834_146122035

7.0. Introduction

In AHPIP-c (**Chart 7.1**), ESIPT predominates over ICT.[206] However, TICT takes places in its methoxy counterpart, AMPIP-c (**Chart 7.1**) in methanol.[206] In the previous chapter, the cause for the absence of TICT emission in AHPIP-c was revealed.

AHPIP-c (I) **AMPIP-c (II)**

Chart 7.1. Structures of AHPIP-c (I) and AMPIP-c (II).

However, TICT takes places in its methoxy counterpart, AMPIP-c (**Chart 7.1**) in methanol.[206] In the previous chapter, AHPIP-c was studied in methanol using TDDFT. Based on the bond lengths, angles, vibrational analysis and potential energy curves in the ground and excited states, we inferred why AHPIP-c gives ESIPT emission in methanol.[276]

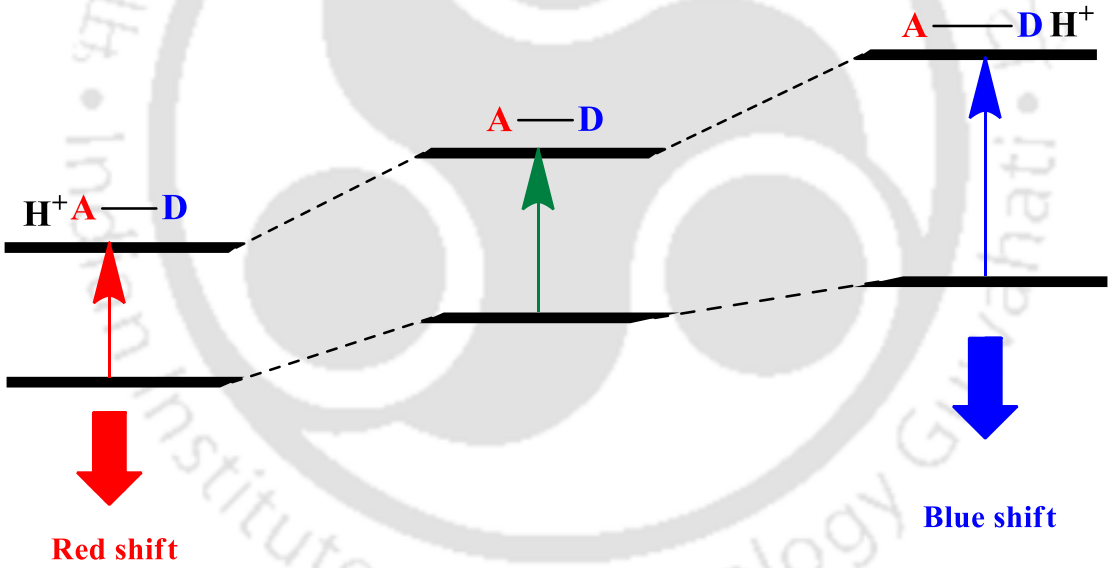

Scheme 7.1. Electronic spectral shifts upon binding of H^+ with donor (D) and acceptor (A) groups.

The binding of proton at the acceptor (pyridyl/imidazole =N-) or donor (-NH_2) groups can influence the proton and charge transfer (**Scheme 7.1**). The binding of the proton to imidazole nitrogen can turn off the ESIPT emission by making the proton acceptor unavailable for proton transfer. The deprotonation of –OH may also turn off the ESIPT emission (**The findings in chapter 3 also corroborate this.**).[277] The protonation at acceptor and deprotonation at the donor enhance the charge transfer. Therefore, the effect of acid and base on AHPIP-c and its methoxy derivative, AMPIP-c, is investigated.

TH-2834_146122035

Table 7.1. Excitation spectral maximum (λ_{ex}^{max}, nm) and emission spectral maximum (λ_{em}^{max}, nm) of different species of AHPIP-c and AMPIP-c in water.

Species	AHPIP-c			AMPIP-c		
	pH/H_0	λ_{ex}^{max}	λ_{em}^{max}	H_/pH/H_0	λ_{ex}^{max}	λ_{em}^{max}
Neutral-enol	8.0	330	392	9.8	329	387
Neutral-keto	8.0	330	444	–	–	–
MA1	10.5	357	425	–	–	–
MA2	10.5	337	~510	–	–	–
MA3	–	–	–	14.0	318	378
MC1	4.0	~275	~385	4.5	~295	–
MC2	4.0	~340	380	4.5	~335	~410
MC3	4.0	360	~505	4.5	~350	~505
DC1	2.0	~280	380	1.7	~285	~365
DC2	2.0	~330	450	1.7	~320	~420
DC3	2.0	367	520	1.7	~370	~500
TC	–10.2	354	430	–10.2	350	430

7.1. Neutral-monoanion equilibria

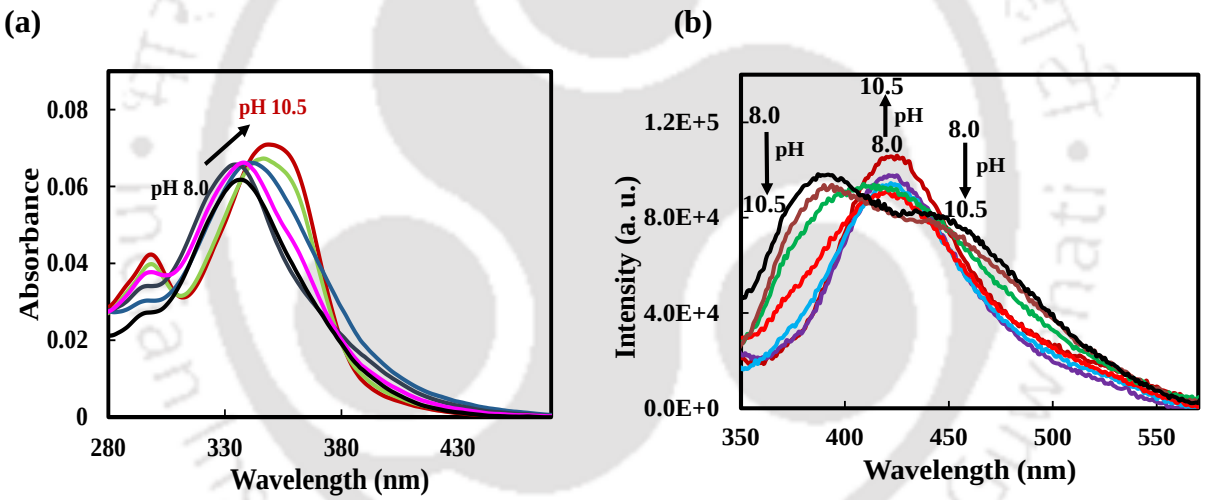

Figure 7.1 (a). Absorption spectra of neutral-monoanionic equilibria of AHPIP-c in water. (b). Emission spectra of neutral-monoanionic equilibria of AHPIP-c in water, λ_{ex} = 300 nm.

AHPIP-c at pH 8.0 shows maximum absorbance at 332 nm (**Table 7.1**). This experimental data is close to other organic solvents.[206] When the pH of the solution increases from 8.0 to 10.5, the 332 nm absorption band of AHPIP-c is red-shifted with an increase in absorbance (**Figure 7.1 (a)**). The increase in pH deprotonates the molecules. Emission spectra of AHPIP-c monitored in the pH range 8.0 to 10.5 are given in **Figure 7.1. (b)**. Neutral AHPIP-c emits at 392 and 444 nm in water (pH 8.0). Like other solvents, the shorter and the longer wavelength emissions in water can be attributed to normal and keto emissions, respectively. The 392 nm band is red-shifted than normal emission in other solvents. The 444 nm band is blue-shifted with respect to the keto band of other less polar solvents.[206] The spectral shift and

TH-2834_146122035

the absence of the keto band in the emission spectrum of methoxy derivative (see later) confirms these assignments. Upon increasing the pH from 8.0 to 10.5, the intensities of both enol and keto band decrease. When the pH was raised, a strong emission emerged at about 425 nm with a very weak emission at ~ 510 nm.

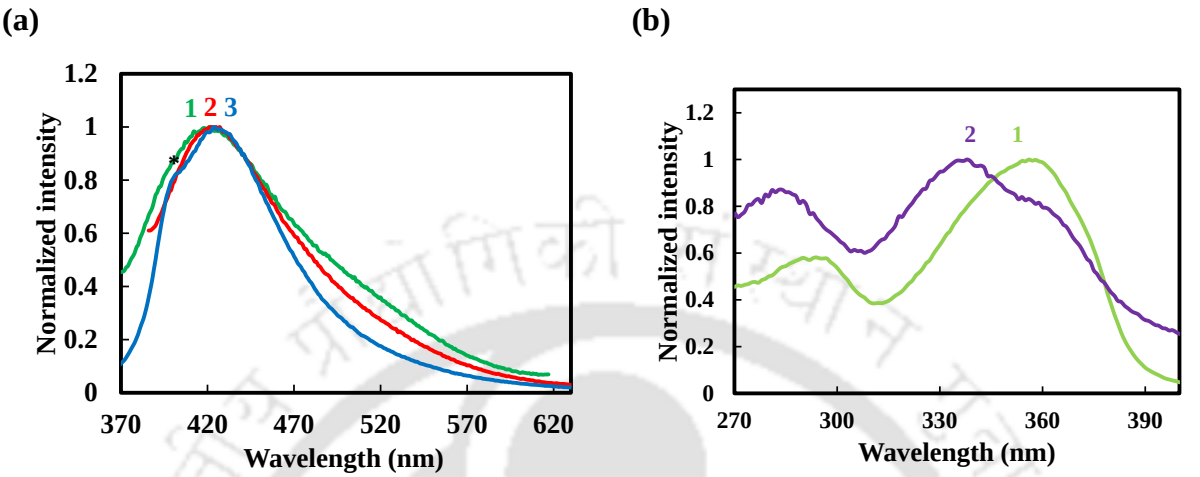

Figure 7.2 (a). Normalized emission spectra of MAs of AHPIP-c in water, λ_{ex} = 320 nm (1), 335 nm (2), 350 nm (3), *water Raman. (b). Normalized excitation spectra of MAs of AHPIP-c in water, λ_{em} = 430 nm (1) and 510 nm (2).

The emission spectra of AHPIP-c at pH 10.5 at different excitations are given in **Figure 7.2 (a)**. Excitation spectra of monoanions were recorded at 430 and 510 nm (**Figure 7.2 (b)**). When monitored at 430 nm, the excitation maximum was observed at 357 nm. On the other hand, when monitored at 510 nm, the excitation band at 357 nm becomes a shoulder, and a new excitation band appears at 337 nm. It shows that the 357 nm excitation band corresponds to the 425 nm emission band. The 337 nm excitation corresponds to the ~510 nm emission band.

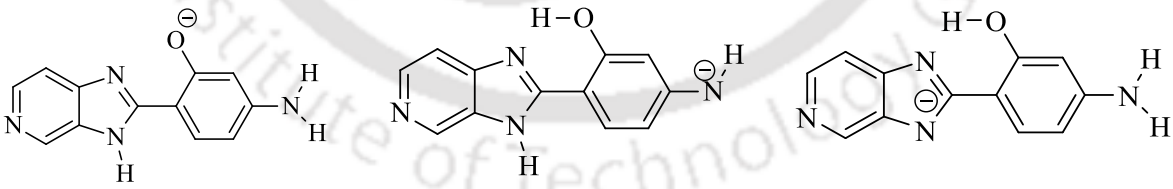

MA1 **MA2** **MA3**

Chart 7.2. Different possible monoanions of AHPIP-c.

AHPIP-c has three acidic groups. Accordingly, three kinds of monoanions are possible and are labelled as MA1, MA2 and MA3 (**Chart 7.2**). Two acidic groups, the 'OH' and 'NH_2' groups, are present on the charge donor aminophenyl ring. Deprotonation of these protons increases charge transfer from the donor, which will produce a red shift in the spectra.

TH-2834_146122035

The molecule has an acidic group, 'NH', on the charge acceptor, and the deprotonation of this proton will reduce the acceptor's ability to accept the proton. This deprotonation will cause a blue shift in the spectrum. Both the excitation spectral bands (337 and 357 nm) are red shifted than the corresponding excitation spectra of the neutral band. The red shift in the excitation suggests that both the monoanions are formed by deprotonation of the acidic groups present in the aminophenol ring. As the 357 nm excitation band corresponds to 425 nm emission, it can be assigned to MA1 formed by the deprotonation of 'OH'. The 'OH' deprotonation causes a red shift in the emission spectrum but eliminates the ESIPT process. The 425 nm emission spectrum is red-shifted than the normal emission and blue-shifted than the tautomer emission. As discussed in chapters 3 and 4, such spectral shift is a characteristic feature of the anion formed by the 'OH' deprotonation in ESIPT molecules.[115,238] The 337 nm band can be attributed to MA2 formed by the deprotonation of the 'NH_2' proton. Though the excitation spectrum of the MA2 is blue-shifted than the excitation spectrum of MA1. The corresponding emission spectrum (~510 nm) is substantially red-shifted. The Stokes shift is also very large (8403 cm^{-1}). The emission (~510 nm) is also close to the TICT emission of the methoxy derivative.[206] As discussed in the previous chapter in APIPs, the TICT emission is formed by the charge transfer from amino group to imidazopyridine ring. The deprotonation of the amino group increases the charge donating ability of the amino group. Therefore, it enhanced the ICT and MA2 gives TICT emission.

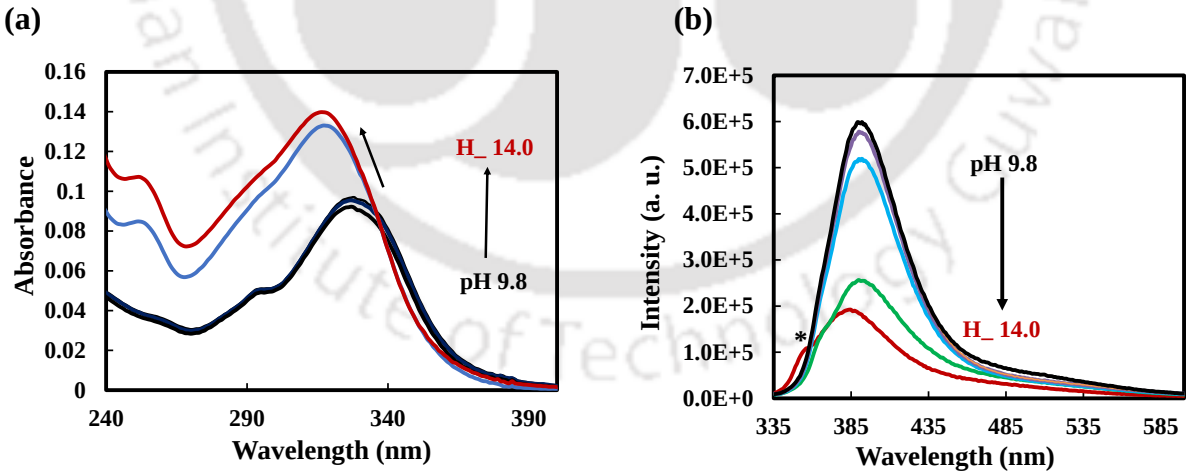

Figure 7.3 (a). Absorption spectra of neutral-monoanionic equilibria of AMPIP-c in water. (b). Emission spectra of neutral-monoanionic equilibria of AMPIP-c in water, λ_{ex} = 300 nm (*water Raman).

The neutral form of AMPIP-c (at pH 9.8) has absorption maximum at 329 nm (**Figure 7.3 (a) and Table 7.1**). Upon increasing the basicity, the absorption spectrum is blue-shifted with an increase in absorbance. The neutral form emits normal fluorescence at 387 nm and a

TH-2834_146122035

weak TICT emission at ~500 nm in water. In methanol also, AMPIP-c emits both normal and a weak TICT emission.[206] In water, both the emissions are red-shifted compared to the respective emission in methanol. Upon increasing the basicity, the fluorescence intensity decreases and the emission maximum is blue-shifted to 378 nm. Unlike hydroxy derivative, AMPIP-c lacks an 'OH' proton; therefore, it cannot form MA1. Although it can form MA2, but both the absorption and emission spectra are blue-shifted than the neutral. This blue shift shows that the methoxy derivative forms MA3, not MA2.

7.2. Neutral-monocation equilibria

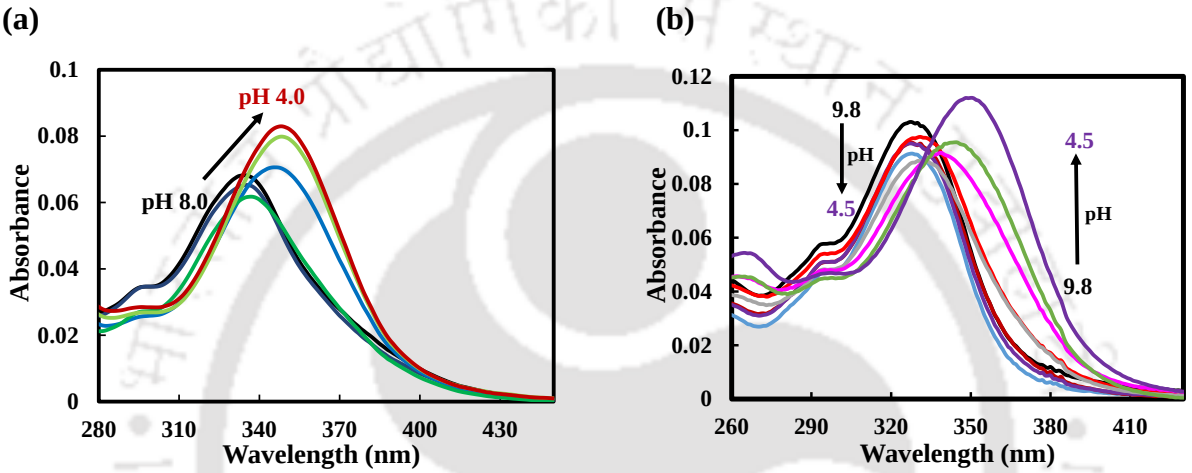

Figure 7.4. Absorption spectra of neutral-monocation equilibrium of (a) AHPIP-c and (b) AMPIP-c in water.

When the pH decreased from 8.0 to 4.0, the absorption maximum of AHPIP-c in water is red shifted with an enhancement in absorbance (**Figure 7.4 (a)**). No clear isosbestic point is observed. The absorption band of AHPIP-c at pH 4.0 has a maximum at 348 nm. Upon reducing the pH, the absorption spectrum of the methoxy derivative, AMPIP-c, also undergoes bathochromic shift with a quasi-isosbestic point at 337 nm (**Figure 7.4 (b)**). At pH 4.5, the absorption maximum of AMPIP-c is observed at 352 nm. The bathochromic shift (332 nm → 352 nm) suggests an increase in conjugation. In both AHPIP-c and AMPIP-c, the imidazopyridine ring is the charge acceptor and the aminophenyl ring is the charge donor (**Chart 7.1**).

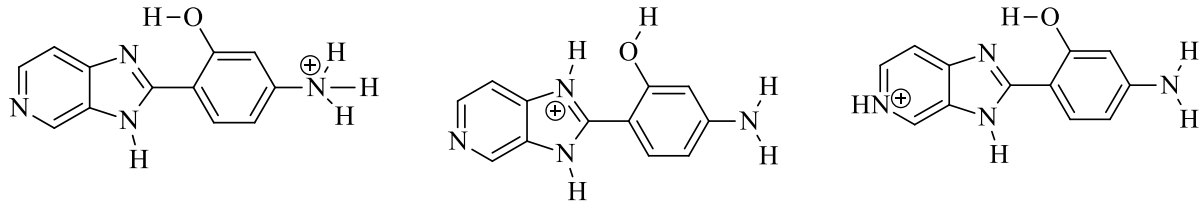

MC1 **MC2** **MC3**

Chart 7.3. Different possible monocations of AHPIP-c.

TH-2834_146122035

Both the molecules have three basic nitrogens, one is present on the donor and two are present on the acceptor. Accordingly, three monocations are possible and they are labelled as MC1, MC2 and MC3 (**Chart 7.3**). The protonation at the acceptor, i.e., the imidazopyridine ring nitrogen, enhances the acceptor's electron withdrawing capacity that increases the conjugation. On the other hand, protonation at the donor, i.e., the amino nitrogen of the amino hydroxyphenyl ring, decreases the donor ability to donate the proton that decreases the conjugation. Therefore, MC1, which is formed by the protonation of 'NH_2' of the amino hydroxyphenyl ring, produces a blue shift. MC2 and MC3, respectively formed by the imidazole and the pyridyl nitrogen protonations produce a red shift in the spectrum. Since protonation at the pyridyl nitrogen increases the conjugation more than that at imidazole nitrogen,[246,278] the red shift in the absorption and emission spectra of the MC3 is expected to be larger than in those spectra of the MC2.

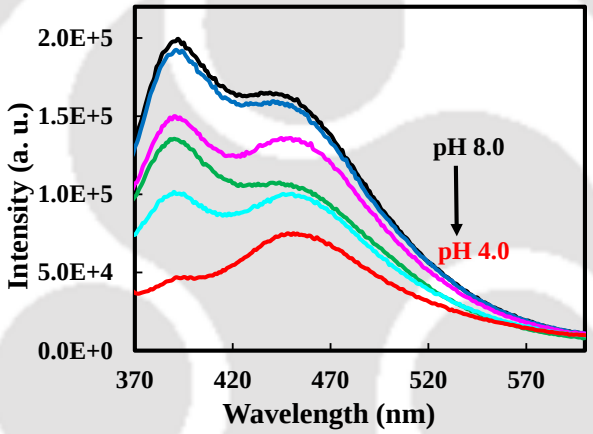

Figure 7.5. Emission spectra of neutral-monocation equilibria of AHPIP-c in water, λ_{ex} = 335 nm.

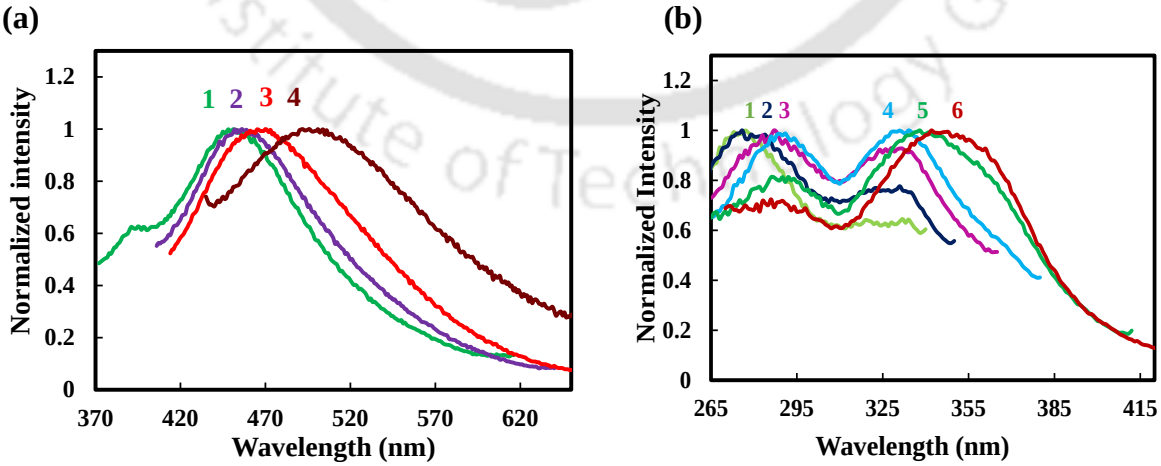

Figure 7.6 (a). Normalized emission spectra of MCs of AHPIP-c in water, λ_{ex} = 320 nm (1), 335 nm (2), 350 nm (3), 370 nm (4). (b). Normalized excitation spectra of MCs of AHPIP-c in water, λ_{em} = 395 nm (1), 410 nm (2), 430 nm (3), 450 nm (4), 490 nm (5), 510 nm (6).

TH-2834_146122035

The fluorescence intensity of the AHPIP-c in water decreases when the pH drops from 8.0 to 4.0 (**Figures 7.5**). Though, two emission bands are observed even at pH 4.0, the intensity ratios are different. It shows the formation of monocations. AHPIP-c has three basic centres and can form MC1, MC2 and MC3 at the same time as discussed. The absence of isosbestic point also suggests that the formation of different monocations. The different monocations absorb at different wavelengths. In such cases, emission spectra (at multiple excitations) and excitation spectra (at multiple emissions) can better represent the existence of various monocations. Therefore, the emission spectra were recorded by exciting at various wavelengths (**Figures 7.6 (a)**). Excitation at 320 nm has an emission band at ~385 nm along a band at ~450 nm. The 450 nm band further shifts towards red when excited at longer wavelengths and emits at ~505 nm when excited at 370 nm.

The excitation spectra at different emission wavelengths are shown in **Figures 7.6 (b)**. The excitation spectra monitored at 395 nm and 410 nm results in a band at ~ 275 nm with a shoulder at ~340 nm. When monitored at 430 nm and 450 nm, both the band shifts red, and the shoulder emerges as a band. When monitored further at wavelengths 490 and 510 nm, it results in another shoulder at 360 nm. The 360 nm excitation band is observed as a weak shoulder even when monitored at 450 nm, but its relative intensity increases when monitored at longer wavelengths. The excitation spectra clearly show the existence of all three different monocations. The ~275 nm excitation band and ~ 385 nm emission bands are blue-shifted than the neutral AHPIP-c. This blue shift shows the reduction in conjugation, therefore, can be assigned to MC1. As stated earlier, protonation at imidazole nitrogen (MC2) produces a lesser red shift in the spectra than pyridyl nitrogen (MC3). Therefore, based on the magnitude of the shift, the ~ 340 nm excitation and ~450 nm emission bands can be attributed to MC2. The ~ 360 nm (shoulder) excitation band and the emission at about 505 nm can be assigned to MC3. The Stokes' shift of MC3 emission is ~8000 cm^{-1}. In DMAPIP-c, Based on the significant Stokes shift, the emission of MC3 may be attributed to TICT emission of MC3.[278] However, due to the feasibility of both ESIPT and TICT, the study of methoxy molecule may be helpful for the assignment.

The normalized emission and excitation spectra of the methoxy derivative, AMPIP-c at pH 4.5 are given in **Figure 7.7 (a) & (b)**, respectively. At pH 4.5, MCs emission spectra consist of two bands centred at ~410 and ~505 nm (**Figure 7.7 (a)**). It indicates that there are at least two different MCs are present at this pH. Three different excitation bands were observed in

TH-2834_146122035

methoxy derivative at ~295, ~335 and ~350 nm like AHPIP-c (**Figure 7.7 (a)**). An excitation band was observed at 295 nm when monitored at 390 nm.

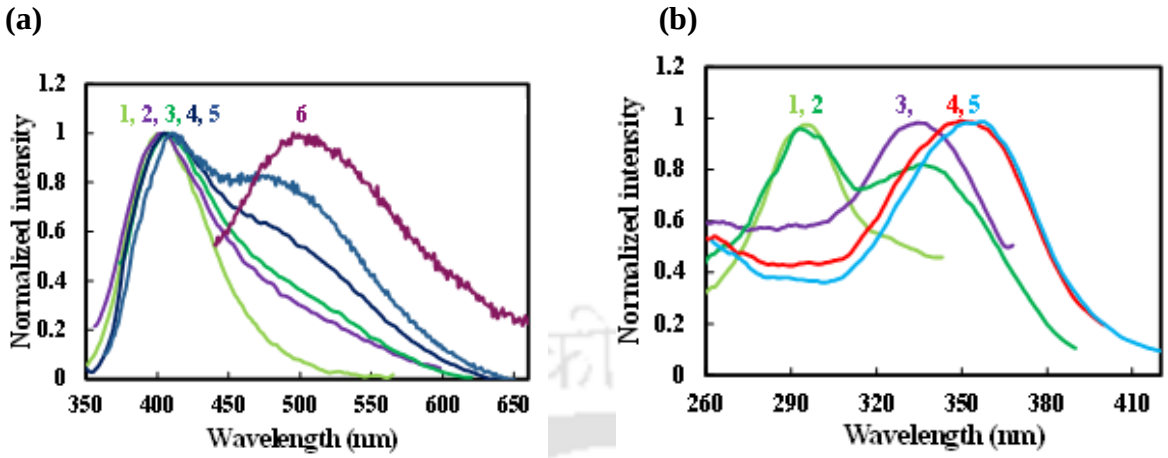

Figure 7.7 (a). Normalized emission spectra of MCs of AMPIP-c in water, λ_{ex} = 290 nm (1), 325 nm (2), 350 nm (3), 370 nm (4). (b). Normalized excitation spectra of MCs of AHPIP-c in acetonitrile, λ_{em} = 390 nm (1), 430 nm (2), 460 nm (3), 480 nm (4), 510 nm (5).

When monitored at 430 nm, another band also emerges at 335 nm along with 290 nm. The 350 nm becomes the sole excitation band when monitored at 460 nm. Monitoring at 480 nm and 510 nm yield another band at 350 nm. Both 410 and 505 nm emissions are red-shifted than the normal band emission (387 nm) of the neutral AMPIP-c. Therefore, they can be assigned to MC2 (410 nm) and MC3 (505 nm), respectively. Like AHPIP-c, the Stokes' shift in the fluorescence spectrum of MC3 is much greater than MC2. Unlike in AHPIP-c, ESIPT is not feasible in AMPIP-c, but it emits TICT emission.[206] The emission is also closely similar to its neutral form's TICT emission. As stated earlier, the proton transfer to pyridyl nitrogen induced the TICT emission in 4'-dimethylaminophenylimidazopyridines.[181,182] Therefore, the 505 nm emission of MC3 can be attributed to the TICT emission of MC3 rather than the normal emission. In DMAPIP-c also, the pyridyl nitrogen protonated monocation (MC3) emits TICT emission.[278] The existence of TICT emission in methoxy derivative (where ESIPT is not feasible) suggests that the 505 nm band of the MC3 of AHPIP-c is also a TICT emission (**Figure 7.15 (a)**). This assignment can be confirmed by solvatochromism. As discussed earlier, ESIPT and TICT will produce negative and positive solvatochromism, respectively. Therefore, the neutral-monocation equilibria were studied in methanol and acetonitrile.

The absorption maximum of AHPIP-c in methanol is at 340 nm.[206] With sulphuric acid addition, the absorption spectrum of AHPIP-c in methanol shifts from 340 nm to 370 nm with a quasi-isosbestic point (**Figure 7.8 (a)**). Similarly, upon sulphuric acid addition, the absorption maximum of AHPIP-c in acetonitrile is shifted batchochromically (**Figure 7.8 (b)**). The

TH-2834_146122035

bathochromic shifts in the absorption spectra suggest that like in water, in these organic solvents, the monocationic equilibrium is dominated by the monocations that absorb at a longer wavelength, i. e. MC2 and MC3.

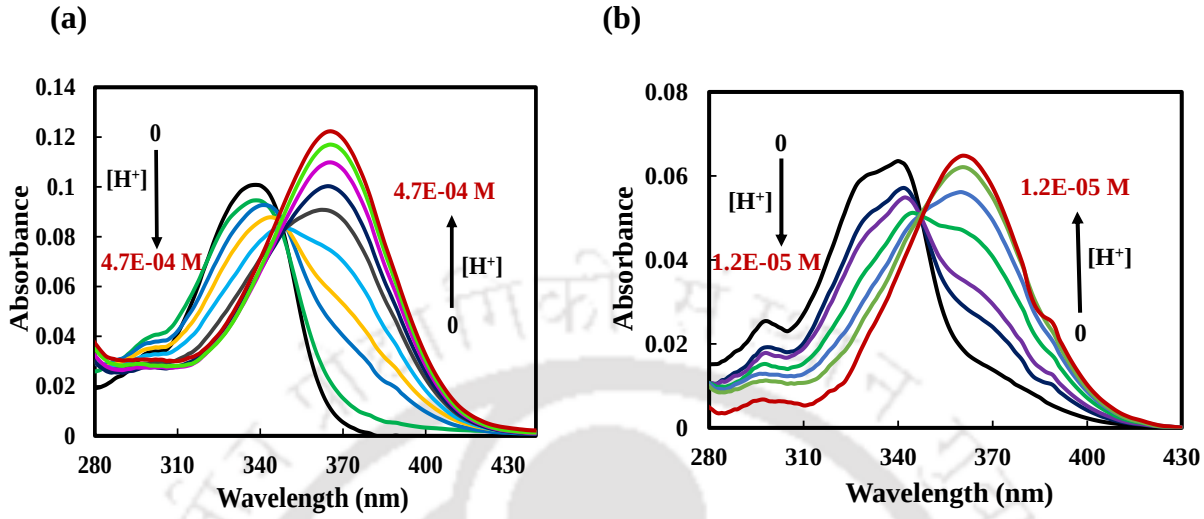

Figure 7.8. Absorption spectra of neutral-monocation equilibrium in (a) methanol and (b) acetonitrile.

AHPIP-c undergoes ESIPT and emits dual emission in both methanol and acetonitrile (**Figures 7.9 (a) & (b)**).[206] The shorter and longer wavelength emissions are normal and tautomer emissions, respectively. Upon increasing the acid concentration, the fluorescence spectra of both the emissions are red-shifted (**Figures 7.9 (a) & (b)**). It also suggests that MC2 and MC3 exist in the excited state and both emit.

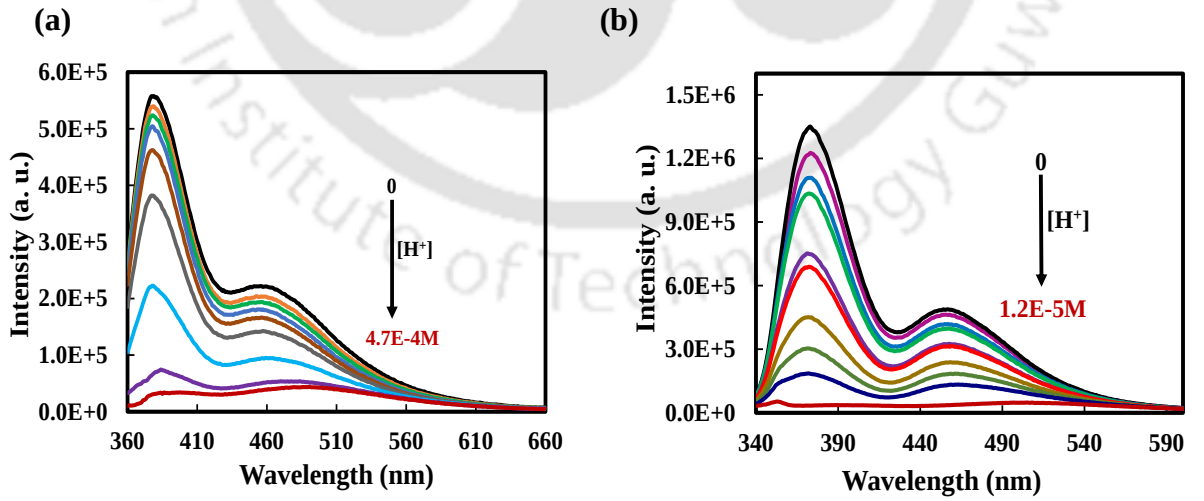

Figure 7.9. Fluorescence spectra of neutral-monocation equilibrium in (a) methanol and (b) acetonitrile, λ_{ex} = 340 nm.

TH-2834_146122035

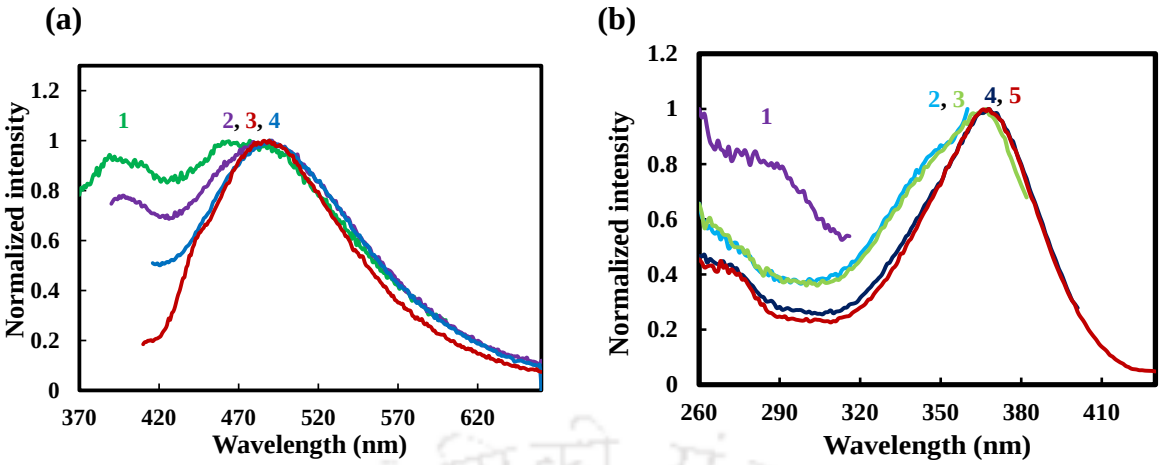

Figure 7.10 (a). Normalized emission spectra of MCs of AHPIP-c in methanol, λ_{ex} = 320 nm (1), 340 nm (2), 360 nm (3), 390 nm (4). (b). Normalized excitation spectra of MCs of AHPIP-c in methanol, λ_{em} = 360 nm (1), 410 nm (2), 440 nm (3), 470 nm (4), 500 nm (5).

The normalized emission and the excitation spectra of MCs in methanol are depicted in **Figure 7.10**. The longer wavelength emission maximum at 490 nm is nearly unaffected when excited at longer wavelengths. The longer wavelength emission in less polar methanol is blue-shifted than the corresponding 505 nm emission of MC3 in water. This blue shift further substantiates the prediction that the ~505 nm of MC3 emission is a TICT emission.

In acetonitrile, excitation at 320 and 340 nm produces band maxima at ~390 nm and 505 nm (**Figure 7.11 (a)**). Interestingly the 505 nm emission maximum is blue shifted when excited at longer wavelengths. The emission maximum is shifted to ~490 nm when excited at 390 nm. It shows the existence of at least two kinds of MC3 in acetonitrile. The excitation spectra at different emission wavelengths are shown in **Figure 7.11(b)**.

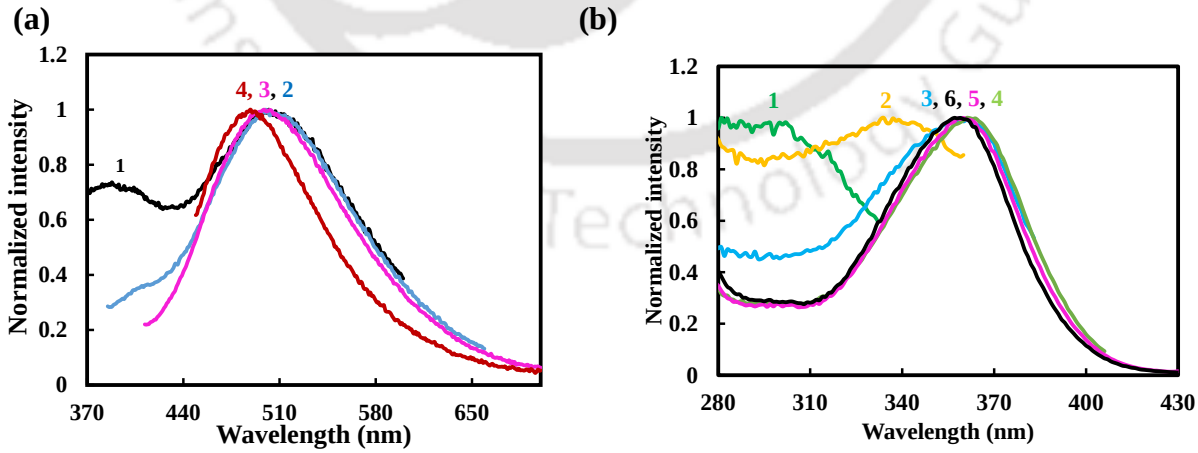

Figure 7.11 (a). Normalized emission spectra of MCs of AHPIP-c in acetonitrile, λ_{ex} = 320 nm (1), 340 nm (2), 360 nm (3), 390 nm (4). (b). Normalized excitation spectra of MCs of AHPIP-c in acetonitrile, λ_{em} = 360 nm (1), 380 nm (2) 410 nm (3), 440 nm (4), 470 nm (5), 500 nm (6).

TH-2834_146122035

The excitation band maximum is blue-shifted from 361 nm to 356 nm for the change in monitoring wavelength from 470 to 500 nm in acetonitrile. It shows that the 490 nm emission corresponds to 365 nm and 505 nm emission corresponds to 361 nm. Like neutral AHPIP-c,[206] MC3 can also exist as *cis*-enol and *trans*-enol conformer (**Chart 7.4**). The *cis*-enol has an intramolecular hydrogen bond; thus it absorbs at a longer wavelength than the *trans*-enol.[237]

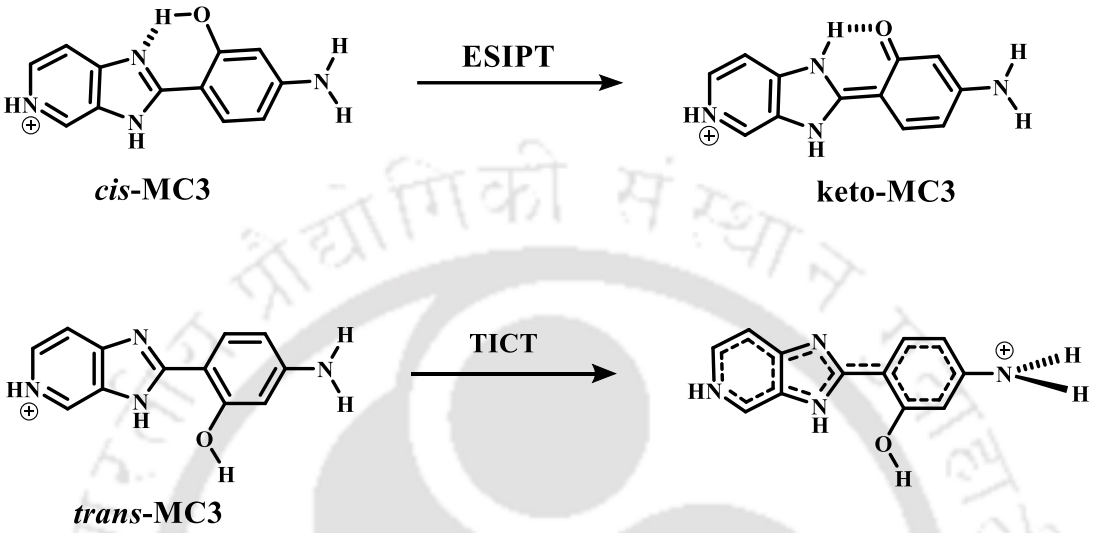

Scheme 7.2. ESIPT and TICT in MC3 of AHPIP-c.

The *cis*-enol of MC3 can undergo ESIPT to form the keto tautomer and *trans*-enol of MC3 (which cannot undergo ESIPT) emits TICT fluorescence (**Scheme 7.2**). The absence of *cis*-enol in protic solvents may be due to breaking of intramolecular hydrogen bonds by intermolecular hydrogen bonds.

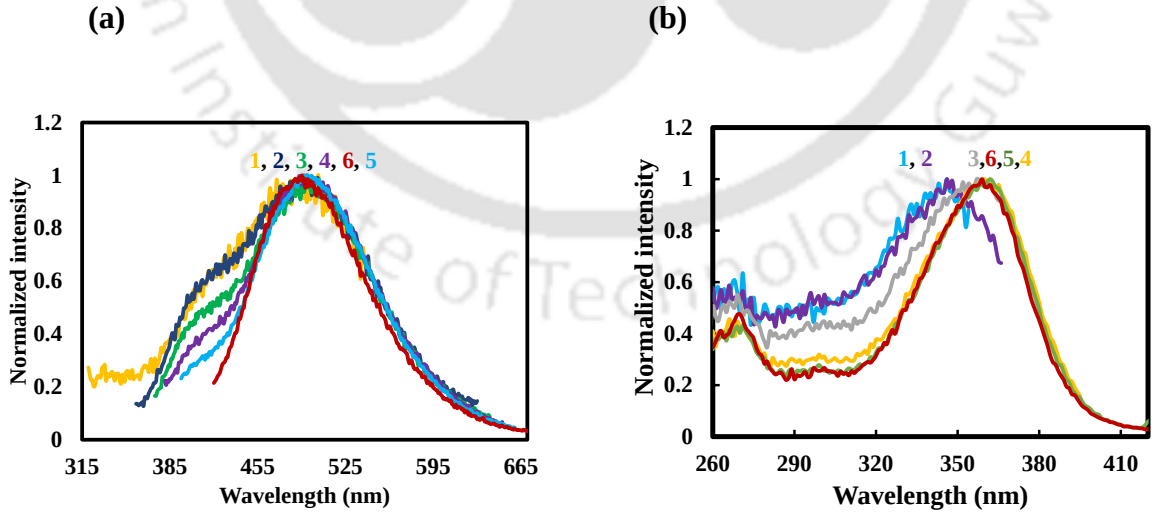

Figure 7.12 (a). Normalized emission spectra of MCs of AMPIP-c in acetonitrile, λ_{ex} = 290 nm (1), 320 nm (2), 330 nm (3), 340 nm (4), 350 nm (5), 370 nm (6). (b). Normalized excitation spectra of MCs of AMPIP-c in acetonitrile, λ_{em} = 400 nm (1), 420 nm (2) 440 nm (3), 460 nm (4), 480 nm (5), 500 nm (6).

TH-2834_146122035

To confirm the ESIPT in MC3, the monocationic equilibrium of methoxy derivative is investigated in acetonitrile (**Figures 7.12 (a) & (b)**). Monocation of AMPIP-c emits at ~410 and ~490 nm. Unlike AHPIP-c, only 5 nm blue shift in longer wavelength emission is independent of excitation wavelength. Therefore, MC3 exists as *cis*- and *trans*- conformers in AMPIP-c also. *cis*-MC3 of AMPIP-c cannot undergo ESIPT due to the absence of 'OH'.

7.3. Monocation-dication equilibria

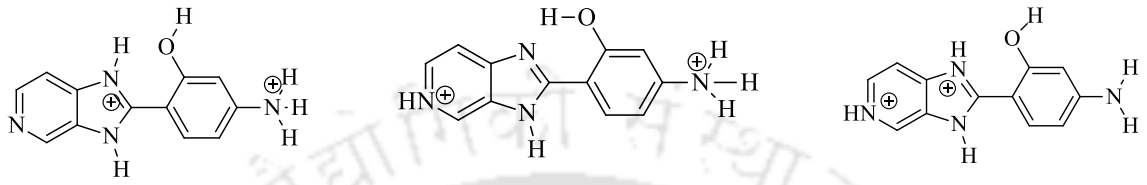

DC1 **DC2** **DC3**

Chart 7.4. Different possible dications of AHPIP-c.

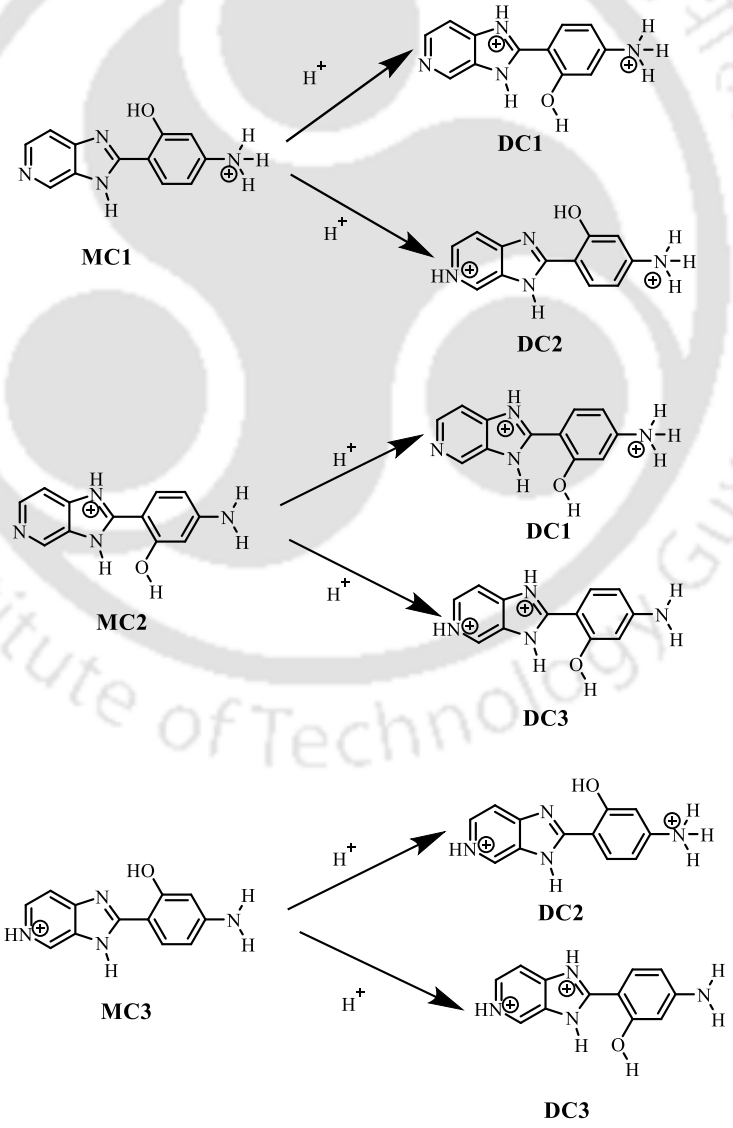

Scheme 7.3. Formation of different dications from monocations.

TH-2834_146122035

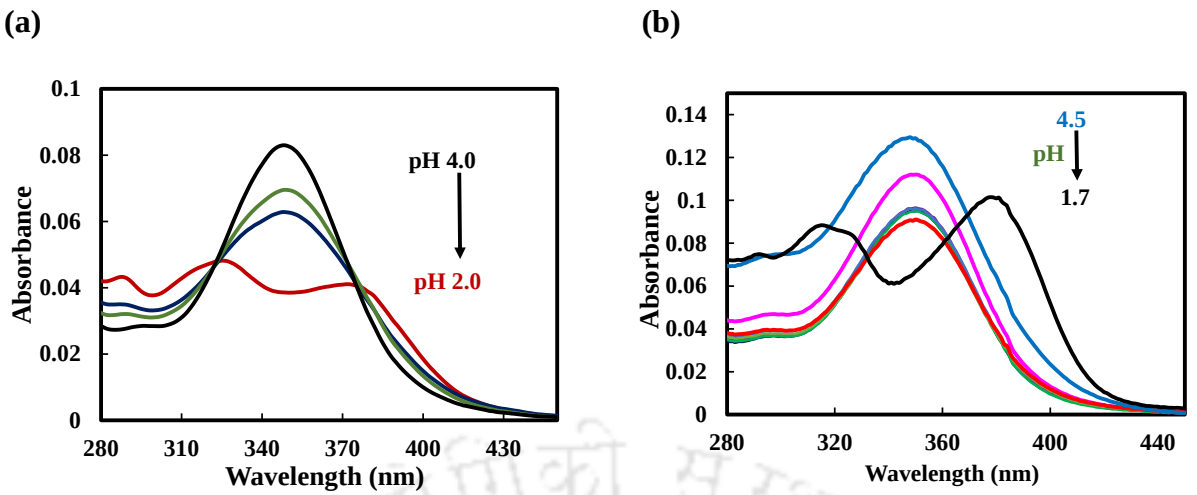

Figure 7.13. Absorption spectra of monocation-dication equilibria of AHPIP-c (a) and AMPIP-c (b) in water.

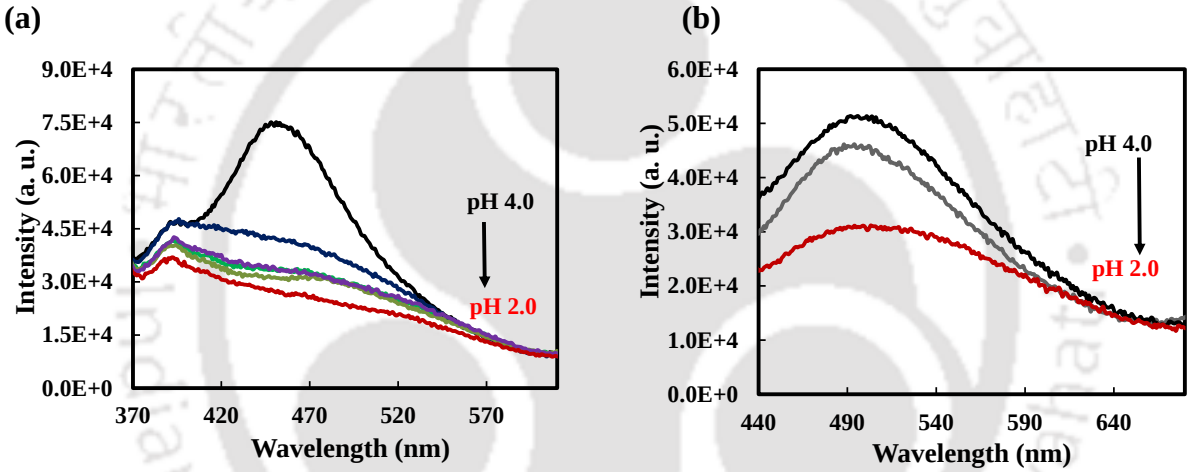

Figure 7.14. Emission spectra of monocation-dication equilibria of AHPIP-c in water, λ_{ex} = 320 nm (a) and λ_{ex} = 350 nm (b).

The absorption spectra of AHPIP-c in the pH range 4.0 to 2.0 are given in **Figure 7.13 (a)**. The absorption spectra of AHPIP-c have three new absorption band at pH 2.0 in water. The positions for the three absorption bands are at ~290, ~325 and ~380 nm. The spectra have two quasi-isosbestic points at 321 and 375 nm. The structures of three dications, DC1, DC2 and DC3, are presented in **Chart 7.4**. Binding on proton on the imidazole nitrogen on MC1 and amino nitrogen of MC2 produces DC1 (**Scheme 7.3**). It will be red-shifted than MC1, but blue-shifted than MC2. Protonation at pyridyl nitrogen of MC1 and amino nitrogen of MC3 leads to the formation of DC2 (**Scheme 7.3**). The difference between DC1 and DC2 is the protonation site at the ring nitrogens. Since, the addition of proton at pyridyl nitrogen causes a large red shift than the protonation at the imidazole nitrogen, DC1 is expected to be red-shifted than the DC2. Protonation of pyridyl nitrogen of MC2 and imidazole nitrogen of MC3 leads to

TH-2834_146122035

the formation of DC3 (**Scheme 7.3**). Accordingly, the absorption bands at ~290, ~325 and ~380 nm can be attributed DC1, DC2 and DC3, respectively.

The absorption spectra of AMPIP-c in the pH range of 4.5 to 1.7 are given in **Figure 7.13 (b)**. In AMPIP-c (pH 1.7), absorption band are present at ~290, ~320 and 370 nm (**Figure 7.13 (b)**). Like AHPIP-c, the absorption band at ~290, ~320 and 370 nm can be assigned to DC1, DC2 and DC3, respectively.

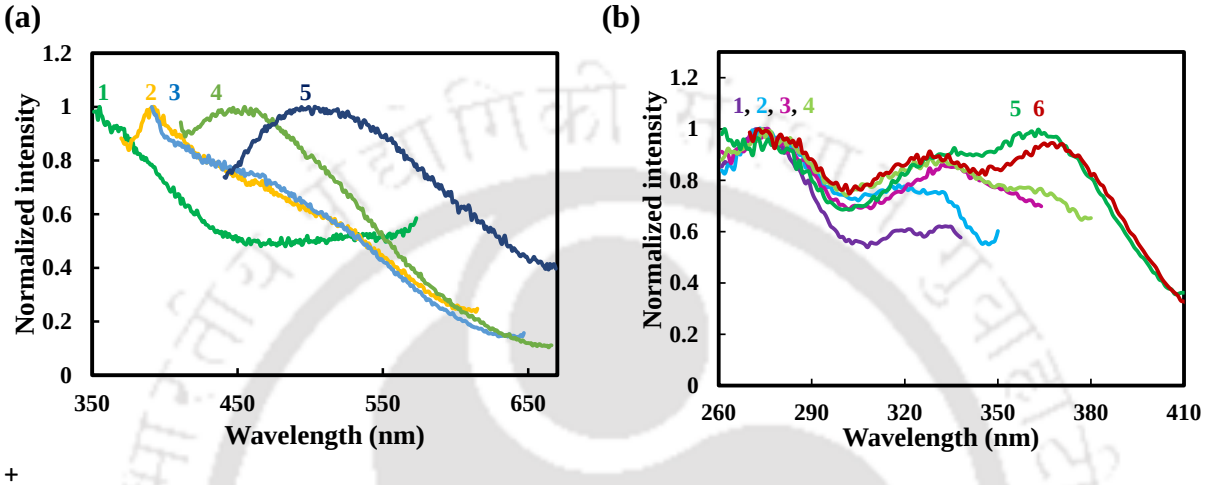

+

Figure 7.15 (a). Normalized emission spectra of DCs of AHPIP-c in water, λ_{ex} = 300 nm (1), 320 nm (2), 335 nm (3), 350 nm (4), 370 nm (5).
(b) Normalized excitation spectra of DCs of AHPIP-c in water, λ_{em} = 395 nm (1), 410 nm (2), 430 nm (3), 450 nm (4), 490 nm (5), 510 nm (6).

Figure 7.15 (a) and (b) represent emission spectra of AHPIP-c in water in the pH range 4.0-2.0. Normalized emission and excitation spectra of DCs are given in **Figure 7.15 (a) and (b)**. At pH 2.0, AHPIP-c emits at ~450 nm at λ_{ex} = 335 nm (**Figure 7.15 (a)**). But at λ_{ex} = 370 nm, the emission is observed at ~520 nm (**Figure 7.15 (a)**). The excitation maximum for ~450 nm band is ~330 nm, while for ~520 nm band, it is ~367 nm (**Figure 7.15 (a)**). The 505 nm emission in MC3 was assigned to TICT emission. As DC3 can form from MC3 (**Scheme 7.3**), ~520 nm emission in DC3 can be assigned to TICT. Unlike MC3, DC3 cannot undergo ESIPT due to protonation at the imidazole ring.

Figure 7.16 (a) and (b) show the normalized emission and excitation spectra of AMPIP-c in water (pH 1.7). At dicationic pH, three emission bands are observed at 365, 420 and 500 nm, respectively. Based on the shift, the emission bands at 365, 420 and 500 nm can be assigned to DC1, DC2 and DC3, respectively. The respective excitation bands of DC1, DC2 and DC3 are also observed at 285 nm, 320 nm and 370 nm.

TH-2834_146122035

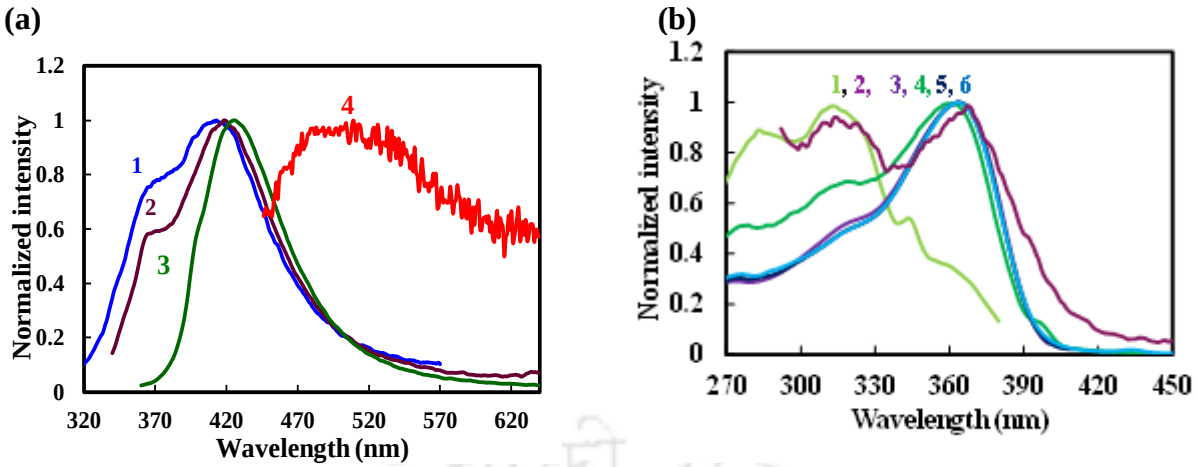

Figure 7.16 (a). Normalized emission spectra of DCs of AMPIP-c in water, λ_{ex} = 292 nm (1), 325 nm (2), 350 nm (3), 420 nm (4). (b). Normalized excitation spectra of DCs of AMPIP-c in water, λ_{em} = 390 nm (1), 430 nm (2), 460 nm (3), 480 nm (4), 510 nm (5).

Like water, in methanol and acetonitrile two isosbestic points were observed (**Figure 7.17 (a) and (b)**). In water, three distinct bands are found for DC1, DC2 and DC3 and their relative absorbance are 1.08: 1.12: 1, respectively. But in methanol, the absorbance of the absorption band of DC3 is higher than that of the DC2 band and no clear band was observed. In acetonitrile, the absorbance of the DC2 further decreases. The ratio of absorbance at 335 nm: 385 nm is 0.68: 1 in methanol and 0.31: 1 in acetonitrile. In other words, the relative population of DC1 reduces compared to DC2 with decreases in polarity and hydrogen bond ability of the solvent; in turn the relative population of DC2 diminishes compared to DC3 with decreases in polarity and hydrogen bond ability of the solvent.

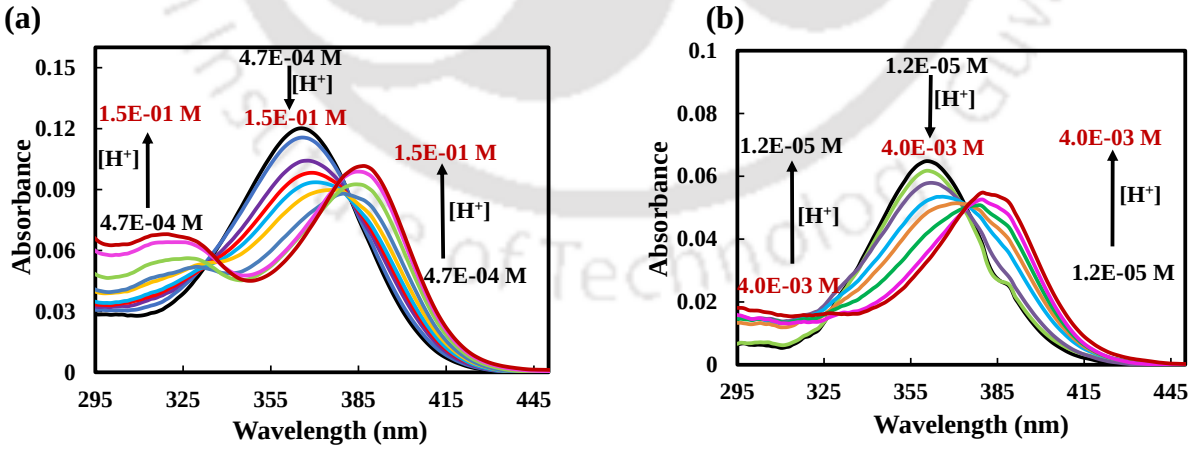

Figure 7.17. Absorption spectra of monocation-dication equilibria of AHPIP-c in (a) methanol and (b) acetonitrile.

7.4. Trication of AHPIP-c and AMPIP-c

In concentrated sulphuric acid at H_o –10.2, AHPIP-c exhibits a single emission at 430 nm that has an excitation band maximum at 352 nm (**Figure 7.18 (a)**). The excitation band is

TH-2834_146122035

red-shifted than the corresponding excitation and emission bands of DC1 and DC2. It is also blue-shifted than the respective excitation and emission band of DC3.

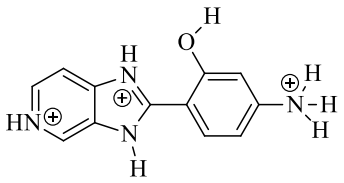

Chart 7.5. Trication of AHPIP-c.

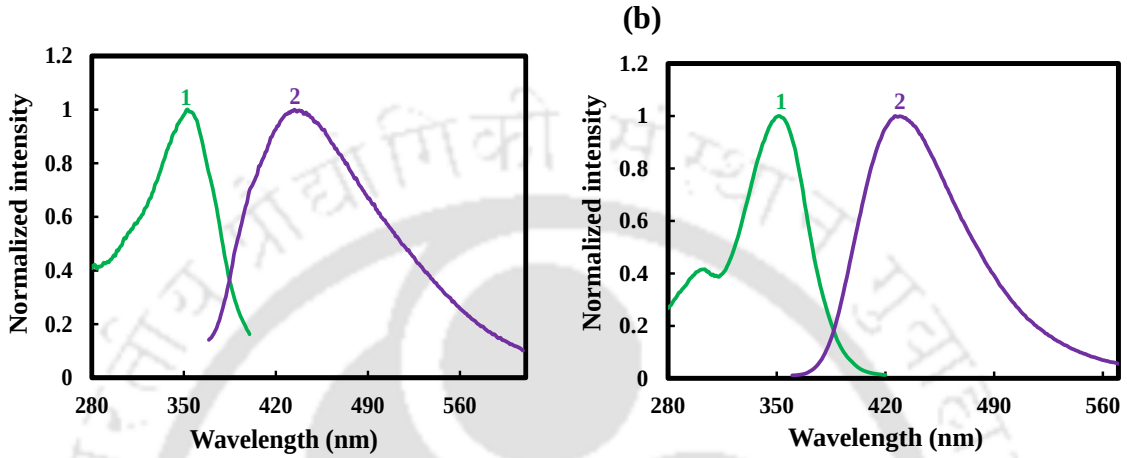

Figure 7.18. Normalized excitation (1) (λ_{em} = 430 nm) and emission (2) spectra (λ_{ex} = 350 nm) of TC of (a) AHPIP-c and (b) AMPIP-c in water.

The protonation of the unprotonated site, i.e., pyridyl/imidazole nitrogen of DC1/DC2, results in the trication (**Chart 7.5**). As protonation at amino nitrogen produces a blue shift in the excitation spectrum, the respective spectrum of trication is blue-shifted than the spectrum of DC3. The same behaviour is found in AMPIP-c and the excitation and emission spectral maxima are at 350 and 428 nm, respectively (**Figure 7.18 (b)**).

7.5. Conclusion

AHPIP-c forms two kinds of monoanions, both MA1 and MA2 are formed by the protonation of charge donor. MA2 emits the TICT emission. On the other hand, deprotonation of AMPIP-c lead to formation of MA3 and it emits both normal and TICT emission. Both AHPIP-c and AMPIP-c forms all three monocations MC1, MC2 and MC3 and dications DC1, DC2 and DC3. MC3 and DC3 of both the molecules emits TICT fluorescence. MC3 and DC2 of AHPIP-c also undergoes ESIPT in acetonitrile to emit tautomer emission. At H_o –10.2 all three basic sites of AHPIP-c are protonated to form trication. The methoxy derivative also form trication at that acid concentration.

TH-2834_146122035

Chapter 8

Summary & Scope of Future Work

TH-2834_146122035

TH-2834_146122035

8.1. Summary of the present work

In this thesis work, intra- and inter-molecular proton transfer have been studied using three azole derivatives as model systems. 1,3,4-Thiadiazole PHBT, a molecule with single intramolecular proton transfer unit was investigated to understand the origin of longer wavelength emission of FABT. Then, bis-HPTA, a molecule with two intramolecular proton transfer unit was investigated to understand the effect of water and microheterogeneous environment. The competing intramolecular proton transfer and intermolecular proton transfer induced TICT was studied theoretically in AHPIP-c. This study was followed by the experimental study of the effect of intermolecular proton transfer that led to protonation/deprotonation of basic/acidic sites of AHPIP-c.

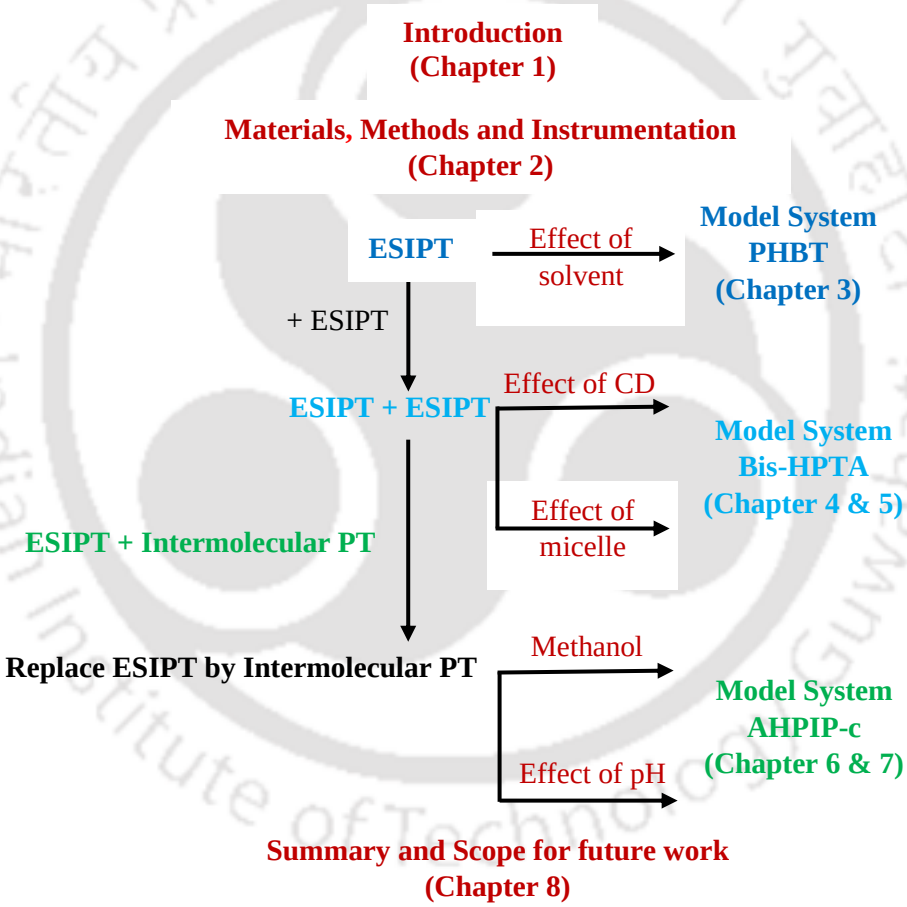

Scheme 8.1. Organisation of the thesis.

The cause for the origin of longer wavelength emission of FABT was investigated. A similar and simpler analogue of FABT, PHBT was synthesized and its emission was studied in various organic solvents and water. The methoxy derivative of PHBT was also synthesized to confirm the role of the 'OH' group in dual emission. PHBT also exhibits dual emission like FABT, but its methoxy derivative emits single emission. PHBT and FABT exist as enol in the

TH-2834_146122035

ground state. Enol form exist in two conformers *cis*- and *trans*- enol. But both the molecules do not exist in keto form in the ground state. However, upon excitation *cis*-enol undergoes intramolecular proton transfer to form keto tautomer in the excited state. Absence of longer wavelength emission in methoxy derivative which is not capable of intramolecular proton transfer confirm this. The *trans*-enol emits the shorter wavelength normal emission. The normal emission is the major emission in most of the organic solvents. However, in non-polar solvents such as toluene, the longer wavelength emission dominates. In water, the aggregation of the molecules, shift the equilibrium from *trans*- to *cis*- enol. As a result, tautomer emission predominates. Upon deprotonation of the 'OH' proton, the anion emits single emission.

Bis-HPTA has two intramolecular hydrogen bond units. It undergoes a special kind of PT called PTTPT where one PT triggers the second PT. The PTTPT of bis-HPTA is affected by solvent nature as well as by encapsulation. This alters the relative population of monoketo and diketo. In *β*-CD, the triazole ring and most part of the α-ring of bis-HPTA remain completely inside. The relative position and orientation of the guest impacts its photophysics. Photoexcitation induced intermolecular proton transfer in anion of bis-HPTA in water. The host guest chemistry prevents the intermolecular proton transfer in anion. No tautomer emission is observed from the anion of bis-HPTA inside *β*-CD.

In micelles, the reduction in nonradiative decay enhanced the tautomer emission of bis-HPTA. Like *β*-CD, the micelles also prevent the formation of tautomer from anion via inter molecular proton transfer. In AOT/*n*-heptane/water reverse micelles the tautomer emission decreases with increases in water content. The β-ring of bis-HPTA is opened by intermolecular hydrogen bond of bis-HPTA with negatively charged polar head group of AOT. The molecule can then undergo ESIPT only in the α-ring to form the monoketo tautomer. On increasing the w_0, the water solvated enol structure emits only normal emission. But the normal emission is very little compared to tautomer emission.

APIP-c emits TICT fluorescence in protic environment due to intermolecular proton transfer induced charge transfer. Introduction of intramolecular hydrogen bond forming 'OH' suppresses the TICT and the new molecule, AHPIP-c emit only TICT emission. Computational studies were carried out to understand the cause for the suppression of TICT emission in AHPIP-c. The studies reveal that the hydrogen bonded solvent bridge between imidazole and pyridyl nitrogen is weaker in AHPIP-c than in DMAPIP-c. The barrier heights for both proton transfer is reduced in the excited states than ground state. However, the barrier height of ESIPT

TH-2834_146122035

is significantly lesser than the intermolecular proton transfer. Thus, the solvent assisted proton transfer is suppressed by ESIPT.

Depending on the pH of the water, intermolecular proton transfer led to protonation/deprotonation of basic/acidic site of AHPIP-c. AHPIP-c forms two kinds of monoanions. The deprotonation of –OH can turn off the ESIPT emission. The deprotonation of 'NH_2' can turn on the charge transfer emission by increasing the charge flow from the donor to acceptor. Both hydroxy and methoxy molecules form all three types of monocations and three types of dications. Protonation at pyridyl nitrogen also induces TICT emission in AHPIP-c. In acetonitrile, MC3 and DC2 exist as two conformers. *cis*-enol of both MC3 and DC2 undergoes ESIPT to form tautomer. The *trans*-enol of both the species emit TICT emission.

8.1. Scope of the future work

In the present work, time resolved emission of the molecules are carried out. But due to the instrumental limitation, the rate of proton transfer could not be followed. A femtosecond time resolved study may provide more information about the rate of proton transfer.

FABT and other 1,3,4-thiadizoles are important class of biological active molecules. Attempts were made to study the anticancer properties of PHBT and PMBT in collaboration. Though the results were promising, the work could not be extended due to solubility issue. However, the issue may be addressed with some modifications in the chemical structure.

Binding of proton at pyridyl nitrogen enhanced the acceptor ability to accept the charge and induced TICT fluorescence. Therefore, the binding of metal ions may induce charge transfer and the molecule may be potential sensor for metal ions. Study of switching between two different states can be crucial for designing molecular photo-switches.

TH-2834_146122035

References

1. J. R. Lakowicz, *Principles of Fluorescence Spectroscopy*, Springer US, 3rd edn., 2006.
2. B. Valeur, M. N. Berberan-Santos, *Molecular Fluorescence: Principles and Applications*, Wiley-VCH Verlag GmbH & Co. KGaA, 2nd edn., 2012.
3. B. Valeur and J.-C. Brochon, Eds., *New Trends in Fluorescence Spectroscopy*, Springer Berlin Heidelberg, Berlin, Heidelberg, 2001, vol. 1.
4. A. Douhal, F. Lahmani and A. H. Zewail, *Chem. Phys.*, 1996, **207**, 477–498.
5. D. D. Pant, H. C. Joshi, P. B. Bisht and H. B. Tripathi, *Chem. Phys.*, 1994, **185**, 137–144.
6. T. Atsbeha, A. M. Mohammed and M. Redi-Abshiro, *J. Fluoresc.*, 2010, **20**, 1241–1248.
7. K. A. Zachariasse, T. von der Haar, A. Hebecker, U. Leinhos and W. Kühnle, *Pure Appl. Chem.*, 1993, **65**, 1745–1750.
8. P. Ashokkumar, V. T. Ramakrishnan and P. Ramamurthy, *J. Phys. Chem. A*, 2011, **115**, 14292–14299.
9. D. Escudero, *Acc. Chem. Res.*, 2016, **49**, 1816–1824.
10. J. Gierschner, S. K. Behera and S. Y. Park, *Angew. Chemie Int. Ed.*, 2020, anie.202009789.
11. J. E. Crooks, in *Proton-Transfer Reactions*, Springer US, 1975, pp. 153–177.
12. R. Ludwig, *ChemPhysChem*, 2007, **8**, 2539–2539.
13. R. B. Gennis, *Front. Biosci.*, 2004, 9, 581–591.
14. M. Y. Okamura and G. Feher, *Annu. Rev. Biochem.*, 1992, **61**, 861–896.
15. S. Xiao, L. Wang, Y. Liu, X. Lin and H. Liang, *J. Chem. Phys.*, 2012, **137**, 195101.
16. J. Catalán and P. Pérez, *J. Theor. Biol.*, 1979, **81**, 213–221.
17. E. A. Kasumov, R. E. Kasumov and I. V. Kasumova, *Photosynth. Res.*, 2015, 123, 1–22.
18. M. Wikström and M. I. Verkhovsky, *Biochim. Biophys. Acta - Bioenerg.*, 2006, 1757, 1047–1051.
19. K. Faxén, G. Gilderson, P. Ädelroth and P. Brzezinski, *Nature*, 2005, **437**, 286–289.
20. E. R. Sayfutyarova, J. J. Goings and S. Hammes-Schiffer, *J. Phys. Chem. B*, 2019, **123**, 439–447.
21. J. Massue, T. Pariat, P. M. Vérité, D. Jacquemin, M. Durko, T. Chtouki, L. Sznitko, J. Mysliwiec and G. Ulrich, *Nanomaterials*, 2019, **9**, 1093.
22. J. Li, Y. Wu, Z. Xu, Q. Liao, H. Zhang, Y. Zhang, L. Xiao, J. Yao and H. Fu, *J. Mater. Chem. C*, 2017, **5**, 12235–12240.
23. T. Fournier, S. Pommeret, J. C. Mialocq, A. Deflandre and R. Rozot, *Chem. Phys. Lett.*, 2000, **325**, 171–175.
24. S. Kundu, B. Sk, P. Pallavi, A. Giri and A. Patra, *Chem. - A Eur. J.*, 2020, 26, 5557–5582.
25. V. R. Mishra, C. W. Ghanavatkar and N. Sekar, *ChemistrySelect*, 2020, 5, 2103–2113.
26. J. E. Kwon and S. Y. Park, *Adv. Mater.*, 2011, 23, 3615–3642.
27. D.-Y. Chen, C.-L. Chen, Y.-M. Cheng, C.-H. Lai, J.-Y. Yu, B.-S. Chen, C.-C. Hsieh, H.-C. Chen, L.-Y. Chen, C.-Y. Wei, C.-C. Wu and P.-T. Chou, *ACS Appl. Mater. Interfaces*, 2010, **2**, 1621–1629.
28. B. Sun, L. Liu, W. Liu, F. Meng and Q. Huang, *J. Lumin.*, 2020, **223**, 117203.
29. P. Muthukumar, M. Surya, M. Pannipara, A. G. Al-Sehemi, D. Moon and S. Philip Anthony, *ChemistrySelect*, 2020, **5**, 3295–3302.
30. Š. Budzák and D. Jacquemin, *J. Phys. Chem. B*, 2016, **120**, 6730–6738.
31. L. Chen, P. Fu, H. Wang and M. Pan, *Adv. Opt. Mater.*, 2021, 2001952.
32. Y. Ma, Y. Yang, R. Lan and Y. Li, *J. Phys. Chem. C*, 2017, **121**, 14779–14786.
33. N. Agmon, *J. Phys. Chem. A*, 2005, **109**, 13–35.
34. D. Huppert and E. Pines, eds. P. M. Rentzepis and C. Capellos, Springer Netherlands, Dordrecht, 1986, pp. 171–178.
35. L. G. Arnaut and S. J. Formosinho, *J. Photochem. Photobiol. A Chem.*, 1993, 75, 1–20.
36. P. Zhou and K. Han, *Acc. Chem. Res*, 2018, **51**, 35.
37. H. Matsumoto, Y. Nishimura and T. Arai, *Org. Biomol. Chem.*, 2017, **15**, 6575–6583.
38. S. J. Formosinho and L. G. Arnaut, *J. Photochem. Photobiol. A Chem.*, 1993, 75, 21–48.
39. J. Zhao, S. Ji, Y. Chen, H. Guo and P. Yang, *Phys. Chem. Chem. Phys.*, 2012, 14, 8803–8817.
40. D. K. Rana, S. Dhar, A. Sarkar and S. C. Bhattacharya, *J. Phys. Chem. A*, 2011, **115**, 9169–9179.
41. G. Burdzinski, M. Sliwa, Y. Zhang and S. Delbaere, *J. Phys. Chem. A*, 2011, **115**, 14300–

TH-2834_146122035

14305.
42. S. Y. Park, Y. S. Lee and D. J. Jang, *Phys. Chem. Chem. Phys.*, 2011, **13**, 3730–3736.
43. A. Bach, C. Tanner, C. Manca, H. M. Frey and S. Leutwyler, *J. Chem. Phys.*, 2003, **119**, 5933–5942.
44. H. C. Joshi and L. Antonov, *Molecules*, 2021, **26**, 1475.
45. J. Zhao and B. Jin, *J. Lumin.*, , DOI:10.1016/j.jlumin.2020.117800.
46. X. Liu, J. Zhao and Y. Zheng, *RSC Adv.*, 2017, **7**, 51318–51323.
47. W. E. Brewer, M. L. Martinez and P.-T. Chou, *J. Phys. Chem.* 1990, **94**, 5, 1915–1918.
48. K.-C. Tang, C.-L. Chen, H.-H. Chuang, J.-L. Chen, Y.-J. Chen, Y.-C. Lin, J.-Y. Shen, W.-P. Hu and P.-T. Chou, , DOI:10.1021/jz201439w.
49. S. Tolosa, J. A. Sansón and A. Hidalgo, *J. Mol. Liq.*, 2018, **251**, 308–316.
50. C. Costentin, M. Robert, J. Savéant and C. Tard, *Angew. Chemie Int. Ed.*, 2010, **49**, 3803–3806.
51. J. K. Lanyi, *Biochim. Biophys. Acta - Bioenerg.*, 2006, 1757, 1012–1018.
52. H. C. Chang, C. C. H. Kung, T. T. Chang, S. C. Jao, Y. T. Hsu and W. S. Li, *PLoS One*, , DOI:10.1371/journal.pone.0190816.
53. E. Freier, S. Wolf and K. Gerwert, *Proc. Natl. Acad. Sci. U. S. A.*, 2011, **108**, 11435–11439.
54. R. Srivastava, *Front. Chem.*, 2019, 7, 536.
55. O. O. Brovarets' and D. M. Hovorun, *RSC Adv.*, 2015, **5**, 99594–99605.
56. Y. Zhang, K. De La Harpe, A. A. Beckstead, R. Improta and B. Kohler, *J. Am. Chem. Soc.*, 2015, **137**, 7059–7062.
57. C. Li, Y. Yang, D. Li and Y. Liu, *Phys. Chem. Chem. Phys.*, 2017, **19**, 4802–4808.
58. D. Jacquemin, J. Zúñiga, A. Requena and J. P. Céron-Carrasco, *Acc. Chem. Res.*, 2014, **47**, 2467–2474.
59. K. Umesaki and K. Odai, *J. Phys. Chem. B*, 2020, **124**, 1715–1722.
60. G. Villani, *Chem. Phys.*, 2005, **316**, 1–8.
61. C. al-Taylor, M. Ashraf el-Bayoumi and M. Kasha, *Proc. Natl. Acad. Sci. U. S. A.*, 1969, **63**, 253–260.
62. A. Douhal, S. K. Kim and A. H. Zewail, *Nature*, 1995, **378**, 260–263.
63. J. Catalán and M. Kasha, *J. Phys. Chem. A*, 2000, **104**, 10812–10820.
64. K. Ando, S. Hayashi and S. Kato, *Phys. Chem. Chem. Phys.*, 2011, **13**, 11118–11127.
65. R. Crespo-Otero, N. Kungwan and M. Barbatti, *Chem. Sci.*, 2015, **6**, 5762–5767.
66. D. E. Folmer, L. Poth, E. S. Wisniewski and A. W. Castleman, *Chem. Phys. Lett.*, 1998, **287**, 1–7.
67. H. Sekiya and K. Sakota, *J. Photochem. Photobiol. C Photochem. Rev.*, 2008, **9**, 81–91.
68. M. Wikström, M. I. Verkhovsky and G. Hummer, *Biochim. Biophys. Acta - Bioenerg.*, 2003, **1604**, 61–65.
69. R. S. Moog and M. Maroncelli, *J. Phys. Chem.*, 1991, **95**, 10359–10369.
70. O. F. Mohammed, D. Pines, J. Dreyer, E. Pines and E. T. J. Nibbering, *Science (80-.).*, 2005, **310**, 83–86.
71. C. Prommin, N. Kanlayakan, W. Chansen, R. Salaeh, K. Kerdpol, R. Daengngern and N. Kungwan, *J. Phys. Chem. A*, 2017, **121**, 5773–5784.
72. H. Fang, *J. Chem. Sci*, 2016, **128**, 1497–1506.
73. K. Sakota, Y. Komoto, M. Nakagaki, W. Ishikawa and H. Sekiya, *Chem. Phys. Lett.*, 2007, **435**, 1–4.
74. Y. H. Liu, M. S. Mehata and J. Y. Liu, *J. Phys. Chem. A*, 2011, **115**, 19–24.
75. D. Yang, J. Zhao, M. Jia and X. Song, *RSC Adv.*, 2017, **7**, 34034–34040.
76. D. Yang, M. Jia, J. Wu and X. Song, *Sci. Rep.*, 2017, **7**, 1–8.
77. Z. Tang, M. Lu, K. Liu, Y. Zhao, Y. Qi, Y. Wang, P. Zhang and P. Zhou, *J. Photochem. Photobiol. A Chem.*, 2018, **367**, 261–269.
78. Y. Tong, J. Fu and J. Ma, *J. Chinese Chem. Soc.*, 2018, **65**, 822–827.
79. N. Dash, F. A. S. Chipem and G. Krishnamoorthy, *Photochem. Photobiol. Sci.*, 2009, **8**, 1708–15.
80. D. Yang, M. Jia, X. Song and Q. Zhang, *J. Phys. Org. Chem.*, 2018, **31**, 1–7.
81. H. Li, Z. Wei, Y. Ma, W. Zhang, D. Wang, X. Wang and G. Jin, *Chem. Phys.*, 2020, **529**, 110553.
82. V. Vetokhina, K. Dobek, M. Kijak, I. I. Kamińska, K. Muller, W. R. Thiel, J. Waluk and J. Herbich, *ChemPhysChem*, 2012, **13**, 3661–3671.

TH-2834_146122035

83. Y. S. Wu, H. C. Huang, J. Y. Shen, H. W. Tseng, J. W. Ho, Y. H. Chen and P. T. Chou, *J. Phys. Chem. B*, 2015, **119**, 2302–2309.
84. D. E. Folmer, E. S. Wisniewski, J. R. Stairs and A. W. Castleman, *J. Phys. Chem. A*, 2000, **104**, 10545–10549.
85. K. Sakota, Y. Kageura and H. Sekiya, *J. Chem. Phys.*, , DOI:10.1063/1.2961031.
86. K. Sakota, N. Inoue, Y. Komoto and H. Sekiya, *J. Phys. Chem. A*, 2007, **111**, 4596–4603.
87. S. Mente and M. Maroncelli, *J. Phys. Chem. A*, 1998, **102**, 3860–3876.
88. O.-H. Kwon, Y.-S. Lee, H. J. Park, Y. Kim and D.-J. Jang, *Angew. Chemie Int. Ed.*, 2004, **43**, 5792–5796.
89. P. Zhou and K. Han, *Acc. Chem. Res.*, 2018, **51**, 1681–1690.
90. D. Hong, Y. Luo, X. He, Z. Zheng, S. Su, J. Wang, C. Wang, C. Chen and B. Sun, *Chem. – A Eur. J.*, 2019, **25**, chem.201900856.
91. P. Toele and M. Glasbeek, *Chem. Phys. Lett.*, 2005, **407**, 487–492.
92. M. Dommett and R. Crespo-Otero, *Phys. Chem. Chem. Phys.*, 2017, **19**, 2409–2416.
93. H. W. Tseng, J. Q. Liu, Y. A. Chen, C. M. Chao, K. M. Liu, C. L. Chen, T. C. Lin, C. H. Hung, Y. L. Chou, T. C. Lin, T. L. Wang and P. T. Chou, *J. Phys. Chem. Lett.*, 2015, **6**, 1477–1486.
94. K. Christmann, O. Schober, G. Ertl, M. Neumann, J. Chem, K. E. Lu and A. Jerry Kresge, *What Makes Proton Transfer Fast?*, 1974, vol. 60.
95. S. Santra and S. K. Dogra, *Chem. Phys.*, 1998, **226**, 285–296.
96. S. Satpathi, K. Gavvala and P. Hazra, *J. Phys. Chem. A*, 2015, **119**, 12715–12721.
97. R. Ghosh and D. K. Palit, *Cite this Photochem. Photobiol. Sci*, 2013, **12**, 987.
98. S. Hammes-Schiffer and J. C. Tully, *J. Chem. Phys.*, 1994, **101**, 4657–4667.
99. F. A. S. Chipem and G. Krishnamoorthy, *J. Phys. Chem. B*, 2013, **117**, 14079–14088.
100. A. Felouat, M. Curtil, J. Massue and G. Ulrich, *New J. Chem.*, 2019, **43**, 9162–9169.
101. Y. P. Li, X. H. Zhu, S. N. Li, Y. C. Jiang, M. C. Hu and Q. G. Zhai, *ACS Appl. Mater. Interfaces*, 2019, **11**, 11338–11348.
102. Y. Yang, Y. Ding, W. Shi, F. Ma and Y. Li, *J. Lumin.*, 2020, **218**, 116836.
103. C.-Y. Peng, J.-Y. Shen, Y.-T. Chen, P.-J. Wu, W.-Y. Hung, W.-P. Hu and P.-T. Chou, *J. Am. Chem. Soc.* 2015, **137**, 14349–14357.
104. F. Plasser, M. Barbatti, A. J. A. Aquino and H. Lischka, *J. Phys. Chem. A*, 2009, **113**, 8490–8499.
105. S. Su and H. Fang, *Mol. Phys.*, 2020, 1–13.
106. R. Gelabert, M. Moreno and J. M. Lluch, *ChemPhysChem*, 2004, **5**, 1372–1378.
107. J. M. Ortiz-Sánchez, R. Gelabert, M. Moreno and J. M. Lluch, *ChemPhysChem*, 2007, **8**, 1199–1206.
108. H. Zhang, P. Van Der Meulen and M. Glasbeek, *Chem. Phys. Lett.*, 1996, **253**, 97–102.
109. G. A. Parada, T. F. Markle, S. D. Glover, L. Hammarström, S. Ott and B. Zietz, *Chem. - A Eur. J.*, 2015, **21**, 6362–6366.
110. F. Rodríguez-Prieto, J. C. Penedo and M. Mosquera, *J. Chem. Soc. - Faraday Trans.*, 1998, **94**, 2775–2782.
111. F. A. S. Chipem and G. Krishnamoorthy, *J. Phys. Chem. A*, 2009, **113**, 12063–12070.
112. D. Yang, M. Jia, Q. Zhang and Y. Wang, *J. Lumin.*, 2020, **219**, 116913.
113. A. Douhal, F. Amat-Guerri, M. P. Lillo and A. U. Acuña, *J. Photochem. Photobiol. A Chem.*, 1994, **78**, 127–138.
114. N. Alarcos, M. Gutiérrez, M. Liras, F. Sánchez and A. Douhal, *Photochem. Photobiol. Sci.*, 2015, **14**, 1306–1318.
115. H. K. Sinha and S. K. Dogra, *Chem. Phys.*, 1986, **102**, 337–347.
116. M. M. Balamurali and S. K. Dogra, *Chem. Phys.*, 2004, **305**, 95–103.
117. J. Han, B. Cao, Y. Li, Q. Zhou, C. Sun, B. Li, H. Yin and Y. Shi, *Spectrochim. Acta - Part A Mol. Biomol. Spectrosc.*, 2020, **231**, 118086.
118. J. Herbich, C. Y. Hung, R. P. Thummel and J. Waluk, *J. Am. Chem. Soc.*, 1996, **118**, 3508–3518.
119. A. Chrayteh, C. P. Ewels and D. Jacquemin, *Phys. Chem. Chem. Phys.*, 2020, **22**, 25066–25074.
120. V. S. Padalkar, A. Tathe, V. D. Gupta, V. S. Patil, K. Phatangare and N. Sekar, *J. Fluoresc.*, 2012, **22**, 311–322.
121. J. Catalán, *J. Phys. Chem. B*, 2009, **113**, 5951–5960.
122. D. P. Kapusta, F. D. Mulashkin and M. G. Khrenova, *Int. J. Quantum Chem.*, ,

TH-2834_146122035

DOI:10.1002/qua.26577.
123. M. Bräuer, M. Mosquera, J. L. Pérez-Lustres and F. Rodríguez-Prieto, *J. Phys. Chem. A*, 1998, **102**, 10736–10745.
124. A. Douhal, F. Lahmani, A. Zehnacker-Rentien and F. Amat-Guerri, *J. Phys. Chem.*, 1994, **98**, 12198–12205.
125. S. R. Vázquez, M. C. Ríos Rodríguez, M. Mosquera and F. Rodríguez-Prieto, *J. Phys. Chem. A*, 2007, **111**, 1814–1826.
126. V. Kachwal, I. S. Vamsi Krishna, L. Fageria, J. Chaudhary, R. R. Kinkar, R. Chowdhury and I. R. Laskar, *Analyst*, 2018, **143**, 3741–3748.
127. Y. P. Chan, L. Fan, Q. You, W. H. Chan, A. W. M. Lee and S. Shuang, *Tetrahedron*, 2013, **69**, 5874–5879.
128. V. S. Patil, V. S. Padalkar, A. B. Tathe and N. Sekar, *Dye. Pigment.*, 2013, **98**, 507–517.
129. S. Su and H. Fang, *Mol. Phys.*, 2020, 1–13.
130. B. K. Paul, A. Samanta and N. Guchhait, *Langmuir*, 2010, **26**, 3214–3224.
131. N. Sarkar, A. Datta, S. Das, K. Das and K. Bhattacharyya, *J. Photochem. Photobiol. A Chem.*, 1997, **109**, 259–265.
132. E. L. Roberts, P. T. Chou, T. A. Alexander, R. A. Agbaria and I. M. Warner, *J. Phys. Chem.*, 1995, **99**, 5431–5437.
133. E. J. Armstrong, H. Galas, R. S. Wylie, S. Zohrehvand, J. van Stam and C. H. Evans, *Can. J. Chem.*, 2021, 2020-0249.
134. A. Douhal, T. Fiebig, M. Chachisvilis and A. H. Zewail, *J. Phys. Chem. A*, 1998, **102**, 1657–1660.
135. S. Mitra, R. Das and S. Mukherjee, *J. Phys. Chem. B*, 1998, **102**, 3730–3735.
136. M. E. D. Garcia and A. Sanz-Medel, *Talanta*, 1986, **33**, 255–264.
137. M. Valero, W. Hu, J. E. Houston and C. A. Dreiss, *J. Mol. Liq.*, 2021, **322**, 114892.
138. P. T. Chou, *J. Chinese Chem. Soc.*, 2001, 48, 651–682.
139. S. Mitra and S. Mukherjee, *J. Lumin.*, 2006, **118**, 1–11.
140. S. Rani, S. Mishra, M. Sharma, A. Nandy and S. Mozumdar, *J. Dispers. Sci. Technol.*, 2020, **41**, 523–536.
141. J. A. Mysona, A. V. McCormick and D. C. Morse, *Phys. Rev. Lett.*, 2019, **123**, 038003.
142. C. Tanford, *J. Phys. Chem.*, 1972, **76**, 3020–3024.
143. C. Tanford, *J. Phys. Chem.*, 1974, **78**, 2469–2479.
144. N. Sarkar, K. Das, S. Das, A. Datta, D. Nath and K. Bhattacharyya, *J. Phys. Chem.*, 1995, **99**, 17711–17714.
145. S. Mondal, S. Basu and D. Mandal, *Chem. Phys. Lett.*, 2009, **479**, 218–223.
146. M. Kotlarchyk, J. S. Huang and S. H. Chen, *J. Phys. Chem.*, 1985, **89**, 4382–4386.
147. M.-L. Arsene, I. Răut, M. Călin, M.-L. Jecu, M. Doni and A.-M. Gurban, *Processes*, 2021, **9**, 345.
148. C. Banerjee, C. Ghatak, S. Mandal, S. Ghosh, J. Kuchlyan and N. Sarkar, *J. Phys. Chem. B*, 2013, **117**, 6906–6916.
149. J. Guha Ray and P. K. Sengupta, *Chem. Phys. Lett.*, 1994, **230**, 75–81.
150. O. H. Kwon and D. J. Jang, *J. Phys. Chem. B*, 2005, **109**, 20479–20484.
151. J. F. Stoddart, *Annu. Rep. Prog. Chem. Sect. B Org. Chem.*, 1988, **85**, 353–386.
152. D. Das and O. A. Scherman, *Isr. J. Chem.*, 2011, **51**, 537–550.
153. Sayo O. Fakayode, Mark Lowry, Kristin A. Fletcher, Xiaodong Huang, Aleeta M. Powe and Isiah M. Warner, *Curr. Anal. Chem.*, 2007, **3**, 171–181.
154. B. V. K. J. Schmidt and C. Barner-Kowollik, *Angew. Chemie Int. Ed.*, 2017, **56**, 8350–8369.
155. B. K. Paul and N. Guchhait, *J. Colloid Interface Sci.*, 2011, **353**, 237–247.
156. B. K. Paul and N. Guchhait, *J. Lumin.*, 2012, **132**, 2194–2208.
157. J. Mohanty, A. C. Bhasikuttan, W. M. Nau and H. Pal, *J. Phys. Chem. B*, 2006, **110**, 5132–5138.
158. Y. Matsushita, T. Suzuki, T. Ichimura and T. Hikida, *J. Phys. Chem. A*, 2004, **108**, 7490–7496.
159. P. Das, A. Chakrabarty, B. Haldar, A. Mallick and N. Chattopadhyay, *J. Phys. Chem. B*, 2007, **111**, 7401–7408.
160. J. Szejtli, *Chem. Rev.*, 1998, **98**, 1743–1753.
161. S. Nigam and G. Durocher, *J. Phys. Chem.*, 1996, **100**, 7135–7142.

TH-2834_146122035

162. W. Sun, Z. H. Wang, M. Y. She, Z. Yang, X. L. Jin, Y. Q. Wang, Z. Shi and J. L. Li, *Chinese Chem. Lett.*, 2016, **27**, 1077–1082.
163. E. L. Roberts, J. Dey and I. M. Warner, *J. Phys. Chem.*, 1996, **100**, 19681–19686.
164. K. Kerdpol, R. Daengngern, C. Sattayanon, S. Namuangruk, T. Rungrotmongkol, P. Wolschann, N. Kungwan and S. Hannongbua, *Molecules*, 2021, **26**, 843.
165. M. K. Singh, H. Pal, A. S. R. Koti and A. V. Sapre, *J. Phys. Chem. A*, 2004, **108**, 1465–1474.
166. G. Krishnamoorthy and S. K. Dogra, *Chem. Phys.*, 1999, **243**, 45–59.
167. R. Misra and S. P. Bhattacharyya, in *Intramolecular Charge Transfer*, Wiley-VCH Verlag GmbH & Co. KGaA, 2018, pp. 29–69.
168. C. Zhong, *Phys. Chem. Chem. Phys.*, 2015, **17**, 9248–9257.
169. S. Sasaki, G. P. C. Drummen and G. I. Konishi, *J. Mater. Chem. C*, 2016, 4, 2731–2743.
170. R. Rattanawan, V. Promarak, T. Sudyoadsuk, S. Namuangruk, N. Kungwan, S. Yuan and S. Jungsuttiwong, *J. Photochem. Photobiol. A Chem.*, 2016, **322–323**, 16–26.
171. C. Cao, X. Liu, Q. Qiao, M. Zhao, W. Yin, D. Mao, H. Zhang and Z. Xu, *Chem. Commun.*, 2014, **50**, 15811–15814.
172. K. Chanda and B. MM, *Chem. Soc. Rev.*, , DOI:10.1039/d0cs01444c.
173. K. A. Zachariasse, M. Grobys, T. Von Der Haar, A. Hebecker, Y. V. Il'ichev, Y. B. Jiang, O. Morawski and W. Kühnle, *J. Photochem. Photobiol. A Chem.*, 1996, **102**, 59–70.
174. W. Rettig, *Angew. Chemie Int. Ed. English*, 1986, 25, 971–988.
175. G. R. Medders, E. C. Alguire, A. Jain and J. E. Subotnik, *J. Phys. Chem. A*, 2017, **121**, 1425–1434.
176. G. J. Zhao and K. L. Han, *Acc. Chem. Res.*, 2012, **45**, 404–413.
177. T. L. Arbeloa, F. López Arbeloa, M. J. Tapia and I. L. Arbeloa, *Chem. Soc. Rev.*, 2021, **50**, 3706-3719.
178. G. Chu and F. Yangbo, *J. Chem. Soc. Faraday Trans. 1 Phys. Chem. Condens. Phases*, 1987, **83**, 2533–2539.
179. M. Józefowicz, K. A. Kozyra, J. R. Heldt and J. Heldt, *Chem. Phys.*, 2005, **320**, 45–53.
180. E. Fasani, A. Albini, P. Savarino, G. Viscardi and E. Barni, *J. Heterocycl. Chem.*, 1993, **30**, 1041–1044.
181. A. Mishra, S. Sahu, N. Dash, S. K. Behera and G. Krishnamoorthy, *J. Phys. Chem. B*, 2013, **117**, 9469–9477.
182. S. K. Behera and G. Krishnamoorthy, *Photochem. Photobiol. Sci.*, 2015, **14**, 2225–2237.
183. S. Ríos Vázquez, J. L. Pérez Lustres, F. Rodríguez-Prieto, M. Mosquera and M. C. Ríos Rodríguez, *J. Phys. Chem. B*, 2015, **119**, 2475–2489.
184. R. I. Cukier and D. G. Nocera, *Annu. Rev. Phys. Chem.*, 1998, **49**, 337–369.
185. Y. Nosenko, G. Wiosna-Sałyga, M. Kunitski, I. Petkova, A. Singh, W. J. Buma, R. P. Thummel, B. Brutschy and J. Waluk, *Angew. Chemie - Int. Ed.*, 2008, **47**, 6037–6040.
186. Y. Kim, M. Yoon and D. Kim, *J. Photochem. Photobiol. A Chem.*, 2001, **138**, 167–175.
187. B. Zhang, M. Gu, C. Liu, X. Liu, N. Gao, Q. Gao, Y. Zhu, M. Tang, C. Du and M. Song, *Eur. J. Inorg. Chem.*, 2017, **2017**, 5366–5371.
188. D. Gormin and M. Kasha, *Chem. Phys. Lett.*, 1988, **153**, 574–576.
189. J. Heldt, D. Gormin and M. Kasha, *Chem. Phys.*, 1989, **136**, 321–334.
190. D. Gormin, J. Heldt and M. Kasha, *J. Phys. Chem.*, 1995, **99**, 7281-7284.
191. C. H. Kim, J. Park, J. Seo, S. Y. Park and T. Joo, *J. Phys. Chem. A*, 2010, **114**, 5618–5629.
192. S. R. Vázquez, M. C. R. Rodríguez, M. Mosquera and F. Rodríguez-Prieto, *J. Phys. Chem. A*, 2008, **112**, 376–387.
193. Y. Hong, J. W. Y. Lam and B. Z. Tang, *Chem. Commun.*, 2009, 0, 4332–4353.
194. Y. Hong, J. W. Y. Lam and B. Z. Tang, *Chem. Soc. Rev.*, 2011, 40, 5361–5388.
195. J. Mei, Y. Hong, J. W. Y. Lam, A. Qin, Y. Tang and B. Z. Tang, *Adv. Mater.*, 2014, 26, 5429–5479.
196. Z. Hu, H. Zhang, Y. Chen, Q. Wang, M. R. J. Elsegood, S. J. Teat, X. Feng, M. M. Islam, F. Wu and B. Z. Tang, *Dye. Pigment.*, 2020, **175**, 108175.
197. L. Meng, X. Ma, S. Jiang, S. Zhang, Z. Wu, B. Xu, Z. Lei, L. Liu and W. Tian, *CCS Chem.*, 2020, **3**, 2084–2094.
198. R. Hu, E. Lager, A. Aguilar-Aguilar, J. Liu, J. W. Y. Lam, H. H. Y. Sung, I. D. Williams, Y. Zhong, K. S. Wong, E. Peña-Cabrera and B. Z. Tang, *J. Phys. Chem. C*, 2009, **113**, 15845–

TH-2834_146122035

15853.
199. Y. Qian, S. Li, G. Zhang, Q. Wang, S. Wang, H. Xu, C. Li, Y. Li and G. Yang, *J. Phys. Chem. B*, 2007, **111**, 5861–5868.
200. S. K. Behera, A. Murkherjee, G. Sadhuragiri, P. Elumalai, M. Sathiyendiran, M. Kumar, B. B. Mandal and G. Krishnamoorthy, *Faraday Discuss.*, 2017, **196**, 71–90.
201. A. Bhattacharyya, S. C. Makhal and N. Guchhait, *J. Photochem. Photobiol. A Chem.*, 2020, **388**, 112177.
202. W. Sun, S. Li, R. Hu, Y. Qian, S. Wang and G. Yang, *J. Phys. Chem. A*, 2009, **113**, 5888–5895.
203. W. Rzeski, J. Matysiak and M. Kandefer-Szerszeń, *Bioorganic Med. Chem.*, 2007, **15**, 3201–3207.
204. A. Matwijczuk, D. Kamiński, A. Górecki, A. Ludwiczuk, A. Niewiadomy, S. Maćkowski and M. Gagoś, *J. Phys. Chem. A*, 2015, **119**, 10791–10805.
205. S. Sahu, M. Das, A. K. Bharti and G. Krishnamoorthy, *Phys. Chem. Chem. Phys.*, 2018, **20**, 27131–27139.
206. S. K. Behera, A. Karak and G. Krishnamoorthy, *J. Phys. Chem. B*, 2015, **119**, 2330–2344.
207. S. J. Singh, S. Rajamanickam, A. Gogoi and B. K. Patel, *Tetrahedron Lett.*, 2016, **57**, 1044–1047.
208. S. Stucky, N. J. Koch, U. Heinz and K. Hegetschweiler, *Chem. Pap.*, 2008, **62**, 388.
209. A. Mishra and G. Krishnamoorthy, *Photochem. Photobiol. Sci.*, 2012, **11**, 1356–1367.
210. W. Koch and M. C. Holthausen, *Wolfram Koch , Max C . Holthausen A Chemist ' s Guide to Density Functional Theory*, 2001, vol. 3.
211. C. Adamo and D. Jacquemin, *Chem. Soc. Rev.*, 2013, **42**, 845–856.
212. Gaussian 09, Revision D.01, M. J. Frisch, G. W. Trucks, H. B. Schlegel, G. E. Scuseria, M. A. Robb, J. R. Cheeseman, G. Scalmani, V. Barone, G. A. Petersson, H. Nakatsuji, X. Li, M. Caricato, A. Marenich, J. Bloino, B. G. Janesko, R. Gomperts, B. Mennucci, H. P. Hratchian, J. V. Ortiz, A. F. Izmaylov, J. L. Sonnenberg, D. Williams-Young, F. Ding, F. Lipparini, F. Egidi, J. Goings, B. Peng, A. Petrone, T. Henderson, D. Ranasinghe, V. G. Zakrzewski, J. Gao, N. Rega, G. Zheng, W. Liang, M. Hada, M. Ehara, K. Toyota, R. Fukuda, J. Hasegawa, M. Ishida, T. Nakajima, Y. Honda, O. Kitao, H. Nakai, T. Vreven, K. Throssell, J. A. Montgomery, Jr., J. E. Peralta, F. Ogliaro, M. Bearpark, J. J. Heyd, E. Brothers, K. N. Kudin, V. N. Staroverov, T. Keith, R. Kobayashi, J. Normand, K. Raghavachari, A. Rendell, J. C. Burant, S. S. Iyengar, J. Tomasi, M. Cossi, J. M. Millam, M. Klene, C. Adamo, R. Cammi, J. W. Ochterski, R. L. Martin, K. Morokuma, O. Farkas, J. B. Foresman, and D. J. Fox, Gaussian Inc., Wallingford CT, 2013
213. A. D. Becke, *J. Chem. Phys.*, 1993, **98**, 5648–5652.
214. C. Lee, W. Yang and R. G. Parr, *Phys. Rev. B*, 1988, **37**, 785–789.
215. T. Yanai, D. P. Tew and N. C. Handy, *Chem. Phys. Lett.*, 2004, **393**, 51–57.
216. S. Grimme, J. Antony, S. Ehrlich and H. Krieg, *J. Chem. Phys.*, 2010, **132**, 154104.
217. E. Cancès, B. Mennucci and J. Tomasi, *J. Chem. Phys.*, 1997, **107**, 3032–3041.
218. T. Lu and F. Chen, *J. Comput. Chem.*, 2012, **33**, 580–592.
219. S. Haider, M. S. Alam and H. Hamid, *Eur. J. Med. Chem.*, 2015, **92**, 156–177.
220. A. Aliabadi, *Anti-Cancer Agents Med. Chem.*, 2016, **16**, 1301–1314.
221. G. Serban, O. Stanasel, E. Serban and S. Bota, *Drug Des., Dev. Ther.*, 2018, **12**, 1545–1566.
222. M. M. Sekhar, U. Nagarjuna, V. Padmavathi, A. Padmaja, N. V. Reddy and T. Vijaya, *Eur. J. Med. Chem.*, 2018, **145**, 1–10.
223. S. Maddila, S. Gorle, C. Sampath and P. Lavanya, *J. Saudi Chem. Soc.*, 2016, **20**, S306–S312.
224. N. Ö. Can, Ö. D. Can, D. Osmaniye and Ü. D. Özkay, *Molecules*, 2018, **23**, 716.
225. J. J. Luszczki, M. Karpińska, J. Matysiak and A. Niewiadomy, *Pharmacol. Rep.*, 2015, **67**, 588–592.
226. B. Chudzik, K. Bonio, W. Dabrowski, D. Pietrzak, A. Niewiadomy, A. Olender, K. Malodobry and M. Gagoś, *Sci. Rep.*, 2019, **9**, 12945.
227. B. Chudzik, K. Bonio, W. Dabrowski, D. Pietrzak, A. Niewiadomy, A. Olender, B. Pawlikowska-Pawlęga and M. Gagoś, *PLoS One*, 2019, **14**, 1–32.
228. M. Juszczak, J. Matysiak, M. Szeliga, P. Pożarowski, A. Niewiadomy, J. Albrecht and W. Rzeski, *Bioorg. Med. Chem. Lett.*, 2012, **22**, 5466–5469.

TH-2834_146122035

229. M. Juszczak, J. Matysiak, A. Niewiadomy and W. Rzeski, *Folia Histochem. Cytobiol.*, 2011, **49**, 436–444.
230. A. Matwijczuk, A. Górecki, M. Makowski, K. Pustuła, A. Skrzypek, J. Waś, A. Niewiadomy and M. Gagoś, *J. Fluoresc.*, 2018, **28**, 65–77.
231. A. A. Hoser, D. M. Kamiński, A. Skrzypek, A. Matwijczuk, A. Niewiadomy, M. Gagoś and K. Woźniak, *Cryst. Growth Des.*, 2018, **18**, 3851–3862.
232. D. M. Kamiński, A. A. Hoser, M. Gagoś, A. Matwijczuk, M. Arczewska, A. Niewiadomy and K. Woźniak, *Cryst. Growth Des.*, 2010, **10**, 3480–3488.
233. Z. Tang, M. Lu, K. Liu, Y. Zhao, Y. Qi, Y. Wang, P. Zhang and P. Zhou, *J. Photochem. Photobiol. A Chem.*, 2018, **367**, 261–269.
234. J. Zhao, S. Ji, Y. Chen, H. Guo and P. Yang, *Phys. Chem. Chem. Phys.*, 2012, **14**, 8803–8817.
235. F. S. Rodembusch, F. P. Leusin, L. F. Campo and V. Stefani, *J. Lumin.*, 2007, 126, 728–734.
236. V. S. Padalkar, A. Tathe, V. D. Gupta, V. S. Patil, K. Phatangare and N. Sekar, *J. Fluoresc.*, 2012, **22**, 311–322.
237. H. K. Sinha and S. K. Dogra, *Chem. Phys.*, 1986, **102**, 337–347.
238. S. Sahu, S. Dutta and G. Krishnamoorthy, *Phys. Chem. Chem. Phys.*, 2016, **18**, 29905–29913.
239. S. Kundu and N. Chattopadhyay, *J. Photochem. Photobiol. A Chem.*, 1995, **88**, 105–108.
240. M. Valero, W. Hu, J. E. Houston and C. A. Dreiss, *J. Mol. Liq.*, 2021, **322**, 114892.
241. O. K. Abou-Zied, *J. Phys. Chem. B*, 2007, **111**, 9879–9885.
242. K. Gavvala, A. Sengupta, R. K. Koninti and P. Hazra, *Phys. Chem. Chem. Phys.*, 2014, **16**, 933–939.
243. M. Das, S. Sahu and G. Krishnamoorthy, *Phys. Chem. Chem. Phys.*, 2019, **21**, 15669–15677.
244. B. K. Paul, A. Samanta and N. Guchhait, *Langmuir*, 2010, **26**, 3214–3224.
245. M. Mosquera, J. C. Penedo, M. C. Ríos Rodríguez and F. Rodrìguez-Prieto, *J. Phys. Chem.*, 1996, **100**, 5398–5407.
246. S. K. Behera and G. Krishnamoorthy, *Phys. Chem. Chem. Phys.*, 2017, **19**, 19234–19242.
247. S. Manne and L. K. Patterson, in *Encyclopedia of Physical Science and Technology (Third Edition)*, ed. R. A. Meyers, Academic Press, New York, Third Edit., 2003, pp. 661–677.
248. N. O. Mchedlov-Petrossyan, N. A. Vodolazkaya and A. O. Doroshenko, *J. Fluoresc.*, 2003, **13**, 235–248.
249. S. Il Yoo, J.-H. Lee, B.-H. Sohn, I. Eom, T. Joo, S. J. An and G.-C. Yi, *Adv. Funct. Mater.*, 2008, **18**, 2984–2989.
250. M. Gaber, T. A. Fayed, S. A. El-Daly and Y. S. El-Sayed, *Photochem. Photobiol. Sci.*, 2008, **7**, 257–262.
251. B. K. Paul, A. Samanta and N. Guchhait, *Langmuir*, 2010, **26**, 3214–3224.
252. G. Krishnamoorthy and S. K. Dogra, *J. Colloid Interface Sci.*, 2000, **228**, 335–343.
253. S. Santra and S. K. Dogra, *Spectrochim. Acta - Part A Mol. Biomol. Spectrosc.*, 2000, **56**, 915–925.
254. S. Das and S. K. Dogra, *J. Chem. Soc. - Faraday Trans.*, 1998, **94**, 139–145.
255. B. K. Paul, A. Samanta and N. Guchhait, *Langmuir*, 2010, **26**, 3214–3224.
256. M. Valero, W. Hu, J. E. Houston and C. A. Dreiss, *J. Mol. Liq.*, 2021, **322**, 114892.
257. S. Das and N. Chattopadhyay, *Colloids Interface Sci. Commun.*, 2017, **16**, 10–13.
258. D. Ghosh, S. Batuta, N. A. Begum and D. Mandal, *J. Lumin.*, 2017, **184**, 64–73.
259. S. Santra and S. K. Dogra, *Spectrochim. Acta - Part A Mol. Biomol. Spectrosc.*, 2000, **56**, 915–925.
260. S. Sasaki, G. P. C. Drummen and G. I. Konishi, *J. Mater. Chem. C*, 2016, 4, 2731–2743.
261. Z. R. Grabowski, K. Rotkiewicz and A. Siemiarczuk, *J. Lumin.*, 1979, **18–19**, 420–424.
262. M. M. Balamurali and S. K. Dogra, *J. Photochem. Photobiol. A Chem.*, 2002, **154**, 81–92.
263. R. Omidyan and M. Iravani, *J. Phys. Chem. A*, 2016, **120**, 1012–1019.
264. F. Abedini and R. Omidyan, *J. Phys. Chem. A*, 2018, **122**, 2653–2662.
265. M. M. Warren, M. Kaucikas, A. Fitzpatrick, P. Champion, J. Timothy Sage and J. J. Van Thor, *Nat. Commun.*, 2013, **4**, 1–8.
266. C. Petermayer and H. Dube, *Acc. Chem. Res.*, 2018, **51**, 1153–1163.
267. D. Yang, M. Jia, J. Wu and X. Song, *Sci. Rep.*, 2017, **7**, 11728.

TH-2834_146122035

268. A. Brenlla, M. Veiga, J. L. Pérez Lustres, M. C. Ríos Rodríguez, F. Rodríguez-Prieto and M. Mosquera, *J. Phys. Chem. B*, 2013, **117**, 884–896.
269. A. Mishra and G. Krishnamoorthy, *Photochem. Photobiol. Sci.*, 2012, **11**, 1356–1367.
270. F. A. S. Chipem, N. Dash and G. Krishnamoorthy, *J. Chem. Phys.*, 2011, **134**, 104308.
271. A. O. Doroshenko, E. A. Posokhov, A. A. Verezubova and L. M. Ptyagina, *J. Phys. Org. Chem.*, 2000, **13**, 253–265.
272. R. L. Martin, *J. Chem. Phys.*, 2003, **118**, 4775–4777.
273. G. Jiang, F. Li, J. Fan, Y. Song, C. K. Wang and L. Lin, *J. Mater. Chem. C*, 2019, **8**, 98–108.
274. C. A. Guido, P. Cortona, B. Mennucci and C. Adamo, *J. Chem. Theory Comput.*, 2013, **9**, 3118–3126.
275. T. Le Bahers, C. Adamo and I. Ciofini, *J. Chem. Theory Comput.*, 2011, **7**, 2498–2506.
276. Ila and G. Krishnamoorthy, *J. Photochem. Photobiol. A Chem.*, 2021, 113199.
277. Ila, R. Dani, S. P. Verma and G. Krishnamoorthy, *Photochem. Photobiol. Sci.*, 2020, **19**, 844–853.
278. G. Krishnamoorthy and S. K. Dogra, *J. Org. Chem.*, 1999, **64**, 6566–6574.

TH-2834_146122035

TH-2834_146122035

Annexure A

भारतीय प्रौद्योगिकी संस्थान गुवाहाटी
Indian Institute of Technology Guwahati

TH-2834_146122035

^{1}H NMR (600 MHz, $CDCl_3$) δ 11.15 (s, 1H), 9.01 (s, 1H), 7.43 – 7.35 (m, 4H), 7.32 – 7.26 (m, 2H), 7.14 (t, J = 6.7 Hz, 1H), 7.05 (d, J = 7.8 Hz, 1H), 6.89 (t, J = 7.5 Hz, 1H).

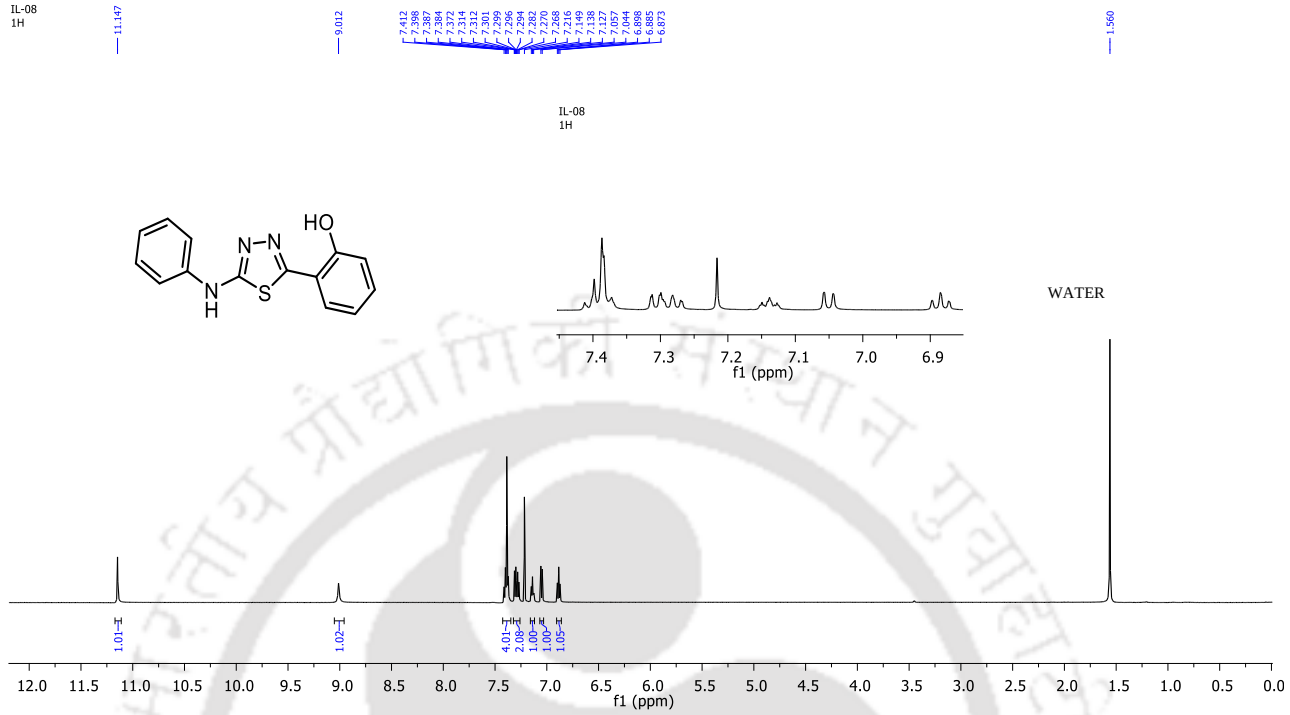

Figure A1. ^{1}H NMR Spectrum of PHBT.

TH-2834_146122035

^{13}C NMR (151 MHz, $CDCl_3$) δ 157.02, 139.95, 131.70, 129.97, 128.59, 124.61, 119.88, 119.07, 117.79, 114.67.

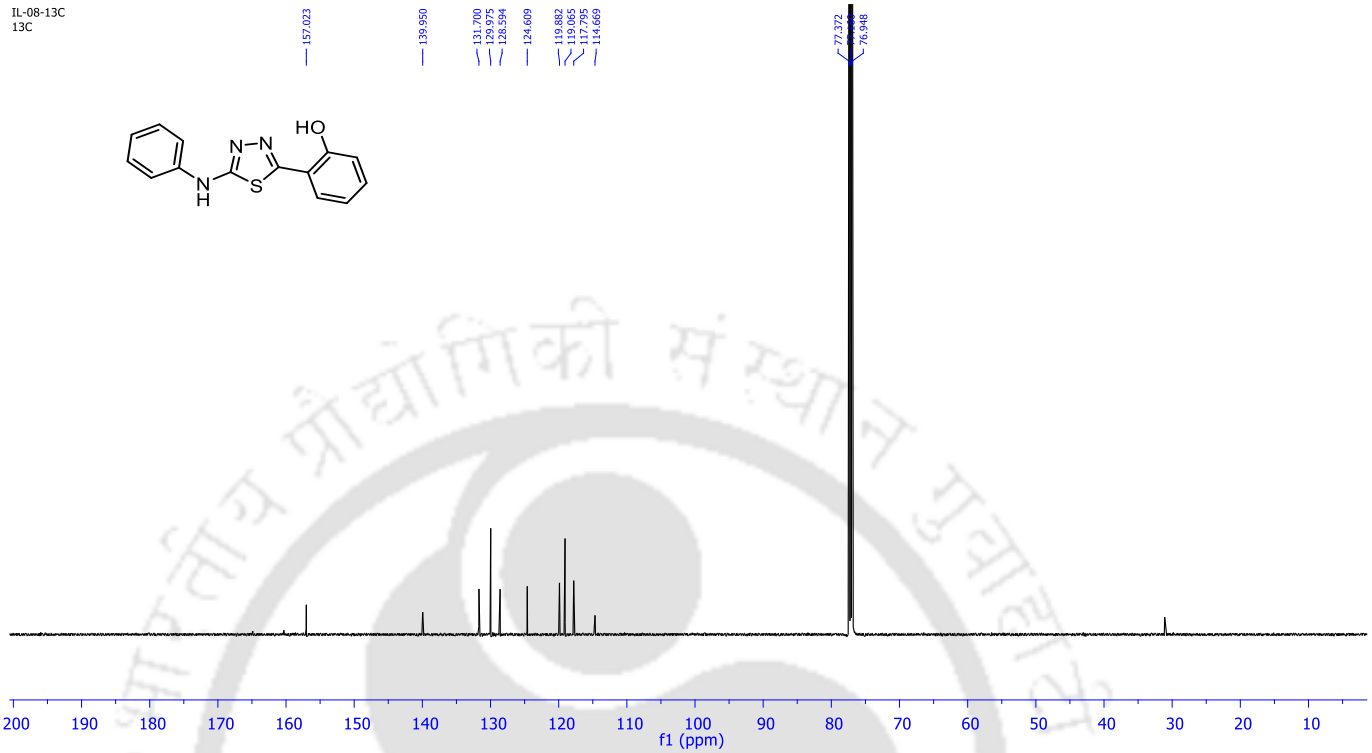

Figure A2. ^{13}C NMR Spectrum of PHBT.

TH-2834_146122035

^{1}H NMR (600 MHz, $CDCl_3$) δ 8.37 (dd, *J* = 7.8, 1.5 Hz, 1H), 7.44 (d, *J* = 7.8 Hz, 2H), 7.39 (dt, *J* = 13.8, 4.9 Hz, 3H), 7.08 (t, *J* = 7.6 Hz, 2H), 6.99 (d, *J* = 8.3 Hz, 1H), 3.96 (s, 3H).

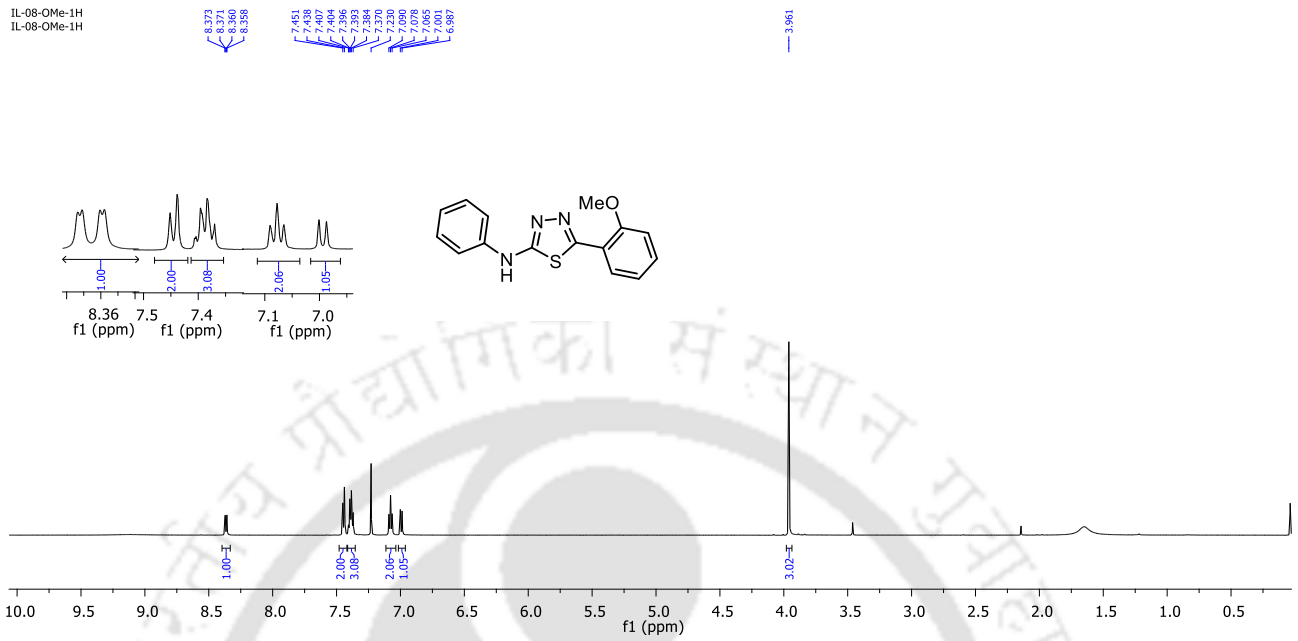

Figure A3. ^{1}H NMR Spectrum of PMBT

TH-2834_146122035

^{13}C NMR (151 MHz, $CDCl_3$) δ 155.2, 140.6, 131.2, 129.7, 128.2, 123.2, 121.5, 119.9, 118.2, 111.5, 55.9.

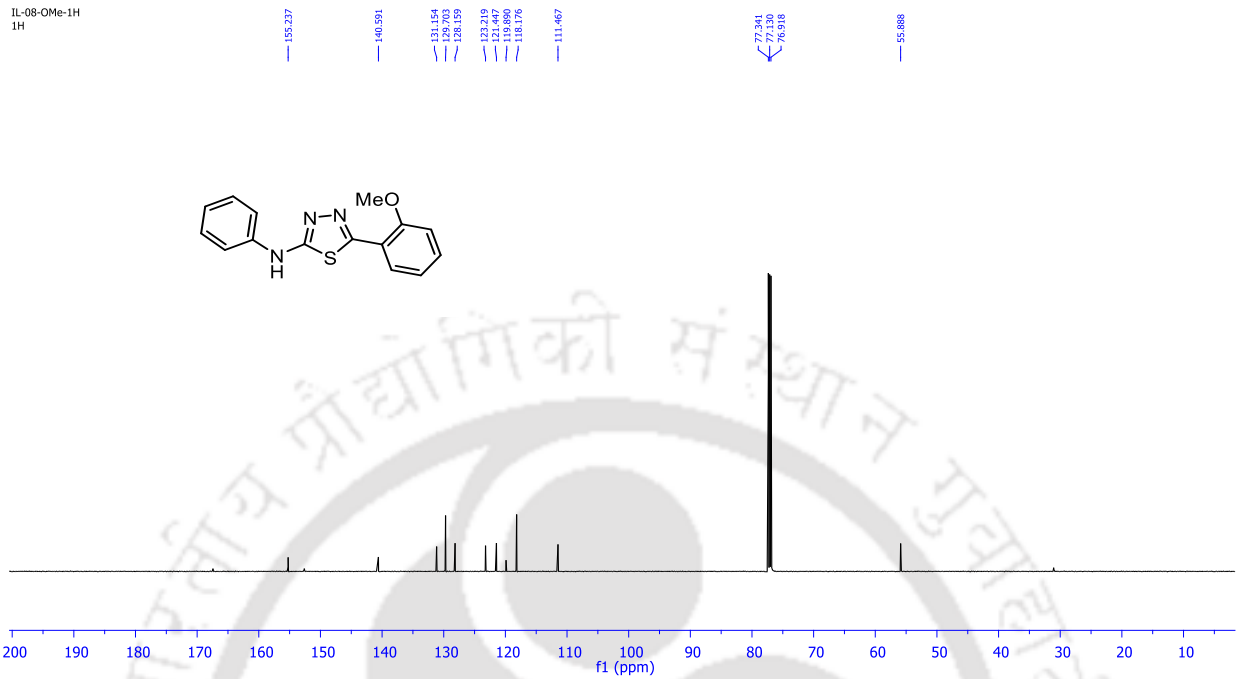

Figure A4. ^{13}C NMR Spectrum of PMBT.

TH-2834_146122035

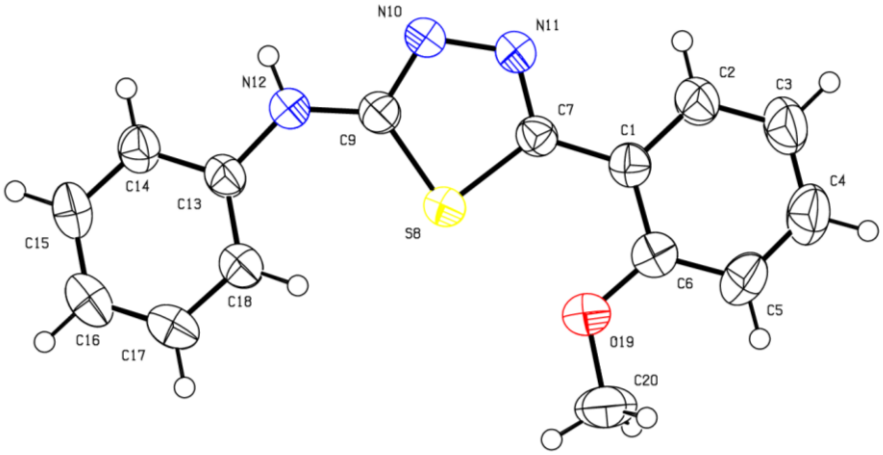

Figure A5. Crystal structure of PMBT (Cambridge Crystallographic Data Centre (CCDC) no. 1921954-1921955).

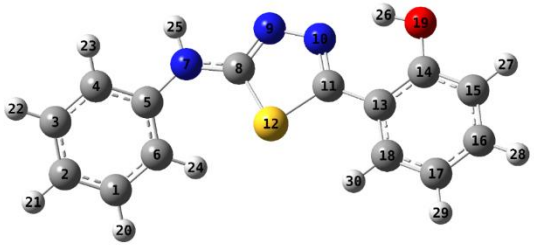

Figure A6. Ground state optimized geometry of PHBT *cis*-enol.

Table A1. Ground state optimized Parameters of PHBT *cis*-enol.

Center Number	Atomic Number	Atomic Type	Coordinates (Angstroms)		
			X	Y	Z
1	6	0	-4.3942	1.7079	0.642138
2	6	0	-5.59938	1.303279	0.065096
3	6	0	-5.68107	0.038284	-0.52697
4	6	0	-4.56932	-0.80061	-0.55756
5	6	0	-3.35474	-0.38994	0.019114
6	6	0	-3.27692	0.868556	0.634265
7	7	0	-2.27559	-1.29419	-0.02181
8	6	0	-0.93016	-1.07818	0.047564
9	7	0	-0.09542	-2.08636	0.173021
10	7	0	1.204662	-1.68701	0.121211
11	6	0	1.392413	-0.39813	-0.02282
12	16	0	-0.13807	0.487485	-0.13006
13	6	0	2.708843	0.225506	-0.06348
14	6	0	3.874834	-0.57544	0.0887
15	6	0	5.139827	0.030821	0.056969

TH-2834_146122035

16	6	0	5.261861	1.403804	-0.12526
17	6	0	4.120967	2.205369	-0.28048
18	6	0	2.864581	1.614031	-0.24942
19	8	0	3.824626	-1.91258	0.265938
20	1	0	-4.31863	2.679523	1.121262
21	1	0	-6.4638	1.959295	0.081044
22	1	0	-6.61125	-0.2955	-0.977
23	1	0	-4.63377	-1.77527	-1.03386
24	1	0	-2.36898	1.188528	1.131318
25	1	0	-2.50758	-2.27395	-0.13358
26	1	0	2.877013	-2.20299	0.25991
27	1	0	6.012154	-0.60325	0.17705
28	1	0	6.249781	1.854221	-0.14845
29	1	0	4.214699	3.276505	-0.42535
30	1	0	1.981649	2.235239	-0.37305

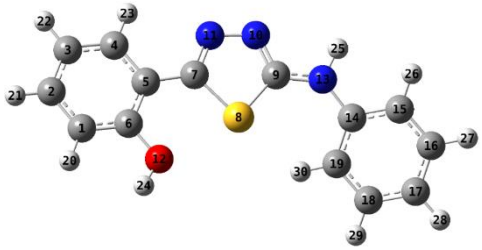

Figure A7. Ground state optimized geometry of PHBT *trans*-enol.

Table A2. Ground state optimized parameters of PHBT *trans*-enol.

Center Number	Atomic Number	Atomic Type	Coordinates (Angstroms)		
			X	Y	Z
1	6	0	-4.47877	1.592418	-0.15943
2	6	0	-5.51506	0.669195	-0.03847
3	6	0	-5.22197	-0.69203	0.104582
4	6	0	-3.8973	-1.1147	0.124997
5	6	0	-2.8292	-0.20217	0.003798
6	6	0	-3.14743	1.163733	-0.13852
7	6	0	-1.45315	-0.71494	0.025536
8	16	0	0.013399	0.284129	-0.05742
9	6	0	0.910741	-1.21699	0.064535
10	7	0	0.146412	-2.28811	0.152488
11	7	0	-1.17869	-1.98969	0.123818
12	8	0	-2.10972	2.051026	-0.25529
13	7	0	2.27053	-1.35858	0.005019
14	6	0	3.308683	-0.41383	0.025925
15	6	0	4.57159	-0.83168	-0.43468
16	6	0	5.652852	0.04545	-0.42519
17	6	0	5.498768	1.358521	0.033493
18	6	0	4.248094	1.771679	0.495516
19	6	0	3.157508	0.897612	0.503611
20	1	0	-4.69544	2.652253	-0.27142
21	1	0	-6.54475	1.013026	-0.05523
22	1	0	-6.02225	-1.41871	0.200448

TH-2834_146122035

23	1	0	-3.65608	-2.16553	0.235415
24	1	0	-2.44393	2.952815	-0.35516
25	1	0	2.547705	-2.32818	-0.09239
26	1	0	4.696656	-1.8457	-0.80554
27	1	0	6.617997	-0.29791	-0.78588
28	1	0	6.340242	2.043942	0.033897
29	1	0	4.112121	2.78265	0.868461
30	1	0	2.21118	1.238175	0.904995

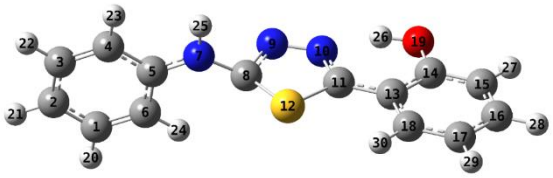

Figure A8. Excited state optimized geometry of PHBT *cis*-enol.

Table A3. Excited state optimized parameters of PHBT *cis*-enol.

Center Number	Atomic Number	Atomic Type	Coordinates (Angstroms)		
			X	Y	Z
1	6	0	-4.3942	1.7079	0.642138
2	6	0	-5.59938	1.303279	0.065096
3	6	0	-5.68107	0.038284	-0.52697
4	6	0	-4.56932	-0.80061	-0.55756
5	6	0	-3.35474	-0.38994	0.019114
6	6	0	-3.27692	0.868556	0.634265
7	7	0	-2.27559	-1.29419	-0.02181
8	6	0	-0.93016	-1.07818	0.047564
9	7	0	-0.09542	-2.08636	0.173021
10	7	0	1.204662	-1.68701	0.121211
11	6	0	1.392413	-0.39813	-0.02282
12	16	0	-0.13807	0.487485	-0.13006
13	6	0	2.708843	0.225506	-0.06348
14	6	0	3.874834	-0.57544	0.0887
15	6	0	5.139827	0.030821	0.056969
16	6	0	5.261861	1.403804	-0.12526
17	6	0	4.120967	2.205369	-0.28048
18	6	0	2.864581	1.614031	-0.24942
19	8	0	3.824626	-1.91258	0.265938
20	1	0	-4.31863	2.679523	1.121262
21	1	0	-6.4638	1.959295	0.081044
22	1	0	-6.61125	-0.2955	-0.977
23	1	0	-4.63377	-1.77527	-1.03386
24	1	0	-2.36898	1.188528	1.131318
25	1	0	-2.50758	-2.27395	-0.13358
26	1	0	2.877013	-2.20299	0.25991
27	1	0	6.012154	-0.60325	0.17705
28	1	0	6.249781	1.854221	-0.14845
29	1	0	4.214699	3.276505	-0.42535
30	1	0	1.981649	2.235239	-0.37305

TH-2834_146122035

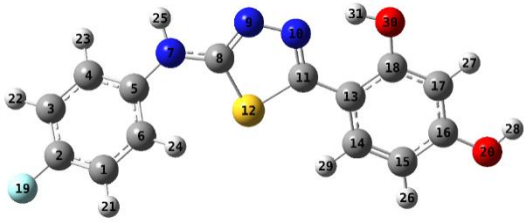

Figure A9. Ground state optimized geometry of FABT *cis*-enol.

Table A4. Ground state optimized parameters of FABT *cis*-enol.

Center Number	Atomic Number	Atomic Type	Coordinates (Angstroms)		
			X	Y	Z
1	6	0	-4.37768	-1.40214	0.791563
2	6	0	-5.51362	-1.0792	0.062577
3	6	0	-5.60309	0.085325	-0.69059
4	6	0	-4.50444	0.942196	-0.7281
5	6	0	-3.33928	0.644382	-0.00182
6	6	0	-3.29021	-0.52603	0.770587
7	7	0	-2.27101	1.564778	-0.04997
8	6	0	-0.92711	1.337917	0.038838
9	7	0	-0.07908	2.327185	0.189711
10	7	0	1.217407	1.906016	0.142162
11	6	0	1.383562	0.615367	-0.01977
12	16	0	-0.16181	-0.24211	-0.15595
13	6	0	2.686146	-0.02843	-0.05485
14	6	0	2.833615	-1.41504	-0.26275
15	6	0	4.074889	-2.0291	-0.2877
16	6	0	5.224451	-1.24292	-0.10226
17	6	0	5.121598	0.13136	0.102098
18	6	0	3.864958	0.748949	0.126382
19	9	0	-6.57839	-1.92842	0.089873
20	8	0	6.428453	-1.88628	-0.13435
21	1	0	-4.35149	-2.31076	1.382985
22	1	0	-6.50762	0.305941	-1.24656
23	1	0	-4.54735	1.844785	-1.33048
24	1	0	-2.42038	-0.75101	1.376592
25	1	0	-2.50421	2.54265	-0.17127
26	1	0	4.175272	-3.09623	-0.44867
27	1	0	6.003321	0.749371	0.244107
28	1	0	7.148983	-1.25606	0.005127
29	1	0	1.947898	-2.02655	-0.40995
30	8	0	3.83271	2.081474	0.326153
31	1	0	2.886809	2.384128	0.311453

TH-2834_146122035

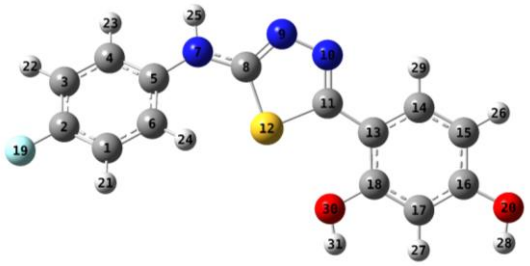

Figure A10. Ground state optimized geometry of FABT *trans*-enol.

Table A5. Ground state optimized parameters of FABT *trans*-enol.

Center Number	Atomic Number	Atomic Type	Coordinates (Angstroms)		
			X	Y	Z
1	6	0	4.282674	-1.46055	-0.61679
2	6	0	5.484731	-1.0498	-0.06035
3	6	0	5.638502	0.205972	0.514849
4	6	0	4.542886	1.065613	0.545057
5	6	0	3.307526	0.680825	-0.00814
6	6	0	3.192501	-0.58666	-0.60122
7	7	0	2.255391	1.610845	0.035112
8	6	0	0.899302	1.43496	-0.05082
9	7	0	0.106385	2.477933	-0.17249
10	7	0	-1.21255	2.141007	-0.1485
11	6	0	-1.44945	0.861206	-0.02375
12	16	0	0.046347	-0.09195	0.100121
13	6	0	-2.80575	0.304623	-0.01333
14	6	0	-3.90351	1.172817	-0.19544
15	6	0	-5.21408	0.721448	-0.18872
16	6	0	-5.46797	-0.64336	0.004786
17	6	0	-4.4084	-1.53343	0.188303
18	6	0	-3.09182	-1.06091	0.178163
19	9	0	6.549927	-1.902	-0.0803
20	8	0	-6.77288	-1.04733	0.002485
21	1	0	4.20176	-2.44178	-1.07165
22	1	0	6.592698	0.497857	0.939644
23	1	0	4.642947	2.043785	1.006608
24	1	0	2.268992	-0.89617	-1.07446
25	1	0	2.512688	2.584255	0.144096
26	1	0	-6.04444	1.403742	-0.33187
27	1	0	-4.59862	-2.59388	0.341052
28	1	0	-6.83428	-2.00289	0.137119
29	1	0	-3.69596	2.226017	-0.3447
30	8	0	-2.03689	-1.91461	0.354419
31	1	0	-2.34593	-2.82122	0.48513

TH-2834_146122035

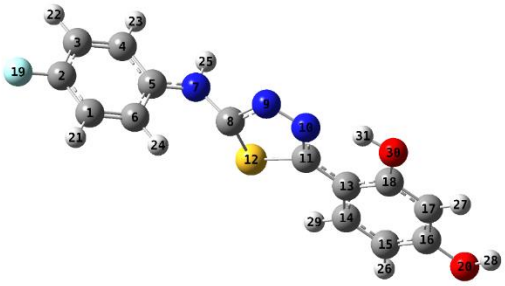

Figure A11. Excited state optimized geometry of FABT *cis*-enol.

Table A6. Excited state optimized parameters of FABT *cis*-enol.

Center Number	Atomic Number	Atomic Type	Coordinates (Angstroms)		
			X	Y	Z
1	6	0	-4.93869	-0.01388	1.434593
2	6	0	-5.99973	-0.13459	0.523093
3	6	0	-5.8136	-0.20268	-0.86864
4	6	0	-4.53209	-0.14844	-1.36052
5	6	0	-3.41526	-0.0249	-0.4631
6	6	0	-3.65219	0.040975	0.952417
7	7	0	-2.17574	0.027714	-0.96245
8	6	0	-0.97429	0.208501	-0.19393
9	7	0	-0.38684	1.44077	-0.32975
10	7	0	0.924742	1.376093	-0.18868
11	6	0	1.465903	0.157488	-0.13458
12	16	0	0.233996	-1.13314	-0.30315
13	6	0	2.884924	-0.07749	-0.00309
14	6	0	3.434946	-1.37725	0.025884
15	6	0	4.801854	-1.60559	0.144402
16	6	0	5.66704	-0.51054	0.242502
17	6	0	5.165332	0.79277	0.219084
18	6	0	3.79193	1.019965	0.098312
19	9	0	-7.24836	-0.18622	0.999274
20	8	0	7.011669	-0.77037	0.362082
21	1	0	-5.15015	0.03555	2.496192
22	1	0	-6.67428	-0.2943	-1.52043
23	1	0	-4.35066	-0.1955	-2.42878
24	1	0	-2.80076	0.139948	1.611143
25	1	0	-2.09701	0.005373	-1.98209
26	1	0	5.203924	-2.61238	0.166261
27	1	0	5.826086	1.65231	0.29088
28	1	0	7.499725	0.061074	0.43224
29	1	0	2.767191	-2.23116	-0.04144
30	8	0	3.3681	2.305738	0.078372
1	1	0	2.377575	2.304203	-0.02327

TH-2834_146122035

Annexure B

भारतीय प्रौद्योगिकी संस्थान गुवाहाटी
Indian Institute of Technology Guwahati

TH-2834_146122035

^{1}H NMR (600 MHz, DMSO-d_6) δ 12.97 (s, 1H), 8.39 (s, 1H), 7.87 (s, 1H), 7.82 (d, J = 9.5 Hz, 1H), 7.42 – 7.38 (m, 1H), 6.86 (dd, J = 13.0, 7.9 Hz, 2H).

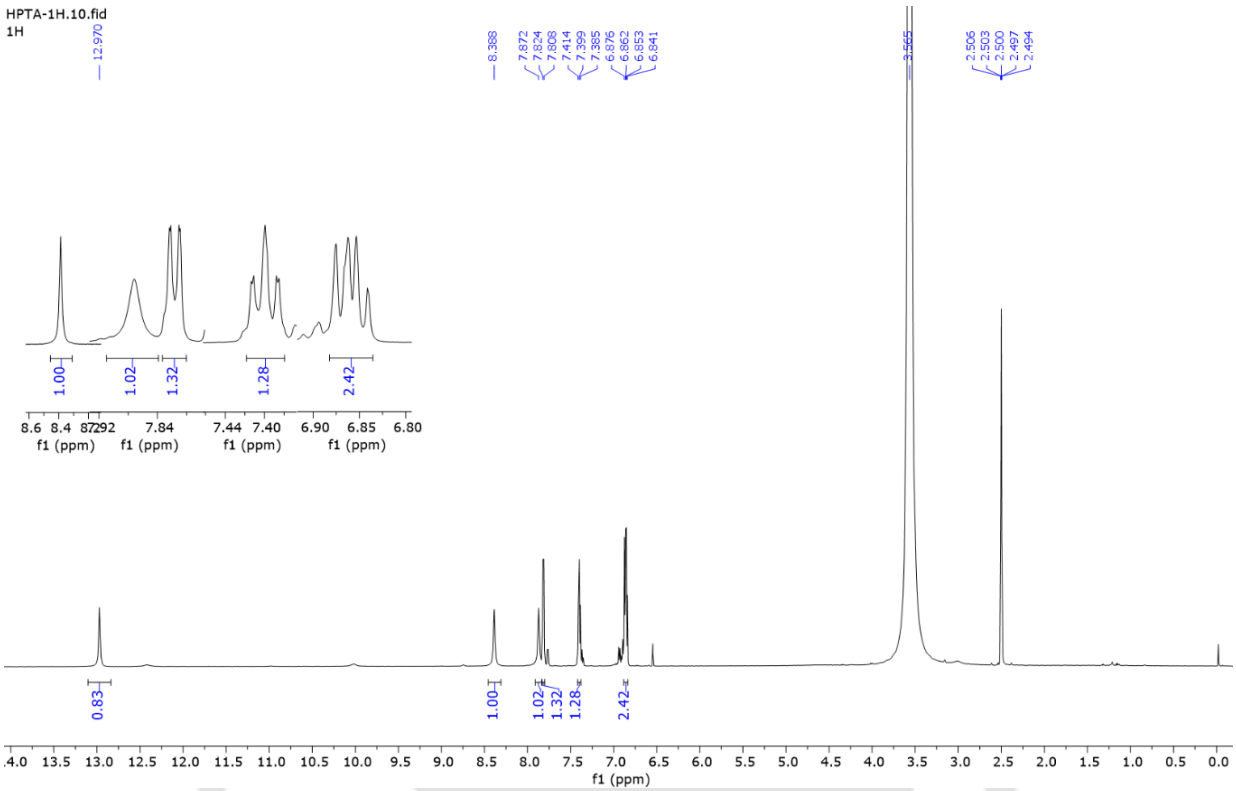

Figure B1. ^{1}H NMR Spectrum of bis-HPTA.

TH-2834_146122035

^{13}C NMR (151 MHz, DMSO-d_6) δ 172.20, 161.09, 134.33, 128.31, 118.66, 117.58, 114.60.

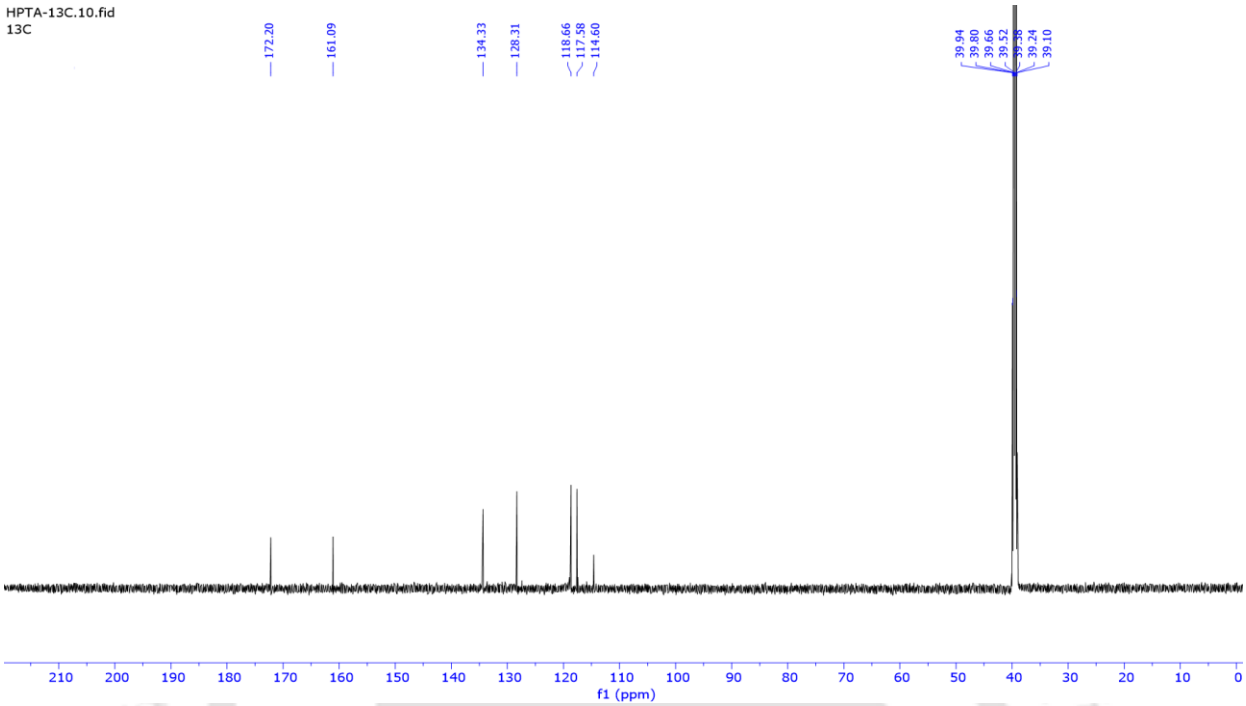

Figure B2. ^{13}C NMR Spectrum of bis-HPTA.

TH-2834_146122035

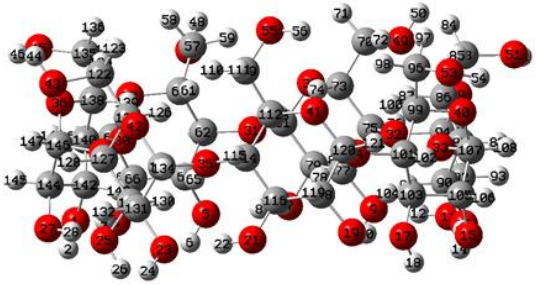

Figure B3. Optimized geometry of bis-HPTA in *β*-CD.

Table B1. Optimized geometry of bis-HPTA in *β*-CD.

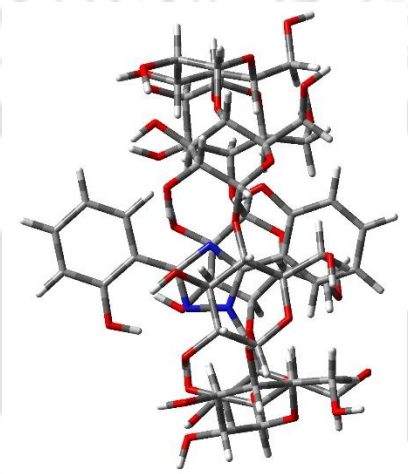

Figure B4. Optimized geometry of bis-HPTA in *β*-CD, orientation I.

Table B2. Optimized geometry of bis-HPTA in *β*-CD.

Center Number	Atomic Number	Atomic Type	Coordinates (Angstroms)		
			X	Y	Z
1	8	0	5.842682	2.835886	2.050834
2	1	0	6.008694	2.407807	2.904323
3	8	0	4.816208	5.519002	1.587827
4	1	0	4.973984	4.574297	1.790909
5	8	0	2.134404	6.505557	2.009299
6	1	0	2.823408	6.489971	2.690566
7	8	0	-0.65245	4.825822	3.18229
8	1	0	-1.16511	4.373519	3.869385
9	8	0	-3.0133	3.327159	2.762231
10	1	0	-2.70126	2.402157	2.829036
11	8	0	-5.75734	2.960765	2.28783
12	1	0	-4.79543	3.068822	2.460494
13	8	0	-6.1836	0.109808	2.090011
14	1	0	-6.0946	0.582134	2.932026
15	8	0	-6.12329	-2.75148	1.851988
16	1	0	-5.93061	-1.79395	1.930477
17	8	0	-4.00649	-4.68806	1.940956

TH-2834_146122035

18	1	0	-4.44811	-4.32829	2.725642
19	8	0	-1.75379	-6.48512	1.919707
20	1	0	-2.3509	-5.71054	1.939095
21	8	0	1.095385	-6.13221	2.227377
22	1	0	1.890453	-5.59557	2.411938
23	8	0	3.665373	-4.7847	2.675899
24	1	0	4.179088	-5.4235	3.188654
25	8	0	5.451419	-2.4803	2.588771
26	1	0	4.99976	-2.67892	3.422684
27	8	0	6.818463	0.109705	2.242088
28	1	0	6.182989	-0.62866	2.333851
29	8	0	5.1807	-0.98284	0.22678
30	8	0	4.097986	3.327133	-0.09246
31	8	0	0.141218	4.930154	0.471043
32	8	0	-3.87894	3.120778	0.026529
33	8	0	-4.97251	-1.1009	-0.1611
34	8	0	-2.09643	-4.54913	-0.109
35	8	0	2.322971	-4.43135	0.265678
36	8	0	6.096345	0.479283	-1.3491
37	8	0	3.159722	4.831235	-1.61435
38	8	0	-1.79039	6.178018	-0.01353
39	8	0	-5.57444	2.3526	-1.33641
40	8	0	-5.02418	-2.89033	-1.66129
41	8	0	-0.65256	-5.75202	-1.50723
42	8	0	4.36193	-4.40569	-0.90662
43	8	0	6.541847	-3.13519	-2.28772
44	1	0	6.970712	-2.90895	-3.12368
45	8	0	6.130644	2.692981	-3.12347
46	1	0	6.863621	2.061355	-3.08438
47	8	0	0.958229	6.170953	-2.83951
48	1	0	0.393924	6.278556	-3.61651
49	8	0	-4.48219	6.45551	-1.04474
50	1	0	-5.02879	6.828839	-1.74893
51	8	0	-6.94161	0.492942	-2.96829
52	1	0	-7.24493	1.406298	-2.8604
53	8	0	-4.02098	-4.99622	-3.25336
54	1	0	-4.95042	-4.72549	-3.27879
55	8	0	0.654458	-4.31586	-3.70066
56	1	0	0.777164	-3.35387	-3.61989
57	6	0	0.940833	4.792736	-2.45665
58	1	0	1.344858	4.162078	-3.25814
59	1	0	-0.07904	4.461162	-2.23784
60	6	0	1.795283	4.589309	-1.21627
61	1	0	1.692379	3.539485	-0.9137
62	6	0	1.378266	5.477667	-0.02328
63	1	0	1.225368	6.50635	-0.36726

TH-2834_146122035

64	6	0	2.433498	5.455551	1.085827
65	1	0	2.367552	4.483666	1.593566
66	6	0	3.856554	5.6309	0.542204
67	1	0	3.9574	6.646185	0.143994
68	6	0	4.127141	4.652061	-0.60397
69	1	0	5.09277	4.857748	-1.07481
70	6	0	-3.4602	5.65083	-1.64222
71	1	0	-2.84866	6.244967	-2.33211
72	1	0	-3.9011	4.815575	-2.20008
73	6	0	-2.55375	5.085027	-0.5624
74	1	0	-1.87257	4.374852	-1.04672
75	6	0	-3.30976	4.32845	0.552167
76	1	0	-4.09381	4.971226	0.965503
77	6	0	-2.32865	3.933348	1.655348
78	1	0	-1.60821	3.216005	1.248933
79	6	0	-1.56724	5.163592	2.149991
80	1	0	-2.2899	5.904647	2.520611
81	6	0	-0.82857	5.821762	0.975183
82	1	0	-0.36786	6.762021	1.283416
83	6	0	-5.5252	0.481419	-2.78202
84	1	0	-5.02933	1.094188	-3.54513
85	1	0	-5.20103	-0.55435	-2.90346
86	6	0	-5.10817	0.985968	-1.40501
87	1	0	-4.01445	0.967314	-1.3452
88	6	0	-5.67727	0.148217	-0.24355
89	1	0	-6.74665	-0.03278	-0.40337
90	6	0	-5.47278	0.854755	1.091654
91	1	0	-4.40214	0.838483	1.328264
92	6	0	-5.95491	2.307489	1.041556
93	1	0	-7.03625	2.319545	0.866091
94	6	0	-5.29244	3.041975	-0.13906
95	1	0	-5.71494	4.044016	-0.25786
96	6	0	-3.24531	-3.85346	-2.88634
97	1	0	-3.34783	-3.0591	-3.6367
98	1	0	-2.20344	-4.17765	-2.86094
99	6	0	-3.63993	-3.28885	-1.52667
100	1	0	-3.02092	-2.40584	-1.3219
101	6	0	-3.4835	-4.28859	-0.36294
102	1	0	-3.99931	-5.22367	-0.61138
103	6	0	-4.08271	-3.69843	0.909724
104	1	0	-3.49303	-2.81988	1.20396
105	6	0	-5.53767	-3.27903	0.670385
106	1	0	-6.11748	-4.17275	0.413688
107	6	0	-5.62096	-2.30812	-0.51846
108	1	0	-6.66268	-2.11842	-0.79293
109	6	0	1.30291	-4.96174	-2.60525

TH-2834_146122035

110	1	0	2.297782	-4.53985	-2.43111
111	1	0	1.426647	-6.01159	-2.89027
112	6	0	0.494003	-4.89928	-1.31124
113	1	0	0.153638	-3.87212	-1.13966
114	6	0	1.285014	-5.38076	-0.07948
115	1	0	1.74524	-6.35282	-0.29693
116	6	0	0.383009	-5.52477	1.156551
117	1	0	0.0388	-4.52395	1.452581
118	6	0	-0.85019	-6.37481	0.832079
119	1	0	-0.51686	-7.39384	0.60466
120	6	0	-1.55323	-5.82381	-0.42274
121	1	0	-2.34635	-6.50553	-0.74294
122	6	0	5.185345	-2.68181	-2.33782
123	1	0	4.631473	-3.19568	-3.13299
124	1	0	5.145247	-1.60275	-2.52053
125	6	0	4.500578	-2.97314	-1.0129
126	1	0	3.505296	-2.51344	-1.04751
127	6	0	5.25292	-2.41346	0.21076
128	1	0	6.298294	-2.73908	0.182517
129	6	0	4.606848	-2.8898	1.50994
130	1	0	3.635462	-2.39214	1.612256
131	6	0	4.403767	-4.405	1.505662
132	1	0	5.385407	-4.88963	1.510619
133	6	0	3.674157	-4.87202	0.233641
134	1	0	3.706172	-5.96244	0.164991
135	6	0	4.938741	2.002717	-2.74455
136	1	0	4.726528	1.183385	-3.44293
137	1	0	4.125208	2.728573	-2.80228
138	6	0	5.009357	1.431684	-1.33288
139	1	0	4.067136	0.910067	-1.12155
140	6	0	5.251418	2.490498	-0.24083
141	1	0	6.124572	3.097943	-0.50695
142	6	0	5.49472	1.816765	1.106109
143	1	0	4.565703	1.32648	1.426046
144	6	0	6.610801	0.77087	1.000868
145	1	0	7.548505	1.286193	0.765995
146	6	0	6.316457	-0.21744	-0.13907
147	1	0	7.174996	-0.86897	-0.32313
148	6	0	0.011075	-0.91891	1.419521
149	6	0	0.016038	-0.45522	-0.67644
150	6	0	-0.3132	0.110515	-1.98608
151	6	0	-1.23683	1.163907	-2.10087
152	6	0	0.266121	-0.41399	-3.1677
153	6	0	-1.58896	1.680411	-3.34424
154	1	0	-1.67774	1.568983	-1.1964
155	6	0	-0.09252	0.103203	-4.41713

TH-2834_146122035

156	6	0	-1.01573	1.142996	-4.50434
157	1	0	-2.30544	2.49222	-3.41225
158	1	0	0.364719	-0.32005	-5.30577
159	1	0	-1.28594	1.537601	-5.47916
160	7	0	-0.56632	-0.11673	0.512459
161	8	0	1.181226	-1.4301	-3.14472
162	1	0	1.392913	-1.63786	-2.20266
163	7	0	0.927082	-1.41661	-0.53912
164	7	0	0.912755	-1.70124	0.785622
165	1	0	1.460284	-2.48865	1.114751
166	6	0	-0.31541	-0.9201	2.841797
167	6	0	-1.36334	-0.08816	3.308592
168	6	0	0.371665	-1.72265	3.774009
169	6	0	-1.70649	-0.08169	4.665229
170	6	0	0.031535	-1.71036	5.121387
171	1	0	1.185469	-2.36126	3.446748
172	6	0	-1.01341	-0.88693	5.564204
173	1	0	-2.51794	0.558469	4.995687
174	1	0	0.574591	-2.33514	5.822176
175	1	0	-1.2868	-0.8722	6.61467
176	8	0	-2.06913	0.717722	2.466299
177	1	0	-1.70036	0.61402	1.542364

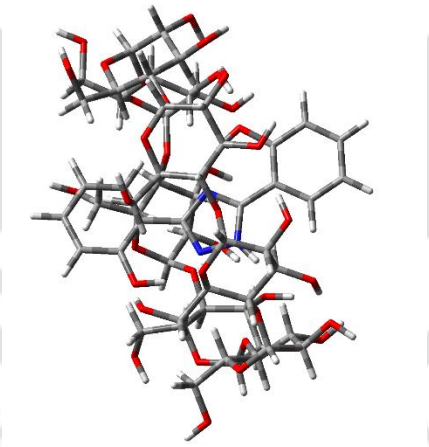

Figure B5. Optimized geometry of bis-HPTA in *β*-CD, orientation II.

Table B3. Optimized geometry of bis-HPTA in *β*-CD, orientation II.

Center Number	Atomic Number	Atomic Type	Coordinates (Angstroms) X	Y	Z
1	8	0	-1.47181	5.966933	2.049892
2	1	0	-0.94564	6.044129	2.860771
3	8	0	-4.23026	5.248088	1.964576
4	1	0	-3.25138	5.284495	1.993416
5	8	0	-5.64201	2.754715	2.095099
6	1	0	-5.3552	3.265007	2.868418

TH-2834_146122035

7	8	0	-6.63142	0.071669	2.283532
8	1	0	-6.1057	0.895162	2.209096
9	8	0	-5.48725	-2.56668	2.339371
10	1	0	-5.61225	-2.01951	3.129977
11	8	0	-4.03715	-5.05999	2.296651
12	1	0	-4.32718	-4.1243	2.283776
13	8	0	-1.26207	-5.80675	2.215172
14	1	0	-1.73456	-5.60141	3.036527
15	8	0	1.495308	-6.46072	2.010834
16	1	0	0.612694	-6.03891	2.074967
17	8	0	3.857591	-4.85821	2.084872
18	1	0	3.385549	-5.19001	2.864564
19	8	0	5.997215	-2.99845	2.202798
20	1	0	5.134459	-3.45922	2.162688
21	8	0	6.197869	-0.14101	2.309811
22	1	0	5.867852	0.777297	2.36388
23	8	0	5.62022	2.65461	2.383068
24	1	0	6.433281	3.011831	2.766135
25	8	0	3.615951	4.702855	2.298367
26	1	0	3.806195	4.248682	3.133149
27	8	0	1.358468	6.455394	2.083115
28	1	0	1.984352	5.703706	2.137751
29	8	0	2.021663	4.662524	-0.02315
30	8	0	-2.45267	4.490996	-0.1322
31	8	0	-5.17107	0.946107	-0.00345
32	8	0	-3.98039	-3.29697	0.086576
33	8	0	0.177753	-5.01119	-0.06242
34	8	0	4.222965	-3.04381	-0.04599
35	8	0	4.947661	1.229953	0.04077
36	8	0	0.688932	5.894316	-1.49451
37	8	0	-4.28273	4.18165	-1.5615
38	8	0	-6.2291	-0.70037	-1.29475
39	8	0	-3.3051	-5.04463	-1.31428
40	8	0	1.924258	-5.53425	-1.52838
41	8	0	5.908214	-2.0651	-1.34548
42	8	0	5.194311	3.190462	-1.22904
43	8	0	4.323207	5.547999	-2.62082
44	1	0	4.169393	5.991455	-3.46552
45	8	0	-1.53397	6.498811	-3.12405
46	1	0	-0.74758	7.06322	-3.0936
47	8	0	-6.22367	2.624489	-2.97365
48	1	0	-6.54778	2.215475	-3.78688
49	8	0	-6.33472	-3.24717	-2.61559
50	1	0	-6.32266	-3.76039	-3.43428
51	8	0	-1.53315	-6.55663	-2.93117
52	1	0	-2.47512	-6.77156	-2.86568
53	8	0	4.229273	-5.15767	-3.10671

TH-2834_146122035

54	1	0	3.729889	-5.98745	-3.10795
55	8	0	5.374639	-0.76584	-3.7891
56	1	0	5.752326	-1.65701	-3.77013
57	6	0	-4.87012	2.208409	-2.76736
58	1	0	-4.22	2.589016	-3.56505
59	1	0	-4.79955	1.115594	-2.74811
60	6	0	-4.36528	2.744711	-1.43927
61	1	0	-3.35937	2.33586	-1.27885
62	6	0	-5.24953	2.357884	-0.23559
63	1	0	-6.28736	2.648884	-0.43238
64	6	0	-4.74534	3.060477	1.021006
65	1	0	-3.74597	2.675583	1.26347
66	6	0	-4.66577	4.572528	0.793592
67	1	0	-5.67337	4.946449	0.579902
68	6	0	-3.78775	4.870043	-0.4321
69	1	0	-3.83195	5.931466	-0.69229
70	6	0	-5.17667	-2.40478	-2.59276
71	1	0	-5.20489	-1.68395	-3.41941
72	1	0	-4.26369	-3.00385	-2.6784
73	6	0	-5.12565	-1.63449	-1.28513
74	1	0	-4.18056	-1.07943	-1.26335
75	6	0	-5.19051	-2.53452	-0.03451
76	1	0	-6.05118	-3.20855	-0.10543
77	6	0	-5.3129	-1.68363	1.225063
78	1	0	-4.3855	-1.1116	1.356523
79	6	0	-6.48993	-0.71112	1.106025
80	1	0	-7.4149	-1.28997	1.004797
81	6	0	-6.32625	0.139498	-0.16316
82	1	0	-7.2082	0.763401	-0.33388
83	6	0	-1.38828	-5.15461	-2.69877
84	1	0	-1.92226	-4.57746	-3.46427
85	1	0	-0.32211	-4.93434	-2.77748
86	6	0	-1.89543	-4.72728	-1.32665
87	1	0	-1.76068	-3.64229	-1.22776
88	6	0	-1.19063	-5.43127	-0.15131
89	1	0	-1.23748	-6.51686	-0.29677
90	6	0	-1.87999	-5.06355	1.15871
91	1	0	-1.74465	-3.98959	1.342617
92	6	0	-3.37701	-5.38578	1.081791
93	1	0	-3.49003	-6.46766	0.949772
94	6	0	-4.00789	-4.69341	-0.13646
95	1	0	-5.03348	-5.03896	-0.29343
96	6	0	3.319586	-4.10435	-2.788
97	1	0	2.536664	-4.0227	-3.55255
98	1	0	3.899201	-3.18011	-2.78486
99	6	0	2.654371	-4.29119	-1.42944
100	1	0	1.952461	-3.46282	-1.26762

TH-2834_146122035

101	6	0	3.645053	-4.34076	-0.249
102	1	0	4.433967	-5.07242	-0.45926
103	6	0	2.90369	-4.73315	1.02569
104	1	0	2.18593	-3.94016	1.274915
105	6	0	2.154259	-6.05343	0.821351
106	1	0	2.885979	-6.83639	0.592754
107	6	0	1.204096	-5.93703	-0.37987
108	1	0	0.774462	-6.91072	-0.63111
109	6	0	5.824759	-0.07928	-2.62303
110	1	0	5.430737	0.937115	-2.68485
111	1	0	6.922168	-0.02608	-2.60337
112	6	0	5.334433	-0.7449	-1.34051
113	1	0	4.2419	-0.83725	-1.36981
114	6	0	5.752216	0.028633	-0.07676
115	1	0	6.809517	0.310231	-0.15187
116	6	0	5.564345	-0.78662	1.213715
117	1	0	4.488763	-0.89384	1.410753
118	6	0	6.175194	-2.1847	1.056555
119	1	0	7.257393	-2.07422	0.922266
120	6	0	5.619056	-2.85903	-0.20832
121	1	0	6.116844	-3.81661	-0.38435
122	6	0	3.612239	4.307242	-2.62381
123	1	0	3.978098	3.647908	-3.42023
124	1	0	2.539061	4.474112	-2.76846
125	6	0	3.813106	3.604398	-1.2913
126	1	0	3.165134	2.719708	-1.297
127	6	0	3.439869	4.472992	-0.07274
128	1	0	3.948948	5.440343	-0.14366
129	6	0	3.844282	3.782996	1.227299
130	1	0	3.215315	2.897175	1.376261
131	6	0	5.309476	3.359385	1.174635
132	1	0	5.933524	4.255798	1.098221
133	6	0	5.595619	2.499301	-0.07051
134	1	0	6.671784	2.345861	-0.17971
135	6	0	-1.12323	5.163531	-2.82701
136	1	0	-0.41583	4.798251	-3.58222
137	1	0	-2.02234	4.545691	-2.86249
138	6	0	-0.47519	5.038571	-1.45258
139	1	0	-0.16236	3.996485	-1.30759
140	6	0	-1.39796	5.448942	-0.2882
141	1	0	-1.81998	6.441076	-0.48778
142	6	0	-0.6074	5.484806	1.015589
143	1	0	-0.28155	4.464994	1.260155
144	6	0	0.619883	6.391639	0.872121
145	1	0	0.276492	7.411933	0.668355
146	6	0	1.474651	5.937798	-0.3211
147	1	0	2.272462	6.656797	-0.52589

TH-2834_146122035

148	6	0	0.59878	0.144953	2.035023
149	6	0	0.84587	0.20655	-0.0948
150	6	0	0.5738	0.146423	-1.52685
151	6	0	-0.74245	-0.14187	-1.97352
152	6	0	1.577454	0.369998	-2.4892
153	6	0	-1.01391	-0.19277	-3.34944
154	6	0	1.303806	0.315998	-3.84967
155	6	0	-0.0025	0.033345	-4.27662
156	1	0	-2.02815	-0.4122	-3.66676
157	1	0	2.095218	0.490104	-4.57044
158	1	0	-0.2299	-0.01123	-5.33742
159	7	0	-0.06952	-0.0253	0.855561
160	7	0	2.021942	0.504931	0.50536
161	7	0	1.879441	0.468041	1.855719
162	6	0	0.001905	0.002608	3.36382
163	6	0	-1.35052	-0.36269	3.497991
164	6	0	0.763313	0.234441	4.535884
165	6	0	-1.94261	-0.49542	4.749808
166	6	0	0.162475	0.100867	5.795337
167	6	0	-1.17797	-0.26076	5.901519
168	1	0	-2.98695	-0.77893	4.83019
169	1	0	0.766406	0.285274	6.678167
170	1	0	-1.62813	-0.36029	6.884754
171	1	0	2.590023	0.586831	-2.1678
172	1	0	-1.9301	-0.5413	2.598682
173	1	0	2.934478	0.7418	0.120837
174	8	0	-1.76797	-0.37301	-1.12238
175	1	0	-1.42986	-0.3127	-0.19065
176	8	0	2.075909	0.59062	4.50736
177	1	0	2.382677	0.646769	3.574415

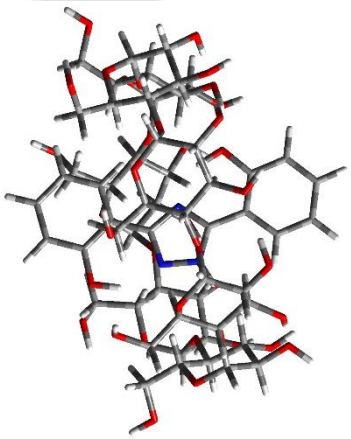

Figure B5. Optimized geometry of bis-HPTA in *β*-CD, orientation III.

Table B3. Optimized geometry of bis-HPTA in *β*-CD, orientation III.

TH-2834_146122035

Center Number	Atomic Number	Atomic Type	Coordinates (Angstroms)		
			X	Y	Z
1	8	0	6.528432	-0.53742	1.977713
2	1	0	6.491313	-1.0354	2.808488
3	8	0	6.973454	2.304842	1.694594
4	1	0	6.636128	1.397247	1.841525
5	8	0	5.177948	4.511256	2.185414
6	1	0	5.747164	4.11249	2.860774
7	8	0	1.891407	4.41395	3.309076
8	1	0	1.208505	4.225077	3.970671
9	8	0	-0.88967	4.24983	2.833025
10	1	0	-1.08142	3.29055	2.833577
11	8	0	-3.44154	5.347826	2.354142
12	1	0	-2.56434	4.94174	2.532618
13	8	0	-5.2631	3.124307	2.076141
14	1	0	-4.9566	3.455417	2.934149
15	8	0	-6.78865	0.730894	1.706283
16	1	0	-6.10968	1.425244	1.839344
17	8	0	-6.00549	-2.02214	1.869252
18	1	0	-6.2428	-1.4739	2.633244
19	8	0	-4.86377	-4.63279	2.098002
20	1	0	-5.04001	-3.67215	2.034995
21	8	0	-2.21432	-5.70769	2.44147
22	1	0	-1.25322	-5.6343	2.599713
23	8	0	0.696284	-5.73572	2.804341
24	1	0	0.897142	-6.45155	3.422308
25	8	0	3.407486	-4.65333	2.610113
26	1	0	2.941513	-4.48404	3.442323
27	8	0	5.951487	-3.36933	2.088469
28	1	0	5.018131	-3.62057	2.24593
29	8	0	3.881285	-3.37306	0.149029
30	8	0	5.231516	0.875587	-0.07528
31	8	0	2.670882	4.226769	0.59597
32	8	0	-1.70477	4.613909	0.100766
33	8	0	-4.81199	1.509117	-0.19687
34	8	0	-4.17776	-2.9229	-0.07581
35	8	0	-0.33751	-4.97101	0.364442
36	8	0	5.365033	-2.55555	-1.45321
37	8	0	5.255499	2.712621	-1.52109
38	8	0	1.602232	6.278547	0.181776
39	8	0	-3.53723	4.805528	-1.28555
40	8	0	-5.71119	0.006996	-1.73998
41	8	0	-3.61698	-4.8083	-1.35103
42	8	0	1.445605	-5.99767	-0.774
43	8	0	3.932064	-6.04514	-2.21538
44	1	0	4.385886	-6.11838	-3.06544
45	8	0	6.507726	-0.64425	-3.20852

TH-2834_146122035

46	1	0	6.790564	-1.57035	-3.21437
47	8	0	4.141604	5.080918	-2.64139
48	1	0	3.737929	5.526159	-3.39808
49	8	0	-0.59993	7.876766	-0.80328
50	1	0	-0.88237	8.502683	-1.48341
51	8	0	-5.589	3.877912	-3.0034
52	1	0	-5.40828	4.821944	-2.8852
53	8	0	-5.8644	-2.32009	-3.33386
54	1	0	-6.50866	-1.60125	-3.4112
55	8	0	-2.00899	-4.66326	-3.65119
56	1	0	-2.97046	-4.75574	-3.71551
57	6	0	3.381908	3.90359	-2.35303
58	1	0	3.415931	3.203444	-3.19678
59	1	0	2.335085	4.153702	-2.15496
60	6	0	3.957609	3.204941	-1.13209
61	1	0	3.307355	2.352098	-0.89999
62	6	0	4.025593	4.108188	0.120441
63	1	0	4.415739	5.093303	-0.15695
64	6	0	4.90491	3.497012	1.214765
65	1	0	4.342166	2.677737	1.681866
66	6	0	6.22179	2.936461	0.664209
67	1	0	6.835471	3.76985	0.305593
68	6	0	5.962107	2.007951	-0.52514
69	1	0	6.902196	1.695481	-0.98925
70	6	0	-0.09658	6.702735	-1.44899
71	1	0	0.730229	6.952914	-2.12467
72	1	0	-0.88637	6.213265	-2.03202
73	6	0	0.411481	5.719728	-0.40789
74	1	0	0.669634	4.791523	-0.93227
75	6	0	-0.63097	5.371137	0.677444
76	1	0	-1.01319	6.292081	1.129415
77	6	0	0.020197	4.501942	1.75132
78	1	0	0.313913	3.545447	1.306646
79	6	0	1.270961	5.191898	2.296391
80	1	0	0.989451	6.174648	2.701197
81	6	0	2.254415	5.456151	1.146198
82	1	0	3.110762	6.038819	1.491183
83	6	0	-4.36902	3.169196	-2.77897
84	1	0	-3.60758	3.46543	-3.51126
85	1	0	-4.59204	2.109417	-2.91936
86	6	0	-3.80781	3.388517	-1.37872
87	1	0	-2.87016	2.828324	-1.28975
88	6	0	-4.76014	2.943255	-0.25283
89	1	0	-5.76224	3.350025	-0.43235
90	6	0	-4.25122	3.418768	1.103315
91	1	0	-3.34335	2.853709	1.347253
92	6	0	-3.92724	4.91537	1.090324

TH-2834_146122035

93	1	0	-4.85183	5.477053	0.917875
94	6	0	-2.97095	5.245407	-0.07129
95	1	0	-2.84319	6.327561	-0.16918
96	6	0	-4.63171	-1.75258	-2.88954
97	1	0	-4.25126	-1.02872	-3.62128
98	1	0	-3.9182	-2.57397	-2.81132
99	6	0	-4.75401	-1.05757	-1.539
100	1	0	-3.77691	-0.63095	-1.2782
101	6	0	-5.21438	-1.9825	-0.39415
102	1	0	-6.1237	-2.51642	-0.69426
103	6	0	-5.49288	-1.15151	0.855615
104	1	0	-4.54932	-0.70823	1.200914
105	6	0	-6.49486	-0.03339	0.54596
106	1	0	-7.44042	-0.48958	0.232626
107	6	0	-5.97909	0.826472	-0.61854
108	1	0	-6.7434	1.536757	-0.94655
109	6	0	-1.59119	-5.31422	-2.45278
110	1	0	-0.50315	-5.24231	-2.41799
111	1	0	-1.86844	-6.37752	-2.47338
112	6	0	-2.18886	-4.66391	-1.20922
113	1	0	-1.93476	-3.59821	-1.19547
114	6	0	-1.71515	-5.33206	0.093333
115	1	0	-1.78449	-6.42196	-0.00849
116	6	0	-2.54589	-4.90726	1.314133
117	1	0	-2.3429	-3.84891	1.530119
118	6	0	-4.04454	-5.05398	1.021317
119	1	0	-4.26256	-6.11636	0.862785
120	6	0	-4.39494	-4.30935	-0.27947
121	1	0	-5.43513	-4.4977	-0.55964
122	6	0	2.978598	-4.98173	-2.30047
123	1	0	2.22664	-5.19169	-3.07083
124	1	0	3.473746	-4.03411	-2.5409
125	6	0	2.268504	-4.8262	-0.96626
126	1	0	1.627505	-3.93941	-1.04097
127	6	0	3.227598	-4.64456	0.226803
128	1	0	3.966252	-5.45333	0.231544
129	6	0	2.454093	-4.65122	1.543444
130	1	0	1.86246	-3.72973	1.596476
131	6	0	1.522952	-5.86083	1.638303
132	1	0	2.133399	-6.76663	1.708898
133	6	0	0.644878	-6.00528	0.383259
134	1	0	0.146673	-6.97768	0.387719
135	6	0	5.146478	-0.60545	-2.77674
136	1	0	4.50343	-1.16251	-3.46972
137	1	0	4.845125	0.443806	-2.78918
138	6	0	4.953874	-1.17202	-1.37477
139	1	0	3.886953	-1.11757	-1.123

TH-2834_146122035

140	6	0	5.762394	-0.43758	-0.28754
141	1	0	6.813105	-0.37279	-0.59383
142	6	0	5.664709	-1.18685	1.037618
143	1	0	4.6283	-1.1309	1.396541
144	6	0	6.060409	-2.65716	0.863677
145	1	0	7.116672	-2.70263	0.57708
146	6	0	5.238725	-3.305	-0.26265
147	1	0	5.61668	-4.30374	-0.49699
148	6	0	-0.45819	-0.89298	1.136116
149	6	0	-0.1709	-0.38138	-0.92847
150	6	0	-0.08051	0.370403	-2.18156
151	6	0	-0.28011	1.763078	-2.19244
152	6	0	0.191969	-0.28529	-3.40868
153	6	0	-0.2209	2.492455	-3.37557
154	1	0	-0.4846	2.265904	-1.25344
155	6	0	0.254283	0.454676	-4.59767
156	6	0	0.047949	1.831083	-4.58179
157	1	0	-0.38378	3.564767	-3.36349
158	1	0	0.463342	-0.0723	-5.52325
159	1	0	0.096836	2.390417	-5.51135
160	7	0	-0.46834	0.15133	0.295794
161	8	0	0.399678	-1.62537	-3.50306
162	1	0	0.320434	-2.03376	-2.61206
163	7	0	0.021699	-1.69905	-0.87569
164	7	0	-0.16157	-2.00817	0.433228
165	1	0	-0.15663	-2.99141	0.700742
166	6	0	-0.7399	-0.80178	2.565532
167	6	0	-1.18829	0.429535	3.103908
168	6	0	-0.5866	-1.89916	3.435455
169	6	0	-1.48886	0.534751	4.466645
170	6	0	-0.88054	-1.79033	4.789687
171	1	0	-0.22051	-2.84737	3.056184
172	6	0	-1.33707	-0.56798	5.302425
173	1	0	-1.83793	1.487004	4.852643
174	1	0	-0.75298	-2.64767	5.441681
175	1	0	-1.57089	-0.47404	6.358309
176	8	0	-1.34718	1.537201	2.326246
177	1	0	-1.06262	1.316053	1.393885

TH-2834_146122035

TH-2834_146122035

Annexure C

TH-2834_146122035

TH-2834_146122035

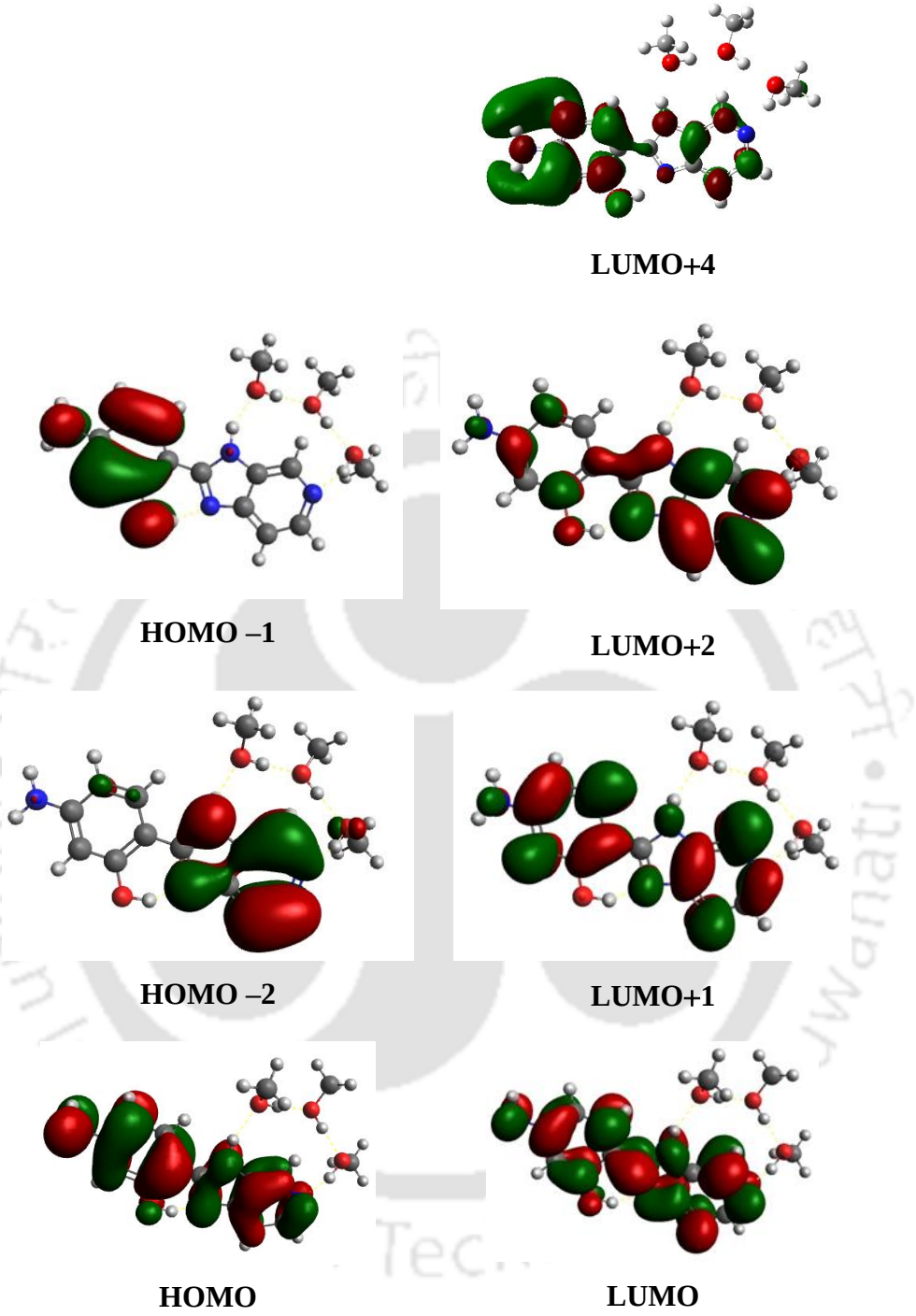

Figure C1. Frontier molecular orbitals of enol forms of AHPIP-c.(MeOH)$_3$.

TH-2834_146122035

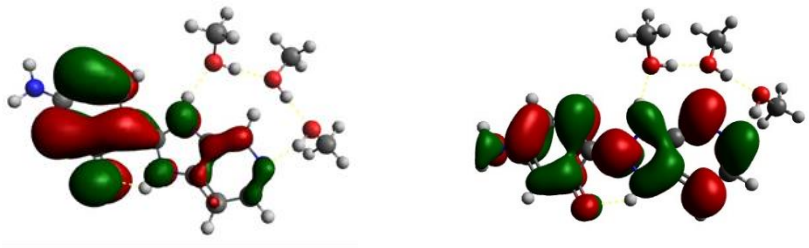

HOMO **LUMO**

Keto Tautomer

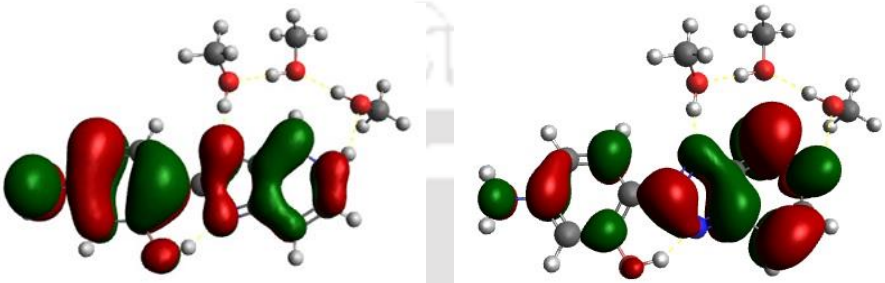

HOMO **LUMO**

Pyridinyl Tautomer (Normal)

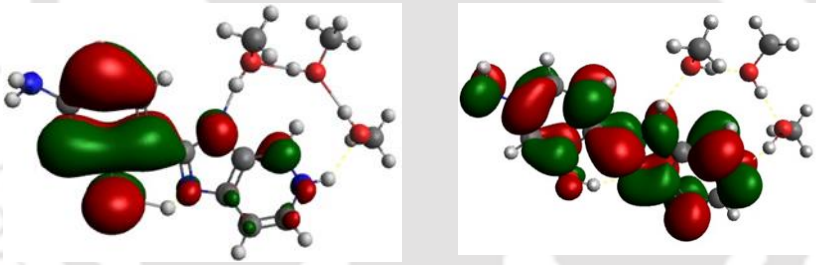

HOMO **LUMO**

Pyridinyl Tautomer (Amino Twisted)

Figure C2. Frontier molecular orbitals of keto (I), pyridinyl tautomer (IIA) and amino twisted pyridinyl tautomer (IIB) of AHPIP-c.$(MeOH)_3$.

TH-2834_146122035

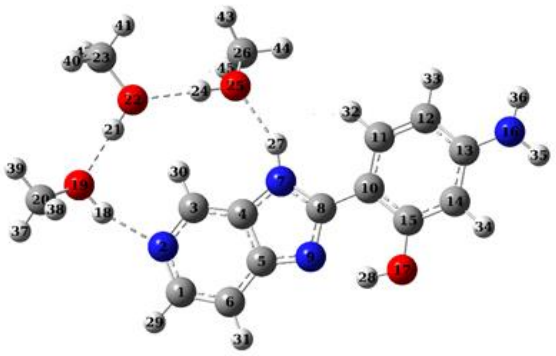

Figure C3. Ground state optimized structure of *cis*-enol of AHPIP-c.$(CH_3OH)_3$.

Table C1. Ground state optimized parameters of *cis*-enol of AHPIP-c.$(CH_3OH)_3$ using B3LYP functional.

Center Number	Atomic Number	Atomic Type	Coordinates (Angstroms)		
			X	Y	Z
1	6	0	-2.3941	-3.11737	-0.36413
2	7	0	-2.96005	-1.89809	-0.53575
3	6	0	-2.16974	-0.81456	-0.56795
4	6	0	-0.79914	-0.94119	-0.39648
5	6	0	-0.19795	-2.20764	-0.21996
6	6	0	-1.02544	-3.33883	-0.21323
7	7	0	0.224257	-0.01852	-0.33515
8	6	0	1.383935	-0.71798	-0.12348
9	7	0	1.160167	-2.04297	-0.06263
10	6	0	2.700471	-0.13125	0.019869
11	6	0	2.918847	1.262311	-0.03716
12	6	0	4.178525	1.81534	0.100041
13	6	0	5.30127	0.974786	0.303113
14	6	0	5.108237	-0.414	0.364984
15	6	0	3.834545	-0.96842	0.2281
16	7	0	6.556282	1.522054	0.489837
17	8	0	3.727021	-2.31601	0.297972
18	1	0	-4.59436	-1.04328	-0.18982
19	8	0	-5.23499	-0.32418	0.03219
20	6	0	-6.11759	-0.7845	1.061028
21	1	0	-4.31513	1.206242	0.374276
22	8	0	-3.78666	2.02366	0.527051
23	6	0	-4.67532	3.13476	0.682171
24	1	0	-2.03217	2.343567	0.038206
25	8	0	-1.10716	2.521169	-0.24013
26	6	0	-1.12441	3.44813	-1.33115
27	1	0	0.051993	0.99148	-0.33579
28	1	0	2.762847	-2.55522	0.185836
29	1	0	-3.08339	-3.95666	-0.34615
30	1	0	-2.64079	0.149779	-0.71906
31	1	0	-0.63355	-4.34163	-0.0822

TH-2834_146122035

32	1	0	2.077887	1.930634	-0.19405
33	1	0	4.31062	2.891815	0.053233
34	1	0	5.949106	-1.08273	0.522074
35	1	0	7.354034	0.916892	0.351361
36	1	0	6.702974	2.46615	0.160015
37	1	0	-6.7009	-1.64898	0.722875
38	1	0	-5.568	-1.05586	1.970808
39	1	0	-6.80428	0.032117	1.294615
40	1	0	-5.34414	2.990174	1.538873
41	1	0	-4.06434	4.022236	0.861555
42	1	0	-5.2771	3.296595	-0.22031
43	1	0	-1.57078	4.40399	-1.03265
44	1	0	-0.08812	3.623306	-1.62847
45	1	0	-1.67559	3.047392	-2.19062

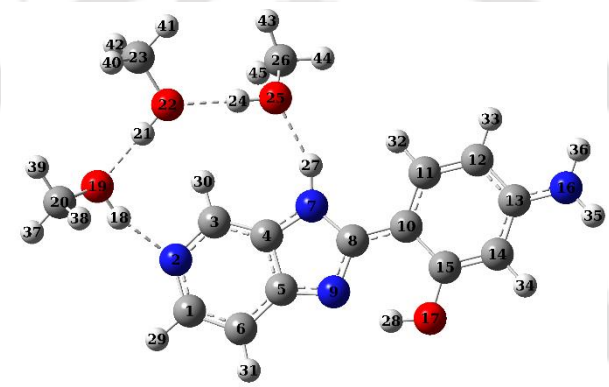

Figure C4. Excited state optimized structure of *cis*-enol of AHPIP-c.$(CH_3OH)_3$.

Table C2. TDDFT optimized parameters of the enol form of AHPIP-c.$(CH_3OH)_3$ using B3LYP functional.

Center Number	Atomic Number	Atomic Type	Coordinates (Angstroms) X	Y	Z
1	6	0	2.441303	-3.07295	0.397932
2	7	0	2.993568	-1.86078	0.660712
3	6	0	2.176603	-0.77807	0.755118
4	6	0	0.806496	-0.91231	0.526366
5	6	0	0.21894	-2.18592	0.249815
6	6	0	1.08507	-3.3175	0.204688
7	7	0	-0.21107	0.001482	0.47659
8	6	0	-1.37979	-0.69848	0.159016
9	7	0	-1.10593	-2.0389	0.040438
10	6	0	-2.67328	-0.13271	0.008345
11	6	0	-2.92682	1.268395	0.141533
12	6	0	-4.1987	1.7872	-0.0182
13	6	0	-5.29928	0.929397	-0.3201
14	6	0	-5.07764	-0.4647	-0.45698

TH-2834_146122035

15	6	0	-3.81335	-0.99469	-0.30168
16	7	0	-6.54735	1.450638	-0.47461
17	8	0	-3.64055	-2.32244	-0.43954
18	1	0	4.541119	-1.01188	0.195949
19	8	0	5.18078	-0.30572	-0.08585
20	6	0	5.996994	-0.80859	-1.14691
21	1	0	4.225442	1.190601	-0.43188
22	8	0	3.701624	2.00963	-0.59717
23	6	0	4.594254	3.089153	-0.88616
24	1	0	1.997626	2.355324	-0.03036
25	8	0	1.087172	2.560226	0.278863
26	6	0	1.168011	3.47955	1.372295
27	1	0	-0.03246	1.010243	0.454977
28	1	0	-2.66675	-2.53573	-0.29549
29	1	0	3.146434	-3.89886	0.337742
30	1	0	2.630558	0.179459	0.980658
31	1	0	0.717684	-4.3169	0.000077
32	1	0	-2.10795	1.940913	0.369533
33	1	0	-4.36819	2.854657	0.083533
34	1	0	-5.90133	-1.13332	-0.68569
35	1	0	-7.33983	0.863121	-0.69069
36	1	0	-6.71774	2.441168	-0.37762
37	1	0	6.593093	-1.66723	-0.81495
38	1	0	5.393456	-1.10666	-2.01359
39	1	0	6.676049	-0.0084	-1.45053
40	1	0	5.184577	2.885653	-1.78772
41	1	0	3.987553	3.980909	-1.0597
42	1	0	5.27517	3.283455	-0.04842
43	1	0	1.633085	4.423734	1.064564
44	1	0	0.147789	3.684102	1.704984
45	1	0	1.734984	3.058383	2.211793

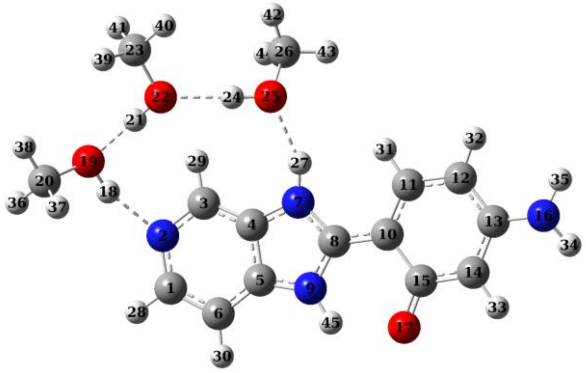

Figure C5. Excited state optimized structure of keto form of AHPIP-c.$(CH_3OH)_3$.

TH-2834_146122035

Table C3. TDDFT optimized parameters of keto form of AHPIP-c.$(CH_3OH)_3$ using B3LYP functional.

Center Number	Atomic Number	Atomic Type	Coordinates (Angstroms)		
			X	Y	Z
1	6	0	2.545955	-3.05705	0.389632
2	7	0	3.056223	-1.8406	0.652693
3	6	0	2.205523	-0.77733	0.743408
4	6	0	0.845504	-0.9508	0.5115
5	6	0	0.319219	-2.23286	0.242007
6	6	0	1.187671	-3.34148	0.191393
7	7	0	-0.20715	-0.05798	0.458239
8	6	0	-1.36693	-0.73459	0.153952
9	7	0	-1.02166	-2.06113	0.045119
10	6	0	-2.68454	-0.1729	0.003593
11	6	0	-2.93455	1.186035	0.145553
12	6	0	-4.23627	1.741638	-0.01102
13	6	0	-5.33492	0.934022	-0.31805
14	6	0	-5.11304	-0.4565	-0.46767
15	6	0	-3.82484	-1.047	-0.31756
16	7	0	-6.60074	1.470676	-0.54045
17	8	0	-3.65722	-2.30787	-0.45683
18	1	0	4.583649	-0.92914	0.187218
19	8	0	5.190089	-0.19796	-0.09761
20	6	0	6.023696	-0.66834	-1.16066
21	1	0	4.176823	1.264037	-0.4395
22	8	0	3.621385	2.06239	-0.60144
23	6	0	4.471578	3.179207	-0.87801
24	1	0	1.91703	2.343934	-0.01218
25	8	0	1.005091	2.512132	0.315685
26	6	0	1.073067	3.420329	1.420272
27	1	0	-0.04679	0.956119	0.460332
28	1	0	3.268745	-3.86704	0.326801
29	1	0	2.630253	0.191773	0.971583
30	1	0	0.844782	-4.3478	-0.01533
31	1	0	-2.12745	1.870635	0.386089
32	1	0	-4.36507	2.812923	0.110464
33	1	0	-5.9348	-1.12521	-0.70623
34	1	0	-7.37845	0.840902	-0.38748
35	1	0	-6.7686	2.383625	-0.13693
36	1	0	6.657968	-1.49873	-0.82795
37	1	0	5.430158	-0.99525	-2.02369
38	1	0	6.665495	0.160116	-1.46913
39	1	0	5.075383	3.00488	-1.77662
40	1	0	3.830214	4.046483	-1.0506
41	1	0	5.13827	3.395574	-0.03436
42	1	0	1.504465	4.381375	1.116697

TH-2834_146122035

43	1	0	0.052084	3.589353	1.769626
44	1	0	1.665113	3.006082	2.245552
45	1	0	-1.74342	-2.74524	-0.17201

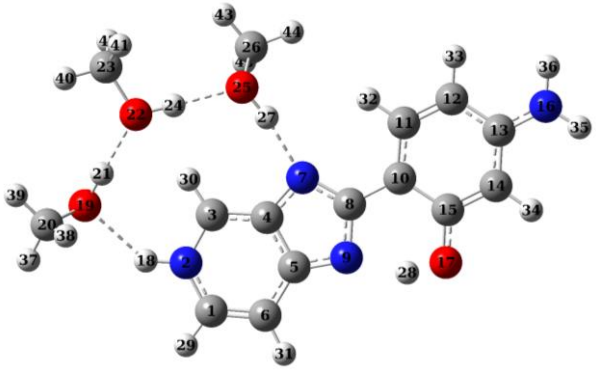

Figure C6. Excited state optimized structure Pyridinyl Tautomer (IIA) form of AHPIP-c.$(CH_3OH)_3$.

Table C4. TDDFT optimized parameters of Pyridinyl Tautomer (IIA) form of AHPIP-c.$(CH_3OH)_3$ using B3LYP functional.

Center Number	Atomic Number	Atomic Type	Coordinates (Angstroms)		
			X	Y	Z
1	6	0	2.336703	-3.23572	0.265255
2	7	0	2.896037	-1.99045	0.437192
3	6	0	2.150487	-0.82034	0.500928
4	6	0	0.762903	-0.95416	0.345604
5	6	0	0.161276	-2.23239	0.171381
6	6	0	0.983673	-3.41361	0.144035
7	7	0	-0.20705	0.013062	0.302159
8	6	0	-1.35612	-0.70676	0.106145
9	7	0	-1.18131	-2.05403	0.024581
10	6	0	-2.67548	-0.11281	-0.00855
11	6	0	-2.87855	1.285663	0.064377
12	6	0	-4.13866	1.836837	-0.05469
13	6	0	-5.27808	0.99004	-0.25669
14	6	0	-5.1031	-0.40933	-0.32814
15	6	0	-3.83877	-0.96245	-0.20881
16	7	0	-6.5072	1.546156	-0.37662
17	8	0	-3.69194	-2.29102	-0.28241
18	1	0	3.90592	-1.8678	0.424906
19	8	0	5.317394	-0.30128	0.086889
20	6	0	6.258244	-0.54652	-0.96011
21	1	0	4.818461	0.517387	-0.12164
22	8	0	3.829781	2.037121	-0.49714
23	6	0	4.491899	3.30458	-0.5209
24	1	0	2.873483	2.173306	-0.29835
25	8	0	1.135141	2.455186	0.092941
26	6	0	0.893315	3.274185	1.240005

TH-2834_146122035

27	1	0	0.572545	1.637009	0.160226
28	1	0	-2.69385	-2.50356	-0.18137
29	1	0	3.039668	-4.05926	0.232799
30	1	0	2.68632	0.101635	0.65328
31	1	0	0.571146	-4.40762	0.018019
32	1	0	-2.0186	1.926687	0.214191
33	1	0	-4.27829	2.911513	0.001165
34	1	0	-5.95405	-1.06499	-0.47933
35	1	0	-7.32924	0.979045	-0.52869
36	1	0	-6.63656	2.546801	-0.33541
37	1	0	6.805378	-1.45687	-0.70314
38	1	0	5.7593	-0.69797	-1.92607
39	1	0	6.976707	0.277172	-1.05703
40	1	0	5.540516	3.123966	-0.76832
41	1	0	4.060293	3.963812	-1.28363
42	1	0	4.442096	3.804086	0.45456
43	1	0	1.514892	4.168175	1.149344
44	1	0	-0.15715	3.585757	1.29151
45	1	0	1.156233	2.755075	2.170371

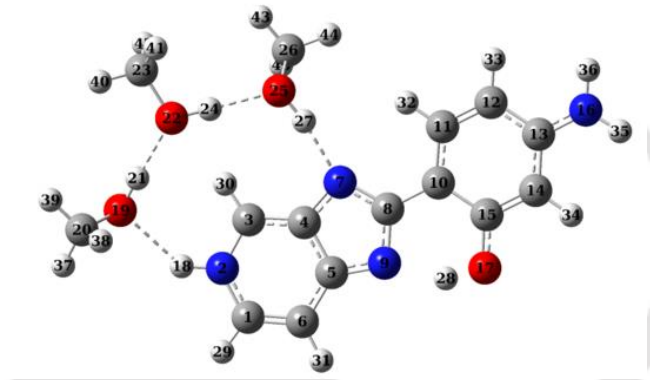

Figure C7. Excited state optimized structure Amino Twisted Pyridinyl Tautomer (II B) form of AHPIP-c.$(CH_3OH)_3$.

Table C5. TDDFT optimized parameters of Amino Twisted Pyridinyl Tautomer (II B) form of AHPIP-c.$(CH_3OH)_3$ using B3LYP functional.

Center Number	Atomic Number	Atomic Type	Coordinates (Angstroms) X	Y	Z
1	6	0	2.431009	-3.21956	0.265879
2	7	0	2.9498	-1.96022	0.461028
3	6	0	2.155403	-0.80983	0.518616
4	6	0	0.785598	-0.99536	0.349964
5	6	0	0.246534	-2.28133	0.165218
6	6	0	1.087763	-3.44227	0.128684
7	7	0	-0.22985	-0.04736	0.304091

TH-2834_146122035

8	6	0	-1.35021	-0.74389	0.095891
9	7	0	-1.10893	-2.0832	0.008973
10	6	0	-2.69576	-0.15594	-0.02657
11	6	0	-2.87415	1.212225	0.051866
12	6	0	-4.15011	1.802853	-0.08216
13	6	0	-5.30014	1.015985	-0.28382
14	6	0	-5.15534	-0.36595	-0.33398
15	6	0	-3.8689	-1.0054	-0.23559
16	7	0	-6.56472	1.673396	-0.39383
17	8	0	-3.76856	-2.27256	-0.3086
18	1	0	3.95326	-1.79992	0.432798
19	8	0	5.31182	-0.20926	0.0792
20	6	0	6.265346	-0.44248	-0.959
21	1	0	4.793027	0.593918	-0.14186
22	8	0	3.770787	2.077721	-0.54367
23	6	0	4.404462	3.358498	-0.61121
24	1	0	2.821879	2.197515	-0.30675
25	8	0	1.092616	2.450389	0.16189
26	6	0	0.895537	3.189702	1.371724
27	1	0	0.540237	1.629671	0.198061
28	1	0	-1.86124	-2.74907	-0.13929
29	1	0	3.157087	-4.0223	0.231132
30	1	0	2.651505	0.12956	0.690159
31	1	0	0.705314	-4.44517	-0.01062
32	1	0	-2.0141	1.853611	0.204802
33	1	0	-4.25073	2.881935	-0.04001
34	1	0	-6.01624	-1.01544	-0.45951
35	1	0	-6.99188	1.799806	0.522709
36	1	0	-7.21585	1.093609	-0.91917
37	1	0	6.83454	-1.33496	-0.68761
38	1	0	5.776653	-0.61869	-1.92602
39	1	0	6.962595	0.39851	-1.06176
40	1	0	5.444374	3.196327	-0.90375
41	1	0	3.924869	3.999088	-1.36088
42	1	0	4.387849	3.868371	0.359937
43	1	0	1.502991	4.095358	1.30901
44	1	0	-0.15448	3.481979	1.49152
45	1	0	1.20863	2.614119	2.251623

TH-2834_146122035

TH-2834_146122035

List of Publications

1. Molecular aggregation to obtain conformer specific enhanced emissions from a triple emissive ESIPT dye, S Sahu, **Ila**, B Shankar, M Sathiyendiran, G Krishnamoorthy, Journal of Photochemistry and Photobiology A: Chemistry 353 (2018), 416-423

2. Comment on "Michael addition based chemodosimeter for serum creatinine detection using (e)-3-(pyren-2-yl)-1-(3,4,5-trimethoxyphenyl)prop-2-en-1-one chalcone", **Ila**, FAS Chipem, G Krishnamoorthy, ACS sensors 3 (2018), 2463-2466

3. Pyridyl substitution control dynamics and shape dependence of fluorescent aggregates, **Ila**, A Malakar, A Gogoi, KA Reddy, M Kumar, BB Mandal, G. Krishnamoorthy, Journal of Photochemistry & Photobiology A: Chemistry 392 (2020), 112405

4. The origin of the longer wavelength emission in 2-(4-fluorophenylamino)-5-(2,4-dihydroxybenzeno)-1,3,4-thiadiazole and its analogue 2-phenylamino-5-(2-hydroxybenzono)-1,3,4-thiadiazole, **Ila**, R Dani, SP Verma, G Krishnamoorthy, Photochemical & Photobiological Sciences 19 (2020), 844-853

5. The suppression of intramolecular charge transfer by tautomerism in 2-(4′-Amino-2′-hydroxyphenyl)-1H-imidazo-[4,5-c]pyridine: Intramolecular proton transfer versus intermolecular proton transfer, **Ila**, G Krishnamoorthy, Journal of Photochemistry & Photobiology A: Chemistry 413 (2021), 113199

6. Modifying the proton transfer by water, confinement and confined water, **Ila**, M Brahma, S Ranjan, P Tripathi, G Krishnamoorthy (Manuscript submitted)

7. Prototropic tuning of proton and charge transfer emission in 2-(4′-Amino-2′-hydroxyphenyl)-1H-imidazo-[4,5-c]pyridine, **Ila**, S K Behera, A D Kanungo, Purushottam, G Krishnamoorthy (Manuscript submitted)

TH-2834_146122035

List of Conference Proceedings

1. **Ila**, S. Chakraborty, G. Krishnamoorthy, Enhancing the anion sensitivity in aqueous media using cationic micelle, NFCFA 2017, BITS Pilani KK Birla Goa campus #

2. **Ila**, S. Sahu, G. Krishnamoorthy, Molecular aggregation to obtain conformer specific enhanced emissions from a triple emissive ESIPT dye, EAS8-2017, CSIR-NIIST, Thiruvananthpuram #

3. **Ila**, R. Dani, S. P. Verma, G. Krishnamoorthy, Spectroscopic study of dual fluorescence and aggregation in 2-((phenyl)amino)-5-(2 hydroxybenzono)-1,3,4-thiadiazole, ICSIMR 2017, CIF, IIT Guwahati

4. **Ila**, A. D. Kanungo, G. Krishnamoorthy, The role of hydroxyl group in metal binding in two thiadiazole derivatives, 23rd CRSI-NSI 2018, IISER Bhopal #

5. **Ila**, S. Ranjan, G. Krishnamoorthy, Intramolecular vs. intermolecular proton transfer in 3,5-bis(2-hydroxyphenyl)-1H-1,2,4-triazole (bis-HPTA): Effect of pH and β-cyclodextrin, ETCS 2020, Gauhati University

#Not a part of the current thesis

TH-2834_146122035